Technische Universität München
Lehrstuhl für Entwicklungsgenetik

The regulation of neuronal progenitor cell migration by cell-cell adhesion factors during zebrafish cerebellar development

Sandra Rieger

Vollständiger Abdruck der von der Fakultät Wissenschaftszentrum Weihenstephan für Ernährung, Landnutzung und Umwelt der Technischen Universität München zur Erlangung des akademischen Grades eines

Doktors der Naturwissenschaften

genehmigten Dissertation.

Vorsitzender:	Univ.-Prof. Dr. A. Gierl
Prüfer der Dissertation:	1. Univ.-Prof. Dr. W. Wurst
	2. apl.-Prof. Dr. J. Graw

Die Dissertation wurde am 15.10.2007 bei der Technischen Universität München eingereicht und durch die Fakultät Wissenschaftszentrum Weihenstephan für Ernährung, Landnutzung und Umwelt am 11.12.2007 angenommen.

Ich erkläre hiermit an Eides statt, dass ich die vorliegende Arbeit selbständig ohne unzulässige fremde Hilfe angefertigt habe.

Die verwendeten Literaturquellen sind im Literaturverzeichnis vollständig zitiert.

München, den 11. Oktober 2007

_____

Sandra Rieger

Acknowledgements

This research project was accomplished in the Zebrafish Neuroimaging group of the Institute of Developmental Genetics at the GSF Research Center for Environment and Health under the supervision of Dr. Reinhard W. Köster and was conducted through the generous support of the BioFuture-Award Grant (0311889) from the German Ministry of Education and Research (BMBF) and the Helmholtz-Association (HGF).

I am truly thankful to Dr. Reinhard W. Köster for his guidance over the past years, and being a member of his lab was a rewarding learning experience. He has greatly contributed to my understanding in the field of developmental neurobiology and has assisted me with his intense and though-provoking discussions.

I would further like to thank my parents, Anita and Martin Rieger, for supporting me during my doctoral program.

I am indebted to the members of the Köster lab - Andreas Barbaryka, Katrin Volkmann, Niklas Senghaas, Martin Distel, Enrico Kühn, Petra Hammerl and Kazuhiko Namikawa - for their excellent assistance and many critical discussions throughout the past years.

I am truly thankful to Ruth Klafke, Annerose Drexler and Thorsten Naserke from the Molecular Neurogenetics Group in the Institute of Developmental Genetics for their histological assistance, materials, helpful discussions and assistance during the preparation of my thesis.

I would like to especially acknowledge Andrea Kneuttinger for her help during the time as a practical student in the lab.

I thank the group of Laure Bally-Cuif and Chichung Lie for providing research materials and supporting me with excellent discussions.

I thank the animal caretakers for their technical assistance and care in the zebrafish facilities.

Acknowledgements

I am thankful to Matthias Hammerschmidt and James Jontes for providing me the N-cadherin plasmid DNA, Martin Distel for supporting me with the 1xUASE1b:Centrin2tdTomato construct and Nathaniel Heintz for contributing the anti-BLBP antibody.

I am grateful to Yoshihiro Yoshihara for sending me the zebrafish NCAM cDNA, Rita Gerardy-Schahn for providing recombinant purified EndoN and to Monika Marx and Martin Bastmeyer for sending the anti-PSA mAb735 antibody.

I would like to thank Thomas Lisse (NIH; Bethesda, Maryland) formerly in the Institute of Experimental Genetics for supporting me with research materials and for helpful suggestions and discussions during the past years.

I would like to thank Prof. Dr. Wolfgang Wurst for giving me the opportunity to accomplish my doctoral work within his institute.

Lastly, I am thankful to Prof. Dr. Wolfgang Wurst, Prof. Dr. Jochen Graw and Prof. Dr. Alfons Gierl for reading this dissertation and supporting the examination.

Table of contents

ACKNOWLEDGEMENTS **3**

TABLE OF CONTENTS **5**

I ABSTRACT **9**

I.I CADHERIN-2 REGULATES DIRECTIONAL AND COHERENT MIGRATION OF CEREBELLAR GRANULE PROGENITOR CELLS 9
I.II NEURONAL MIGRATION IN THE DIFFERENTIATING CEREBELLUM IS LINKED TO POLYSIALYLTRANSFERASE EXPRESSION AND POLYSIALYLATION OF NCAM 10

II ZUSAMMENFASSUNG **11**

II.I CADHERIN-2 REGULIERT DIE DIREKTIONALE UND KOHÄRENTE MIGRATION VON GRANULÄRZELLVORLÄUFERN IM ZEBRAFISCH KLEINHIRN 11
II.II NEURONALE MIGRATION IM DIFFERENZIERENDEN ZEBRAFISCH KLEINHIRN WIRD ÜBER DIE POLYSIALYLIERUNG VON NCAM VERMITTELT 12

III ABBREVIATIONS **14**

1 INTRODUCTION **1**

1.1 SHAPING THE CEREBELLAR SYSTEM FROM A SIMPLE TISSUE INTO A FUNCTIONAL BRAIN COMPARTMENT 1
1.1.1 Anatomical organization of the cerebellar domains 1
1.1.2 Morphogenetic movements of the cerebellum 2
1.1.3 Specification of cell types from the precerebellar system and ventricular zone of the cerebellum 3
1.1.4 The upper rhombic lip and its derivatives 5
1.2 MIGRATION DYNAMICS AND CELL POLARITY CONTROL OF NEURONAL PROGENITORS 8
1.2.1 Routes of migrating URL-derived neuronal progenitors in the developing zebrafish cerebellum 8
1.2.2 Neuronal progenitor migration via nucleokinesis 9
1.2.3 Cytoskeletal coordination of nucleokinesis 10
1.2.4 Establishment of cell polarity and adhesion in migrating cells 12
1.3 CLASSIC CADHERIN-MEDIATED NEURONAL MIGRATION 14
1.3.1 Structure and regulation of type I classic Cadherins 14
1.3.2 N-cadherin mediated neuronal migration in the CNS 17
1.3.3 PSA-NCAM and its regulation in the CNS by polysialyltransferase expression 19
1.4 AIM OF THE STUDY 21
1.4.1 Zebrafish as model organism 21
1.4.2 Analysis of Cadherin-2 during cerebellar granule cell progenitor migration in zebrafish 22
1.4.3 Investigation of the function of PSA-NCAM and polysialyltransferase expression during zebrafish cerebellar development and in the adult brain 24

2 MATERIALS AND METHODS **25**

2.1 MATERIALS 25
2.1.1 Suppliers of chemicals and consumables 25
2.1.2 Equipment 25
2.1.2.1 Gel electrophoresis *25*
2.1.2.2 Electroporation *25*
2.1.2.3 Histology *25*
2.1.2.4 Microinjection and Transplantation *26*
2.1.2.5 Microscopes *26*
2.1.2.6 Microscope cameras *27*
2.1.2.7 Microscope objectives (Zeiss) *27*
2.1.2.8 Molecular biology and cell culture *27*
2.1.2.9 Western blotting *28*
2.1.2.10 Software *28*
2.1.3 Buffers and solutions 28
2.1.3.1 Fixation of embryos *28*
2.1.3.2 Laemmli sample buffer (4x) *28*
2.1.3.3 In-situ hybridization (adopted from R.W. Köster and J. Wittbrodt) *29*
2.1.3.4 Dot blot *30*

Table of contents

2.1.3.5 Immunohistochemistry ... *30*
2.1.3.6 Embryo solutions ... *31*
2.1.3.7 Post-Fixative Solution ... *31*
2.1.3.8 Epon embedding resin ... *31*
2.1.3.9 Toluidine Blue Working Solution ... *32*
2.1.4 Kits ... 32
2.1.5 RNA *in situ* probes ... 33
2.1.6 Antibodies ... 33
2.1.6.1 Primary antibodies ... *33*
2.1.6.2 Secondary antibodies ... *33*
2.1.7 Enzyme injection ... 34
2.1.8 Nucleic acid injection ... 34
2.1.8.1 Vectors ... *34*
2.1.8.2 Fluorescent proteins ... *34*
2.1.8.3 Plasmid construction ... *35*
2.1.8.4 Plasmids used for RNA and DNA injections ... *36*
2.1.9 Primers used for amplification of specific zebrafish cDNAs by RT-PCR ... 37
2.1.10 Fluorescent dyes ... 37
2.1.11 Bacteria strains for plasmid amplification ... 38
2.1.12 Cell culture ... 38
2.1.13 Fish strains ... 38
2.2 METHODS ... 38
2.2.1 Molecular biology ... 38
2.2.1.1 Transformation of plasmids into bacteria ... *38*
2.2.1.2 Mini preparations for plasmid DNA isolation from bacteria ... *39*
2.2.1.3 Maxi preparations for plasmid DNA isolation ... *39*
2.2.1.4 DNA gel electrophoresis ... *39*
2.2.1.5 DNA gel extraction ... *40*
2.2.1.6 Purification of DNA fragments from restriction digests or PCR reactions using kits ... *40*
2.2.1.7 DNA precipitation ... *40*
2.2.1.8 DNA restriction digest ... *40*
2.2.1.9 DNA ligation ... *41*
2.2.1.10 Calculation of nucleic acid concentrations ... *41*
2.2.1.11 Polymerase chain reaction (PCR) ... *41*
2.2.1.12 Removal of 5' overhangs ... *42*
2.2.1.13 Dephosphorylation of vector DNA ... *42*
2.2.1.14 cDNA preparation from zebrafish by RT-PCR ... *43*
2.2.1.15 Transient gene expression using heatshock induction ... *44*
2.2.2 Protein techniques ... 44
2.2.2.1 SDS-Polyacrylamide gel electrophoresis (PAGE) ... *44*
2.2.2.2 Western blotting ... *44*
2.2.3 Cell culture ... 45
2.2.3.1 Maintenance of zebrafish PAC2 fibroblast cells ... *45*
2.2.3.2 Nanofectin transfection of PAC2 fibroblasts ... *45*
2.2.4 Zebrafish manipulations ... 46
2.2.4.1 Fish maintenance and strains used ... *46*
2.2.4.2 Tail clip genotyping of parachute R2.10 embryos ... *46*
2.2.4.3 Synthesis of capped mRNA for microinjection into zebrafish embryos ... *48*
2.2.4.4 Preparation of plasmid DNA for microinjection into zebrafish embryos ... *49*
2.2.4.5 Microinjection into zebrafish embryos ... *49*
2.2.4.6 Temporal rescue of parachute R2.10 ... *50*
2.2.4.7 Genetic mosaic analysis by single cell transplantation ... *50*
2.2.4.8 Electroporation ... *50*
2.2.4.9 Enzymatic removal of endogenous PSA ... *51*
2.2.4.10 Fluorescent dye labeling of zebrafish embryos ... *51*
2.2.4.11 In-situ hybridization ... *52*
2.2.4.12 Immunohistochemistry ... *54*
2.2.4.13 Cell death analysis by acridine orange staining ... *54*
2.2.5 Microscopy methods ... 55
2.2.5.1 Transmission electron microscopy (TEM) ... *55*
2.2.5.2 Confocal microscopy ... *55*
2.2.5.3 Time-lapse analyses settings for confocal microscope ... *56*

Table of contents

2.2.5.4 Image processing ... *56*
2.2.5.5 Statistical analysis ... *56*

3 RESULTS ... 58

3.1 CADHERIN-2 MEDIATES COHERENT AND DIRECTIONAL MIGRATION OF ZEBRAFISH CEREBELLAR GRANULE PROGENITOR CELLS ... 58
3.1.1 Cerebellar granule progenitor cells migrate in a homotypic neurophilic manner ... 58
3.1.2 Cadherin-2 is a candidate to mediate cerebellar granule progenitor cell migration ... 62
3.1.3 Temporal rescue of *parachute* mutant embryos to reveal a direct role for Cadherin-2 in regulating cerebellar granule progenitor cell migration ... 64
3.1.4 Cadherin-2 mediates directionality and coherence of cerebellar granule progenitor cell migration ... 67
3.1.5 Cadherin-2 mediates stable GPC-interactions in migratory chains ... 68
3.1.6 Cadherin-2 influences polarization of migrating cerebellar GPCs ... 69
3.1.7 Loss of Cadherin-2 leads to a randomized positioning of the centrosome in GPCs ... 71
3.1.8 GPC motility is not affected in the absence of Cadherin-2 ... 73
3.1.9 Cadherin-2 deficient GPCs are misrouted when transplanted into wild type environment ... 74
3.1.10 Granule cells begin to differentiate despite impaired directional migration ... 78
3.1.11 Construction of Cadherin-2 deletion variants to monitor Cadherin-2 localization within migrating GPCs ... 82
3.1.12 GPCs dynamically relocate Cadherin-2 clusters during forward migration ... 86
3.1.13 Directed relocation of Cadherin-2 within the cell membrane ... 87
3.2 PSA-NCAM ... 90
3.2.1 Cloning of the zebrafish polysialyltransferases STX and PST ... 90
3.2.2 Polysialyltransferase expression in the developing zebrafish central nervous system ... 90
3.2.3 *stx* and *pst* are both expressed in common and differential domains in the adult zebrafish brain ... 93
3.2.4 Co-expression of *ncam*, *stx* and PSA in domains of neuronal migration in the developing zebrafish cerebellum ... 95
3.2.5 PSA removal impairs migration of neuronal progenitor cells from the URL ... 96

4 DISCUSSION ... 100

4.1 CADHERIN-2 REGULATES MIGRATION OF GRANULE PROGENITOR CELLS IN THE DIFFERENTIATING ZEBRAFISH CEREBELLUM ... 100
4.1.1 Glia cell-independent migration of cerebellar GPCs ... 100
4.1.2 Cadherin-2 has several migration-regulating functions for zebrafish cerebellar GPCs ... 101
4.1.3 Cadherin-2 is the prominent classic Cadherin mediating homotypic contacts between migrating cerebellar GPCs ... 102
4.1.4 Impaired differentiation and increased cell death of GPCs in dorsal domains of rescued *pac*-/-R cerebelli ... 102
4.1.5 Cadherin-2 mediates GPC polarization in the URL ... 103
4.1.6 Coherent migration of GPCs mediated by dynamic shifts of Cadherin-2 along cell-cell contacts ... 104
4.1.7 Dynamics of Cadherin-2 in migrating GPCs ... 105
4.1.8 Possible guidance mechanisms for GPC migration towards the MHB ... 106
4.1.9 Model of coherent and directional GPC migration ... 107
4.1.10 Outlook ... 109
4.2 PSA-NCAM REGULATES NEURONAL PROGENITOR MIGRATION IN THE ZEBRAFISH CEREBELLUM ... 112
4.2.1 Divergence of PST and STX expression in the zebrafish embryo ... 112
4.2.2 STX polysialylates NCAM in the developing zebrafish cerebellum ... 113
4.2.3 Differential expression of STX and PST may establish functional differences for PSA-NCAM in the adult CNS ... 114
4.2.4 Outlook ... 114

5 REFERENCES ... 118

6 APPENDIX ... 134

6.1 SUPPLEMENTARY FIGURES ... 134
6.2 MOVIE LEGENDS ... 137
6.3 LIST OF FIGURES ... 143
6.4 LIST OF TABLES ... 146
6.5 PREPARATION OF ZEBRAFISH EMBRYOS FOR TRANSMISSION ELECTRON MICROSCOPY – ONLINE PUBLICATION ... 147
6.6 QUANTUM DOTS ARE POWERFUL MULTIPURPOSE VITAL LABELING AGENTS IN ZEBRAFISH EMBRYOS ... 148
6.7 LIST OF PUBLICATIONS ... 152

Table of contents

6.7.1 Publications 152
6.7.2 Submitted Publications & publications under review 152
6.7.3 Publications in preparation 152
6.8 LEBENSLAUF 153

I Abstract

I.I Cadherin-2 regulates directional and coherent migration of cerebellar granule progenitor cells

Long distance migration of neuronal progenitor cells from the upper rhombic lip into prospective target regions is a prominent feature of zebrafish cerebellar development. While the migratory paths of these progenitors have been well described, their mode of migration and the molecules that control their migratory behavior remain largely unknown. *In vivo* time-lapse imaging of migrating granule progenitor cells (GPCs) in the differentiating zebrafish cerebellum revealed that GPCs exhibit a chain-like migration behavior via homotypic neurophilic interactions. A candidate factor to mediate such homotypic interactions is the cell-cell adhesion factor Cadherin-2, being expressed by migratory cerebellar GPCs. Temporal rescue of *parachute* R2.10 (*pac*-/-R) mutant embryos, lacking functional Cadherin-2, indicates a direct role for Cadherin-2 in the establishment and maintenance of GPC polarization and orientation, as well as in the directional migration of GPCs along chains. In the absence of Cadherin-2, GPCs lack migratory directionality and coherence, thus leading to their ectopic positioning and subsequent cell death in the dorsal cerebellum.

Expression of the centrosomal marker Centrin2-tdTomato in *pac*-/-R embryos showed a randomized positioning of the centrosome in migrating cerebellar GPCs, whereas the centrosome in wild type GPCs located predominantly anteriorly during migration. This is in good agreement with the randomized migration behavior of cerebellar GPCs. Genetic mosaic analyses in addition demonstrated that mutant donor GPCs retained their migration defects in the wild type cerebellum, suggesting that the impaired directional migration results mainly from cell-autonomous effects.

Rather than mediating rigid interactions, *in vivo* time-lapse imaging revealed that Cadherin-2 containing adherens junctions are dynamically relocated in migrating GPCs via directed intra-membranous transport of Cadherin-2 clusters. These findings uncover a key role for zebrafish Cadherin-2 in the establishment and maintenance of polarization and in mediating cell-cell adhesion during chain-like migration of cerebellar GPCs. This directional and coherent migration along chains is achieved through the dynamic remodeling of Cadherin-2-containing adherens junctions along cellular contacts.

Abstract

I.II Neuronal migration in the differentiating cerebellum is linked to polysialyltransferase expression and polysialylation of NCAM

Modulation of cell-cell adhesion is crucial for the regulation of neuronal migration and maintenance of structural plasticity in the embryonic and mature brain. Such modulation can be obtained by the reversible attachment of polysialic acid (PSA) to the neural cell adhesion molecule (NCAM) via the two known polysialyltransferases STX and PST. PSA-NCAM function is likely regulated by the differential expression of STX and PST in the CNS. In mammals, PSA-NCAM has been implicated in the regulation of neuronal migration, whereas such a role remained elusive in zebrafish.

To investigate the function of both polysialyltransferases and PSA-NCAM in the zebrafish CNS, homologues of *stx* (*st8sia2*) and *pst* (*st8sia4*) were isolated from embryonic cDNA. Their expression patterns were subsequently compared to PSA-NCAM in the embryonic and adult zebrafish brain. During development, strong polysialyltransferase expression was often confined to regions of neuronal migration, with *stx* being the exclusive enzyme for polysialylation of NCAM in the differentiating cerebellum where neuronal migration is especially pronounced. Furthermore, expression analysis on adult brain sections showed that *stx* and *pst* are found in complementary and overlapping domains in the cerebellum, suggesting a synergistic or redundant function for both enzymes in the regulation of adult neurogenesis, neuronal migration and plasticity via enzymatic modulation of NCAM. The role for PSA-NCAM in the regulation of migrating neuronal progenitors in the differentiating zebrafish cerebellum was further examined by *in vivo* time-lapse imaging after enzymatic ablation of PSA, as addition of polysialic acid residues on NCAM has been suggested to promote motility of migrating cells by reducing cell-cell adhesion. The absence of PSA in the cerebellum resulted in strong immobilization of neuronal progenitors, normally migrating from the upper rhombic lip in anteroventral directions. These findings unravel a novel function for PSA-NCAM in the regulation of progenitor cell motility in the differentiating zebrafish cerebellum.

II ZUSAMMENFASSUNG

II.I Cadherin-2 reguliert die direktionale und kohärente Migration von Granulärzellvorläufern im Zebrafisch Kleinhirn

Ein Hauptmerkmal der Zebrafisch Kleinhirnentwicklung ist die Migration neuronaler Vorläuferzellen über weite Distanzen von der Kleinhirn-Rautenlippe in Gehirnregionen die das vestibuläre und nicht-vestibuläre System bilden. Obwohl die Migrationswege dieser Vorläuferzellen detailliert beschrieben wurden, ist bisher wenig über das Verhalten und die Moleküle bekannt, die diese Zellwanderung im Zebrafisch steuern. *In vivo* Zeitrafferaufnahmen von migrierenden Granulärzellvorläufern im differenzierenden Kleinhirn haben gezeigt, dass sich diese Zellen in kettenähnlichen Formationen mittels homotypischer neurophiler Interaktionen fortbewegen. Ein Adhäsionsmolekül, das solche Zell-Zellkontakte vermitteln kann ist Cadherin-2. Dieses Protein ist in Granulärzellvorläufern des differenzierenden Kleinhirns exprimiert und daher ein viel versprechender Kandidat zur Regulierung der Kettenwanderung dieser Zellen. Die Injektion von *cadherin-2* messenger RNA in *Parachute* R2.10 Mutanten, denen endogenes Cadherin-2 fehlt führt zum zeitlich begrenzten „Rescue“ früher embryonaler Defekte dieser Mutante. Allerdings wird das Protein über die Zeit wieder abgebaut und fehlt daher zu Beginn der Granulärzellvorläufermigration im differenzierenden Kleinhirn. Dieser „Rescue“ von *Parachute* Mutanten konnte zeigen, dass Cadherin-2 eine direkte Funktion in der Etablierung und Aufrechterhaltung von Zellpolarität sowie der Ausrichtung von Granulärzellvorläufern hat. Weiterhin vermittelt Cadherin-2 deren direktionale Migration entlang von Ketten. Fehlt Cadherin-2 kommt es zu einer ungerichteten inkohärenten Migration in ektopische Kleinhirnregionen. Obwohl solche ektopisch lokalisierten Zellen zu differenzieren beginnen sterben sie nach weiteren ein bis zwei Tagen. Durch die Markierung des Centrosoms über einen Centrin2-tdTomato Fluoreszenzreporter in „Rescue“ Mutanten konnte weiterhin gezeigt werden, dass die Position des Centrosoms in Cadherin-2-defizienten Granulärzellvorläufern randomisiert ist, während es zumeist im anterioren Teil von migrierenden Wildtypzellen gefunden wurde. Diese randomisierte Positionierung des Centrosoms in“ Rescue“ Mutanten ist ein zusätzlicher Hinweis auf den Direktionalitätsverlust migrierender Granulärzellvorläufer im Kleinhirn. Mit Hilfe von genetisch mosaiken Embryonen konnte zudem gezeigt werden, dass die ungerichtete inkohärente Migration von Cadherin-2-defizienten Granulärzellvorläufern großteils zellautonom erfolgt. Anhand von *in vivo* Zeitrafferaufnahmen konnte weiterhin

nachgewiesen werden, dass Cadherin-2 in migrierenden Granulärzellvorläufern innerhalb der Zellmembran transportiert wird. Das zeigt, dass Cadherin-2 nicht nur am Aufbau starrer Zell-Zellverbindungen beteiligt ist, sondern dynamisch in migrierenden Zellen relokalisiert werden kann. Diese Ergebnisse weisen auf eine Schlüsselposition von Cadherin-2 in der Etablierung und der Aufrechterhaltung der Polarisation und Zell-Zelladhäsion von Granulärzellvorläufern bei deren Kettenwanderung hin. Die dynamische Umgestaltung von Cadherin-2-vermittelten Adhärenzverbindungen entlang von Zell-Zellkontakten ermöglicht eine direktionale und kohärente Migration im Zebrafisch Kleinhirn, welche entscheidend für die Positionierung, terminale Differenzierung und das Überleben von Granulärzellvorläufern ist.

II.II Neuronale Migration im differenzierenden Zebrafisch Kleinhirn wird über die Polysialylierung von NCAM vermittelt

Die Modulierung von Zell-Zelladhäsion ist notwendig für die Regulation neuronaler Migration and der Aufrechterhaltung von Plastizität im embryonalen und adulten Gehirn. Eine solche Modulation wird in Zellen durch die reversible Addition von Polysialylsäure (PSA) an das Adhäsionsmolekül NCAM durch zwei bekannte Polysialyltransferasen STX und PST erzielt. Der Grad der Polysialylierung von NCAM wird durch die differenzielle Expression der beiden Polysialyltransferasen reguliert. In Säugetieren wurde eine Funktion für PSA-NCAM in der Regulation neuronaler Migration beschrieben, welche jedoch bisher im Zebrafisch nicht bekannt ist. Zur genaueren Untersuchung der Funktion von PSA-NCAM wurden zuerst die homologen Gene der beiden Zebrafisch Polysialyltransferasen *stx* und *pst* mittels embryonaler cDNA kloniert. Die Expressionsmuster von *stx* und *pst* wurden anschließend mit der Expression von PSA-NCAM im embryonalen und adulten zentralen Nervensystem verglichen. Dadurch konnte gezeigt werden, dass *stx* und *pst* während der Embryonalentwicklung großteils in Regionen neuronaler Migration exprimiert sind. *stx* ist zudem als einzige Polysialyltransferase im Kleinhirn, in dem neuronale Migration besonders ausgeprägt ist, exprimiert und daher ausschließlich für die Polysialylierung von NCAM in dieser Region verantwortlich. Zusätzlich zeigten Expressionsstudien an adulten Gehirnpräparaten, dass *stx* und *pst* in teils komplementären, aber auch überlappenden Kleinhirndomänen exprimiert sind. Das könnte auf eine Funktion beider Polysialyltransferasen in der Regulation adulter Neurogenese, neuronaler Migration und Plastizität im adulten Kleinhirn hinweisen.

Zusammenfassung

Es wird angenommen, dass die enzymatische Polysialylierung von NCAM die neuronale Migration positiv beeinflusst, indem Zell-Zelladhäsion in PSA-NCAM exprimierenden Zellen reduziert wird. *In vivo* Zeitrafferstudien sollten deshalb klären, ob migrierende neuronale Vorläuferzellen im sich entwickelnden Zebrafisch Kleinhirn in ihrer Migration beeinflusst werden, wenn PSA enzymatisch von der Zelloberfläche entfernt wird. Durch *in vivo* Konfokalmikroskopie konnte gezeigt werden, dass die Ablation von PSA zum Motilitätsverlust früher neuronaler Zellen im Kleinhirn führt. Diese Ergebnisse deuten auf eine neuartige Funktion für PSA-NCAM in der Zebrafisch Kleinhirnanlage bei der Regulation der Motilität von neuronalen Vorläuferzellen hin.

III Abbreviations

aa	amino acids
AP	alkaline phosphatase
BCIP	5-Bromo-4-chloro-3-indolylphosphate
bHLH	basic helix-loop-helix
BLBP	brain lipid binding protein
BMP	bone morphogentic protein
bp	base pairs
cb	cerbellum
Cdh2ΔEC2-4ΔC	Cadherin-2 lacking EC2-4 and the cytoplasmic domain
Cdh2ΔN	dominant-negative Cadherin-2, lacking EC1-4
cDNA	complementary DNA
CNS	central nervous system
Cy2	cyanine-2 (green)
Cy5	cyanine-5 (far red)
ΔC	deletion of the cytoplasmic domain
DAB	diaminobenzidine tetrahydrochloride
DCN	deep cerebellar nuclei
DCX	doublecortin
dEosFP	dimerized monomeric Kaede variant
DIG	digoxigenin
DiI	1,1'-dioctadecyl-3,3,3',3'-tetramethylindocarbocyanine perchlorate
DMSO	dimethylsulfoxide
DNA	desoxy-ribonucleic acid
DNase	desoxy-ribonuclease
dNTP	desoxy-nucleotide-tri-phosphate
dpf	days post fertilization
DTT	1,4-Dithioerythritol
E	Embryonic day
EC	ectodomain
ECL	enhanced chemiluminescence
ECM	extracellular matrix
ECN	external cuneate nucleus
EGFP	enhanced green fluorescent protein
EGL	external granule cell layer
EGTA	ethylene glycol tetraacetic acid
EndoN	Endoneuraminidase
fabp7a	fatty acid binding protein 7a
FBS	Fetal bovine serum
GABA	gamma-aminobutyric acid
$gaba_A R\alpha 6$	$gaba_A$ receptor alpha 6 subunit
GCL	granule cell layer
GPC	granule progenitor cell
GFAP	glial fibrilliary acidic protein
GFP	green fluorescent protein
HAV	Histidine-Alanine-Valine
hb	hindbrain
hpf	hours post fertilization
HRP	horse-radish peroxidase
HSE	oligomerized heatshock binding elements
Hyb-mix	Hybridization mixture
IGL	internal granule cell layer
ION	inferior olivary nucleus
IQGAP1	IQ motif containing GTPase activating protein 1
ISH	in-situ hybridization
KalTA4	kozak gal4 transactivator domain 4
LB	Luria Bertani
LRL	lower rhombic lip

Abbreviations

LRN	lateral reticular nucleus
LWR	length – width ratio
LynGFP	Lyn kinase domain fused to GFP
mCherry	monomeric Cherry
MCS	multiple cloning site
MHB	mid-hindbrain boundary
ML	molecular layer
MNCD2	monoclonal anti-Cadherin-2 antibody
mRNA	messenger ribonucleic acid
MT	microtubule
MTOC	microtubule organizing center
MW	molecular weight
n	sample number
NA	numerical aperture
NBT	Nitro blue tetrazolium
Ncad	neural cadherin
NCAM	neural cell adhesion molecule
NeuroD	neurogenic differentiation
NGS	normal goat serum
NIH	National Institute of Health
OB	olfactory bulb
OD	outer diameter
P	postnatal day
pac	*parachute*
***pac*R2.10**	*parachute* carrying the R2.10 allele
***pac*-/-R**	rescued *parachute* R2.10 mutant
PBS	phosphate buffered saline
PC	Purkinje cell
PCL	Purkinje cell layer
PCR	polymerase chain reaction
PenStrep	Penicillin/Streptavidin
PFA	Paraformaldehyde
PGN	pontine gray nucleus
PMZ	pre-migratory transitory zone
PSA	polysialic acid
PSA-NCAM	polysialylated neural cell adhesion molecule
PST	polysialyltransferase st8siaIV
Ptf1	pancreas transcription factor 1
PTU	1-phenyl-2-thiourea
PVDF	Polyvinylidene fluoride
r1	rhombomere 1
RMS	rostral migratory stream
RNA	ribonucleic acid
RNase	ribonuclease
rpm	rotations per minute
RTN	reticulotegmental nucleus
RT-PCR	reverse transcription PCR
SD	standard deviation
SDS	sodium dodecyl sulfate
SEM	standard error of the mean
SVZ	subventricular zone
TEM	transmission electron microscopy
TAE	Tris-Acetate-EDTA
TBE	Tris-Borate-EDTA
TBS	Tris-buffered saline
td	tandem dimer
UBCs	unipolar brush cells
URL	upper rhombic lip
Vglut1	vesicular glutamate transporter 1
VN	vestibular nucleus
VZ	ventricular zone

Abbreviations

WT	wild type

1 Introduction

The cerebellum (Latin: little brain) makes up about 10% of the brain volume. It is part of the hindbrain, where it covers the dorsal surface of the pons and medulla. Although the cerebellum is of considerable size it bears relatively few classes of neurons. Its major cell type, the cerebellar granule cells are highly abundant and present the largest cell population. Only seven other cell types, including Purkinje cells, Golgi cells, Lugaro cells, basket cells, stellate cells, unipolar brush cells and candelabrum cells constitute the remaining cell types of the cerebellum (Sotelo, 2004). The cerebellum evolved in association with the electric and vestibular senses from the evolutionary ancient vertebrate central nervous system (Paulin, 2005). Its development, anatomical organization and functional properties have been largely conserved among vertebrate species, ranging from teleost fish to mammals (Altman, 1997). The cerebellum is the primary center for motor coordination and motor learning through feedback regulation. It furthermore functions in maintaining muscular tone, control of body posture, and it has been recently shown to contribute to cognitive processing and emotional control (Schmahmann, 2004, Schmahmann and Caplan, 2006).

1.1 Shaping the cerebellar system from a simple tissue into a functional brain compartment

1.1.1 Anatomical organization of the cerebellar domains

The anatomical structure of the cerebellum highly correlates with its function, thus allowing for tremendously fast and synchronized processing of information. The cerebellum in zebrafish is composed of three major components, the vestibulolateralis lobe (in zebrafish termed auricles, including the eminentia granularis and lobus caudalis), the corpus cerebelli and the valvula cerebelli, being further subdivided into medial and lateral valvula (Fig. 1.1). The valvula cerebelli is special with respect to its uniqueness in ray-finned fish species. The cerebellum receives input from the precerebellar system through afferent fibers, while most cerebellar neurons within the cerebellum project efferents to the deep cerebellar nuclei and Purkinje cells, which in turn send their axons into the brain (Wullimann, 1998).

The cerebellar granule cell population outnumbers other cell types in the cerebellum. Granule cells in teleost fish receive input from different precerebellar nuclei (Wullimann and Northcutt, 1988, Wullimann and Northcutt, 1989). In addition, granule cells in the corpus cerebelli receive mossy fiber afferents from spinal and tectal neurons that synapse

with dendrites of the granule neurons, thereby transmitting proprioceptive and other sensory input to the cerebellum. The corpus cerebelli is most homologous to the non-vestibular system in mammals and coordinates locomotion and higher motor functions. In contrast, granule cell that are situated in the eminentia granularis and lobus caudalis receive mainly input from the vestibular and lateral line systems (Puzdrowski, 1989, Wullimann, 1998), thereby processing information for coordination of balance and body posture.

Figure 1.1 Anatomical view of the zebrafish cerebellum

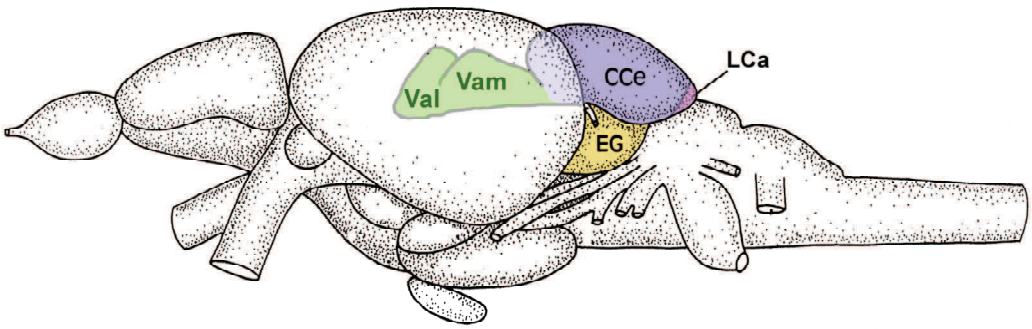

(Fig. 1.1) The cerebellum in context of the zebrafish brain. The scheme shows a lateral view of the brain. Cerebellar components that are covered by the optic tectum are represented in pale colors. The corpus cerebelli (blue) constitutes the largest part of the cerebellum and is located in the dorso-medial domain of the hindbrain, with the lobus caudalis (purple) residing at its posterior edge. The eminentia granularis (yellow) is positioned adjacent to the corpus cerebelli in ventrolateral domains. The valvula cerebelli (pale green), comprising the lateral (Val) and medial (Vam) valvula, is buried deep in the midbrain and covered by the optic tectum. It is bounded to the corpus cerebelli at its posterior edge. Adapted from (Reichert, 1996). Abbr.: CCe: corpus cerebelli, EG: eminentia granularis, LCa: lobus caudalis, Val: valvula lateralis, Vam: valvula medialis.

1.1.2 Morphogenetic movements of the cerebellum

Cerebellar development results from a complex interplay of gene expression and local cellular interactions. These events are largely conserved among zebrafish and mammals and follow a spatially and temporally precisely controlled pattern. Development of the cerebellum involves the unitary specification of the midbrain-hindbrain boundary (MHB) that first establishes rhombomere 1 (r1)/cerebellar identity along the antero-posterior axis in the rostral hindbrain (Wurst and Bally-Cuif, 2001). Morphological changes then lead to a rotation of the cerebellar anlage from an initially anteroposterior into a mediolateral

orientation (Fig.1.2, see Supplementary Movie 1). This process occurs concomitantly with the opening of the fourth ventricle in the hindbrain, placing the ventricle with its anterior limit to the caudal aspect of r1 (Sgaier et al., 2005, Distel et al., 2006). It has been proposed that this rotation might help to bring the precerebellar primordium of the caudal hindbrain closer to the cerebellum during differentiation of the brain, to facilitate the establishment of connections between both systems (Altman, 1997).

Figure 1.2 Rotation of the cerebellar anlage

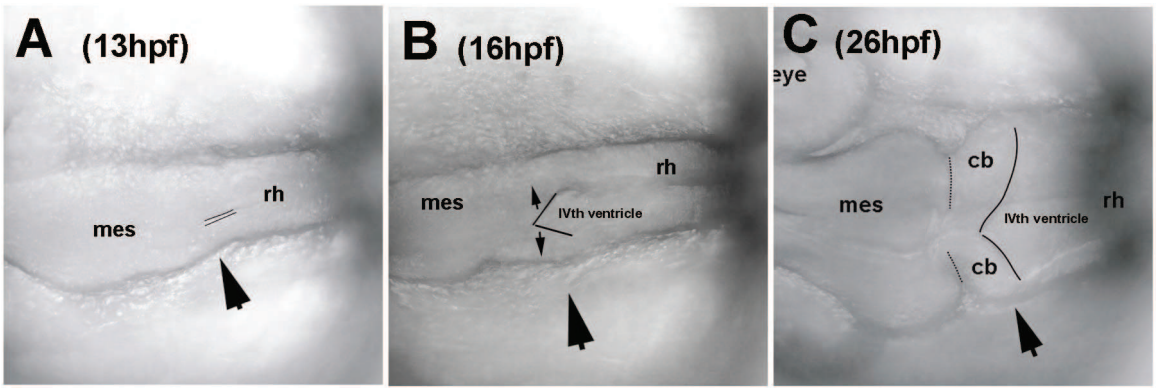

(Fig. 1.2) (A-C) Dorsal view *in vivo* time-lapse sequence showing the cerebellar anlage as it rotates from an initially anteroposterior (A) into a mediolateral position (B, C). Confocal stacks were projected to single images for each time-point. (A) The fourth ventricle (black lines, arrow) starts to open at the posterior edge of the cerebellar anlage at approx. 13hpf. (B) Three hours later, the cerebellar anlage has begun to rotate as the ventricle further expands (black lines, arrow). (C) At 26hpf, the cerebellar primordium is recognizable by its typical morphology, with both cerebellar halves extending now in mediolateral orientation (arrow, black lines mark the posterior edge of the cerebellar anlage, while the anterior border of the cerebellar anlage along the MHB is depicted by a dashed line, see also Supplementary Movie 1). Abbr.: cb: cerebellum; mes: mesencephalon; rh: rhombencephalon.

1.1.3 Specification of cell types from the precerebellar system and ventricular zone of the cerebellum

Following the morphogenetic reorganization, both the precerebellar and cerebellar primordium start to generate diverse neuronal cell lineages. Neurons of the precerebellar system arise from the caudal hindbrain in the rhombencephalon and form six symmetrical bilaterally positioned nuclei along the anteroposterior axis, including the pontine gray (PGN), reticulotegmental (RTN), vestibular (VN), lateral reticular (LRN), external cuneate (ECN), and inferior olivary (ION) nuclei (Altman, 1997, Rodriguez and Dymecki, 2000).

Neurons of LRN, ECN, RTN, VN and PGN derive from the lower rhombic lip (LRL) and express Atonal1. These neurons have been characterized in mammals and found to project afferent mossy fibers to dendrites of the cerebellar granule cells and to glutamatergic deep cerebellar nuclei (DCN). Atonal1-positive lower rhombic lip descendants are furthermore defined by expression of high levels of Wnt1 (Rodriguez and Dymecki, 2000, Wang and Zoghbi, 2001). In contrast, progenitors of the ION do not express Atonal1 and derive from regions in the anterior spinal cord (Landsberg et al., 2005, Wang et al., 2005). Mature ION neurons project climbing fibers into the cerebellum (Sotelo, 2004), where they synapse with dendrites of GABAergic Purkinje cells (Desclin, 1974, Sotelo et al., 1975) and some DCN, giving them excitatory glutamatergic input.

Neurons of the cerebellum originate from two germinative zones, the upper rhombic lip (URL) and the ventricular zone (VZ) (Fig. 1.3A). These zones give rise to distinct neuronal cell populations that are born in sequential slightly overlapping waves, as being revealed by fate mapping studies in chick and mouse (Goldowitz and Hamre, 1998, Hoshino et al., 2005, Machold and Fishell, 2005, Wang et al., 2005, Wingate, 2005). The induction and patterning of the temporally and spatially distinct cell types along the dorso-ventral axis is crucially dependent on signaling from the r1 roofplate, which overlies the cerebellar primordium (Fig. 1.3A). In mouse, the roofplate is defined by expression of the LIM homeodomain transcription factor Lmx1a and members of the bone morphogenetic protein (BMP) family such as Bmp6, Bmp7 and Gdf7 (Alder et al., 1999). The importance of the roofplate has been demonstrated in dreher mice, bearing a mutation in the Lmx1a gene. Homozygous mutants lacking the roofplate, exhibit patterning and differentiation defects of neurons along the entire dorsal CNS. While r1 roofplate cells do not contribute to cerebellar cell populations themselves (Chizhikov et al., 2006), their secretion of BMPs is crucial for the induction of Atonal1 in cells of the URL, located just beneath the roofplate (Alder et al., 1999). The role of roofplate induction for cell fate specification in the zebrafish cerebellum remains elusive.

Induction of cerebellar progenitor pools in more proximal domains, such as in the underlying VZ are not dependent on r1 roofplate signaling, although the roofplate has been shown to be necessary for their proliferation and positioning along the dorso-ventral axis (Chizhikov et al., 2006). Purkinje cells (PCs) are the first neurons to arise from the VZ and are defined by expressing the transcription factor Ptf1a (Hoshino et al., 2005, Pascual et al., 2007). The VZ gives further rise to other GABAergic cells, such as interneurons, including some deep cerebellar nuclei, basket, stellate and golgi cells (Goldowitz and Hamre, 1998,

Hoshino et al., 2005). PC development has been well characterized in mammals. Soon after final mitosis, PCs start to express calbindin and begin to migrate along radial glial fibers into the cerebellar cortex (Hatten and Heintz, 1995). Once arrived in the cerebellar cortex their maturation is critically dependent on Wnt3 expression (Salinas et al., 1994). PC neurons in the cerebellum are easily identifiable by their large soma and their extensive two-dimensional dendritic arbors that synapse with the parallel fiber axons of the cerebellar granule neurons (Hatten and Heintz, 1995). Purkinje cell axons and that of DCN, which are the teleost equivalent of eurydendroid cells, provide the sole output of the cerebellum.

1.1.4 The upper rhombic lip and its derivatives

The zebrafish upper rhombic lip extends along the medio-lateral aspect of caudal rhombomere 1 (Fig. 1.2C), adjacent to the fourth ventricle above the VZ and below the r1 roofplate (Fig. 1.3A). The URL is a germinal layer that gives rise to several cerebellar neuronal cell types that migrate over long distances in order to reach their final target regions (Fig. 1.3B, C). URL-descendants are specified by expression of the bHLH transcription factor Atonal1 (Fig. 3.5G). Atonal1 expression has been conserved but its function has been poorly characterized in zebrafish. The importance of this transcription factor in the specification of rhombic lip derivatives was first revealed by analyses of Math1$^{(-/-)}$ mutant mice, lacking functional Atonal1 (mouse, Math1). In these mutants, several rhombic lip derivatives including early born neuronal populations and granule cells are missing (BenArie et al., 1997, Machold and Fishell, 2005).

Neuronal progenitor cells generated in the URL emerge in temporal waves and subsequent to their final mitosis migrate over long distances into respective neuronal clusters that are located either within or outside the cerebellar domain (Köster and Fraser, 2001, Machold and Fishell, 2005, Wang et al., 2005, Wingate, 2005, Köster and Fraser, 2006, Volkmann et al., 2007) (Fig. 1.3A, B). Fate mapping studies in mouse, chick and zebrafish have recently identified several neuronal cell lineages that emerge from the URL (Wingate and Hatten, 1999, Karam et al., 2001, Köster and Fraser, 2001, Luckner et al., 2001, Gilthorpe et al., 2002, Machold and Fishell, 2005, Wang et al., 2005, Wilson and Wingate, 2006, Volkmann et al., 2007).

In mouse, the earliest neuronal progenitors arise from the URL between E10 and E12.5 and constitute neurons of the cholinergic mesopontine tegmental system as well as large glutamatergic neurons of the DCN (Machold and Fishell, 2005). Following the generation

of these early populations, glutamatergic granule progenitor cells (GPCs) are produced from E12.5 onward in mouse (Machold and Fishell, 2005, Wang et al., 2005) and ~ 48hpf in zebrafish (Volkmann et al., 2007).

Figure 1.3 Cerebellar proliferation zones and migration routes of URL-derived progenitors in zebrafish

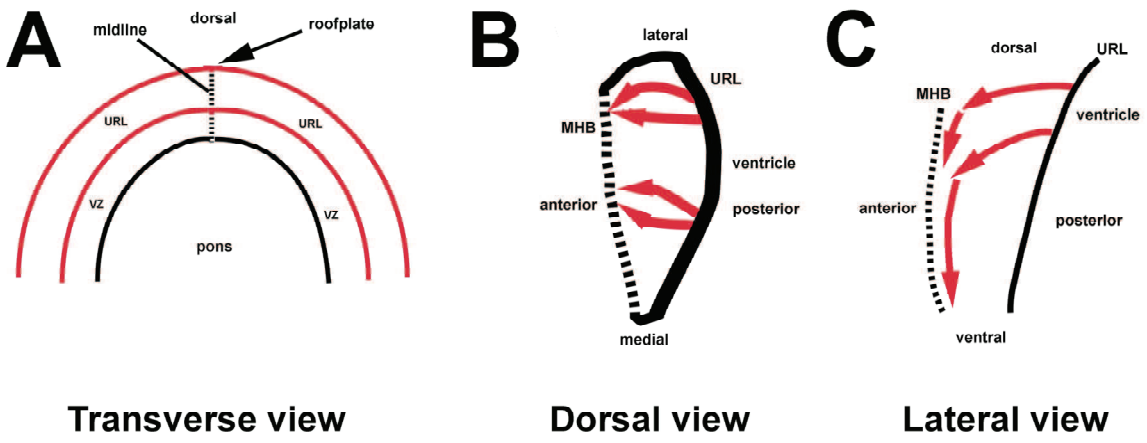

(Fig. 1.3) (A) The URL is a proliferating neuroepithelium located at the dorsal aspect of the cerebellum (demarcated by the red lines), below the r1 roofplate (arrow) and above the ventricular zone (black and red lines). (B) Dorsal view showing one cerebellar lobe. The URL is located at the caudal aspect of the cerebellum, anterior to the fourth ventricle. Soon after birth, URL-derived neuronal progenitors migrate (red arrows) towards the MHB (dashed line). (C) Lateral view of the cerebellum. Upon arrival at the MHB, cells either remain in this domain or migrate further ventrally towards the brain stem (red arrows). Abbr.: MHB: mid-hindbrain boundary, URL: upper rhombic lip, VZ: ventricular zone.

In addition, to the observed temporal differences in the generation of distinct neuronal cell lineages, the URL has been further shown to be spatially subdivided along its medio-lateral aspect during granule cell development (Mathis et al., 1997, Machold and Fishell, 2005, Sgaier et al., 2005, Volkmann et al., 2007). GPCs destined for distinct cerebellar domains arise in parallel but remain within their parasagittal subdivisions during migration. For example in the differentiating zebrafish cerebellum, GPCs that arise medially migrate into rostromedial directions and differentiate into granule neurons of the corpus cerebelli, while GPCs that originate in more lateral positions migrate ventrolaterally and populate the future eminentia granularis (Fig. 3.6C). A third granule cell population with large soma remains posteriorly, along the entire aspect of the medio-lateral extension of the cerebellum. These cells become granule neurons of the lobus caudalis.

Analyses of the mammalian cerebellum showed that granule cell-specification depends on several molecular factors. Atonal1 is thereby the earliest transcription factor to be expressed, starting as early as E9 during mouse development (BenArie et al., 1997, Kim et al., 1997), and in zebrafish at ~18hpf. Soon after departure from the URL, GPCs in the mammalian cerebellum start to express Nestin, a marker for undifferentiated neuronal progenitors. Several other transcription factors including Pax6, the zinc-finger domain genes Zic1, Zic3, Zipro1 and the cell cycle genes cyclin D1 and D2 are also upregulated at this stage and necessary for granule cell proliferation (Aruga et al., 1994, Engelkamp et al., 1999, Huard et al., 1999, Machold and Fishell, 2005, Wang et al., 2005, Pogoriler et al., 2006, Su et al., 2006). Proliferating GPCs sequentially populate the external granule cell layer (EGL), which forms at the dorsal-most surface of the cerebellar anlage (Alder et al., 1996, Wingate and Hatten, 1999, Wingate, 2001).

During postnatal cerebellar development, postmitotic GPCs start to migrate inward along radial glia fibers to form the internal granule cell layer (IGL). It has been suggested that early migration of GPCs in the prenatal rat cerebellum occurs mainly without glial-guidance (Liesi et al., 2003). Whether a glial-dependent or independent migration mode is used by GPCs in the zebrafish cerebellum remains to be investigated. Postmitotic GPCs in the PMZ downregulate Atonal1 before onset of radial migration and start to upregulate differentiation factors such as the bHLH transcription factors NSCL1 (Duncan et al., 1997) and NeuroD (Miyata et al., 1999). NeuroD is required for granule cell survival, as mutant mice lacking NeuroD show increased apoptosis of differentiating granule cells. Prior to migration into the deep cerebellar cortex, a transient population of radial Bergmann glia fibers arises, which derive from Golgi epithelial cells (Goldowitz and Hamre, 1998). In preparation for radial migration, differentiating granule cells in the PMZ adopt a bipolar shape (Edmondson and Hatten, 1987) and extend parallel fiber axons perpendicular to the radial migration direction (Wang et al., 2007). A third short leading process is further extended towards the IGL, perpendicular to the parallel fibers. Radial migration into the IGL depends on the interaction of neurons and glia through specialized interstitial junctions (Hatten, 1999). In meander (*mea*) tail mutant mice, these interactions are disturbed and radial glia fibers are disorganized and atrophic. These mice further reveal reduced survival rates of granule cells (Ross et al., 1990). Interestingly, the effects of glial abnormalities are secondary to the granule cell phenotype (Hamre and Goldowitz, 1997), reflecting the importance of neuron-glia interactions during radial migration. Factors being involved in glial-guided migration include the brain-lipid binding protein (BLBP), which is expressed by differentiating radial

glia cells, neuregulin and ErbB4, which are important for the induction of radial glia morphologies (Rio et al., 1997) and neuron-glia interactions (Hatten, 1999), and the ECM molecules thrombospondin (Adams and Tucker, 2000) and tenascin (Husmann et al., 1992), being involved in axon extension of migrating neurons. Final maturation of granule cells in the IGL involves expression of $GABA_A$ receptor alpha 6 subunit (Raetzman and Siegel, 1999) and glutamate vesicular transporters (Miyazaki et al., 2003), being highly conserved for their expression throughout vertebrates species (Higashijima et al., 2004, Volkmann et al., 2007).

The last cells arising from the upper rhombic lip are unipolar brush cells (UBCs). This class of interneurons is defined by the expression of Tbr2/Eomes in mouse. UBC progenitors migrate in two distinct dorsal and rostral streams (Kalinichenko and Okhotin, 2005, Englund et al., 2006). The dorsally migrating progenitors disperse throughout the white matter of the cerebellum and from there migrate into the IGL. Progenitors of a second rostral stream migrate first along the ventricular zone and then towards the brainstem into the cochlear nucleus. UBCs are involved in vestibular functions (Dino et al., 1999) and two subtypes have been identified, expressing either calretinin or the metabotropic glutamate receptor 1 (mGluR1) (Nunzi et al., 2002). Both subtypes are further defined by the expression of GluR2 (Sekerkova et al., 2004). UBCs function in the amplification of inputs from the vestibular ganglia by spreading and prolonging excitation signals within the IGL (Nunzi et al., 2001). The origin and existence of unipolar brush cells in the zebrafish cerebellum has not been described until now.

1.2 Migration dynamics and cell polarity control of neuronal progenitors

1.2.1 Routes of migrating URL-derived neuronal progenitors in the developing zebrafish cerebellum

Neuronal migration is a key event during vertebrate brain development with postmitotic progenitor cells migrating over significant distances in order to reach their prospective target regions. For example, neuronal progenitor cells from the ventricular zone of the lateral ganglionic eminence migrate up to 120μm to the ventrolateral surface of the telencephalic vesicle in the rat forebrain (Wichterle et al., 1999). Also, migrating neuronal progenitors in the developing zebrafish cerebellum migrate over 100μm from the URL into regions of the brainstem (Köster and Fraser, 2001).

Migration in the differentiating zebrafish cerebellum starts at ~30hpf. Up to this stage, single neuronal cells span the entire width of the cerebellar anlage (Fig 1.4), while displaying frequent interkinetic nuclear movements. Analysis of early migrating progenitors in the differentiating cerebellum of zebrafish by time-lapse confocal microscopy revealed that migrating cells exhibit distinctive migration characteristics (Köster and Fraser, 2001). They change their cellular morphologies from a unipolar to a bipolar shape after initiation of migration, thus leaving the cell anchored in the URL via a trailing process. Upon reaching the MHB, the trailing process is retracted and a unipolar cell shape is adopted again. Progenitor cells subsequently extend a long perpendicular leading process, sometimes up to 50μm into ventral directions, which is then being followed by the soma. These observations suggest that the MHB may serve as an attractant for migrating progenitor cells, whereas other guidance cues direct these cells ventrally upon arrival at the MHB (Köster and Fraser, 2001).

Figure 1.4 Neuronal progenitor cells span the entire width of the early cerebellar anlage in zebrafish

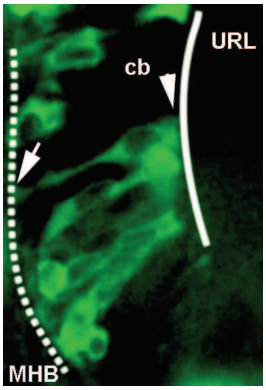

(Fig. 1.4) Confocal projection of the zebrafish cerebellar anlage at 28hpf, showing neuronal progenitor cells transiently expressing cytoplasmic GFP in a mosaic manner. At this early stage, neuronal progenitors span the entire width of the cerebellar anlage and exhibit interkinetic nuclear movements, while being attached via two process (arrowhead and arrow) to the URL (solid line) and MHB (dashed line), respectively.

1.2.2 Neuronal progenitor migration via nucleokinesis

In the differentiating cerebellum, migrating neuronal progenitor cells execute a carefully choreographed series of movements (Köster and Fraser, 2001) by exhibiting saltatory forward movements typical of nucleokinesis (Schaar and McConnell, 2005, Tsai et al., 2005). Nucleokinesis is a repeated two-step process involving extension of a leading process

and displacement of the nucleus towards the leading edge. During the first step of nucleokinsesis, the neuronal cell rapidly extends and retracts neurites, and one of them becomes subsequently stabilized ahead of the soma into the direction of cell movement. Thereby, a characteristic dilation is formed in the leading process. The large over-proportional nucleus is then translocated into this dilation, while the soma contracts at the rear end and pushes the nucleus forward (Schaar and McConnell, 2005). At the same time the trailing process retracts. Extension of the leading process and nuclear displacement are not synchronized, thus the mechanisms that control nucleokinetic movements seem to be rather loosely linked.

1.2.3 Cytoskeletal coordination of nucleokinesis

Ultrastructural examinations of migrating neuronal cells from the postnatal rat SVZ revealed that nuclei of migrating cells are significantly elongated just before nuclear translocation (Schaar and McConnell, 2005). Similarly, such elongated nuclei have been found in progenitors of the differentiating zebrafish cerebellum, as revealed by TEM studies (Fig.3.3A). Nuclear elongation most likely results from pulling of microtubules (MTs) that are anchored in the nuclear membrane. MT plus-ends grow from the centrosome, also termed the microtubule organizing center (MTOC), towards opposing directions, anteriorly into the leading edge and posteriorly around the nucleus of the migrating neuronal cell (Fig 1.5A). The nucleus becomes thereby enveloped in a cage-like manner (Rivas and Hatten, 1995). MTs can however also terminate in the vicinity of the nuclear membrane at the anterior edge of the nucleus (Xie et al., 2003).

Nucleokinesis is critically dependent on the coupling of the nucleus to the centrosome. The centrosome has been shown to be translocated into the leading process prior to nucleokinetic movement and was sometimes found as far as 8μm ahead of the nucleus (Tanaka et al., 2004, Schaar and McConnell, 2005). Current studies suggest two models that lead to nuclear translocation. In the first model, a complex of Lis1, Nde1 (an ortholog of NudE) and dynein, being localized to the nuclear membrane seems to be crucial in this process, with doublecortin (DCX) further stabilizing MTs at the perinuclear cage. In this model, displacement of the nucleus is achieved by the minus-end activity of dynein on MTs, which subsequently pulls the nucleus towards the centrosome (Tsai et al., 2005, Higginbotham and Gleeson, 2007) (Fig. 1.5B). Interference with the function of dynein, Lis1 or Nde1 results in the disruption of nuclear translocation and defective nucleus

centrosomal coupling (Hirotsune et al., 1998, McManus et al., 2004, Shu et al., 2004, Tanaka et al., 2004).

Figure 1.5 Microtubule-based nuclear translocation in migrating neuronal cells

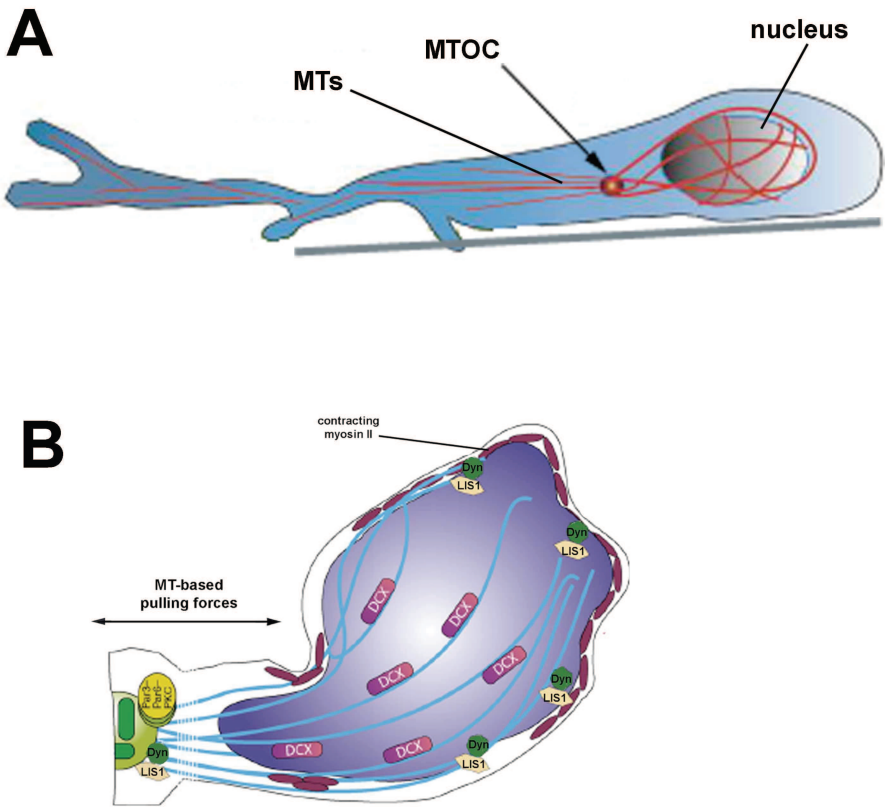

(Fig. 1.5) Model for nuclear translocation established by pulling forces from the centrosome. (A). Microtubule plus-ends emanating from the centrosome grow anteriorly into the leading process and posteriorly around the nucleus to form a perinuclear cage. Adapted from (Solecki et al., 2006). (B) The centrosome (MTOC) is positioned in front of the nucleus in the direction of migration. Microtubules are coupled via Par proteins and Lis1/dynein to the centrosome. MTs are further anchored in the nuclear membrane through Lis1 and dynein/dynactin, whereby DCX additionally stabilizes MTs along the nucleus. The dynein motor complex at the centrosome generates force on MT minus-ends, which then tears the nucleus towards the centrosome and leading edge. Additional contraction of myosin II at the rear end generates membrane blebbings that pinch the nucleus forward. Adapted from (Higginbotham and Gleeson, 2007).

Nuclear translocation seems to be additionally regulated by the interactions of MTs and myosin II. Myosin II serves different functions in this process. Myosin II located in the rear end of the cell helps breaking down cell adhesion just before the onset of nuclear translocation. In addition, it acts as contractile force by generating membrane blebbings in the posterior cell compartment that squeeze the nucleus towards the leading edge (Schaar

and McConnell, 2005). Its role in the front of the cell during nucleokinesis is controversial but it seems to counteract the activity of MTs (Schaar and McConnell, 2005).

In a second model, the pulling forces of MTs from the cell cortex are crucial for nuclear translocation into the leading process, being mediated by the dynein-dynactin motor complex, which anchors MTs in the cortex. These forces then reorient the centrosome and Golgi apparatus into the direction of migration (Gundersen, 2002, Ridley et al., 2003) (Fig. 1.6). This has been suggested to further facilitate the growth of MTs into lamellipodia, thereby enabling vesicular transport along MTs into the leading process. MT anchoring and centrosome repositioning seems to be required to pull the nucleus into the leading process. Rather than using a single mechanism, it is likely that the interplay of both mechanisms leads to nuclear translocation and nucleokinetic movement. Many of the investigations of nuclear translocation have been carried out in cell culture, as these cells are easily manipulated and accessible for time-lapse imaging. So far, it remains however unclear whether similar mechanisms for nucleokinesis may also apply to migrating cells of the differentiating zebrafish cerebellum.

1.2.4 Establishment of cell polarity and adhesion in migrating cells

Migrating cells dynamically polarize in response to extracellular cues, which leads to the reorientation of the centrosome into the leading edge (Schaar and McConnell, 2005, Higginbotham and Gleeson, 2007). This process is tightly linked to reorganization of the actin cytoskeleton and to the growth and anchoring of MTs in the leading edge (Noritake et al., 2004, Watanabe et al., 2004). Several molecular pathways control the protrusive activity of the leading edge in migrating cells (Fig. 1.6). For example, partitioning-defective (Par) genes have been shown to play a crucial role in the process of cell polarization.

Par genes were first discovered in genetic screens searching for mutations in C. elegans that perturb AP-polarity of the zygote (Kemphues et al., 1988) and it has been discovered that Par genes are evolutionary highly conserved. For example, Par pathway components appear crucial for polarity establishment of neural cells in the vertebrate nervous system (Shi et al., 2003, von Trotha et al., 2006).

In response to integrin-mediated signaling in cultured astrocyte monolayers, a complex of mPar6 and the kinase PKCζ is recruited to the cell cortex at the leading edge. This complex in conjunction with the polarized activity of the small Rho-family GTPase Cdc42, which

stabilizes APC at the cell periphery, is necessary for the direct phosphorylation of glycogen-synthase kinase (GSK)-3β and localized inhibition of its kinase activity, thus promoting cell polarization and centrosomal reorientation towards the site of protrusion (Etienne-Manneville and Hall, 2001, Etienne-Manneville and Hall, 2003).

Figure 1.6 Model for cell polarization and centrosomal repositioning in response to cell-cell adhesion

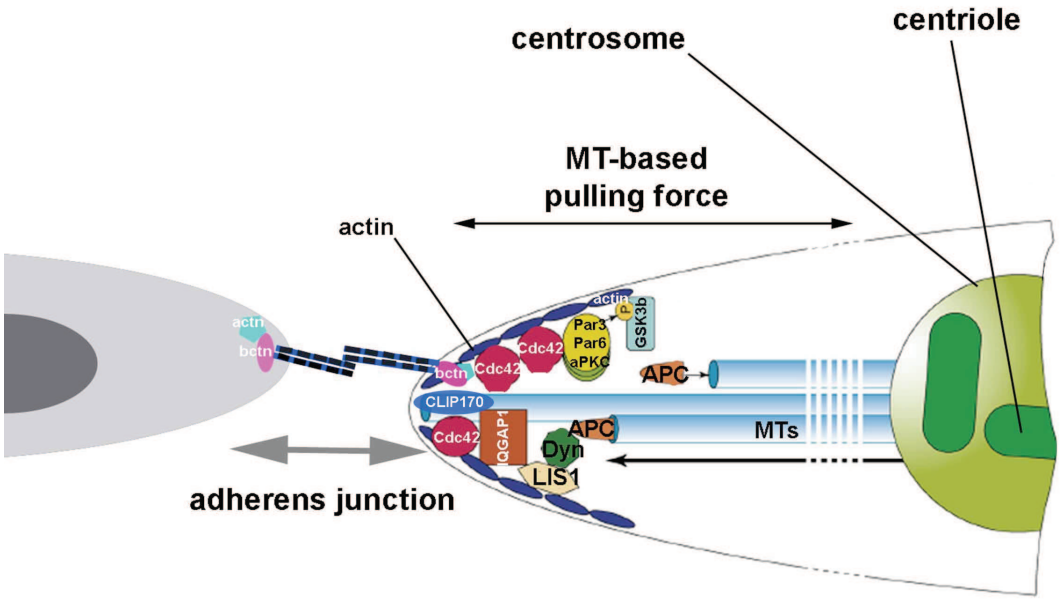

(Fig. 1.6) In response to guidance cues assembly of adherens junctions and actin polymerization is stimulated by activation of Cdc42, which in turn recruits a complex of Par-3, Par-6 and aPKC to the leading edge. Formation of this complex promotes phosphorylation and inactivation of GSK3-β, whereby APC can bind to MT plus-ends and stabilize them, thus enabling cell polarization. IQGAP1 provides the link between MT plus-ends, adherens junctions and the actin cytoskeleton. IQGAP1 acts as molecular switch between adhesion and non-adhesion, also interacting with MT plus-ends through binding to CLIP-170. Lis1 and the dynein/dynactin motor activity in the cortex of the leading edge promote centrosomal reorientation, by applying pulling force on MTs, thereby leading to the repositioning of the centrosome towards the direction of migration. Adapted from (Higginbotham and Gleeson, 2007). Abbr.: MTs: microtubules.

APC together with the dynein-dynactin complex localizes in clusters at cortical regions near the plus-ends of growing MTs in migrating cells (Mimori-Kiyosue et al., 2000, Barth et al., 2002). There, it helps to stabilize MTs within the leading edge at sites of adherens junctions during reorientation of the centrosome. For example, the cell-cell adhesion molecule N-

cadherin has been shown to co-localize with APC, β-catenin and the small scaffolding protein IQGAP1 in actin-positive membrane ruffles of migrating NIH3T3 cells to regulate their adhesive activity (Sharma et al., 2006).

IQGAP1, which binds actin, is an effector of Cdc42 and Rac1 and has been shown to act as molecular switch for cell-cell adhesion. For example, it has been shown that activated Rac1 and Cdc42 positively regulate E-cadherin mediated cell-cell adhesion in epithelial cells through binding and inhibition of IQGAP1 at adherens junctions, thereby tethering actin filaments to the Cadherin-Catenin complex (Kuroda et al., 1998, Noritake et al., 2004, Noritake et al., 2005). In contrast, inactivation of Rac1 and Cdc42 leads to the accumulation of IQGAP1 at adhesion sites and to its increased binding to β-catenin. This causes α-catenin to dissociate from adherens junctions, thereby reducing cell-cell adhesion. The regulation of E-cadherin-mediated adhesion through IQGAP1 has been proposed to depend on a dynamic equilibrium state between two complexes, involving E-cadherin-β-catenin-α-catenin and E-cadherin-β-catenin-IQGAP1 (Noritake et al., 2004).

IQGAP1 further binds the MT plus-end capping protein CLIP-170 (Fukata et al., 2002). For example, in fibroblast cells MT plus-ends containing CLIP-170 grow towards sites in the cell cortex that have been marked by the expression of Cdc42/Rac1, thus promoting leading edge formation (Noritake et al., 2005). IQGAP1 therefore seems to link leading edge formation and cell polarization to Cadherin-mediated cell adhesion and Cdc42/Rac1 in migrating neuronal cells.

1.3 Classic Cadherin-mediated neuronal migration

1.3.1 Structure and regulation of type I classic Cadherins

The classic Cadherins are membrane integral cell-surface glycoproteins that mediate homophilic cell-cell adhesion in a Ca^{2+}-dependent manner (Redies, 2000). Classic Cadherins comprise five extracellular (EC) repeat domains, a single transmembrane and a cytoplasmic domain. Binding of Ca^{2+} to the ectodomain linker regions confers rigidity to the protein structure and resistance to proteolysis (Pokutta et al., 1994, Steinberg and McNutt, 1999), whereas the removal of Ca^{2+} by the calcium chelator EGTA leads to a collapse of the ectodomains and their subsequent internalization (Fig. 1.7). Strand-dimer formation in cis and trans configuration plays an important role for type I classic Cadherins in the homophilic binding to other type I Cadherins (Shapiro et al., 1995, Brieher et al., 1996, Yap

et al., 1997, Tamura et al., 1998). For example, clustering has been shown to increase E- and N-cadherin mediated adhesion by formation of zipper-like structures. This lateral clustering seems to be a prerequisite for the formation of trans dimers (Tamura et al., 1998, Kim et al., 2005). Cis- and trans-dimerization is at least in part mediated by a conserved tryptophane at amino acid position 2 of the mature peptide, within the first ectodomain (Shapiro et al., 1995, Ahrens et al., 2002, Kim et al., 2005, Patel et al., 2006). An evolutionary conserved Histidine-Alanine-Valine (HAV) motif in EC1 also plays an important role in trans-adhesive interactions. Evidence for this has been derived from studies, in which HAV inhibitory peptides were applied to cells. Blocking the HAV motif interfered with different biological processes such as neurite outgrowth (Doherty et al., 1991), myoblast fusion (Mege et al., 1992) or embryonic compaction (Blaschuk et al., 1990).

Although the importance of the EC1 domain in mediating cis and trans dimers has been confirmed, other ectodomains may also be involved and necessary for dimerization (Chappuis-Flament et al., 2001, Ahrens et al., 2002). For example, it has been shown that a conserved aspartic acid residue in ectodomain 2 at amino acid position 134 of the mature peptide is necessary for the formation of trans dimers. The mutation of this aspartic acid to alanine in E-cadherin and N-cadherin prevents cell aggregation (Ozawa, 2002, Kim et al., 2005), while cis interactions still occur. In addition, the cytoplasmic domain of E-cadherin has also been shown to play a role in dimerization. A 70 amino acid deletion in the cytoplasmic tail of E-cadherin prevents trans but not cis dimer formation (Ozawa, 2002), demonstrating that several structural features in type I Cadherins contribute to homophilic interactions.

Classic Cadherin-mediated adhesion is largely regulated through intracellular signaling pathways and several mechanisms have been proposed (Gumbiner, 2000). First, the composition of the adherens junction core complex, involving Cadherin, β-catenin and α-catenin seems to influence the strength of cell-cell adhesion. The cytoplasmic levels of Cadherin thereby determine the increase in adhesion, whereas the levels of cytoplasmic β-catenin play only minor roles (Bradley et al., 1993, Hinck et al., 1994). Cytoplasmic levels of Cadherins may be controlled by the metalloproteinase ADAM10, which regulates ectodomain shedding of Cadherin-2 and thereby the overall levels of Cadherin-2 at the cell surface (Reiss et al., 2005). In some cell types however, changes in cell-cell adhesion do not necessarily depend on the levels of surface Cadherins. For example, signaling from certain growth factors leads to morphogenetic movements that result in the loss of Cadherin-mediated adhesion without changing the morphology of adherens junction complexes at the

cell surface (Weidner et al., 1990, Shibamoto et al., 1994). These observations suggest that adhesion in these cells is regulated by phosphorylation, such as tyrosine-phosphorylation of β-catenin through receptor tyrosine kinases (Matsuyoshi et al., 1992, Behrens et al., 1993, Shibamoto et al., 1994, Daniel and Reynolds, 1997, Rhee et al., 2002).

Figure 1.7 The adherens junction complex

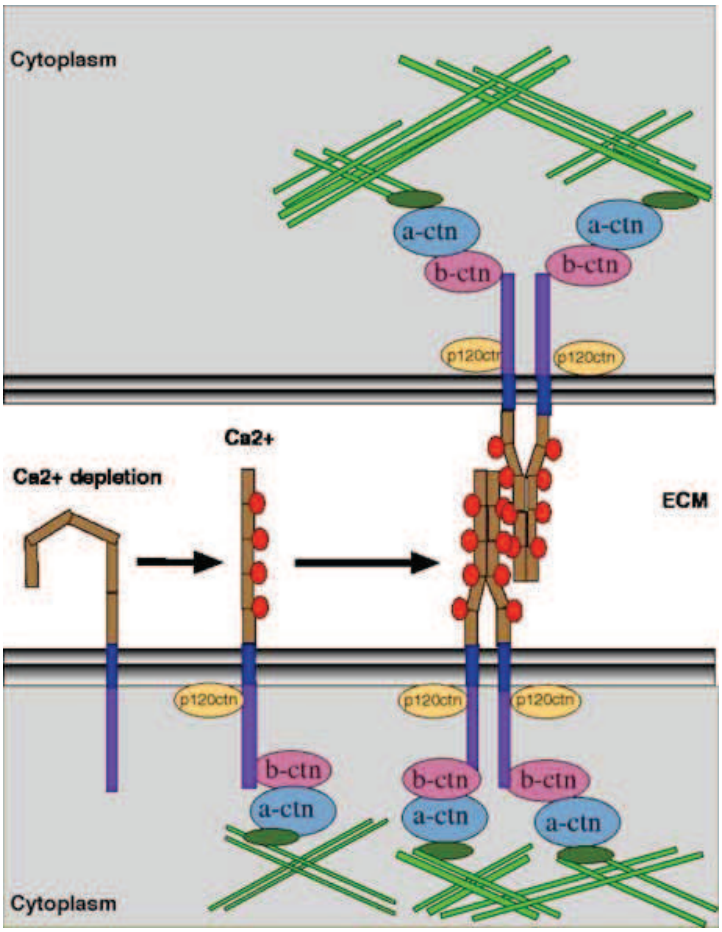

(Fig. 1.7) Type I classic Cadherins comprise five extracellular (EC) repeat domains (brown). Ca^{2+} (red) is bound in Ca^{2+}-binding pockets located at the interface of two ectodomains, thereby conferring rigidity to the protein, whereas Ca^{2+} depletion leads to destabilization of the protein at the cell surface. Classic Cadherins possess a single transmembrane domain (dark blue) and a cytoplasmic domain (purple), which is being bound to β-catenin in a complex with α-catenin. This adherens junction core complex furthermore interacts with the actin cytoskeleton (green) to establish stable cell-cell adhesion complexes. The small molecule p120 catenin (yellow) acts as signaling molecule through binding to the juxtamembrane domain of classic Cadherins.

Cell migration requires the rapid response to different extracellular signaling cues and the continuous relocation of adherens junctions. In recent years, data accumulated suggesting that Cadherins are recycled and transported back to the membrane via vesicular trafficking

(Le et al., 1999, Fujita et al., 2002, Lock and Stow, 2005, Jones et al., 2006, Sharma and Henderson, 2007). The recycling may be more economical for the cell, thus facilitating the rapid transport of Cadherins within the membrane. Different mechanisms have been proposed although mostly for the recycling of E-cadherin, which has been investigated in mouse cell lines. The recycling of Cadherins in zebrafish cells however still remains to be elucidated. E-cadherin recycling occurs mostly through the endosomal pathway and is in part mediated by Rab11 (Jones et al., 2006). Also the E3 ubiquitin ligase Hakai has been implicated in the recycling of E-cadherin. Evidence supports the idea that ubiquitination of membrane proteins does not necessarily lead to their degradation by proteasomes (Bonifacino and Weissman, 1998). Hakai has been shown to bind to E-cadherin in response to tyrosine phosphorylation of the E-cadherin complex. This promotes subsequent ubiquitination of E-cadherin through Hakai. The subsequent endocytotic/recycling mechanism of the E-cadherin complex remains however still poorly understood. A mechanism has been proposed whereby the E-cadherin/Hakai complex is targeted to clathrin-coated vesicles, although a mechanism is lacking that explains the recycling of E-cadherin back to the plasma membrane. However participation of members of the Rab family of small GTPases and their effectors seems to be involved (Pece and Gutkind, 2002). Recently, it has been further shown that the internalization and recycling of adherens junctions proteins can also be regulated by macropinocytosis in a β-catenin-dependent manner, through the activity of the GTPase Arf6 (Sharma and Henderson, 2007).

1.3.2 N-cadherin mediated neuronal migration in the CNS

The adhesion factor family of classic Cadherins is known to play important roles during many steps of central nervous system (CNS) development. For example in vertebrates they are critically involved in the formation of the neural tube (Bronner-Fraser et al., 1992) (Hong and Brewster, 2006), the morphogenesis and maintenance of brain compartments (Inoue et al., 2001) (Junghans et al., 2005), the regulation of neuronal migration (Taniguchi et al., 2006) (Kadowaki et al., 2007), the elongation and fasciculation of axons (Riehl et al., 1996) (Matsunaga et al., 1988) as well as in the establishment of dendritic spines and synapses (Walkenhorst et al., 2000) (Togashi et al., 2002).

Cadherin-2 (neural Cadherin, N-cadherin), a member of the family of type I classic Cadherins represents the most common classical Cadherin in the vertebrate CNS, being expressed broadly throughout the developing and mature brain. Inactivation of Cadherin-2

in mice results in severe cardiogenesis, somitogenesis and neural tube formation defects and leads to early prenatal death (Radice et al., 1997). The specific rescue of the cardiac phenotype however allows Cadherin-2 deficient mice to develop further. Similarly, zebrafish Cadherin-2 mutants survive early developmental defects, likely due to their independence of proper cardiac functions until late organogenesis stages (Sehnert and Stainier, 2002) (Hove et al., 2003). While the severely malformed neural tube in mutant mice and in zebrafish mutants unravels the importance of Cadherin-2 in nervous system development, the massive lack of structural integrity makes it difficult to assess its detailed functions during later stages of brain differentiation (Luo et al., 2001) (Lele et al., 2002) (Malicki et al., 2003) (Hong and Brewster, 2006). Conditional inactivation of Cadherin-2 in the CNS via application of function-interfering antibodies or dominant-negative variants have revealed crucial roles for this adhesion factor, such as during neural crest delamination, but these methods are dependent on the accessibility of the tissue of interest for direct manipulations (Bronner-Fraser et al., 1992) (Ganzler-Odenthal and Redies, 1998) (Nakagawa and Takeichi, 1998).

Classical studies have attributed Cadherin-2 function mostly to rigid cell-cell adhesion thus mediating tissue integrity as well as the segregation of different cell populations during nervous system development (Kostetskii et al., 2001), such as the upregulation of Cadherin-2 in neural ectoderm during neural tube formation. The expanded availability of conditional gene inactivation methods in mice, the development of electroporation technologies in chicken and mouse embryos as well as the identification of specific Cadherin-2 inhibitors, which allow to overcome early lethal phenotypes in Cadherin-2 mutants now allow for more precise investigations of Cadherin-2 function, also during later stages of brain differentiation. More recently, studies have implied the importance for the dynamic regulation of Cadherin-2-mediated adhesion in migratory cells. For example, disruption of Cadherin-2 function in chick neural crest cells reduced their migratory velocity (Kasemeier-Kulesa et al., 2006). Similarly, precerebellar neurons in the caudal hindbrain migrate at reduced speed, when Cadherin-2 function is impaired (Taniguchi et al., 2006). Thus the significance for a role of Cadherin-2 in regulating cellular and in particular neuronal migration is emerging.

Among few other cell types cerebellar granule cells serve as a paradigm to investigate the cellular and molecular mechanisms underlying neuronal migration. Studies on sorting cerebellar neuronal progenitors suggested a correlation between Cadherin-2 expression and granule cell migration in the mouse cerebellum (Wang et al., 2007). Moreover, application

of Cadherin-2 antagonizing peptides to cultured GPCs reduced their migration and affected their orientation on cerebellar slice cultures, arguing for a direct role of Cadherin-2 mediated adhesion not only in regulating GPC motility but also directionality (Wang et al., 2007). The underlying cellular mechanisms of how Cadherin-2 could affect migration remain however elusive.

Besides the attachment to neighboring cells, classic Cadherin-containing adherens junctions have been implicated in the regulation of cellular polarity, as their loss results in poorly polarized cellular morphologies and failures in polarized cell behavior (Hong and Brewster, 2006) (Kadowaki et al., 2007). Intriguingly, Cadherin-2 indirectly interacts with the microtubule cytoskeleton through the scaffolding protein IQGAP1, which has been recently shown to influence cerebellar GPC migration (D'Souza-Schorey, 2005) (Kholmanskikh et al., 2006). Cerebellar GPCs migrate via nucleokinesis, marked by the characteristic sequential forward transport of cellular organelles along microtubule fibers. Key component of this migratory mode is the centrosome, which positions in front of the nucleus to initiate and orchestrate directional nucleokinetic migration (Gregory et al., 1988) (Solecki et al., 2004) (Tsai and Gleeson, 2005) (Higginbotham and Gleeson, 2007). Currently, not much is known about the relation between Cadherin-2-mediated adhesion and centrosomal re-positioning during migration of cerebellar GPCs. Given that Cadherin-2 co-localizes together with IQGAP1 at the cell cortex in the leading edge of polarized cells (Sharma et al., 2006) and thus influences MT growth into the leading edge, Cadherin-2 is a good candidate to regulate centrosomal re-positioning and thus directional movement of GPCs in the zebrafish cerebellum.

1.3.3 PSA-NCAM and its regulation in the CNS by polysialyltransferase expression

The neural cell adhesion molecule (NCAM) plays multiple roles during the development of the central nervous system (CNS). It has been shown to be involved in regulating embryonic neurogenesis (Ponti et al., 2006), neuronal migration (Ono et al., 1994, Wang et al., 1994, Hu et al., 1996), axonal pathfinding (Tang et al., 1992, Daston et al., 1996, Cremer et al., 1997, Marx et al., 2001) as well as synaptogenesis (Seki and Rutishauser, 1998). Furthermore, in the mature brain NCAM has been implicated in regulating adult neurogenesis (Vutskits et al., 2006), neuronal migration (Cremer et al., 1994), survival of neural stem cell derived neuronal progenitors (Gascon et al., 2007a), synaptic plasticity and learning (Becker et al., 1996, Muller et al., 1996). During these processes the properties of

NCAM are modulated by the reversible attachment of polysialic acid (PSA) to its extracellular domain. For example, PSA weakens the adhesive properties of NCAM by steric hindrance and thus promotes migration of neuronal progenitors in the rostral migratory stream of the vertebrate olfactory system (Ono et al., 1994, Rutishauser and Landmesser, 1996, Rutishauser, 1998). In addition, PSA-bearing NCAM regulates the expression of the low-affinity neurotrophin receptor p75 and thereby promotes survival of migrating neuronal progenitors (Gascon et al., 2007a).

PSA attached to NCAM has also been involved in binding and presenting growth factors, thereby regulating long-term potentiation (Becker et al., 1996, Muller et al., 1996, Muller et al., 2000). Thus reversible attachment and removal of PSA is crucial for modulating NCAM-activity and thus CNS development and function. PSA-synthesis on NCAM is mediated by two polysialyltransferases, STX and PST, which specifically attach α2,8-linked sialic acid residues on NCAM. Both polysialyltransferases can act in a differential as well as synergistic manner (Angata et al., 1998, Nakayama et al., 1998, Ong et al., 1998, Angata and Fukuda, 2003, Angata et al., 2004, Weinhold et al., 2005). Based on their differential expression, PSA-synthesis during embryogenesis has mainly been attributed to STX, whereas adult PSA-synthesis in mammals is thought to be mediated preferentially by PST (Becker et al., 1996, Ganzler-Odenthal and Redies, 1998, Hildebrandt et al., 1998). The expression and function of these polysialyltransferases has attracted increasing biomedical interest for several reasons: 1) high PSA-levels as well as expression of STX can serve as diagnostic markers for neuroblastoma with poor prognostic outcome (Seidenfaden et al., 2003, Cheung et al., 2006), 2) polysialyltransferase activity promotes metastasis formation and thus represents an interesting pharmaceutical target and 3) the migration promoting activity of either STX- or PST-mediated PSA-synthesis in genetically engineered Schwann cells significantly supports regeneration by increasing axon outgrowth and Schwann-cell mediated remyelination (Lavdas et al., 2006, Zhang et al., 2007)

Due to their small size, transparency and extracorporal development, zebrafish embryos allow one to observe highly dynamic cell behaviors such as neuronal migration (Köster and Fraser, 2006), axon pathfinding (Fricke et al., 2001) or synaptogenesis (Niell et al., 2004, Mumm et al., 2006) directly *in vivo* and are thus well suited to address PSA-NCAM and polysialyltransferase function *in vivo*. Moreover, in contrast to mammals, adult zebrafish show significant levels of neurogenesis in almost all regions of the adult brain and have a pronounced capability to regenerate CNS-lesions (Becker et al., 2004, Zupanc et al., 2005, Adolf et al., 2006, Grandel et al., 2006, Zupanc and Zupanc, 2006). For example, stab

wounds in the adult zebrafish cerebellum are repaired within several days by an upregulation of neurogenesis in the cerebellar molecular layer, followed by directed migration of these neuronal progenitors towards the lesion site (Liu et al., 2004, Zupanc and Zupanc, 2006). Such adult neurogenesis, migration and regeneration in zebrafish could likely involve PSA-NCAM function, but research on PSA-NCAM in zebrafish has only been initiated recently.

In a recent study, polysialylation of NCAM in zebrafish embryos has been demonstrated to play a crucial role in axon fasciculation, but also commissural axonal guidance during midline crossing (Marx et al., 2001). Furthermore, the cloning and expression analysis of the highly conserved zebrafish STX- and PST-homologues was reported and both were shown to be capable of synthesizing PSA (Marx et al., 2007). Consistent with its predominant expression during embryogenesis antisense-morpholino injection revealed that STX is likely to be solely responsible for PSA-synthesis during zebrafish embryogenesis. This finding is in good agreement with mammalian embryonic STX- and PST-function (Eckhardt et al., 2000, Angata et al., 2004). Surprising is however that in the adult zebrafish brain only STX-expression was found to correlate with PSA synthesis, while PST-expression was either weak or absent, suggesting that STX may be the sole PSA-synthesizing enzyme relevant in the developing and adult CNS in zebrafish (Marx et al., 2007).

1.4 Aim of the study

1.4.1 Zebrafish as model organism

The zebrafish was chosen as a vertebrate model organism to study neuronal migration in the cerebellum as zebrafish combine many beneficial features of other vertebrates. Similar to xenopus, zebrafish embryos develop extracorporal. In addition zebrafish embryos are optically transparent. The expression of fluorescent fusion proteins in migrating neurons can therefore be readily observed by using *in vivo* time-lapse imaging methods. Zebrafish embryos can be further transiently manipulated during all stages of development by injection or electroporation of nucleic acids. Like in mice, zebrafish can be as well genetically modified and stable transgenic lines created. Due to their massive production with a female zebrafish laying up to 300 eggs at the time and their short generation interval of only 2 to 3 months, zebrafish analyses can be performed very rapidly.

Many large-scale screens have been carried out in zebrafish to discover new genes or

genes involved in a particular developmental process or disease. Due to teleost genome duplication, for almost every gene in humans exist several counterparts in zebrafish, thus making zebrafish well suitable for studying human genetic disorders. Based on these properties, zebrafish is an excellent and suitable model organism to study neuronal migration, developmental and disease mechanisms, which can be moreover applied to humans, as these mechanisms are largely conserved.

1.4.2 Analysis of Cadherin-2 during cerebellar granule cell progenitor migration in zebrafish

In the present study, the aim was to identify mechanisms that regulate the migration of cerebellar granule progenitor cells (GPCs). Although their migratory routes and terminal differentiation domains had been already studied in detail (Köster and Fraser, 2006, Volkmann et al., 2007), their mode of migration and the factors controlling their migratory behavior remained to be investigated. This analysis was based on the recent identification of the cerebellar granule cell population in the gata1:GFP transgenic line, which expresses green fluorescent protein (GFP) in migrating granule progenitor cells of the differentiating zebrafish cerebellum (Long et al., 1997, Volkmann et al., 2007).

A common feature of mammalian cerebellar development is the migration of GPCs along radial Bergmann glia fibers into the deep cerebellar cortex (Hager et al., 1995, Kawaji et al., 2004) but evidence indicated that GPC migration can also occur in a glia-independent manner towards the IGL. It remained elusive what migratory mode is used by GPCs in the zebrafish cerebellum. To analyze this, it was intended to examine the presence of glia cells by dye labeling and by performing expression studies using glial-specific markers at stages of prominent neuronal progenitor migration. In addition, it was aimed to examine the migration behavior of GFP-expressing cerebellar GPCs in the gata1:GFP transgenic line, using high-resolution *in vivo* time-lapse imaging to identify types of interactions for these cells during migration.

The migratory behavior of GPCs suggested the involvement of cell-cell adhesion molecules in mediating interactions between these cells. One candidate factor for the regulation of GPC adhesion was Cadherin-2. Disruption of Cadherin-2 function in zebrafish embryos results in severe cerebellar defects (Lele et al., 2002, Liu et al., 2004). While these malformations are likely to be attributed to more general neurulation defects, the mispositioning of neurons throughout the brain in homozygous larvae of the zebrafish

Cadherin-2 mutant *parachute* (*pac*) as well as the upregulation of Cadherin-2 expression during regeneration processes in the adult cerebellum further supported a role for zebrafish Cadherin-2 in regulating neuronal migration (Lele et al., 2002, Liu et al., 2004). To identify a role for Cadherin-2 in mediating cell-cell adhesion between migrating cerebellar GPCs, it was intended to perform time-lapse imaging on homozygous *pac* embryos crossed into the gata1:GFP transgenic line for investigation of the migratory behavior of cerebellar GFP-expressing GPCs. Furthermore, genetic mosaic analyses and the expression of a dominant-negative Cadherin-2 variant were expected to confirm a role for Cadherin-2 in the regulation of GPC migration.

Neuronal progenitors in the zebrafish cerebellum are likely to migrate via nucleokinesis (M. Distel & R.W. Köster, unpublished results). Such migrating cells polarize towards the direction of migration. Recent studies discovered that the centrosome is a key marker of neuronal polarity and nucleokinesis (Higginbotham and Gleeson, 2007). MTs emanating from the centrosome are anchored in the leading edge at sites of adherens junctions (Noritake et al., 2004, Noritake et al., 2005), thus reorganizing the MT network and preparing the cell for somal translocation (Higginbotham and Gleeson, 2007). In this study, the aim was to explore whether cerebellar GPCs in *pac* embryos exhibit migratory defects, and whether these defects are caused by a mispositioning of the centrosome due to the loss of Cadherin-2. For this analysis, a centrosomal marker Centrin2 fused to a fluorescent protein tdTomato was planned to be injected into wild type and *pac* gata1:GFP embryos to fluorescently label the centrosome in migrating GFP-expressing cerebellar GPCs, thus allowing the investigation of their migratory behavior by *in vivo* time-lapse microscopy.

A cell has to liberate itself from its initial position in order to migrate. One idea is that adherens junctions are thereby disassembled to reduce cell-cell adhesion. However, rather than mediating rigid cell-cell interactions, it was hypothesized that Cadherin-2-mediated adherens junctions dynamically reposition in migrating cerebellar progenitors, which had not been shown before. To investigate this, a non-functional variant of Cadherin-2 fused to the red fluorescent protein mCherry was planned to be constructed. This variant was intended to still locate at the cell surface but lacking adhesive properties. Being expressed in cerebellar GPCs of the gata1:GFP line, this variant could then serve as adhesion reporter for investigation of the dynamics of Cadherin-2 in migrating cerebellar GPCs by *in vivo* time-lapse imaging.

1.4.3 Investigation of the function of PSA-NCAM and polysialyltransferase expression during zebrafish cerebellar development and in the adult brain

PSA-NCAM has been shown to regulate axon fasciculation and guidance during zebrafish CNS development. Additional roles, such as in the regulation of neuronal migration during zebrafish embryogenesis remained however unclear. In order to address whether PSA-NCAM might be involved in the regulation of migrating cerebellar progenitor cells in zebrafish, the two known polysialyltransferases STX and PST, which add α2,8-linked polysialic acid residues on NCAM, first needed to be cloned. Their expression and that of PSA-NCAM in the cerebellum at stages of pronounced neuronal migration should be analyzed in order to identify a potential function in mediating neuronal migration in the differentiating cerebellum. It was conjectured that PSA-NCAM plays a role during adult neurogenesis and ongoing neuronal migration in the adult zebrafish cerebellum. To test this, STX and PST expression were further planned to be analyzed in the adult zebrafish brain by *in situ* hybridization, using tissue brain sections, and their expression compared to the expression patterns of PSA-NCAM in the cerebellum.

Addition of the long carbohydrate chains of polysialic acid on NCAM is widely believed to reduce cell-cell adhesion by steric hindrance. In contrast, the enzymatic ablation of polysialic acid in the differentiating zebrafish cerebellum after onset of migration was expected to increase cellular adhesive interactions and thus to slow down migration. To test this hypothesis, the enzyme EndoN should be injected into the hindbrain ventricle of zebrafish embryos, expressing GPF in migrating cerebellar progenitor cells. EndoN specifically degrades polysialic acid residues from NCAM. The specific ablation of PSA at stages of pronounced neuronal migration in the differentiating cerebellum was intended to reveal a function for PSA-NCAM in promoting migration of cerebellar neuronal progenitor cells.

2 Materials and Methods

2.1 Materials

2.1.1 Suppliers of chemicals and consumables

Standard chemicals were obtained from Sigma-Aldrich, Fluka, Merck, Roth GmbH, Serva Electrophoresis GmbH and Biozym. Enzymes and polymerases were obtained from MBI Fermentas, Invitrogen, Roche, Stratagene and New England Biolabs (NEB). Components used for western blotting were bought from Invitrogen, BioRad, BioTrace, Kodak and Amersham. Microinjection, electroporation and transplantation equipment was derived from Narishige, Harvard Apparatus and World Precision Instruments. Plastic ware was ordered from Roth GmbH, Eppendorf and Greiner. Glassware was obtained from Schott.

2.1.2 Equipment

2.1.2.1 Gel electrophoresis

Gel documentation system (Herolab)

Gel systems (Shelton Scientific, Amersham/ BD Biosciences)

N36 UV table (BENDA Laborgeräte)

Power supply Electron EC105 (Thermo)

2.1.2.2 Electroporation

BTX ECM810 electroporator (BTX)

Electrodes (World Precision Instruments)

Glass capillaries (Harvard Apparatus)

Microinjection needle holder (Narishige)

2.1.2.3 Histology

Microtome 355S for paraffin sections (MICROM)

Diamond knives (Diatom)

EG 1160 paraffin embedding station (Leica)

Vibratome HM650V (MICROM)

Microtome Reichert Ultracut E for electron microscopy (Leica Microsystems)

Hybridization oven Hybaid Shake'n'stack (Thermo)

Ultrastainer for electron microscopy sections (Leica Microsystems)

2.1.2.4 Microinjection and Transplantation

FemtoJet Express (Eppendorf)

Microinjection needle holder (Narishige)

Horizontal needle puller (Narishige)

Vertical needle puller (Narishige)

2.1.2.5 Microscopes

Stereomicroscope SV11 (Zeiss)

Fluorescent Stereomicroscope MZ 16FA equipped with filters for UV, GFP, FITC/Cy-3, YFP, Rhodamine and Texas Red (Leica)

Axioplan 2 (Zeiss)

Zeiss LSM510 equipped with Argon laser (451, 477, 488, 514nm) and Helium-Neon lasers (561, 594, 633nm)

Zeiss LSM510 Meta equipped with Argon laser (451, 477, 488, 514nm) and Helium-Neon lasers (543, 633nm)

EM10CR transmission electron microscope (Zeiss)

Light source KL2500 (Leica)

Light source KL1500 (Zeiss)

2.1.2.6 Microscope cameras

Axiocam HRc digital camera (Zeiss)

DFC 350 FX camera (Leica)

2.1.2.7 Microscope objectives (Zeiss)

C-Apochromat 40x/NA1.20 water immersion corrected

C-Apochromat 63x/NA1.20 water immersion corrected

Plan-NeoFluar 5x/NA0.15

Plan-NeoFluar 10x/NA0.3

Plan-NeoFluar 20x/NA0.5

Plan-NeoFluar 40x/NA0.75

2.1.2.8 Molecular biology and cell culture

BioPhotometer (Eppendorf)

BV SW 85 slide warmer (Adamas instrument)

Centrifuge 5415 D (Eppendorf)

Centrifuge Universal 32R (Hettich)

Cooling Centrifuge 5415 R (Eppendorf)

Centrifuge Evolution (Servall)

LC 6201S scale (Sartorius)

Microflow 2 cell culture work bench (Nunc)

Microwave oven 8020 (Privileg)

pH meter 720 (WTW inolab)

Polymax 1040 wave shaker (Heidolph instruments)

PTC-100 Thermocycler (MJ Research)

Rotator (LabInco BV)

Thermo Incubators (Heraeus Instruments)

Thermomixer comfort (Eppendorf)

Centrifuge Varifuge 3.0R (Heraeus Instruments)

Waterbath (Memmert, Isotemp 205, Lauda Ecoline E100)

2.1.2.9 Western blotting

Curix 60 developing machine (AGFA)

XCell SureLock gel chamber (Invitrogen)

XCell II blot module (Invitrogen)

2.1.2.10 Software

LSM510 version 4.0

GraphPad Prism 4 (GraphPad, Inc.)

NIH ImageJ 1.34s (Wayne Rasband, NIH)

2.1.3 Buffers and solutions

Standard buffers were prepared according to Sambrook and Fritsch, "Molecular Cloning", third edition, 2001, Cold Spring Harbor, New York. Embryo solutions and standard zebrafish protocols were derived from M. Westerfield, “THE ZEBRAFISH BOOK; A guide for the laboratory use of zebrafish (Danio rerio)”, 2000, Eugene, University of Oregon Press.

2.1.3.1 Fixation of embryos

<u>Fixation buffer</u>

1x PBS/ 0.1%Tween-20/ 4% paraformaldehyde (PFA)

2.1.3.2 Laemmli sample buffer (4x)

<u>Upper buffer</u>

0.5M Tris-HCl/ 0.4% SDS

4x sample buffer

Upper buffer	1.25ml
10% SDS	100μl
Glycerol	1ml
0.05% bromophenol blue	400μl
β-mercaptoethanol	550μl

2.1.3.3 In-situ hybridization (adopted from R.W. Köster and J. Wittbrodt)

Hyb-Mix

25ml 100% Formamide/ 12.5ml 20x SSC/ 150μl Heparin (50mg/ml)/ 250mg solid Torula RNA (Sigma)/ 500μl 10% Tween-20/ ad 50ml H_2O

Proteinase K buffer

1x PBST/ 10μg/ml Proteinase K (Roche)

Wash buffers

50% Formamide/ 2xSSC/ 0.1%Tween-20

2x SSCT

0.2x SSCT

Block and antibody solution

1xPBST/ 10% Normal Goat Serum

Staining buffer

0.1M Tris-HCl, pH9.5/ 0.1M NaCl/ 0.05M $MgCl_2$/ 0.1% Tween-20

Substrate solution

Staining buffer/ 3.75μl/ml BCIP (50mg/ml)/ 4.5μl/ml NBT (50mg/ml)

2.1.3.4 Dot blot

PI solution

100mM Tris-HCl, pH7.5/ 150mM NaCl

PII solution

1xPBS/ 0.1% TritonX-100

PIII solution

100mM Tris-HCl, pH9.5/ 100mM NaCl/ 50mM $MgCl_2$

Substrate solution

PIII solution/ 3.75μl/ml BCIP (50mg/ml)/ 4.5μl/ml NBT (50mg/ml)

2.1.3.5 Immunohistochemistry

Wash buffer

1xPBS/ 1% TritonX-100/ 1% DMSO

Blocking and antibody solution

Wash buffer/ 10% Normal goat serum

Staining solution

0.1M Tris-HCl, pH7.5/ 0.1% Tween-20

One DAB tablet (Sigma) was dissolved in 1ml staining solution, filtered (0.2μm) and 500μl of the concentrated solution was dissolved in 10ml staining solution.

DAB staining solution

0.05% DAB/ staining solution
0.3% H_2O_2 in water

2.1.3.6 Embryo solutions

Anesthesia

0.002g/ml Tricaine in 30% Danieau

Anti-Pigmentation agent

0.15mM 1-phenyl-2-thiourea (PTU)

2.1.3.7 Post-Fixative Solution

Dalton's osmium and potassium-bichromate buffer

1. Buffered solution: Adjust pH 7.2 of 5% Potassium dichromate solution ($K_2Cr_20_7$) with 2,5N KOH (100 ml solution with about 12 ml KOH)
2. Salt solution: 3,4 % NaCl
3. Osmium solution: 2% OsO_4 acid

Mix 1, 2 and 3 as follows:

1 part buffered solution (1),

1 part salt solution (2),

2 parts 2% OsO_4 acid (3)

2.1.3.8 Epon embedding resin

Mixture A

- 62 ml 2-Dodecenylsuccinic-acid anhydride (DDSA)
- 100 ml Glycid ether 100 (Epon-812)

Mixture B

- 89 ml Methyl nadic anhydride (MNA)
- 100 ml Glycid ether 100 (Epon 812)

Note: The mixtures are at least 6 months stable, if stored at -20 °C

Combine both mixtures A and B at a 1:1 ratio to 10 ml and add 0.15 ml of the hardener 2,4,6 –Tris (dimethylaminomethyl)-phenol (Merck, Germany), under stirring. This will yield medium hard blocks.

Note: Depending on the desired hardness of the blocks proportions of both mixtures can be varied, according to the Glycid ether 100 preparation manual from Serva Electrophoresis GmbH.

2.1.3.9 Toluidine Blue Working Solution

Toluidine blue stock solution	5 ml
1% Sodium chloride, pH 2.3	45 ml

2.1.4 Kits

Ambion mMESSAGE mMACHINE® SP6 Kit

DIG RNA-Labeling mix (Roche)

ECL Detection kit (Amersham)

Gel Extraction kit (Eppendorf)

GeneClean Turbo kit (Q-BIOgene)

Nanofectin kit (PAA)

NucleoBond PC100/500 kit (Macherey-Nagel)

QIAGEN Nucleotide Removal kit (QIAGEN)

QIAquick PCR Purification kit (QIAGEN)

RNeasy Mini kit (QIAGEN)

2.1.5 RNA *in situ* probes

	RNA probes	Received from
Adhesion	*cadherin-2*	Matthias Hammerschmidt
	ncam	Yoshihiro Yoshihara/ RIKEN
	pst *(st8siaIV)*	Cloned by RT-PCR from 54hpf zebrafish cDNA
	stx *(st8siaII)*	Cloned by RT-PCR from 54hpf zebrafish cDNA
Differentiation	*neurod*	Dr. Gong/ Vladimir Korzh
	gaba$_A$Rα6	Adult brain zebrafish cDNA
	vglut1	Shin-ichi Higashijima
Glia-specific	*fabp7a*	Stephen L. Johnson
	gfap	Cloned by RT-PCR from 31hpf zebrafish cDNA
	vimentin	Joan Cerda/ Harald Herrmann
Rhombic lip specification	*atonal1a*	Masahiko Hibi
Dorsal CNS	*wnt1*	Matthias Hammerschmidt

Table 1 RNA probes used for in-situ hybridization sorted according to their function in the zebrafish central nervous system.

2.1.6 Antibodies

2.1.6.1 Primary antibodies

Antibodies	dilution factor	Supplier
mouse anti-PSA	1:750	Monika Marx, Martin Bastmeyer
mouse anti-BLBP	1:1500	Nathaniel Heintz
rabbit-anti GFP	1:500	Torrey Pines Biolabs
mouse anti-Cdh2 MNCD2	1:1000	Developmental Studies Hybridoma Bank
rat anti-Tenascin	1:1000	GSF, Dr. Kremmer

2.1.6.2 Secondary antibodies

Antibodies	dilution factor	Supplier
anti-DIG-AP	1:2000	Roche
anti-mouse-Cy2	1:1000	Dianova
anti-rabbit-Cy5	1:1000	Dianova
anti-mouse-HRP	1:1500	Dianova
anti-rat-HRP	1:1500	Dianova

2.1.7 Enzyme injection

Purified endoneuraminidase (EndoN) was received from Rita Gerardy-Schahn and stored at -80°C.

2.1.8 Nucleic acid injection

2.1.8.1 Vectors

pCRIITOPO (Invitrogen)

pCS2+ (Rupp et al., 1994)

pBluescriptII-SK+/- (Stratagene)

2.1.8.2 Fluorescent proteins

Protein	Excitation	Emission	Intracellular localization	Special features
GFP	488	505	cytoplasm and nucleus	
LynGFP	488	505	plasma membrane	Lyn sequence derived from ten amino acid sequence in the N-terminal end of lyn kinase with conserved myristoylation and palmitoylation sequences (MGCIKSKRKD) (Teruel et al., 1999)
UncGFP	488	505	cytoplasm	unc76:EGFPpA fragment from XEX-76eGFP (Dynes and Ngai, 1998)
DEosFP	506/390	516/581	cytoplasm and nucleus	EosFP derived from stony coral *Lobophyllia hemprichii* converts from green (516nm) to red (581nm) emission upon UV-irradiation near 390nm (Wiedenmann et al., 2004)
TdTomato	554	581	cytoplasm and nucleus	tandem dimer Tomato (Shaner et al., 2004)
MCherry	587	610	cytoplasm and nucleus	monomeric Cherry (Shaner et al., 2004)

Table 2 Fluorescent proteins used for intravital labeling

2.1.8.3 Plasmid construction

p14xUASE1b:CdhΔN-mCherry-pA: The mCherry coding region (Shaner et al., 2004) was isolated via PCR amplification using primers AgeI-Cherry_up 5' ATA CCG GTC ATG GTG AGC AAG GGC 3' and Cherry-NotI_lo 5'GGG CGG CCG CTC TTA CTT GTA CAG C 3'. p14xUASE1b:Cdh2ΔN-EGFP (Jontes et al., 2004) was digested with AgeI and NotI and mCherry as AgeI/NotI fragment ligated into the vector, thereby replacing EGFP with mCherry.

pCS2+CdhΔN-mCherry-pA: CdhΔN-mCherry was isolated as Asp718/ NotI fragment and ligated as blunt fragment into StuI/ SnaBI sites of pCS2+.

pCS2+Cdh2ΔC-mCherry-pA: The cytoplasmic fusion of Cadherin-2 was generated by replacing aa Δ739-892 of the cytoplasmic domain with mCherry. For this, the coding region for Cdh2ΔC was PCR isolated from plasmid p14xUASE1b:Cdh2-EGFP (Jontes et al., 2004) using primers Ncad-up BamHI 5' ACG GGA TCC CCA CCA TGT ACC CCT CCG GAG GCG TGA TGC T 3' and Ncad-low SalI 5' TGT GTC GAC TTA TCC CGT CTC TTC ATC CAC ATC ACA AAC A 3'and as BamHI/ SalI fragment ligated into pCS2+, thereby generating a N–terminal fusion of Cdh2ΔC to mCherry.

pCS2+ Cdh2Δ2-4ΔC-mCherry-pA: Ectodomains 2-4 were deleted by digestion with BglII to remove bp 770 – 1845, followed by subsequent re-ligation of both vector arms.

pCS2+Cdh2ECΔ2-4ΔC-EosFP-pA: mCherry of vector pCS2+Cdh2Δ2-4ΔC-mCherry-pA was excised as SalI/ Asp718 fragment and dEosFP (Shaner et al., 2004) ligated into these sites.

pBSK+8xHSE:MCS-pA: The vector *pBSK+pA-GFP:8xHSE:MCSpA* (Bajoghli et al., 2004) allows for bi-directional activation of GFP and a target gene by the inserted 8 repeated heatshock-binding elements that activate bi-directional gene expression upon heat stress. To generate a unidirectional activator cassette, the GFP was excised by SalI restriction, followed by subsequent re-ligation of both vector arms.

pBSK+8xHSE:Cdh2ΔN-mCherry-pA: Cdh2ΔN-mCherry-pA was excised from pCS2+Cdh2ΔN-mCherry-pA as StuI/ NotI fragment. The vector pBSK+ 8xHSE:MCSpA was subsequently opened using EcoRV and NotI restriction sites and Cdh2ΔN-mCherry-pA was ligated as blunt/ NotI fragment into this vector.

pBSK+8xHSE:Cdh2ECΔ2-4ΔC-mCherry-pA: Cdh2ECΔ2-4ΔC-mCherry-pA was excised as BamHI/ NotI fragment and ligated into the same sites of pBSK+ 8xHSE:MCS.

pBSK+8xHSE:Cdh2ECΔ2-4ΔC-EosFP-pA: Cdh2ECΔ2-4ΔC-EosFP-pA was excised from pCS2+ as Asp718/blunt and BamHI fragment. pBSK+ 8xHSEMCS-pA was opened using NotI/ blunt and BamHI restriction sites, thereby removing the polyA sequence. Cdh2ECΔ2-4ΔC-EosFP-pA was subsequently ligated into the vector as BamHI/ blunt-fragment.

pBSK-1xUASE1b:Centrin2-tdTomato: The Centrin2tdTomato fragment was excised from pCS2+ using HindIII/ blunt and EcoRI and ligated into the EcoRI/ SnaBI sites of pBSK-1xUASE1b (M. Distel & R.W. Köster, unpublished).

All final constructs were sequenced using either of the following services: GSF Sequencing service, Sequiserve and MWG.

2.1.8.4 Plasmids used for RNA and DNA injections

Plasmid name	RNA injection	DNA injection	Reference
pCS2+Cdh2-pA	X		M.Hammerschmidt
pCS2+Cdh2ΔN-mCherry-pA	X		see 2.1.8.3 for plasmid construction
pCS2+Cdh2Δ2-4ΔC-mCherry-pA	X	X	see 2.1.8.3 for plasmid construction
pCDNA3 lynGFP-pA	X		Jack Horne
pCS2+KalTA4-pA		X	R.W. Köster, unpublished
pBSK-tub-GVP-Uunc-pA		X	(Köster and Fraser, 2001)
14xUASE1b:Cdh2-EGFP-pA		X	(Jontes et al., 2004)
pBSK-1xUASE1b:centrin2-tdTomato-pA		X	M. Distel, unpublished
pBSK+8xHSE:Cdh2ΔN-mCherry-pA		X	see 2.1.8.3 for plasmid construction
pBSK+8xHSE:Cdh2Δ2-4ΔC-mCherry-pA		X	see 2.1.8.3 for plasmid construction
pBSK+8xHSE:Cdh2Δ2-4ΔC-dEosFP-pA		X	see 2.1.8.3 for plasmid construction

Table 3 Plasmids used for RNA and DNA injections into zebrafish embryos

2.1.9 Primers used for amplification of specific zebrafish cDNAs by RT-PCR

Gene	NCB accession number	Isolation from	Primer name	Primer sequence
Gfap	BC091942	Adult brain	gfap up	5' CGC GAG GTG GAC AGG GTG ATG GGG CTG 3'
			gfap lo	5' CCA GGG CCA GTT TGA CAT TGA GCA GAT 3'
Vimentin	BC091942	Adult brain	vimentin up	5' GAG CTT CAA CAA TAA CCC GCA AAC 3'
			vimentin lo	5' TGG ATC TTC AGT GCC TCG GGT TCA 3'
centrin2	Cloned by M. Distel, unpublished	Adult brain	centrin2 up	5'TTG GAT CCA TGG CGT CCG GCT TCA GGA A3
			centrin lo	5'TTT CTA GAT CAG TAC AGA TTG GTT TTC TTC3'
stx (st8siaII)	AY055462	54hpf	stx up	5' TAC TCG AGA TGT CTT TTG AAT TCC GAA TAC TGA 3
			stx lo	5' TAT CTA GAT CAT GTA GGA GGT TTG CAT GGT CCC 3'
pst (st8siaIV)	DQ779599	54hpf	pst up	5' TCT CGA GAT GCG GCT TTC ACG 3'
			pst lo	5' TAG ATT AAG TTG ATG TGC ATT TAG ATG TC 3'
cadherin-2	AF418565	24hpf	Ncad a long up	5' ATC AGT GCC AGA GAG AGA CGG AGG AAC GA 3'
			Ncad d long down	5' GCG GGA TTG GTT GTA CTC GTT CTC GGT GA 3'

Table 4 Oligonucleotides for zebrafish cDNA amplification.

2.1.10 Fluorescent dyes

Bodipy Ceramide (Fl C5) (Molecular Probes)

DiI (Invitrogen)

Rhodamine-dextran 10,000MW (Molecular Probes)

TOPRO (Molecular Probes)

Acridine Orange

2.1.11 Bacteria strains for plasmid amplification

DH5α

Top10 (Invitrogen TA-cloning kit)

XL1Blue

2.1.12 Cell culture

Zebrafish PAC2 embryonic fibroblast cells (Chen et al., 2002)

2.1.13 Fish strains

Wild type AB strain (ZFIN)

Wild type brass strain (EkkWill Waterlife Resources, Gibbonston, FLorida)

*pac*R2.10 mutant strain (Lele et al., 2001)

gata-1:GFP (strain781) (Long et al., 1997)

2.2 Methods

2.2.1 Molecular biology

2.2.1.1 Transformation of plasmids into bacteria

For transformation of DNA into bacterial cells, -80°C frozen cells were thawed on ice for 10 min and 100ng-1μg of plasmid DNA added to 50μl bacteria. The mixture was incubated 30 min on ice, while swirling the tube every 15 min to allow for binding of plasmids to bacterial wall. The bacteria were then heatshocked at 42°C for 1 min to induce plasmid DNA uptake by bacteria and immediately placed on ice, allowing to cool down the cells for 1 min. The bacteria were transferred into 500μl Luria Bertani (LB) medium and incubated by shaking with 250rpm for 30 min - 1h at 37°C to allow transformed bacteria to express the antibiotic resistance gene. The cultures were subsequently plated onto 20ml LB agar in Petri dishes, containing antibiotics according to the plasmid resistance and incubated 12-16h to allow bacteria colonies to grow.

2.2.1.2 Mini preparations for plasmid DNA isolation from bacteria

For preparations of small amounts of purified plasmid DNA for analytical purposes, 3ml of plasmid-containing bacteria in LB medium were incubated with respective antibiotics in 37°C, shaking at 250rpm overnight. Initial steps of plasmid isolation were performed using Macherey-Nagel buffers (see 2.1.4). First, bacterial cultures were transferred into 2ml tubes and pelleted by centrifugation at 10,000rpm for 10 min. The supernatant was decanted and pellets were re-suspended in 200μl S1 (RNase-containing buffer). After complete re-suspension of the pellet, 200μl S2 lysis buffer was added and incubated for 5 min to allow bacterial walls to be broken down, thus releasing its plasmid DNA content. Subsequently, 300μl of S3 buffer was added to precipitate the bacteria debris. The debris was removed by centrifugation and the supernatant transferred into a fresh 2ml tube. Typically, the centrifugation step was repeated to remove remaining protein. Then 500μl Isopropanol was added to precipitate the DNA, followed by centrifugation at 4°C and 13,000rpm for 30 min. The supernatant was decanted and the pellet washed with 70% ethanol, followed by centrifugation at 4°C and 13,00rpm for 20 min. The DNA was finally air-dried and re-suspended in 30μl ddH_2O.

2.2.1.3 Maxi preparations for plasmid DNA isolation

For preparations of large amounts of purified plasmid DNA, 200ml of plasmid-containing XL1Blue, DH5α or Top10 bacteria in LB medium were incubated with respective antibiotics, either 100μg/ml of Ampicillin or 50μg/ml Kanamycin at 37°C, shaking with 250rpm, overnight. Isolation of plasmids from bacteria cultures was performed using the NucleoBond PC100/500 kit (Macherey-Nagel) according to the manufacturer's protocol.

2.2.1.4 DNA gel electrophoresis

Agarose gel electrophoresis takes advantage of the negative charge of DNA and thus through the application of a current DNA fragments can be separated according to their molecular weight. For gel electrophoresis, DNA (100-200ng for analytical purposes) or 1-10μg (for preparative purposes) was diluted 5:1 in 6x loading dye and loaded together with a 1kb standard DNA ladder (MBI Fermentas) onto 0.8% - 2% agarose gels. The gels were run at 100-140V in 1x TAE buffer using Amersham and Shelton Scientific gel chamber systems. Following electrophoresis, the gels were incubated in 1xTAE buffer containing 1μg/ml

ethidium bromide for 30 min. DNA fragments containing intercalated ethidium bromide were visualized by UV light at 254 nm and documented on the Herolab gel system.

2.2.1.5 DNA gel extraction

DNA fragments of desired size were excised from agarose gels and transferred into a fresh 2ml tube. The slices were extracted according to the manufacturer's protocol using the Gel Extraction kit (Eppendorf).

2.2.1.6 Purification of DNA fragments from restriction digests or PCR reactions using kits

For purification of digested DNA fragments or PCR products either the Nucleotide Removal kit or QIAquick PCR Purification kit (QIAGEN) was used, according to the manufacturer's protocol.

2.2.1.7 DNA precipitation

Alternatively, DNA fragments were purified by precipitation as follows: 1/2 volume 5M NH_4OAc and 3 volumes 100% ethanol were added to the DNA sample and mixed by pipetting. The reactions were incubated overnight at -20°C for precipitation. The samples were pelleted by centrifugation, the supernatant decanted and the pellet washed with 500μl 70% ethanol. Following 20 min of centrifugation at 4°C, the DNA was air-dried at 37°C for 20 min. The pellet was re-suspended in ddH_2O.

2.2.1.8 DNA restriction digest

For analytical digestions, typically 1μg plasmid DNA was digested with 1-5U of restriction enzyme. For preparative purposes, typically 10μg plasmid DNA was used. Buffer conditions were adopted from the manufacturer's protocol. The reactions were incubated for at least 1h at 37 °C if 1μg DNA was used, and for a minimum of 4h when 10-15μg was digested. Success of the restriction digests was checked by gel electrophoresis using 0.5μl of digested DNA.

2.2.1.9 DNA ligation

T4 DNA ligase catalyzes the ligation of DNA fragments. For ligation reactions typically 50ng of vector DNA was mixed with 3x the molar amount of insert DNA and 2.5U T4 DNA ligase in a total volume of 15μl. The reactions were incubated at 16 °C overnight. Alternatively incubation was performed at room temperature between 30 min - 4h. For TA-cloning typically 4μl PCR product was ligated into 1μl of pCRIITOPO vector, according to the manufacturer's manual.

2.2.1.10 Calculation of nucleic acid concentrations

Nucleic acid samples were diluted 1:100 in ddH_2O before determining the absorbance at 260nm (A260nm) using the BioPhotometer (Eppendorf). The absorbance of one unit single-stranded RNA at 260nm corresponds to 40μg/ml (A260 = 1 unit = 40μg/ml) and the absorbance of one unit double-stranded DNA at 260nm corresponds to 50μg/ml (A260 = 1 unit = 50μg/ml). Therefore, the RNA and DNA concentrations were calculated by using the formula A260 x dilution factor (100) x 40 (RNA)/ or x 50 (DNA) = μg/ml.

2.2.1.11 Polymerase chain reaction (PCR)

For amplification of DNA fragments from isolated cDNA or plasmid DNA the following reaction was prepared:

50ng	DNA template
5μl	10x PCR buffer
5-7μl	2mM dNTP mix (Fermentas)
5μl	25mM $MgCl_2$ (Fermentas)
2μl	each primer (50pmol/μl)
1μl	DNA-Polymerase
Ad 50μl	H_2O

The PCR conditions were chosen according to the primers and template lengths used. In general, DNA was first denatured at 94°C. The temperature for primer annealing is dependent on the melting temperature of the oligonucleotides and was therefore determined empirically. Usually 45 sec were sufficient for annealing. Elongation was performed with DNA-Polymerase at 72°C for 1 min/kb fragment length. Typically Taq Polymerase (MBI

Fermentas) was used for PCR reactions that did not depend on the proof reading capacity of the polymerase. For cloning procedures, where point mutations were not desired, polymerases with proof-reading activity such as Pfu Ultra II, Pfu Turbo and EasyA (Stratagene) were used. All PCR reactions were performed using the MJ Research Thermocycler PTC-100.

2.2.1.12 Removal of 5' overhangs

To fill in 5' overhangs produced by restriction digestion of plasmid DNA with 5' cutting enzymes the following reaction mixture was prepared:

Restriction digest (not purified)
1x Klenow buffer (Roche)
20μM each dNTP
1U Klenow DNA polymerase (Roche)

The reaction was incubated 15 min – 30 min at 37°C and purified using either DNA precipitation or the QIAGEN Nucleotide Removal kit.

2.2.1.13 Dephosphorylation of vector DNA

To prevent re-ligation of vector arms after blunt-end or single enzyme digestions, the DNA was typically dephosphorylated using calf intestinal phosphatase (CIP). First, the reaction was purified to remove salts, using the QIAGEN Nucleotide Removal kit. Then, dephosphorylation was performed as follows:

linearized DNA
1x Phosphate buffer (Roche)
1-2μl CIP (Roche)
Ad ddH_2O

The reaction was incubated for 30 – 45 min at 37°C and the reaction purified either by DNA precipitation or using the QIAGEN Nucleotide Removal kit.

2.2.1.14 cDNA preparation from zebrafish by RT-PCR

For generation of zebrafish embryonic or adult brain cDNA, about 100 embryos or 10 adult brains were pooled and transferred into a 15ml Falcon tube. 5ml TRIzol (Invitrogen) containing water-saturated phenol was added and the tissue homogenized. 2.5ml of chloroform ($CHCl_3$) was added to separate phases by vigorously mixing the tube for 15 sec. This solution was incubated at room temperature for 3 min, followed by centrifugation for 30 min at 5,000rpm at 4°C to separate the aqueous phase, containing the RNA. The RNA was transferred into fresh 2ml tubes for precipitation with 1ml Isopropanol. Samples were incubated 10 min at room temperature and then pelleted by centrifugation at 10,000rpm for 20 min. The supernatant was discarded and the pellet washed with 75% Ethanol, followed by centrifugation at 10,000rpm for 20 min. The pellet was air dried for 5 min at 37°C and dissolved in RNase-free water. Genomic DNA was removed by digestion with 1μl DNase at 37°C. The reaction was heat-inactivated at 65°C for 10 min and subsequently purified using the QIAGEN RNeasy Mini kit. The isolated DNA-free RNA was stored at -80°C.

Reverse transcription of whole embryo and adult brain RNA was performed using the following conditions:

2μl random hexamer primers (Promega) together with 5μl freshly isolated RNA were denatured by incubation at 70°C for 5 minutes. Then, a mixture containing

10μl	5x SSII reverse transcriptase buffer (Invitrogen)
5μl	DTT (Fermentas)
1μl	RNase-Inhibitor (RNasin) (Promega)
0.2μl	100mM dNTP mix
1μl	SSII superscript enzyme (Invitrogen)
Ad 50μl ddH_2O	

was added, and the reaction incubated at 42°C for 60 – 90 min to reverse transcribe cDNA from isolated RNA. The enzymatic reaction was inactivated by incubation at 70°C for 10 minutes. Subsequently, the cDNA was purified using the DNA precipitation method (see 2.2.1.7). The amplified cDNA was stored at -20°C or immediately used for PCR amplification (2.2.1.11).

2.2.1.15 Transient gene expression using heatshock induction

For transient control of gene expression a heatshock-inducible system was used (Bajoghli et al., 2004). This system is based on stress-inducibility of endogenous heatshock proteins, by binding of heatshock factors (HSF) to the heatshock response elements in the promoter of heatshock proteins upon heat stress, thus activating transcription. These heatshock response elements contain several short binding sequences, which have been optimized to allow for temporary transcriptional activation of genes of interest, either transiently injected or stably integrated into the zebrafish genome. The heatshock promoter used in this study consists of eight multimerized heat shock elements (HSE) with the idealized sequence AGAACGTTCTAGAAC, being alternately separated by 3 and 6 bp, followed by a CMV minimal promoter on either side. For heatshock-dependent gene transcription, the genes of interest were cloned behind the HSE promoter (see 2.1.8.3) and heatshock-inducible plasmid DNA was injected into 1-cell stage zebrafish embryos (see 2.2.4.5). To activate transcription at 48hpf, the embryos were transferred into 4-well plastic dishes and covered with 30% Danieau/PTU medium. The dishes were sealed with Parafilm and placed into a 40°C pre-heated water bath for 1h. The embryos were subsequently transferred to a 28°C incubator for a minimum of 2h until protein expression was observed. To maximize gene expression this heatshock procedure was repeated once at 51hpf.

2.2.2 Protein techniques

2.2.2.1 SDS-Polyacrylamide gel electrophoresis (PAGE)

For analysis of Cadherin-2 expression, embryonic protein extracts were prepared from pooled embryos of each wild type, *pac*R2.10 and *pac*-/-R. Following addition of protease inhibitor, samples were dissolved in 1x SDS sample buffer and denatured at 94°C for 5min. 10μl sample and 2μl SeeBlue pre-stained protein standard (Invitrogen) for estimation of protein sizes were loaded onto 10% tris-glycine acrylamide pre-cast gels (Invitrogen) and run at 100-140V using the XCell SureLock system (Invitrogen). After completion, gels were prepared for western blotting.

2.2.2.2 Western blotting

Following SDS-PAGE, gels were blotted onto PVDF membrane (BioTrace) using the XCell II blotting module according to the manufacturer's manual (Invitrogen). To check

transfer efficiency, blotted gels were subsequently stained with Coomassie Blue staining solution (BioRad) for 1h and de-stained with 7 % acetic acid. To detect blotted protein samples, PVDF membranes were blocked with 5% skim milk in 1xTBS/ 0.1%Tween-20 (TBST) for 1h and probed with primary mouse anti-cdh2 MNCD2 antibody (1:1000) at 4°C overnight (see 2.1.6). Following overnight incubation the membrane was washed 5 times in 5% skim milk/TBST for 15min each. The membrane was subsequently probed with the secondary antibody anti-mouse IgG conjugated to horseradish peroxidase (HRP) at a 1:1500 dilution in 5% skim milk/TBST, at room temperature for 1h, rocking. After 5 repeated washes in 5% skim milk/TBST for 15min each, the blotted membrane was developed using the ECL Detection system (Amersham, BD Biosciences), according to the manufacturer's protocol. Kodak x-ray film was used for development in the AGFA Curix 60 developing machine. The membranes were stripped and processed for control antibody detection using rat anti-Tenascin (1:1000) (see 2.1.6 for antibodies) and secondary anti-rat-HRP (1:1500, Dianova) antibodies.

2.2.3 Cell culture

2.2.3.1 Maintenance of zebrafish PAC2 fibroblast cells

PAC2 zebrafish fibroblast cells (Chen et al., 2002) were maintained at 30°C in L-15 medium (Leibovitz's, PAA), supplemented with 6ml non-essential amino acids, 6ml penicillin/streptavidin and 75ml fetal bovine serum. To prepare cells for transfection PAC2 cells were washed in 10ml cold Dulbecco's 1x PBS and lysed with 1ml Trypsin-EDTA. Subsequently, 9ml L-15 medium was added and cells were transferred into a 50ml Falcon tube for centrifugation at 2,500rpm for 2min. The supernatant was decanted and cells re-suspended in 5ml L-15 medium. The cells were then quantified using a Double Neubauer counting chamber and about $1x10^5$ cells were plated per well using 6-well plastic dishes, containing ethanol-purified glass cover slips. Alternatively, the glass cover slips were pre-treated with 32% HCl to enhance the adherens of cells. PAC2 cells were allowed to reach 70% confluence before transfection.

2.2.3.2 Nanofectin transfection of PAC2 fibroblasts

Transfection was performed according to the Nanofectin kit protocol (PAA). Briefly, for one transfection reaction 5μg DNA (pCS2+ Cdh2ΔEC2-4ΔC-EosFP, see 2.1.8.3 for plasmid

construction) was diluted in 250μl diluent. In a second tube, 16μl Nanofectin was diluted in 250μl diluent. The Nanofectin solution was subsequently added to the DNA solution and the reaction mixed by vortexing. The reaction was incubated for 30 min at room temperature to allow for the formation of liposomes and 500μl of this mix was subsequently added to one well of a 6-well dish containing adhering PAC2 cells. The dish was swirled for mixing and then incubated at 30°C for at least 12h. Before imaging cells were washed with fresh L-15 medium to remove Nanofectin. The cells were kept in darkness to prevent photo-conversion of dEosFP.

2.2.4 Zebrafish manipulations

2.2.4.1 Fish maintenance and strains used

Raising, spawning, and maintaining of zebrafish lines was performed as described (Kimmel et al., 1995, Westerfield, 1995). Wild type fish of the brass strain were used for microinjections, embryonic *in situ* hybridizations and immunohistochemistry. Wild type fish of the AB strain were used for *in situ* hybridization on adult paraffin sections. For analysis of Cadherin-2, heterozygous mutant fish of the *parachute* (*pac*R2.10) strain (Lele et al., 2002) were crossed into homozygous fish of the stable transgenic gata-1:GFP line (strain 781) (Long et al., 1997). For transplantation experiments, embryos of the brass strain, the gata1:GFP transgenic line and the *pac*R-/- gata1:GFP mutant transgenics were used. Embryos of the brass strain were used for single cell electroporation.

Terminology: Embryos resulting from crosses of *pac*R2.10 and gata-1:GFP transgenic fish are named *pac*R2.10 gata1:GFP in this study; rescued mutant embryos of *pac*R2.10 gata1:GFP are named *pac*-/-R gata1:GFP.

2.2.4.2 Tail clip genotyping of *parachute* R2.10 embryos

For RNA isolation, a small portion of embryonic tail was removed from anesthetized embryos at 24hpf using a razor blade, and transferred into 2ml tubes. The tails were quick-frozen using liquid nitrogen and stored at –80°C. To prepare RNA from single tails, the tissue was thawed to room temperature and dissolved in 50μl TRIzol by pipetting. Another 350μl TRIzol was added, and after mixing 200μl Chloroform was added. The solution was vigorously shaken for 15 sec and incubated at room temperature for 3 min before centrifugation at 10,000rpm and 4°C for 15min. The aqueous phase was transferred into a

fresh 1.5ml tube and 50μl Glycogen (5mg/ml Ambion) as carrier was added, before the addition of 200μl Isopropanol. Samples were incubated 10 min at room temperature for precipitation and then pelleted by centrifugation at 10,000rpm for 30 min. The supernatant was discarded and the pellet washed with 75% Ethanol, followed by centrifugation at 10,000rpm for 20 min. The pellet was air dried for 5 min at 37°C and dissolved in 22μl RNase-free water. To digest genomic DNA, the re-suspended sample was incubated with 1μl DNase at 37°C for 15 min and subsequently the DNase was inactivated at 65°C for 10 min. 11μl of this solution was immediately used for RT-PCR:

11μl of non-purified isolated RNA and 1μl random hexamer primers were mixed by pipetting at room temperature without centrifugation and then pre-annealed by incubation at 70°C for 5 min. The reaction was incubated at 25°C for 5 min to cool the reaction down and to allow the primers to anneal. Meanwhile, the reverse transcription mixture was prepared as follows:

10μl	5x SSII reverse transcriptase buffer
5μl	DTT
1μl	RNase-Inhibitor
0.2μl	100mM dNTP mix
1μl	SSII superscript enzyme
Ad 50μl	ddH_2O

This mixture was added to the denatured and pre-annealed RNA and cDNA synthesized as follows:

42°C - 60 minutes for extension
70°C - 10 minutes for inactivation of the reverse transcriptase
8°C for storage in PCR cycler

The synthesized cDNA was thereafter stored at -20°C for long-term storage or immediately used for PCR.

To subsequently PCR amplify *cadherin-2* transcripts, the following PCR reaction was prepared:

11μl	template tail cDNA
10μl	5x Taq buffer
0.2μl	100mM dNTP mix
5μl	25mM $MgCl_2$
1μl	forward primer Ncad a long (50pmol/μl) (Lele et al., 2002)
1μl	reverse primer Ncad d long (50pmol/μl) (Lele et al., 2002)
0.5μl	Taq Polymerase (Fermentas)
Ad 50μl ddH_2O	

The PCR conditions were further set as follows and splice transcripts amplified.

Step	Cycles	Temperature	Time
1	1	94°C	5 minutes
2	2-39	94°C	30 seconds
	2-39	47°C	45 seconds
	2-39	72°C	1 minute
3	40	72°C	10 minutes
4	41	8°C	storage

Table 5 PCR conditions for genotyping of wild type and *pac*R2.10 alleles

PCR products were separated according to their different sizes using 15% TBE gels (Invitrogen) at 100V for 30 min in 1xTBE buffer. The gels were subsequently stained in 1xTBE buffer containing 1μg/ml ethidium bromide and visualized by UV light using the Herolab gel documentation system.

2.2.4.3 Synthesis of capped mRNA for microinjection into zebrafish embryos

For capped mRNA synthesis from pCS2+ plasmids, typically 10μg DNA was digested with 3μl NotI for linearization at 37°C for 2h. The digest was checked for completion by gel electrophoresis on a 1% agarose gel and the transcription template subsequently purified

using the QIAGEN Nucleotide Removal kit. *In vitro* synthesis of capped mRNA was performed using the Ambion mMESSAGE mMACHINE® SP6 Kit according to the manufacturer's protocol. Briefly, 5μl of linearized DNA template, 10μl 2x NTP/CAP, 2μl 10x reaction buffer, 1μl nuclease free water and 2μl Enzyme Mix was mixed. The reaction was incubated at 37°C for 4h to allow for synthesis of capped mRNA, after which the DNA template was digested by treatment with 1μl DNase (Roche) for 15 min. Capped mRNA was subsequently purified using the QIAGEN RNeasy Mini kit and dissolved in 25μl RNase-free water. The efficiency of RNA synthesis was checked on a 1% agarose gel. For this, 1μl capped mRNA was diluted in 4μl of 5x RNA loading dye (Ambion) and run at 100V for 30 minutes. The concentration of the mRNA was further determined using the BioPhotometer (see 2.2.1.10)

2.2.4.4 Preparation of plasmid DNA for microinjection into zebrafish embryos

For microinjections, purified plasmid DNA was re-purified using the GeneClean Turbo kit (Q-BIOgene) according to the manual. Briefly, 15μg DNA was diluted with 5 volumes of TurboSalt solution and allowed to bind to the column during 5 sec of centrifugation at 10,000rpm. The flow-through was decanted and 500μl wash buffer applied. The wash buffer was removed by centrifugation at 10,000rpm for 5 sec and a dry spin was performed for 5 min. The DNA was eluted from the column with 30μl ddH_2O for 1 min at room temperature and subsequently centrifuged at 10,000rpm for 1 min. Centrifugation of the eluted DNA was repeated at 10,000rpm for 6 min to pellet column debris. The DNA concentration was subsequently determined photometrically (see 2.2.1.10).

2.2.4.5 Microinjection into zebrafish embryos

First, 1mm OD filamentous glass microcapillaries (Harvard Apparatus) were pulled to generate tips of 1-3μm diameters, using a vertical needle puller (Narishige). For vital injections, about 1-2nl of 50ng/μl (50-100pg/embryo) purified plasmid DNA (see 2.2.4.4) in ddH_2O containing 0.02%PhenolRed was injected into 1-cell stage embryos. For injections of capped messenger RNA 50–100ng/μl (50-200pg/embryo) of mRNA (see 2.2.4.3) in ddH_2O containing 0.02%PhenolRed was injected into 1 to 64-cell blastula stage embryos. For injection of KalTA4/UAS DNA construct, injection concentrations were lowered to a final

DNA concentration of 50ng/μl. For this, about 15-30pg of activator DNA was co-injected with 25-50pg of effector DNA.

2.2.4.6 Temporal rescue of *parachute* R2.10

To rescue the neurulation defects in *pac*R2.10 embryos, caused by a lack of functional Cadherin-2, about 1.5nl of 35ng/μl (approx. 70pg) wild type *cadherin-2* mRNA was injected into early 1-cell stage embryos (see 2.2.4.5). Embryos being rescued for their neurulation defects were generally identified between 24 and 36hpf and judged based on their morphological appearance (see Fig. 3.7C, compare to A and B). For example, *pac*-/-R embryos were identified as mutants if both cerebellar primordia were abutting each other at the dorsal midline indicating their proper neurulation. In addition, mutant embryos having wild type appearing cerebelli often showed an inflation of the hindbrain ventricle, containing loose cell aggregates, which is typical of the *parachute* mutant phenotype.

2.2.4.7 Genetic mosaic analysis by single cell transplantation

Donor embryos were injected with rhodamine-dextran 10,000MW (Molecular Probes) at the 1-cell stage. Transplantation needles without filament at 1mm OD were pulled using a horizontal needle puller (Narishige). Embryos were dechorionated at the 4 to 16-cell stage, using Pronase (Roche) and placed dorsal side up into 1.5% agarose/ 30% Danieau molds. The embryos were kept in 30% Danieau/ 1% pen/strep during all steps. For transplantations of wild type donor gata1:GFP into wild type acceptor or *pac*-/-R gata1:GFP donor into wild type acceptor embryos, a small group of sphere-stage cells was transferred between the animal poles of both embryos. Embryo pairs were screened at 24hpf to identify homozygous *pac*R2.10 donor and the respective acceptor embryos. The transplantation efficiency was furthermore monitored by incorporation of rhodamine-labeled cells into acceptor embryos.

2.2.4.8 Electroporation

Electroporation allows for the delivery of charged molecules, such as nucleic acids into cells. Application of a brief high voltage pulse from the outside of the plasma membrane induces sufficient transmembrane potential to disrupt the electrostatic forces maintaining the lipid bilayer structure. This causes temporarily the formation of small pores in the cell membrane. DNA and other charged molecules are then electrophoretically transferred into

the cell through these pores. Following pulse termination, pores reseal over 10s to 100s of ms (Tawk and Clarke, UCL).

To electroporate Cadherin-2 expression constructs into single cells of the upper rhombic lip at 48hpf, a pulled filamentous glass microcapillary with 1mm OD was filled with 100ng/μl purified plasmid DNA in 0.01% Fast Green (Sigma)/H_2O. A silver wire microelectrode (World Precision Instruments) was inserted into the capillary, serving as anode. The electrode was secured onto a microinjection holder (Narishige) and connected to the ECM810 electroporator (BTX). The tip of the glass needle was subsequently tapped to produce an opening of about 1μm. Embryos were embedded in 1.2% ultra-low gelling agarose/30% Danieau/PTU/0.01%Tricaine, such that their dorsal side was facing-up. The electrode-containing needle was then placed adjacent to the neuronal progenitor cells in the URL. The cathode, which was prepared from a platinum wire, was positioned next to the embryo in direction of the desired DNA flow. To introduce plasmid DNA into single cells, 7 square pulses of 600μs length each, paused by 100 ms between each pulse were given in at least two repetitions using 255V. Embryos were subsequently excised from the agarose and allowed to recover in 30%Danieau/PTU for 8h before time-lapse recordings.

2.2.4.9 Enzymatic removal of endogenous PSA

Polysialic acid (PSA) can be enzymatically degraded by treatment with EndoN. For removal of PSA from the embryonic nervous system at 33hpf, embryos were anesthetized with 30% Danieau/PTU/Tricaine and embedded in 1.2% ultra-low gelling agarose with their dorsal side facing up. A pulled filamentous needle filled with 100ng/μl purified EndoN in 1xPBS was inserted into the fourth ventricle of the hindbrain and about 1-3nl of enzyme was injected. The embryos were allowed to recover at 28°C.

2.2.4.10 Fluorescent dye labeling of zebrafish embryos

The lipophilic dye Bodipy Ceramide (Fl C5) (Molecular Probes) was used to outline plasma membranes, while TOPRO (Molecular Probes) was used to label cell nuclei of fixed embryos. Both dyes were dissolved in DMSO to make 1mM stock solutions, and stored at –20°C until use. Embryos were fixed in 4% PFA/PBST, washed 3x in 1xPBST and dechorionated before staining. Embryos were soaked overnight in 1:1000 dilutions of either dye in 1xPBST and washed three times in 1xPBST to remove excessive dye before

processing for imaging. Images were captured on the Zeiss inverted LSM510 Meta, using the Plan-NeoFluar 20x objective.

To label glial fibers emanating from the upper rhombic lip, a sharpened tungsten needle with DiI crystals (Invitrogen) at the tip was applied to the embryonic URL at 32hpf to mark individual cells or cell clusters. The lipophilic dye was allowed to bind to the plasma membrane for 16 hours and embryos were imaged at 48hpf using the Zeiss LSM510 Meta and 40x objective.

2.2.4.11 In-situ hybridization

2.2.4.11.1 Synthesis of RNA for in-situ hybridization

Antisense riboprobes were generated from linearized DNA template and labeled by digoxigenin incorporation using the DIG RNA-Labeling mix (Roche), according to the manufacturer's protocol. The DNA template was subsequently digested with 1μl DNase at 37°C for 15 min and DIG-labeled RNA was purified using the QIAGEN RNeasy Mini kit, according to the manufacturer's protocol.

2.2.4.11.2 Paraffin embedding and sectioning of adult zebrafish brains

To prepare adult brain paraffin sections, 9-month brains were fixed in 4% PFA/PBST for 4h at 4°C and dehydrated in an ethanol series of 70%, 90%, 95% and twice 100% for 10 min each step. The brains were then incubated in 100% Xylene for 7-8 min until almost clear and infiltrated with fresh paraffin. The brains were incubated in paraffin at 65°C overnight and blocks were prepared for sectioning. Sections of 8μm were subsequently cut on a microtome (MICROM 355S) and mounted onto frosted glass slides.

2.2.4.11.3 Whole-mount in-situ hybridization

Embryos were fixed in 4% PFA/PBST overnight at 4°C and subsequently washed 3x with 1xPBST. Embryos were dechorionated and dehydrated in 100% methanol. This was followed by storage of the embryos in 100% fresh methanol at –20°C for a minimum of 24h. Following re-hydration by using a series of 75, 50, 25% methanol/PBST, embryos were washed 3x in 1xPBST for 5 min each. Embryos were digested with 10μg/μl Proteinase K for 10-30 min, depending on the developmental age of the fixed embryos. The reaction was

stopped by incubation in 20μg/μl freshly prepared glycine/PBST. Embryos were fixed again in 4% PFA/PBST for 20 min and washed 3x in 1xPBST. Embryos were transferred into 1ml Hyb-mix and pre-hybridized in a pre-heated water bath at 57°C for 1h. The digoxigenin-labeled RNA probes were denatured at 94°C for 10 min and added to the pre-hybridized embryos. Embryos were incubated with RNA probes at 57°C, overnight. Next day, embryos were washed at 57°C for 45 min each in the following order: 2x in 2xSSCT/ 50%Formamide, 1x in 2xSSCT and 2x in 0.2xSSCT. For subsequent blocking, 10% normal goat serum (NGS)/PBST was added and embryos were incubated 1h at room temperature, agitating. Following the blocking step, embryos were incubated with a 1:2000 dilution of anti-DIG antibody (Roche) conjugated to alkaline phosphatase (AP) in 10%NGS/PBST at 4°C overnight. Embryos were washed 6 x 15 min in 1xPBST the next day. For staining, embryos were first equilibrated 2x 5 min in staining buffer and then incubated in substrate solution for the color reactions to develop (see 2.1.3.3). Stained embryos were washed 3x in 1xPBST and subsequently incubated in 90% glycerol before preparation of flat-mounts. Pictures of mounted embryos were recorded using the Zeiss Axioplan2 and Axiocam HRc camera. For transverse sections, embryos were kept in 1xPBST and then processed for vibratome sections.

2.2.4.11.4 In-situ hybridization on adult paraffin-embedded brain sections

Before ISH, sections were re-hydrated in order: 100% Xylene for 5 min, followed by a graded ethanol series of 100% 95%, 90%, 70% and 3 final washes in 1xPBS, for 10 min each.

The in-situ hybridization procedure for paraffin sections was similar to whole-mount ISH, except that slides were kept in a Tupper ware box, serving as humidity chamber during RNA hybridization at 69°C and antibody incubation in an ISH oven. Tween-20 was omitted from all buffers except for the Hyb-mix. Stained sections were photographed using the Zeiss Axioplan2 equipped with an Axiocam HRc camera.

2.2.4.11.5 Vibratome sections

For transverse sectioning of embryos after whole-mount ISH, embryos were embedded in 5% agarose/ 1xPBS. Sections of 20-50μm were cut on a vibratome (MICROM HM650V), equipped with standard razor blades.

2.2.4.12 Immunohistochemistry

For re-hydration, embryos stored in 100% methanol were transferred into 100% acetone and incubated for 7 min at –20°C. Embryos were subsequently washed 2x in ddH_2O for 1 minute each, followed by three washes in 1xPBS/ 1%Triton-X100 (PBSTr). Subsequently, embryos were blocked with 10% NGS/PBSTr for 1 hour at room temperature, agitating and then incubated with primary antibody in 10% NGS/PBSTr at 4°C, overnight. Next day, embryos were washed several times in PBSTr for 45 min each, followed by incubation with secondary antibody in 10% NGS/PBSTr at 4°C, overnight. For GFP and BLBP immunostaining, the fluorescence-coupled antibodies anti-rabbit IgG conjugated to Cy-2 and anti-mouse IgG conjugated to Cy-5 were used at 1:1000 dilutions (Dianova). For secondary detection of PSA-NCAM by DAB, anti-mouse IgG conjugated to HRP (Dianova) was used at a 1:300 dilution. For the DAB color reaction, embryos were washes 5 times in 1xPBST for 45 min each and subsequently incubated in staining solution (see 2.1.3.5) for 15 min, while shaking at room temperature. The solution was then exchanged by DAB staining solution and embryos were incubated for 30 min at room temperature. Subsequently, 20μl 0.3% H_2O_2 in ddH_2O was added to the solution and the color reaction was allowed to develop in the dark. After sufficient staining of the embryos the reaction was stopped by replacing the DAB staining solution with 1xPBST. The embryos were subsequently washed 5 times in 1xPBST at room temperature for 15 min each and stored at 4°C.

For fluorescence immunolabeling, embryos were washed 8 times in 1xPBST for 45 min each, after incubation with secondary antibodies. For long-term storage of fluorescently labeled embryos, the fluorescence was fixed by incubation in 4% PFA/PBST for 20 min and subsequently washed 3 times in 1xPBST for 5 min each. Embryos were stored at 4°C before mounting and imaging.

2.2.4.13 Cell death analysis by acridine orange staining

Acridine orange staining was performed on living embryos at 4dpf and 5dpf using wild type and *pac*-/-R specimens. Acridine orange enters dead cells when the cellular wall has been broken and binds to nucleic acids, either electrostatically or by intercalation. Depending on the excitation/ emission wavelengths used, both DNA and RNA can be separated. Anesthetized embryos were soaked in 30%Danieau/PTU containing 5μg/ml acridine orange for 20 min, followed by three 1-minute washes in 30%Danieau/PTU. The

embryos were immediately mounted in 1.2% ultra-low gelling agarose/ 30%Danieau/PTU and scanned on the LSM510 using the 40x C-Apochromat objective.

2.2.5 Microscopy methods

2.2.5.1 Transmission electron microscopy (TEM)

Zebrafish embryos were fixed at 55hpf for 2h at room temperature in 2% PFA/ 0.2% glutaraldehyde/PBS and washed 3x 1xPBS for 10 min each before a 1h incubation at room temperature with post-fixative solution osmium tetroxide (see 2.1.3.7). Post-fixation was followed by three washes in ddH_2O for 10 min each. Embryos were subsequently ethanol dehydrated in the following order: 30%, 50%, 70%, 90%, 96% for 10 min each, then 3x in 100% Ethanol for 10 min each. For the infiltration process with epon embedding medium (see 2.1.3.8), embryos were transferred into fresh 2ml tubes and first incubated 2x with intermediate solvent 100% propylene oxide for 20 min each, followed by incubation in a 1:1 mixture of epon embedding resin: propylene oxide for 1h. The epon embedding resin: propylene oxide mixture was exchanged with pure epon embedding resin and embryos incubated at room temperature, overnight. Embryos were transferred into standard flat molds and re-oriented before polymerization at 60ºC for 24 hours. Blocks were first cut into 20μm sagittal sections. The sections being close to the region of interest were stained with toluidine blue and analyzed by light-microscopy before cutting 60-80nm ultra-thin slices with Diamond knives (Diatom) on a microtome (Reichert Ultracut E Microtome). Subsequently, ultrathin sections were mounted on a grid and stained in order with 0.5% uranyl acetate for 30 min and 3% lead citrate for 2 min as contrast agents, using the Leica Ultrastainer. Single washes with ddH_2O were performed between each step. Sections were scanned using the EM10CR transmission electron microscope (Zeiss). This protocol has been described in detail (Rieger, 2007).

2.2.5.2 Confocal microscopy

Imaging was performed using a modified imaging chamber, which was prepared by drilling a hole into the bottom of a small Petri dish and attaching a glass cover slip to the hole, using silicon grease. For embedding, a drop of 1.2% ultra-low gelling agarose (Sigma) containing the embryo was placed onto the glass coverslip. Following orientation of the

embryo and solidification of the agarose, the imaging chamber was filled with medium to cover the embryo in order to prevent drying out.

2.2.5.3 Time-lapse analyses settings for confocal microscope

Specimen/ Cell line	Recordings/ Injected construct	Section interval (stack/single)	Time interval (min)	Objective C-Apochromat
gata1:GFP	Chain migration	1μm (stack)	12	63x
gata1:GFP	8xHSE:NcadΔN-mCherry	1μm (stack)	12	63x
gata1:GFP	8xHSE:Cdh2Δ2-4ΔC-mCherry	1μm (stack)	12	63x
gata1:GFP	8xHSE:Cdh2Δ2-4ΔC-EosFP	1μm (stack)	5	63x
PAC2	pCS2+ Cdh2Δ2-4ΔC-EosFP	1μm (single)	1	40x
gata1:GFP	wild type into wild type transplantation	3μm (stack)	12	40x
gata1:GFP	*pac*-/-R into wild type transplantation	3μm (stack)	12	40x
gata1:GFP	wild type GPC migration	3μm (stack)	12	40x
gata1:GFP	pBSK-1xUASE1b:centrin2-tdTomato/ CMV:KalTA4	1μm (stack)	12	63x
brass	pBSK- tub-GVP-Uunc	3μm (stack)	12	40x

Table 6 Conditions used for time-lapse recordings of living specimens

2.2.5.4 Image processing

Digital images were processed for brightness, contrast and size using Adobe Photoshop 7.0 D and the NIH open source software ImageJ1.34s. Z-stacks from time-lapse recordings were projected to single images for each time point. Image projections were assembled into movies using QuickTime Player 7.2. Time-lapse imaging and analysis of results used herein has been described in detail (Köster and Fraser, 2004).

2.2.5.5 Statistical analysis

Statistical analyses were performed, using the GraphPad software Prism 4:

Contact stabilities: For statistical quantification of contact stabilities the unpaired, two-tailed Student t test was used. GPC pairs (n=8) for each of four independent wild type and *pac*-/-R embryos were quantified.

Length-width ratio: For statistical analyses of the LWR, wild type, *pac*-/-R, *pac*R2.10 and non-migrating control group were analyzed by one-way ANOVA and post testing, using a multiple comparison test.

Cell tracing, migration distance and velocity: The means of total tracked distances and velocities were determined and the two-tailed Student's t-test applied for statistical analysis.

Cell death analysis: Dead cells were counted in both cerebellar halves and total numbers compared between wild type and *pac*-/-R. For statistical analyses, the unpaired, two-tailed Student t test was used.

3 RESULTS

3.1 Cadherin-2 mediates coherent and directional migration of zebrafish cerebellar granule progenitor cells

3.1.1 Cerebellar granule progenitor cells migrate in a homotypic neurophilic manner

The gata1:GFP stable transgenic line (Long et al., 1997) expresses GFP in migrating granule progenitor cells (GPCs) of the differentiating cerebellum starting at ~48hpf. Time-lapse confocal microscopy revealed that GPCs migrate into distinct terminal differentiation domains, depending on their medio-lateral positions within the upper rhombic lip (URL) (Volkmann et al., 2007). GPCs emanating from the URL migrate towards the mid-hindbrain boundary (MHB) and then either remain there or migrate ventrally towards the brain stem. In order to reveal cellular and molecular mechanisms that regulate migration of cerebellar GPCs, it was first addressed whether glial cells are present in the zebrafish cerebellum prior to and during onset of GPC migration at 36 and 48hpf, respectively. While migration of earlier born cerebellar neuronal cell populations is well under way at ~36hpf, GPCs arise from the URL and migrate in anteroventral directions at ~48hpf and later. To detect glia-like cell morphologies in the cerebellum, mRNA encoding for the membrane-targeted fluorescent fusion protein lynGFP (Teruel et al., 1999) was injected into 8 and 16-cell stage embryos for mosaic labeling, thus outlining individual cellular morphologies. The cerebellum and caudal hindbrain of injected embryos was subsequently analyzed at 36hpf and 48hpf by confocal microscopy. In rhombomeres posterior to the cerebellum, cells with morphologies similar to radial glia were spanning the neural tube, being attached to the apical and basal membrane via typical glia-like endfeet. In some cases, individual cells appeared as if they progressed along these fibers (Fig. 3.1A, blue arrow). In contrast, such glia-like cellular morphologies could not be observed in the developing cerebellum. Rather, cells appeared to migrate via the formation of chain-like structures extending from the URL towards the MHB (Fig. 3.1.A white arrowhead), similar to previous observations (Köster and Fraser, 2001). In addition to this mosaic analysis by mRNA injection of lynGFP, individual cells were labeled by applying DiI crystals onto cells of the URL at 32hpf (Fig. 3.1B, white asterisk marks site of injection in the URL), thus outlining the morphologies of glial cells, if present, which were expected to span from the URL towards the MHB.

Figure 3.1 Absence of glial-like cell morphologies in the early differentiating cerebellum

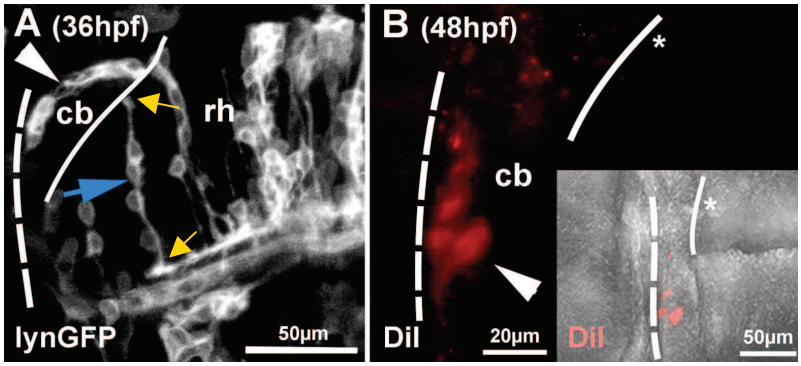

(Fig. 3.1) Neither mosaic expression of membrane-targeted lynGFP at 36hpf (A) nor DiI labeling of URL cells at 48hpf (B) revealed glial-like cellular morphologies in the cerebellum. Both images show lateral views. The dashed line marks the MHB while the solid line depicts the URL. (A) Cerebellar GPCs display chain-like structures (white arrow) subsequent to their emigration from the URL, while glial fiber-like morphologies are not present. In contrast, such cells with glial-like morphologies having fibers attached to the apical and basal membranes via typical glial-like end feet (yellow arrows) are found in the caudal hindbrain (blue arrow). (B) DiI injection at 32hpf reveals the presence of labeled neuronal progenitors close to the MHB at 48hpf but no glial-like morphologies. Abbr.: cb: cerebellum; rh: rhombencephalon.

DiI was allowed to incorporate into the lipid bilayer of cells for 16 hours before analyzing the embryos by confocal microscopy at 48hpf. Such analyses never revealed any cells with glia-like morphologies (n=5 embryos). Rather, DiI-labeled cells displayed morphologies that were reminiscent of neuronal progenitors with a typical elongated leading process (Fig. 3.1B, white arrowhead). These findings suggest that glia cells are absent in the zebrafish cerebellum before and during onset of GPC migration.

To further substantiate this finding, expression of the glial specific genes *gfap*, *vimentin* and *fabp7a* was examined by *in situ* hybridization at 48hpf. While gene expression was found posterior to the cerebellum in the caudal hindbrain, no expression could be detected in the differentiating cerebellum itself (Fig. 3.2A-C), up to 100hpf (not shown) when major GPC migration has already ceased (Volkmann et al., 2007). Furthermore, immunohistochemistry in gata1:GFP transgenic embryos at 48hpf against Brain Lipid-Binding protein (BLBP), which is expressed in radial glia cells, supported the gene expression data, with BLBP staining being prominent in the caudal hindbrain but not detectable in the differentiating cerebellum (Fig. 3.2D).

Figure 3.2 Expression of glial markers in the caudal hindbrain but not in the differentiating cerebellum

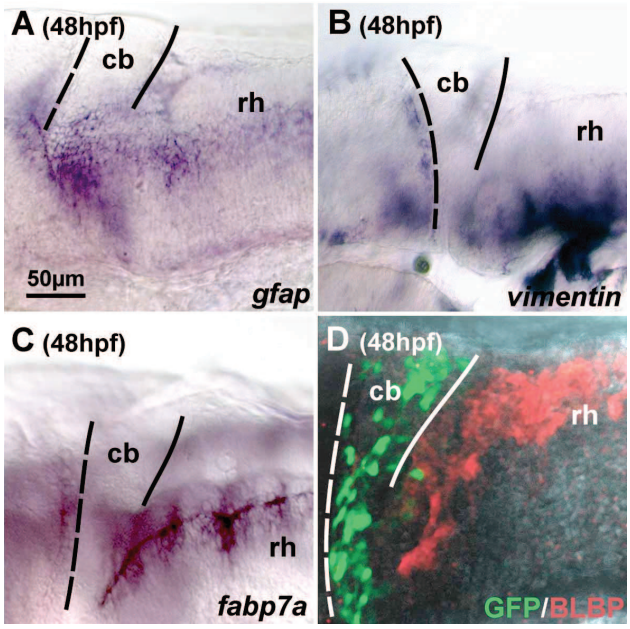

(Fig. 3.2) Glial-specific gene expression is absent in the differentiating cerebellum during onset of GPC migration. Lateral views of the zebrafish cerebellum and caudal hindbrain are shown at 48hpf. The MHB is marked with a dashed line, while a solid line depicts the URL. (A-C) *In situ* hybridization reveals *gfap* (A), *vimentin* (B) and *fabp7a* (C) gene expression in the caudal hindbrain but not in the cerebellum. (D) BLBP protein expression (red) is found in the caudal hindbrain of gata1:GFP embryos as revealed by immunohistochemistry. GFP-expressing cerebellar GPCs can be recognized by their green fluorescence. Abbr.: cb: cerebellum, rh: rhombencephalon.

Intriguingly, ultrastructural analysis of the cerebellum using transmission electron microscopy (TEM) revealed a highly parallel organization of cerebellar cells being oriented from the URL towards the MHB (Fig. 3.3A, black arrowheads). Moreover, cerebellar cells displayed many direct cell-cell contacts mediated by electron dense structures, indicative of adherens junctions (Fig. 3.3B, black arrowhead). In contrast, in the caudal hindbrain several cells with fiber-like processes were present (Fig. 3.3C, black arrows), substantiating the findings made by mosaic labeling of hindbrain cells. These results suggest that GPCs migrate in a glia-independent manner.

To directly reveal such a migratory behavior for zebrafish GPCs, high resolution intravital time-lapse confocal microscopy was performed on gata1:GPF transgenic embryos (n=6 movies). This demonstrated that GPCs migrate from the URL towards the MHB in close apposition while intimately interacting with each other through formation of chain-like structures (Wichterle et al., 1997) (Fig. 3.4, and Supplementary Movie 3.1).

These findings indicate that zebrafish cerebellar GPCs use a homotypic neurophilic migration mode.

Figure 3.3 Ultrastructural analyses of the differentiating cerebellum and caudal hindbrain

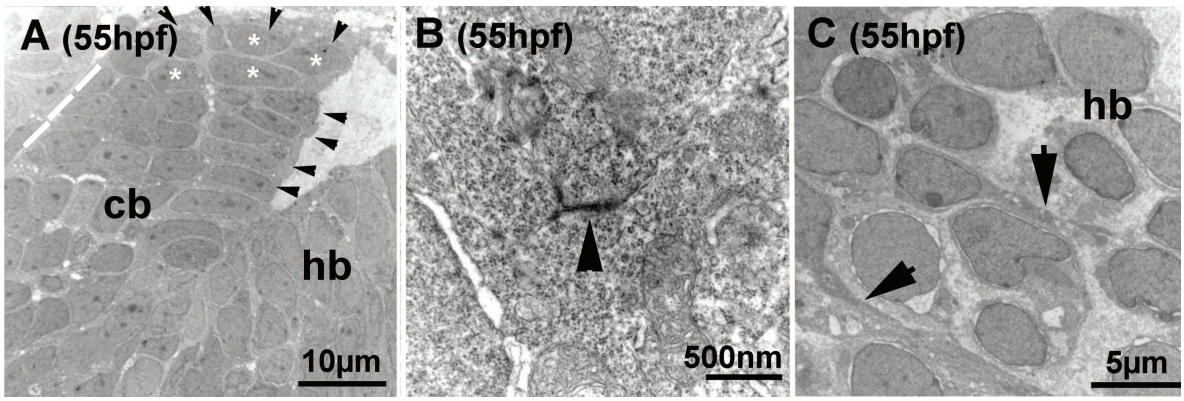

(Fig. 3.3) Transmission electron microscopy (TEM) analysis of the differentiating cerebellum and caudal hindbrain at 55hpf, anterior is left. (A) A lateral view of the differentiating cerebellum and part of the caudal hindbrain is shown. Ultrastructural analysis demonstrates that cells in the differentiating cerebellum are arranged in a highly ordered manner (arrowheads), with nuclei (asterisk) being elongated towards the MHB (white dashed line). (B) Electron dense structures indicate that adherens junctions are established at sites of cell-cell contacts (arrowhead). (C) In the hindbrain, cells are loosely arranged and some cells with fiber-like processes are present (arrows), probably serving to guide neuronal migration. Such fibers do not exist in the cerebellum at this stage (compare to A). Abbr.: cb: cerebellum, hb: hindbrain.

Figure 3.4 Chain-like migration behavior of cerebellar GPCs

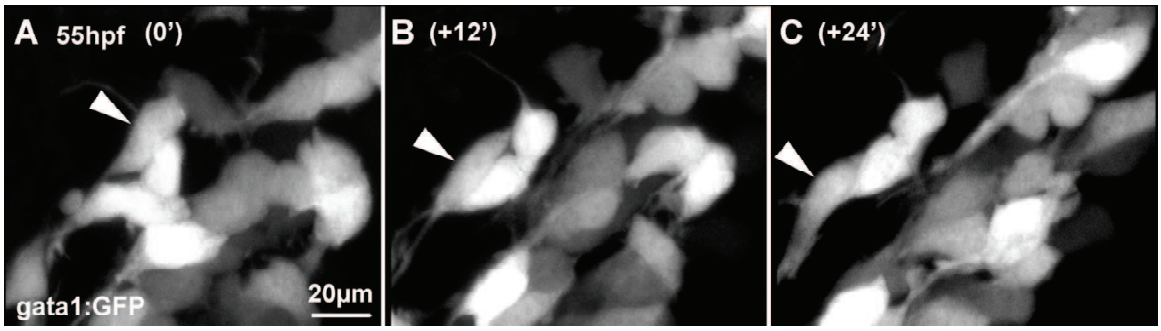

(Fig. 3.4) Cerebellar GPCs interact in a homotypic neurophilic manner during migration. Lateral view of the zebrafish cerebellum at 55hpf. High-resolution 1μm optical sections showing a time-lapse confocal sequence of migrating fluorescent GPCs in the gata1:GFP stable transgenic line, recorded in 12-minute intervals. Intense interactions occur among GPCs as an individual cell migrates along other GPCs that are arranged in a chain-like manner (white arrowhead, Supplementary Movie 3.1).

3.1.2 Cadherin-2 is a candidate to mediate cerebellar granule progenitor cell migration

Cadherins have been shown to be involved in the homophilic formation of cellular interactions between neurons via adherens junctions. Classic Cadherins are good candidates to mediate chain-like GPC migration in the differentiating cerebellum of zebrafish embryos as their presence along cell-cell contact sites was revealed by TEM analyses, appearing in electron dense structures (Fig. 3.3B, black arrowhead). Neural Cadherin-2 (zebrafish homolog of mouse N-cadherin) is the most prominent representative of the classic Cadherin family in the zebrafish nervous system and has been shown to be expressed in the differentiating zebrafish nervous system (Bitzur et al., 1994). To re-examine its expression in the cerebellum, *in situ* hybridization was performed at stages of ongoing GPC migration. *cadherin-2* was confirmed to be strongly expressed in the zebrafish cerebellum at 48hpf and 72hpf, when GPC migration is most prominent (Fig. 3.5A, B), similar to previous findings (Liu et al., 2004). Furthermore, combined *in situ* hybridization and immunohistochemistry revealed that *cadherin-2* mRNA expression in the cerebellum co-localizes with migratory GFP-expressing GPCs in embryos of the stable transgenic gata1:GFP line (Fig. 3.5C, D). This makes zebrafish Cadherin-2 a candidate to mediate cellular interactions among migratory cerebellar GPCs.

The zebrafish *parachute* R2.10 (termed *pac*R2.10) mutant harbors an amorph loss of function allele of zebrafish *cadherin-2* (Lele et al., 2002). Despite strong neurulation defects mutant embryos still develop a cerebellum although its morphology is altered and much smaller lobes are formed than those seen in wild type embryos (Fig. 3.5E, F). In addition, a cerebellar upper rhombic lip is still present as revealed by gene expression analysis of the rhombic lip marker *atonal1a* (Fig. 3.5G, H). To address whether Cadherin-2 regulates cerebellar GPC migration, *pac*R2.10 mutants were crossed into the gata1:GFP line and GFP-expressing GPCs of homozygous transgenic mutant embryos were analyzed by *in vivo* time-lapse confocal microscopy. First, wild type cerebellar GPCs of gata1:GFP embryos were examined by time-lapse confocal microscopy. GPCs in these embryos started migration from the URL at 48hpf in an anterior direction towards and along the MHB (Fig. 3.6 A-C, n = 4 movies, Supplementary Movie 3.2). At the MHB they formed lateral and medial clusters that will differentiate into the granule cell populations of the eminentia granularis (Fig. 3.6 C, blue dashed circle) and the corpus cerebelli (Fig. 3.6 C, orange dashed circle), respectively (Köster and Fraser, 2006) (Volkmann et al., 2007). In contrast to this observed long distance migration of wild type GPCs, *in vivo* time-lapse

analysis revealed that GFP-expressing GPCs of *pac*R2.10 mutant embryos arose in a scattered and irregular manner in the URL of the rudimentary cerebellum (Fig. 3.6D).

Figure 3.5 Zebrafish Cadherin-2 is a candidate to mediate adhesive contacts between migrating GPCs

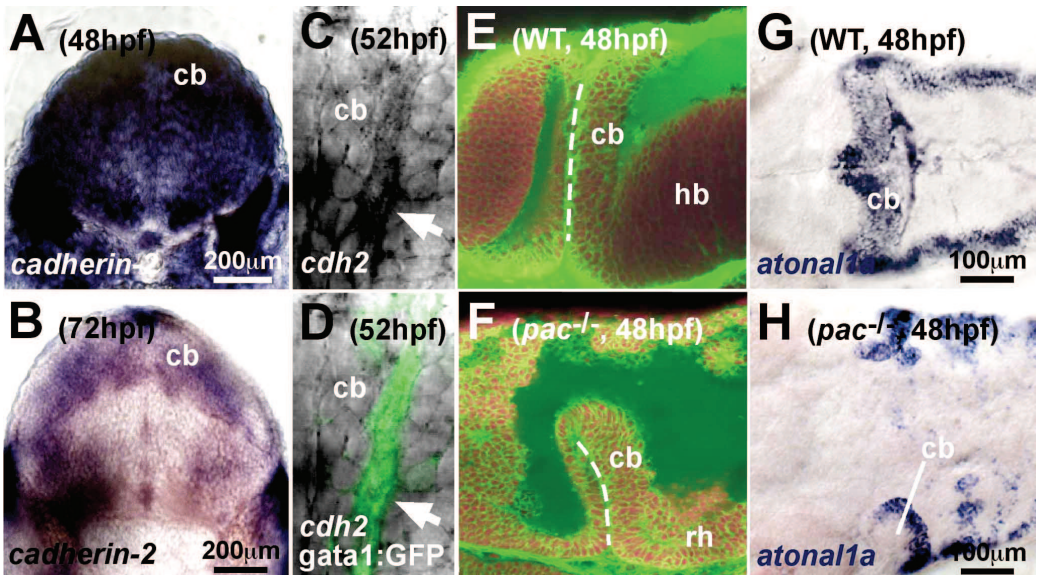

(Fig. 3.5) (A, B) Transverse sections through the developing zebrafish cerebellum after *in situ* hybridization of *cadherin-2*, which is expressed during stages of prominent GPC migration at 48hpf (A) and 72hpf (B). (C, D) High-magnification confocal microscopy reveals *cadherin-2* expression in cerebellar cells (white arrow) at 52hpf. These cells co-localize with GFP (D, green fluorescence, white arrow), thus showing that migratory GPCs in embryos of the gata1:GFP transgenic line express *cadherin-2*. (E, F) Lateral views of wild type (E) and *pac*R2.10 mutant embryos (F) co-stained with TOPRO and Bodipy Ceramide to outline cytoplasmic membranes and nuclei. This reveals that *pac*R2.10 mutants still form a cerebellum despite their strong defects in the CNS, although it is rudimentary when compared to the wild type sibling. (G, H) The rhombic lip is still present in *pac*R2.10 mutants (H) as demarcated by *atonal1a* gene expression (wild type in G and *pac*R2.10 mutant in H, dorsal views). Abbr.: WT: wild type, cb: cerebellum, cdh2: *cadherin-2*, *pac*-/-: *parachute* R2.10 mutant.

Although being moderately motile, GPCs of the later corpus cerebelli remained close to the URL during all stages analyzed (Fig. 3.6 E and F, orange dashed circle). These cells were moving back and forth along the medio-lateral aspect of the URL rather than migrating anteriorly and thus failed to form characteristic clusters close the MHB (n = 4 movies, see Supplementary Movie 3.3). A similar stationary migration behavior, although to a lesser extent was observed for GPCs that normally migrate into clusters of the eminentia granularis. This is consistent with previous findings that dorsal-most neuronal structures, such as in the future corpus cerebelli, are more strongly affected in *pac*R2.10

mutants (Lele et al., 2002). These findings suggest that loss of Cadherin-2 influences the migration of cerebellar GPCs.

Figure 3.6 Atypical migration behavior of GPCs in *pac*R2.10 mutant embryos

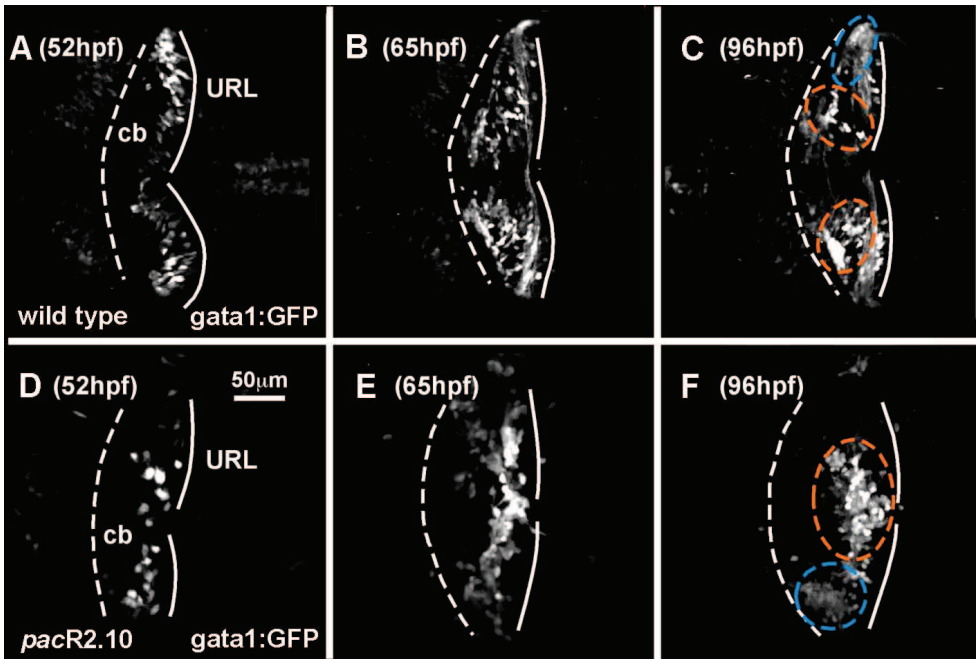

(Fig. 3.6) Individual projected stacks of *in vivo* time-lapse recordings showing migrating GPCs in wild type gata1:GFP transgenic embryos (A-C) and *pac*R2.10 gata1:GFP mutant embryos (D-F). The dashed line depicts the MHB, whereas the solid line marks the URL. (A-C) Wild type GPCs migrate towards and along the MHB to form distinct granule cell clusters that are destined to become the corpus cerebelli (C, orange dashed circle) and the eminentia granularis (C, blue dashed circle, see Movie 3.2). (D-F) In contrast, GPCs of *pac*R2.10 mutants, in particular cells that are located medially and constituting the later corpus cerebelli remain close to the URL and settle in ectopic clusters (F, orange dashed circles, see Movie 3.3). Abbr. cb: cerebellum, URL: upper rhombic lip.

3.1.3 Temporal rescue of *parachute* mutant embryos to reveal a direct role for Cadherin-2 in regulating cerebellar granule progenitor cell migration

Homozygous mutant *pac*R2.10 embryos exhibit defects in neurulation, leading to the development of smaller sized cerebellar lobes that fail to fuse at the dorsal midline (Fig. 3.5 F, H). As neurulation occurs early in development these defects do not allow one to discriminate between an indirect or direct function of Cadherin-2 in regulating zebrafish GPC migration. Therefore, *pac*R2.10 mutant embryos were temporally rescued for their neurulation phenotype by injecting wild type *cadherin-2* mRNA (~70pg) into single cell stage zebrafish embryos. At 24hpf, morphological analysis revealed that the cerebellar

primordium in rescued *pac*-/-R mutants, termed *pac*-/-R, appeared similar to wild type cerebelli (Fig.3.7A) with both cerebellar halves connected at the dorsal midline (Fig. 3.7C), in contrast to non-rescued *pac*R2.10 mutants that exhibit severe neurulation defects (Fig. 3.7B). Rescue of the neurulation defects in mutant embryos was further supported by the proper expression of *wnt1* along the dorsal midline (Fig. 3.7D-F). Furthermore expression of *atonal1a* along the URL of wild type cerebellar primordia (Fig. 3.7G) was largely restored in rescued *pac*-/-R (Fig. 3.7I, black arrow) when compared to non-rescued *pac*R2.10 mutant embryos (Fig. 3.7H), although some injected embryos showed deviations of the lower rhombic lip tissue (Fig. 3.7I, white asterisk). These findings indicate that the neurulation defects of *pac*R2.10 embryos can be rescued to a large extent by *cadherin-2* mRNA injections at the single cell stage.

To unambiguously identify such rescued homozygous *pac*R2.10 carriers, embryonic tails of wild type, *pac*R2.10 and rescued *pac*-/-R embryos were genotyped by RT-PCR using primers that anneal within the 5'UTR and in the first exon of *cadherin-2* (see 2.1.9). Homozygous *pac*R2.10 mutants carry a splice mutation and therefore produce transcripts of different lengths, whereas only a single transcript is found in wild type embryos (Fig. 3.7L, note RT-PCR results in both lanes on the right were obtained from tails of the same embryos displayed in 3.7F and 3.7I, respectively) (Lele et al., 2002).

To further examine the stability of *cadherin-2* mRNA in injected mutant embryos, *in situ* hybridization was performed on rescued (Fig. 3.7K) and non-rescued (Fig. 3.7J) *parachute* mutants at 24hpf. This revealed that *cadherin-2* mRNA was completely degraded in *pac*-/-R embryos at this developmental stage. Although *cadherin-2* mRNA was not detectable by *in situ* hybridization anymore, Cadherin-2 protein levels in *pac*-/-R mutant embryos were comparable to those in wild type embryos at 24hpf, as detected by western blot analysis (Fig. 3.7M, lane 1 and 3). At 48hpf, the stage at which GPCs initiate migration, Cadherin-2 protein levels mostly declined in *pac*-/-R embryos probably due to high protein turnover rates (Fig. 3.7M, lane 6, black arrow). The phenotypic rescue of *pac*-/-R embryos is therefore temporally restricted to stages before onset of GPC migration (Volkmann et al., 2007), thus allowing an investigation of direct functions of Cadherin-2 in regulating cerebellar GPC migration.

Figure 3.7 Neurulation defects are rescued in *parachute* mutants by *cadherin-2* mRNA injection

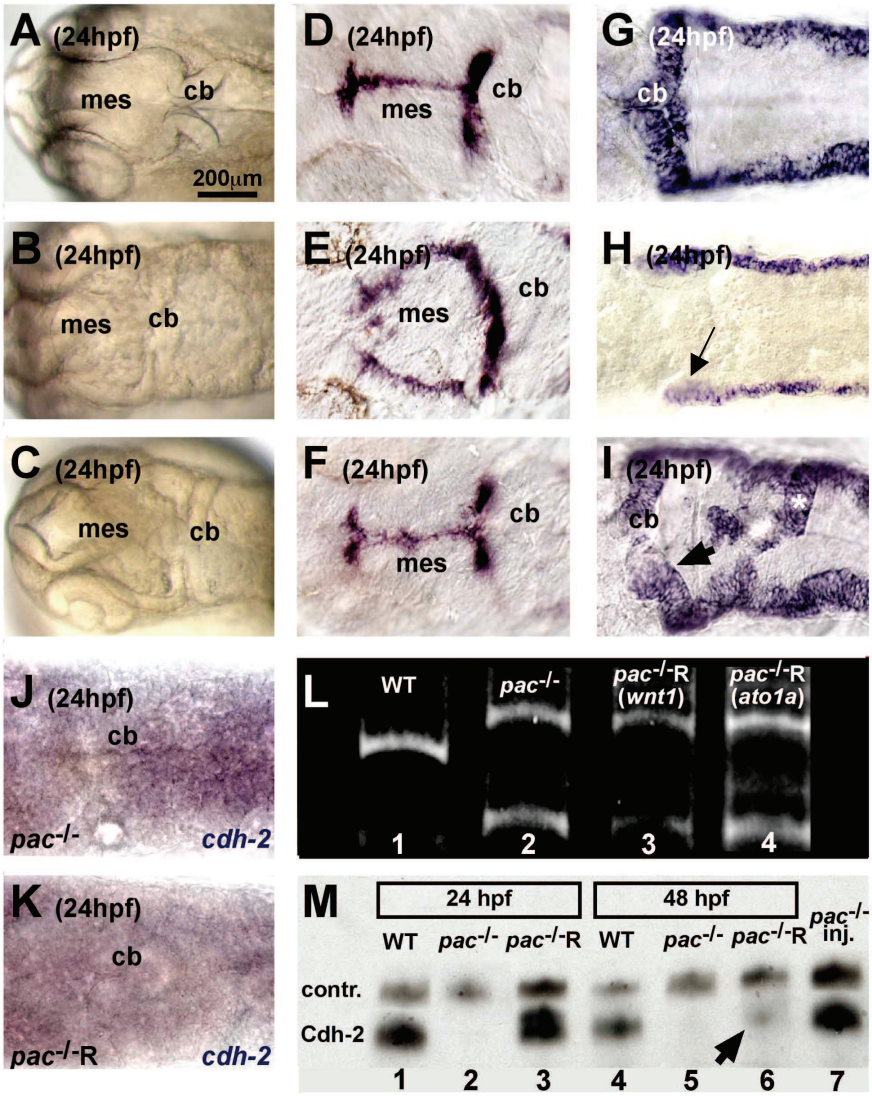

(Fig. 3.7) Temporal rescue of *pac*-/-R embryos is restricted to developmental stages prior to cerebellar GPC migration. (A-K) Dorsal views of the embryonic brain at 24hpf. (A-C) Morphological appearance of wild type (A) *pac*R2.10-embryos (B) and rescued *pac-/-R embryos* (C). (D-I) This rescue is further confirmed by whole mount *in situ* hybridization. (D-F) Expression of *wnt1* is detected along the dorsal midline in wild type (D) and *pac*-/-R (F), while the neural tube is not fused in *pac*R2.10 mutants and *wnt1* expression is found in two parallel stripes along the antero-posterior axis (E). (G-I) A*tonal1a* expression is found in the rhombic lip and marks the fusion of both cerebellar halves at the dorsal midline in wild type (G) and *pac*-/-R (H), while both cerebellar lobes are laterally located in *pac*R2.10 mutants (I, arrow). (L) Detected *cadherin-2* splice transcripts via RT-PCR in *pac*-/-R embryos (lane 3+4, note RT-PCR was performed on tails of embryos displayed in F and I, respectively), also being present in homozygous carriers of the *pac*R2.10-allele (lane 2), which can be distinguished from a single transcript present in wild type embryos (lane 1). (J, K) Whole-mount *in situ* hybridization of *cadherin-2* reveals that injected *cadherin-2* mRNA is not detectable anymore at 24hpf in rescued *pac*-/-R embryos (K, compare to *pac*R2.10-embryo in J). (M) In contrast to little or no *cadherin-2* gene expression in rescued mutants, western blot analysis indicates that Cadherin-2 protein is still present at 24hpf (lane 3) in comparable levels to wild type embryos (lane 1), but is mostly degraded in *pac*-/-R embryos until

48hpf (lane 6, black arrow, compare band to wild type (lane 4) and *pac*R2.10-embryos (lane 5) before granule progenitor cells emigrate from the URL. Lane 7 shows levels of Cadherin-2 protein expression in *pac*R2.10-embryos after plasmid DNA injection of Cadherin-2, resulting in stable protein expression even beyond 48hpf. Equal amounts of protein were loaded, control: TenascinR. Abbr.: ato1: *atonal1a*, cb: cerebellum, contr.: control antibody, mes: mesencephalon.

3.1.4 Cadherin-2 mediates directionality and coherence of cerebellar granule progenitor cell migration

Intravital time-lapse studies and cell tracing analyses of individual GPCs in wild type and *pac*-/-R gata1:GFP embryos indeed revealed a direct role for Cadherin-2 in governing GPC migration. Imaging migrating GPCs in one cerebellar lobe at high magnification confirmed that both wild type and *pac*-/-R GPCs migrated in typical anterior and antero-lateral routes towards the MHB after emigration from the URL (Fig. 3.8A-E) (Supplementary Movie 3.4, n=5). Furthermore, cerebellar GPCs in rescued *pac*-/-R embryos were capable of long-distance migration (Fig. 3.8F-J), in contrast to GPCs in homozygous *pac*R2.10 mutant embryos (Fig. 3.6D-F, Supplementary Movie 3.3). GPCs in *pac*-/-R however migrated mostly as individual cells rather than interacting intensely with one another. More strikingly, individual GPCs severely deviated from their antero-lateral routes towards and along the MHB, migrating in random directions, sometimes even exhibiting circling behavior (Supplementary Movie 3.5, n=5). These findings demonstrate that cerebellar GPCs in *pac*-/-R embryos lack coordinate and directional migration towards the MHB.

To further substantiate this finding, the migratory tracks of individual GPCs in wild type and *pac*-/-R gata1:GFP embryos were compared. This demonstrated that GPC migration in wild type gata1:GFP transgenic embryos is highly coherent with migratory tracks aligning almost parallel to one another (Fig. 3.8K, L). This high degree of coherence was likely caused by the chain-like migration behavior of cerebellar GPCs in gata1:GFP embryos. Furthermore, the overall migratory routes of individual GPCs strictly followed antero-lateral directions, as revealed when starting and end-points of individual tracks were connected (Fig. 3.8L). This shows that GPC migration in the zebrafish cerebellum is highly directional. In contrast, tracing of GPCs in *pac*-/-R embryos revealed a random and dispersed orientation of individual tracks, being suggestive of a non-coherent undirected migration (Fig. 3.8M, N, e. g. pink and dark blue tracks). These findings indicate that Cadherin-2 influences directionality and coherence of migrating GPCs.

Figure 3.8 GPCs in *pac*-/-R mutant embryos lack coherent and directional migration behavior

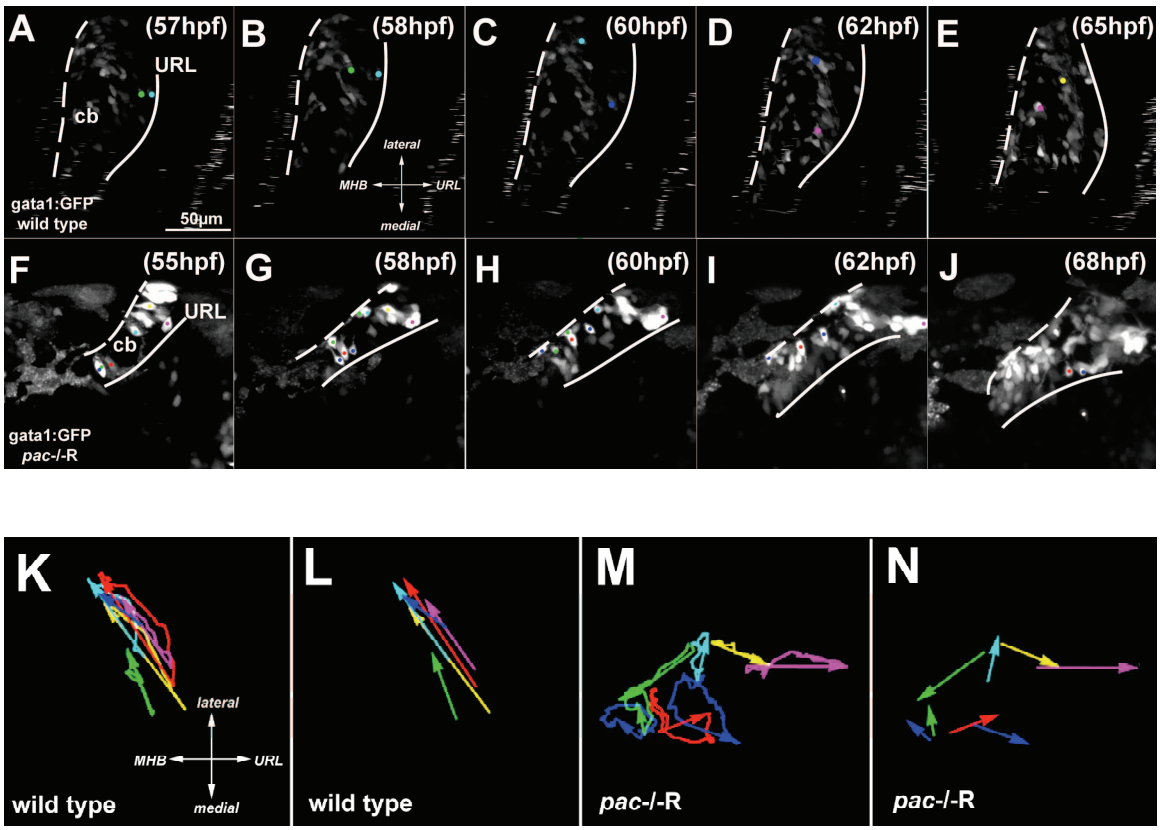

Fig. 3.8 Cadherin-2 regulates coherence and directionality of migrating cerebellar GPCs. (A-J, dorsal views showing only one cerebellar lobe) Maximum intensity projections from individual time-points of a time-lapse confocal movie are shown. Stacks were recorded in 12-minute intervals and individual GPCs were subsequently traced using ImageJ software and the manual tracking tool plug-in. Frames of a movie sequence show individually traced migrating cerebellar GPCs of wild type gata1:GFP embryos (A-E) and rescued *pac*-/-R gata1:GFP embryos (F-J). The dashed line depicts the MHB and the solid line the URL. Traced GPCs are marked in differently colored dots. (A-E) Wild type GPCs migrating from the URL towards anterior and antero-lateral regions. (F-J) GPCs in *pac*-/-R embryos display a migratory behavior mostly occurring on the individual level, being dispersed with cells also heading back to the URL (blue and red dots, compare Supplementary Movie 3.4 and Movie 3.5). (K-N) Tracks of migrating GPCs are displayed from wild type (K, L) and *pac*-/-R embryos (M, N), with starting and end points of each track being connected by an arrow showing the overall migration direction. Wild type tracks reveal that GPC migration is highly coherent and directional, while migration of GPCs in *pac*-/-R gata1:GFP embryos occurs on the single level with some cells migrating in circles (M, e.g. dark blue tracks). Abbr.: MHB: midbrain-hindbrain boundary, URL: upper rhombic lip.

3.1.5 Cadherin-2 mediates stable GPC-interactions in migratory chains

In order to analyze in more detail why migrating Cadherin-2 deficient cerebellar GPCs in *pac*-/-R embryos fail to migrate in a coherent manner, the stability of cell-cell contacts among GPCs was determined. For this, the contact length between two migrating GPCs in the cerebellum was measured using 1μm confocal sections of four independent wild type

and *pac*-/-R time-lapse movies. The elapsed time from the first contact of two GPCs and the time point of release was thereby measured. Individual stacks were recorded in 12-minute intervals for a maximal duration of 252 minutes. In wild type gata1:GFP transgenic embryos, robust contacts between migrating GPCs (Fig. 3.9A-D, white arrowhead) lasted for an average duration of 95.3 ± 10.9min (Fig. 3.9E, n=29 analyzed cell contacts). In contrast, in *pac*-/-R embryos cell-cell contacts were less stable and lasted significantly shorter with an average duration of 36.8 ± 5.6min (Fig. 3.9E, n=29 analyzed cell contacts). These findings further support that Cadherin-2 deficient GPCs are unable to engage in chain-like migration and may explain the lack of coherence between migrating GPCs in rescued *pac*-/-R embryos.

To explain why GPC contacts were dramatically reduced in *pac*-/-R embryos, ultrastructural analysis of the differentiating cerebellum at 55hpf by transmission electron microscopy was performed (Fig. 3.9). This revealed that cerebellar cells in *pac*-/-R embryos lack adherens junctions (Fig. 3.G vs. H, white arrowhead), therefore most likely leading to the reduction of stable contacts and resulting in the disorganized appearance of cerebellar cells (Fig. 3.9F). This finding moreover suggests that Cadherin-2 is the primary classic Cadherin, mediating homotypic neurophilic cell-cell interactions during chain-like migration of cerebellar GPCs in the zebrafish embryo.

3.1.6 Cadherin-2 influences polarization of migrating cerebellar GPCs

In order to address cellular changes underlying the disoriented migration behavior of Cadherin-2 deprived GPCs, the length-width ratios (LWRs) of migrating GPCs were determined (Fig. 3.10). Cells were generally considered clearly polarized with LWR values above 1.65 (Shih and Keller, 1992) (Wallingford et al., 2000). LWRs above 1.65 were found for migrating wild type GPCs of gata1:GFP embryos, displaying a mean LWR of 2.1 ± 0.51 (n=50). Also temporally rescued *pac*-/-R gata1:GFP embryos showed a mean LWR of 1.91 ± 0.61 (n=41) and thus GPCs of wild type and rescued mutants were polarized and did not significantly differ from each other. However, these LWRs differed from GPCs of non-rescued *pac*R2.10 mutant embryos, which showed a mean LWR of 1.5 ± 0.5 (n=51), indicating their lack of polarization (**$p<0.001$) (Fig. 3.10C). The mean LWR of these GPCs was rather similar to the LWR-value of terminally differentiated non-migratory granule cells, which already ceased migration and displayed a mean LWR of 1.28 ± 0.16 (n=34).

Figure 3.9 Reduction of contact stabilities among GPCs in *pac*-/-R embryos due to the absence of Cadherin-2

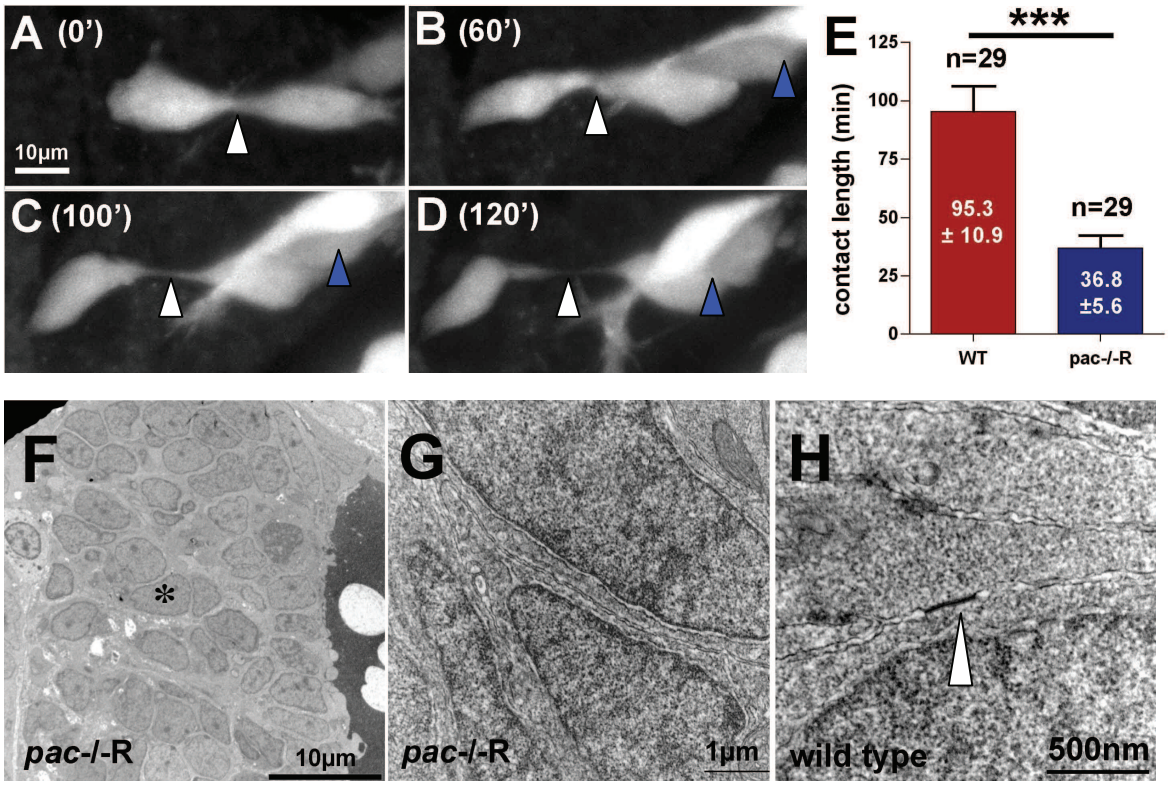

(Fig. 3.9) Quantification of contact stabilities among individual GPCs in wild type and *pac*-/-R embryos by time-lapse analysis (A-D) High-resolution 1μm confocal sections of a time-lapse movie showing the contact formation and release between two GPCs. (A, B) Initially, both GPCs form a stable contact with the leading edge of one GPC being attached to the rear end of another GPC (white arrowhead). (B-D) As a third GPC moves along the chain (blue arrowhead) the contact between the two GPCs is released (C, D, white arrowhead). (E) Measurements of contact stabilities among GPCs in *pac*-/-R embryos revealed significantly reduced contact durations (approx. 50%). (F-H) Transmission electron microscopy of the differentiating cerebellum shows disorganized cell arrangements in *pac*-/-R embryos (F, nuclei appear dark, asterisk). Furthermore, adherens junctions are clearly lacking, as shown in the representative image (G). Compare (G) to wild type (H), white arrowhead. Asterisks in (E) show significant differences at ***$p<0.0001$ (Student t test). Values and error bars represent mean ± SD, standard deviation).

These findings indicate that the impairment in directional migration of Cadherin-2 deficient GPCs in *pac*-/-R embryos is not caused by their failure in polarization. Rather this suggests that Cadherin-2 might function earlier, most likely in mediating polarization of GPCs within the URL before onset of GPC migration. It is therefore likely that the loss of GPC polarization in homozygous *pac*R2.10 embryos before onset of migration causes the stationary behavior and thus final mispositioning of GPCs close to their place of origin (see Fig. 3.6D-F for *pac*R2.10 GPC migration behavior).

In contrast to the similar LWRs of wild type and *pac*-/-R GPCs, clear differences could be found by quantifying their orientation angles with respect to a typical anterolateral migration direction for wild type GPCs. In this analysis, the angle between the long axis of a GPC and the AP-axis of the cerebellum was measured. Values were given from 0º to 90º in the positive range, when GPCs were oriented in anterolateral/ posteromedial direction, while negative values from 0º to -90º indicated an aberrant orientation towards anteromedial/ posterolateral directions. The measured angles of individual GPCs were then plotted against their length-width ratios, as shown in the diagram (Fig. 3.10D). Almost all cerebellar GPCs of wild type gata1:GFP transgenic embryos (83%) displayed angles in the positive range from 0º to 90º, thus revealing an orientation towards their future migration direction (Fig. 3.10D, n=58, red dots). Only 17% of wild type GPCs displayed negative values ranging from 0 to -45º, pointing into anteromedial/ posterolateral directions. In contrast, cerebellar GPCs of *pac*-/-R gata1:GFP embryos showed no preference in their orientations with angles, equally covering values in the positive and negative range (Fig. 3.10D, n=66, blue dots). Whereas only 56% of these GPCs displayed angles similar to the majority of wild type GPCs, ranging from 0º and 90º, almost as many (44%) were oriented in the negative range between 0º and -90º.

3.1.7 Loss of Cadherin-2 leads to a randomized positioning of the centrosome in GPCs

Neuronal cells migrate via nucleokinesis, with the centrosome serving as an intrinsic polarity marker that is repositioned in front of the nucleus towards the leading edge during active forward movement of the cell (Gregory et al., 1988) (Solecki et al., 2004) (Tsai et al., 2005) (Higginbotham and Gleeson, 2007). To test whether the oriented migratory behavior of GPCs is influenced by Cadherin-2, 25pg of the expression construct pBSK-1xUASCentrin2-tdTomato was co-injected with 15pg of the activator pCSKalTA4 (unpublished) into wild type and *pac*-/-R gata1:GFP embryos at the 1-cell stage to mark the position of the centrosome in GPCs, after onset of migration. The cerebelli of injected wild type and *pac*-/-R gata1:GFP embryos were scanned by confocal microscopy at 55hpf - 68hpf. To determine the position of the centrosome within GPCs, single optical sections of cerebellar halves were analyzed at individual time points. A rostro-caudal and medio-lateral axis was used to divide individual cells into 4 quadrants. Each of the 4 quadrants was further subdivided, producing a total of 8 sections (Fig.3.11A, B).

Figure 3.10 Length-width ratios and orientation angles of cerebellar GPCs

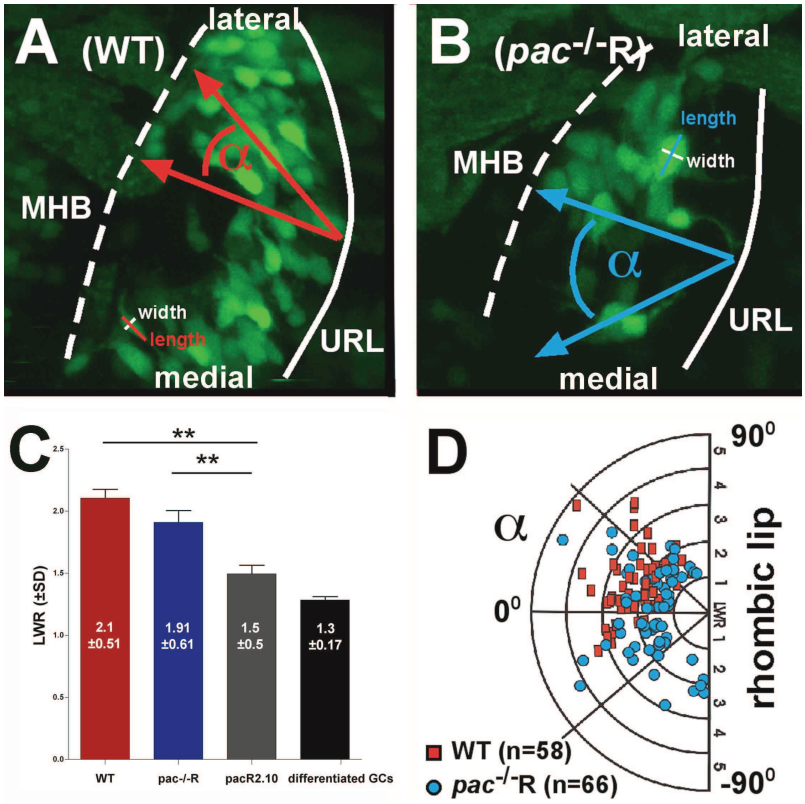

(Fig.3.10) GPCs of temporally rescued *pac*-/-R embryos are polarized but disoriented. (A, B) Confocal projections showing dorsal views of cerebellar halves in wild type gata1:GFP (A) and *pac*-/-R gata1:GFP (B) embryos. The LWRs of cerebellar GFP-expressing GPCs as well as their orientation angles were quantified by measuring the angle between the AP-axis of the cerebellum and the long axis of a GPC, as depicted. (C) The column graph shows LWRs of GPCs in wild type (n=50 cells), *pac*-/-R (n=41 cells), *pac*R2.10 (n=51 cells) and differentiated granule cells of wild type embryos (n=34 cells). The mean LWRs of wild type and *pac*-/-R GPCs indicate that they are polarized in contrast to cerebellar GPCs of *pac*R2.10 embryos and differentiated granule cells of wild type gata1:GFP embryos. (D) Whereas wild type GPCs are preferentially polarized in anterolateral/posteromedial directions (red squares, n=58, between 0° and 90°), GPCs in *pac*-/-R embryos display no preference in polarization being equally oriented towards all directions within the cerebellum (blue dots, n=66, from 0° to 90° and 0° to -90°). Asterisks show significant differences at **p<0.001 (ANOVA). Values and error bars represent mean ± SD, standard deviations). Abbr.: MHB: mid-hindbrain boundary, URL: upper rhombic lip, WT: wild type.

The centrosome position was subsequently determined with respect to these 8 sections. A total of n= 99 cells for wild type and n= 120 cells for *pac*-/-R were analyzed (Fig. 3.11 C, D). In three quarters of all wild type GPCs analyzed (74%, n=72/98) the centrosome was positioned in direction of the MHB, thus being consistent with the typical migratory direction of the GPC. Strikingly, in GPCs of *pac*-/-R embryos the centrosome did not display any favored orientation, as reflected in the almost equal distribution of the

centrosome within Cadherin-2 deficient GPCs. The centrosome in Cadherin-2 deficient GPCs pointed anteriorly towards the MHB in 21% (n=25/120), towards the lateral edge of the cerebellum in 30% (n=36/120), towards the URL in 21% (n=25/120) and towards the midline in 28% (n=34/120) of the analyzed cells. This shows that the directionality defects of migrating cerebellar GPCs in *pac*-/-R embryos are consistent with the randomized positioning of the centrosome within the cell.

Figure 3.11 Randomized centrosomal positioning in GPCs of *pac*-/-R embryos

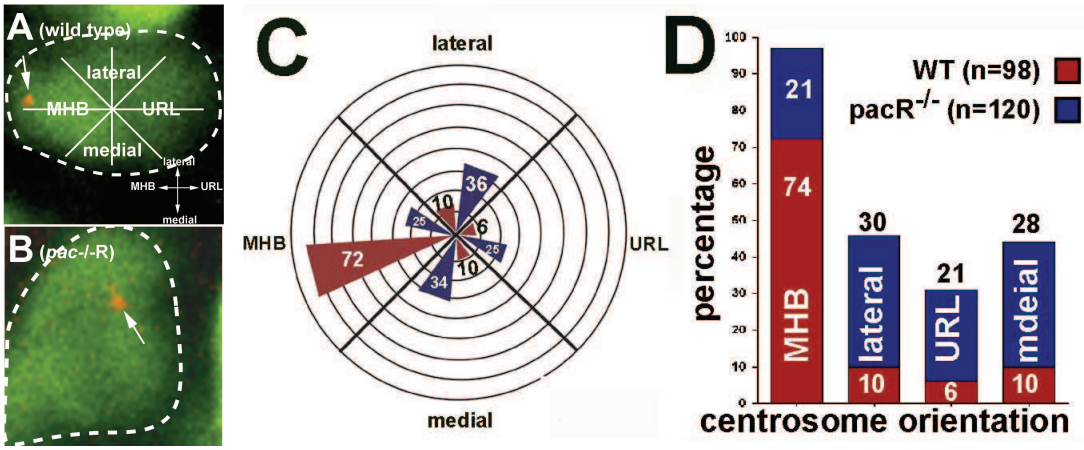

(Fig. 3.11) Quantification of the centrosome position in cerebellar GPCs of wild type and *pac*-/-R gata1:GFP. The centrosome in migrating GPCs of wild type gata1:GFP (A) and *pac*-/-R (B) embryos has been marked by expression of the red fluorescent centrosome localization marker Centrin2:tdTomato (arrows). (A, B) The centrosome position for each cell was determined as depicted (A, see also text). Examples for differently positioned centrosomes are shown. The white dashed line marks the cell soma, while the white arrow marks the centrosome. The centrosome in the GPC of the *pac*-/-R mutant embryo points in posterior direction (B), as compared to the anterior centrosome position in the wild type GPC (A, white arrow). (C, D) The centrosome positions for wild type and *pac*-/-R GPCs were plotted as absolute values in the diagram (C) and as percentages in the column graph (D). While 74% (72 analyzed GPCs) in wild type embryos positioned their centrosome towards the MHB (red bars, n=98), GPCs of *pac*-/-R gata1:GFP embryos did not reveal any preferential centrosome position (C, D, blue bars, n=120).

3.1.8 GPC motility is not affected in the absence of Cadherin-2

To address whether *pac*-/-R derived migrating GPCs solely lack directionality or also display alterations in their migration distances and velocities, migratory cerebellar GPCs of wild type and *pac*-/-R gata1:GFP embryos were analyzed by time-lapse confocal microscopy and cell tracing, using the manual tracking tool plug-in of the ImageJ open source software (NIH). Initially, the linear distance between starting and end time points for GPCs was determined by analyzing a 4-hour migration period. This distance was then

plotted against the angle of migrating GPCs to reveal the migration direction of these cells during 4 hours. This analysis showed that the migration angle of wild type GPCs correlated well with their preferred orientation of polarization and the positioning of the centrosome in anterolateral directions, pointing towards the MHB (Fig. 3.12A, n=30/33, 91%, red dots), whereas cerebellar GPCs in *pac*-/-R embryos randomly migrated throughout the differentiating cerebellum without displaying any preferred direction. In fact, more than one third of the analyzed cells (Fig. 3.12A, n=11/28, 39%, blue dots) demarcated posteriorly to their initial position, which is in good agreement with their aberrant centrosome position in a significant fraction of the analyzed GPCs (Fig. 3.11C, D).

Intriguingly, when the linear distance between starting and end time point of migrating cells was compared, it appeared as if GPCs in wild type gata1:GFP transgenic embryos migrated almost three times as far as their *pac*-/-R counterparts (Fig. 3.12B, 31.2±2.8μm versus 12.9±1.3μm, ***$p<0.0001$). However, the average migratory velocities (Fig. 3.12C, 0.154±0.06μm/min versus 0.141±0.05μm/min) as well as the total length of the migratory tracks (Fig. 3.12D, 26.3±2.5μm versus 22.4±2.1μm) did not differ significantly between wild type and *pac*-/-R GPCs when traced in each time frame of a 4-hour movie. The atypical, often circling routes of migratory GPCs can explain these discrepancies. While GPCs in wild type gata1:GFP cerebelli maintained their initial orientation and migrated almost linearly into anterolateral direction (Fig. 3.8K, L), cerebellar GPCs of *pac*-/-R embryos did not maintain this orientation and instead often changed directions during migration (Fig. 3.8M, N). These findings reveal that the lack of Cadherin-2 does not influence cellular motility but changes polarity and directionality of migratory GPCs.

3.1.9 Cadherin-2 deficient GPCs are misrouted when transplanted into wild type environment

If Cadherin-2 enables migrating GPCs to engage in chain-like structures and to maintain intrinsic polarity, it was expected that Cadherin-2 deficient GPCs will be unable to migrate properly in a wild type cerebellar environment. To address this idea, small groups of cells were transplanted at the sphere stage (3hpf) from wild type gata1:GFP or *pac*-/-R gata1:GFP embryos into wild type hosts of the same developmental stage. The migratory behavior of GFP-expressing cerebellar GPCs was subsequently analyzed by *in vivo* time-lapse imaging, starting at 55hpf.

Figure 3.12 Migrating GPCs in *pac*-/-R embryos lack directionality but not motility

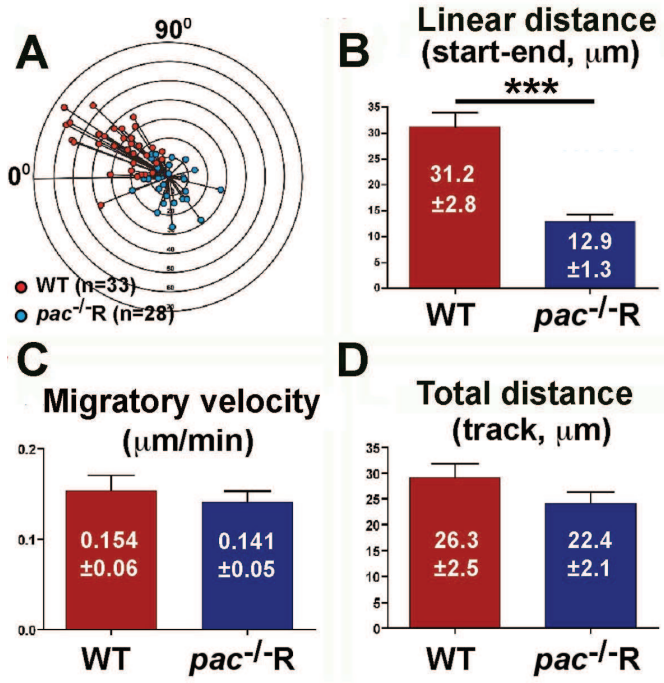

(Fig. 3.12) Comparison of migration distances and migration velocities of wild type and *pac*-/-R gata1:GFP GPCs. (A) The migration angle for GPCs was plotted against the linear migration distance over a time interval of 4 hours (red circles, n=33), showing that the majority of wild type GPCs migrate in anterolateral direction, whereas GPCs of *pac*-/-R embryos migrate randomly without any preferred orientation (blue circles, n=28). (B) The linear distance between starting and end time point of migrating cerebellar GPCs is dramatically reduced in *pac*-/-R embryos (12.9±1.3mm) when compared to the migration distance of wild type GPCs (***$p<0.0001$). (C, D) Nevertheless, when GPCs were traced in individual time frames of a movie the migratory velocities (C) and tracked distances (D) of individual cells did not significantly differ. Values and error bars represent ±SD, standard deviations. Asterisks show significant differences in (B) at ***$p<0.0001$ (Student t test).

GFP-expressing donor cells from wild type gata1:GFP embryos emanated from the URL and migrated in antero-lateral directions (Fig. 3.13A, B) towards the MHB (Supplementary Movie 3.6, n=4). Such donor-derived GPCs were clearly polarized (Fig. 3.13G, LWR 2.22±0.45, n=29) and displayed a directional coherent migratory behavior (Fig. 3.13C), as revealed from cell tracing studies. When their direction was plotted against the distance of migration over a time-period of 4 hours (Fig. 3.13H, n=28, overlay from Fig. 3.12A), the migratory behavior could not be distinguished from non-transplanted GPCs of wild type gata1:GFP transgenic embryos (Fig. 3.13H, n=28, red dots marking non-transplanted and purple dots transplanted GPCs). This demonstrated that wild type donor GPCs migrate similar to non-transplanted GPCs and are not affected by the transplantation procedure.

Next, donor cells from *pac*-/-R gata1:GFP embryos were transplanted into wild type hosts and the migration behavior of cerebellar GPCs subsequently analyzed (Fig. 3.13D, E, Supplementary Movie 3.7, n=4). *Pac*-/-R GPCs also initiated migration after emanating from the URL. Intriguingly however, manually traced cells lacked coherence and directionality of migration, while being clearly polarized similar to non-transplanted Cadherin-2 deficient GPCs in *pac*-/-R embryos (Fig. 3.13G, LWR 1.73±0.36, n=16). This indicated that a wild type cerebellar environment is not capable of rescuing the impaired directional and coherent migration of Cadherin-2 deficient GPCs. In fact, plotting the migration direction of *pac*-/-R donor GPCs against their distance of migration after 4 hours revealed that their migratory behavior was indistinguishable from that of non-transplanted Cadherin-2 deficient GPCs (Fig. 3.13H, green dots, overlay from Fig. 3.12A).

Interestingly, not all mutant donor GPCs were capable of migrating far from the URL in a wild type environment. A reason for this may be that low amounts of Cadherin-2 protein are still present in transplanted embryos at 48hpf due to the temporal rescue of *pac*-/-R embryos (Fig. 3.7M black arrow). Thus, the initially proper onset of migration of mutant donor GPC from the URL in a wild type host environment could be attributed to residual Cadherin-2 levels remaining in the mutant donor cells. In contrast, cells that became stationary close to the URL likely had already lost Cadherin-2 protein before or during onset of migration.

To validate this hypothesis, a dominant-negative variant of zebrafish Cadherin-2, termed Cdh2ΔN (Suppl. Fig. 4B) (Jontes et al., 2004), was fused to the red fluorescent protein mCherry (Shaner et al., 2004). Subsequently, this variant was expressed under control of an oligomerized heatshock consensus sequence (Bajoghli et al., 2004) to drive transient expression after onset of GPC migration by means of increasing the environmental temperature. The plasmid pBSK8xHSE:Cdh2ΔN-mCherry (70pg) was injected into single cell stage gata1:GFP-embryos and Cadherin-2 function was abolished in a mosaic manner by two repeated 1-hour heatshocks at 40°C at 48hpf and 51hpf. Two hours after heatshock application, strong red fluorescent cells were observed inside the URL (Fig. 3.13I, white asterisks) and chosen for subsequent *in vivo* time-lapse analysis, as they contained high levels of dominant-negative Cadherin-2 and thus were likely to be fully deprived of functional Cadherin-2. These fluorescent URL cells were clearly polarized, showing a mean LWR of 1.99±0.56 (Fig. 3.13G, n=18) and oriented in an antero-lateral direction towards the MHB. Nevertheless they never engaged into chains of

migrating GPCs that emanated from the URL in their vicinity (Fig. 3.13I-K, GPCs marked with yellow or blue dots, Supplementary Movie 3.8, n=4).

Figure 3.13 Genetic mosaic analysis and expression of Cadherin-2 deletion variants

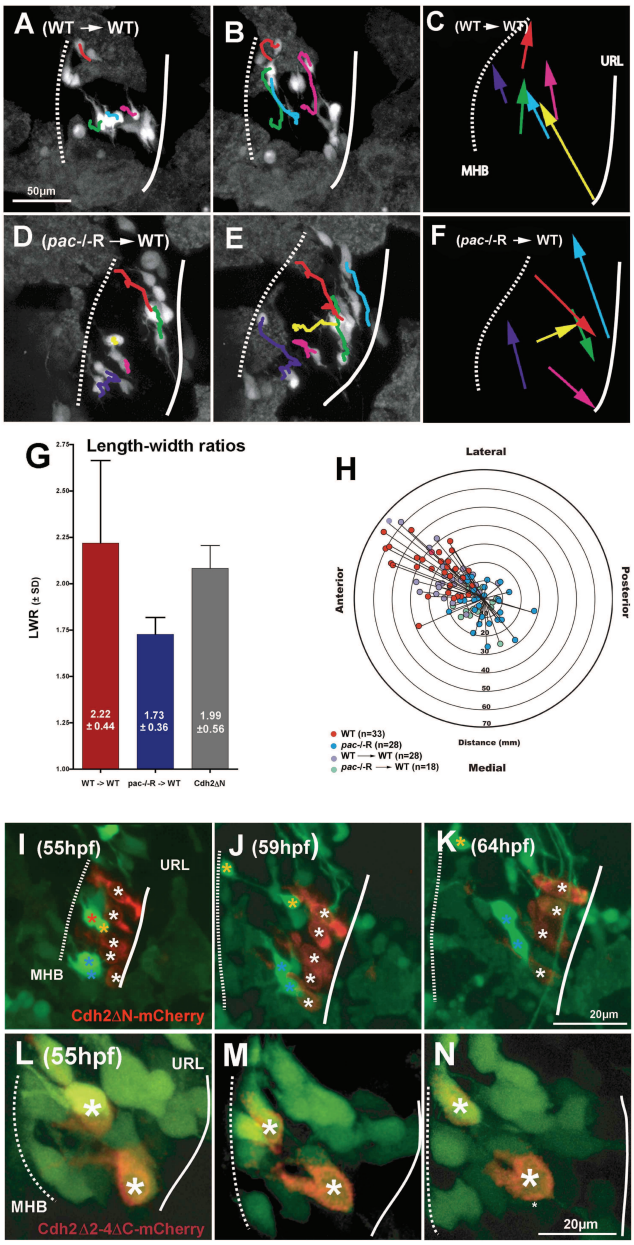

(Fig. 3.13) (A-H) Cadherin-2 deficient GPCs fail to migrate properly in a wild type environment. (A, B and D, E) Maximum intensity projections (dorsal view) from individual time points of *in vivo* time-lapse analysis showing transplanted wild type (A, B) and *pac*-/-R (D, E) gata1:GFP donor GPCs in wild type host cerebelli. (A-C and G) GFP-expressing GPCs of wild type donors are clearly polarized when transplanted into wild type hosts (G, red column, n=29) with GPCs migrating in a directional and coherent manner as indicated by their individual tracks (C, see also Supplementary Movie 3.6). (D-F and G) In contrast, cerebellar GPCs derived from *pac*-/-R gata1:GFP donors, although being polarized (G, blue column, n=16) migrate in a non-directional

manner within wild type host cerebelli, as indicated by their tracks (F, see also Supplementary Movie 3.7). (H) Plotting the migration distance of donor GPCs against their directions (wild type: purple dots, n=28 and *pac*-/-R: light green dots, n=18) reveals that wild type and Cadherin-2 deficient donor cells do not differ in their migration routes from non-transplanted GPCs (WT: red dots and *pac*-/-R: dark blue dots, overlay from Fig. 3.12A), with mutant donors also exhibiting a randomized migration behavior. (I-N) Maximum intensity projections (dorsal view) from individual time points of *in vivo* time-lapse movie starting at 54hpf, showing cerebellar GPCs of gata1:GFP embryos. Transient expression of a dominant-negative Cadherin-2 variant fused to monomeric cherry Cdh2ΔN-mCherry (I-K) and a non-functional Cadherin-2 variant Cdh2Δ2-4ΔC-mCherry (L-N) is achieved by a heatshock-inducible promoter element. (I-K) Cells inside the URL strongly express the dominant-negative variant after heatshock activation, as indicated by their strong red fluorescence (white asterisks). Such URL-cells are normally polarized (G, gray column, n=6), despite the lack of Cadherin-2 activity. These cells however remain inside the URL and fail to join neighboring GPCs, engaging in chain-like migration (GFP-expressing GPCs marked by yellow and blue dots, see Supplementary Movie 3.8). (L-N) In contrast, control GPCs, expressing a non-functional Cadherin-2 variant activate GFP-expression and migrate away from the URL towards the MHB along co-migratory GPCs (asterisks) (see Supplementary Movie 3.9). Abbr.: MHB: mid-hindbrain boundary, URL: upper rhombic lip, WT: wild type.

Moreover, URL cells expressing this dominant-negative Cadherin-2 variant did never activate GFP-expression. Recently, it was shown that onset of GFP expression in GPCs of the gata1:GFP line is linked to their onset of migration and differentiation (Volkmann et al., 2007). These findings suggest that GPCs expressing the dominant-negative Cadherin-2 variant are incapable to emanate from the upper rhombic lip and initiate differentiation.

In contrast to the expression of this dominant-negative variant, expression of 70pg of a non-functional control Cadherin-2 deletion variant (see below and Suppl. Fig. 4D), having ectodomains 2-4 deleted and termed Cdh2Δ2-4ΔC-mCherry, did not affect the onset of migration and differentiation, as revealed by GFP co-expression in these GPCs (Fig. 3.13L-N, white asterisks, Supplementary Movie 3.9, n=5). These findings show that heatshock conditions and expression of the mCherry fusion protein *per se* does not alter the differentiation program of cerebellar GPCs and their migration. Rather these findings suggest that Cadherin-2 is essential for proper onset of GPC migration within the URL. Thus, the absence of Cadherin-2 results in the inability of GPCs to join cohorts of migrating cells in their vicinity.

3.1.10 Granule cells begin to differentiate despite impaired directional migration

Rhombic lip-derived cells in the cerebellum of gata1:GFP transgenic embryos differentiate into cerebellar granule cells (Volkmann et al., 2007). To examine whether impaired directional migration of GPCs in *pac*-/-R embryos affects granule cell

differentiation, several granule cell-specific differentiation markers were analyzed for their expression at different developmental stages. At 3dpf *neuroD* was found strongly expressed in the cerebellum in both wild type (Fig. 3.14A) and *pac*-/-R embryos (Fig. 3.14B). However in the latter *neuroD* expression appeared patchy and non-homogeneously scattered throughout the dorsal cerebellum.

Figure 3.14 Expression patterns of granule cell differentiation markers in the wild type and *pac*-/-R cerebellum

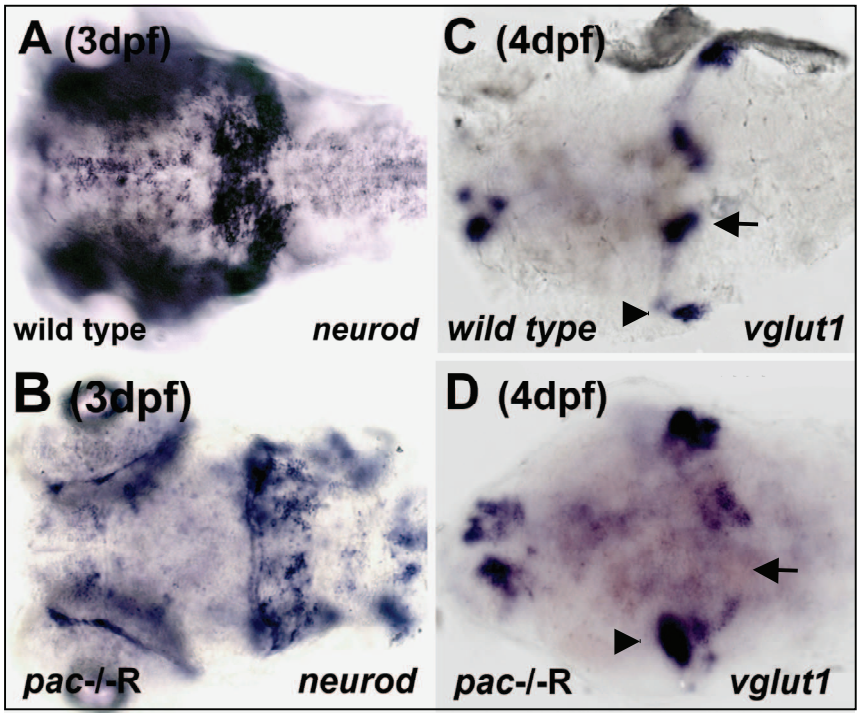

(Fig. 3.14) Migrating GPCs deprived of Cadherin-2 continue to differentiate. (A-F) Dorsal views of WT (A, C) and *pac*-/-R (B, D) embryos after *in situ* hybridization for cerebellar differentiation markers *neuroD* (A, B, 3dpf) and *vglut1* (C, D, 4dpf). The ectopic expression of *neuroD* in *pac*-/-R embryos likely reflects the positioning of misrouted GPCs in these embryos. While *neuroD*-expression in the cerebellum of *pac*-/-R embryos is initiated at similar levels as in wild type embryos, expression of the terminal differentiation marker *vglut1* is strongly reduced in dorsal cerebellar domains of *pac*-/-R embryos (compare C and D, arrows), while ventral clusters are present (compare C and D, arrowheads).

This finding indicated that despite the lack of migratory directionality and coherence, neuronal differentiation of GPCs is properly initiated in *pac*-/-R embryos. One day later, expression domains of the *vesicular glutamate transporter 1* (*vglut1*) was detected in cerebellar granule cells of *pac*-/-R embryos, however being strikingly smaller, at aberrant

positions and lacking the two prominent medio-dorsal clusters (Fig. 3.14D, black arrows) when compared to the *vglut1* expression domains in wild type embryos (Fig. 3.14C).

While this indicated that GPCs continue to differentiate into cerebellar granule neurons in *pac*-/-R embryos, their maintenance may be affected in dorsal regions of the cerebellum due to the mispositioning. This was supported by the complete absence of *vglut1* (Fig. 3.15) and $gaba_A$ *receptor alpha6* subunit ($gaba_AR\alpha6$) (Fig. 3.16) expression in dorsal regions of the cerebellum in *pac*-/-R embryos at 6dpf. The $gaba_AR\alpha6$ subunit is a highly conserved terminal and specific cerebellar granule neuron marker (Bahn et al., 1996) (Volkmann et al., 2007).

The small remaining patches of $gaba_AR\alpha6$ expression in more ventrolateral regions in the cerebellum of *pac*-/-R embryos (Fig. 3.16B, D, black arrows) may be due to the fact that ventral populations, such as GPCs of the eminentia granularis are affected to a lesser extent by the loss of Cadherin-2. This is in good agreement with the cell tracing experiments (Fig. 3.6, F blue dashed circle and Supplementary Movie 3.3) and previous observations, showing that homozygous *pac*R2.10 mutants exhibit more severe defects in dorsal regions of the CNS (Lele et al., 2002).

Consistent with the gene expression results showing the loss of cerebellar granule neurons in dorsal cerebellar domains of *pac*-/-R embryos, only few GFP-expressing cells could be detected by confocal microscopy in the cerebellum of *pac*-/-R gata1:GFP embryos at 6dpf (Fig. 3.17B), as compared to the large numbers found in wild type gata1:GFP embryos (Fig. 3.17A). This absence suggested that dorsal granule cells might undergo cell death. To support this idea, wild type and *pac*-/-R cerebelli were analyzed by acridine orange staining to visualize cell death in living embryos. For this, embryos were soaked in acridine orange solution for 20 minutes, thus allowing dead cells to incorporate the dye, which then binds to the DNA. Individual cerebelli of wild type and *pac*-/-R embryos were subsequently analyzed by confocal microscopy at 4 and 5dpf. This is the time point when differentiated granule neurons start to disappear in dorsal cerebellum. While the increase in cell death was minimal in the dorsal cerebellum of wild type embryos between 4 and 5dpf (Fig. 3.17C, E, n=10 embryos, 2.0 ±2.0 vs. 7.85 ±3.891), *pac*-/-R embryos showed a significant increase (Fig. 3.17D, n=8 embryos, 4dpf: 13 ±1.826 vs. 5dpf: 34.5 ±6.191, ***$p<0.0001$), which was about five times higher than that found in wild type embryos ($p<0.0001$).

Figure 3.15 Absent expression of *vglut1* in the dorsal cerebellum of *pac*-/-R embryos at 6dpf

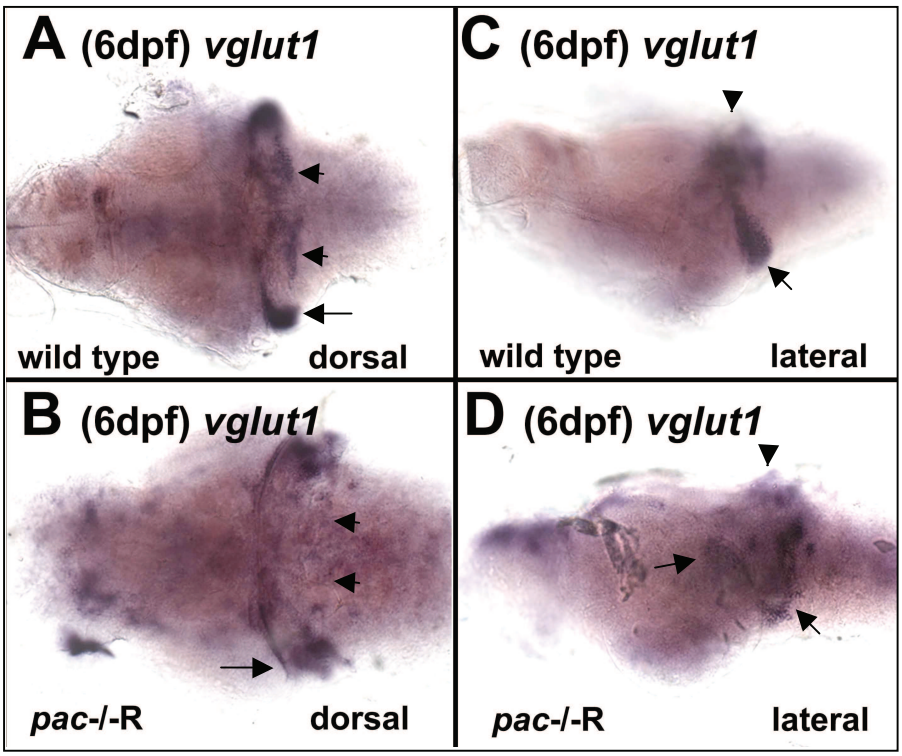

(Fig. 3.15) Granule cells fail to terminally differentiate in the dorsal cerebellum of *pac*-/-R embryos. The expression of *vglut1* in wild type (A, C) and *pac*-/-R (B, D) embryos is shown at 6dpf. (A, C) Dorsal (A) and lateral (C) views of wild type brain showing *vglut1* expression in anteriorly located medio-lateral stripes along the MHB and in posterior stripes along the URL. *vglut1* is further expressed in ventrolateral domains of the cerebellum (C, arrow). (B, D) Expression of *vglut1* in the dorsal cerebellum of *pac*-/-R brains is lacking (compare B, D, arrowheads to wild type A, C, arrowheads), while ventral clusters fail to condense (B, D, arrows compare to A, C, arrows).

In contrast, no significant differences between wild type and *pac*-/-R embryos could be detected using TUNEL assay or activated caspase-3 staining at 4, 5 and 6dpf (not shown), suggesting that the observed cell death is not mediated by apoptotic pathways. Currently, it cannot be excluded that the observed increase in cell death in the dorsal cerebellum of *pac*-/-R embryos may be caused by a general decline in health, including the lack of proper blood supply by misrouted blood vessels. Quantum dot 605-injection into the heart ventricle, which allows for the staining of the vascular system (Rieger et al., 2005), revealed however that blood vessels are present in the dorsal cerebellum of *pac*-/-R embryos although appearing irregularly formed (not shown). Furthermore, *pac*-/-R mutants die only later than 7dpf, and therefore the lack of blood supply is likely not responsible for the early increase in cell death, which increases already between 4 and 5dpf. Thus, these

findings suggest that the maintenance of granule cells in the dorsal cerebellum of *pac*-/-R embryos is affected due to failures in proper migration.

Figure 3.16 Expression of $gaba_A R\alpha 6$ is absent in the dorsal cerebellum of *pac*-/-R embryos at 6dpf

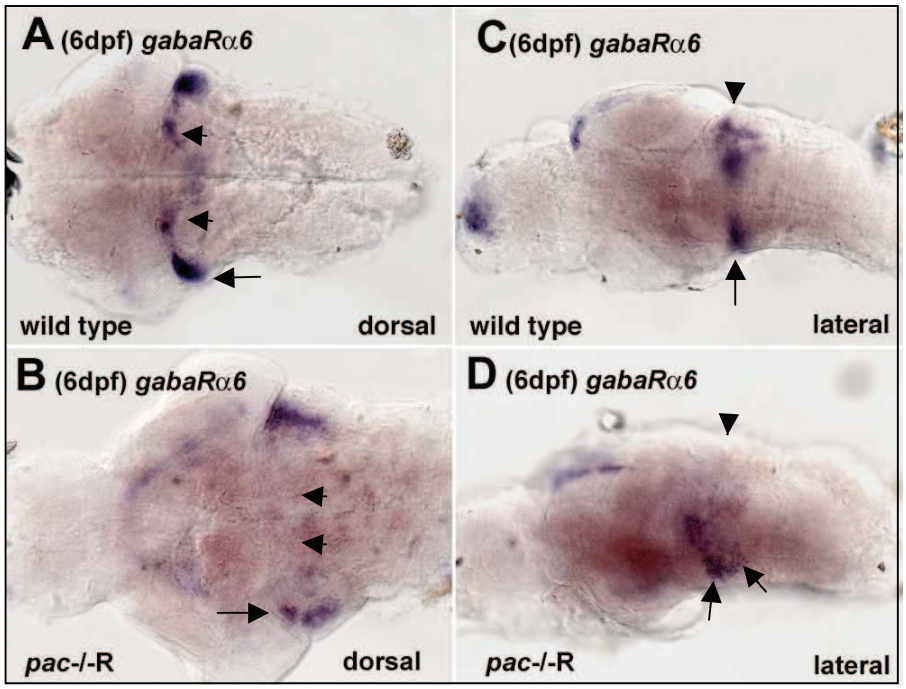

(Fig. 3.16) The absence of $gaba_A R\alpha 6$ expression in the dorsal cerebellum of *pac*-/-R embryos is consistent with lacking *vglut1*-positive cells in this domain. (A, C) Wild type $gaba_A R\alpha 6$-expression at 6dpf is found in medio-lateral stripes along the MHB (A) and in ventral clusters (C, arrow). In contrast, $gaba_A R\alpha 6$-expression in the dorsal cerebellum of *pac*-/-R is missing (compare B, D, arrowheads with A, C, arrowhead) while ventral clusters appear less condensed (compare B, D, arrows to A, C, arrows).

3.1.11 Construction of Cadherin-2 deletion variants to monitor Cadherin-2 localization within migrating GPCs

To address the localization of Cadherin-2-containing adherens junctions in migrating cerebellar GPCs of gata1:GFP embryos, several Cadherin-2 deletion variants were generated and tested in serving as an effective adhesion reporter. First, full-length Cadherin-2 (Cdh2) and dominant-negative Cadherin-2 (Cdh2ΔN) were ectopically expressed by injection of 70pg mRNA into 1-cell stage embryos. This resulted in severe malformations of the hindbrain, as indicated by gene expression analysis of *atonal1a* at 24hpf (Fig. 3.18).

Figure 3.17 Increased neuronal cell death in *pac*-/-R embryos

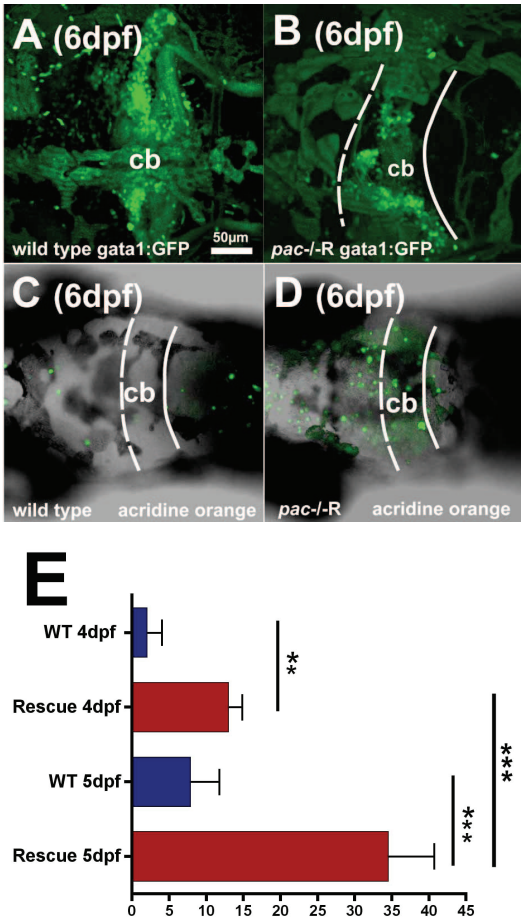

(Fig. 3.17) (A-D) Maximum intensity projections of 100μm confocal stacks showing a dorsal view of the cerebellum. (A, B) Comparison of wild type (A) and *pac*-/-R (B) gata1:GFP cerebelli indicates that the number of GFP-expressing GPCs in the rescued mutants is severely reduced in dorsal domains (n=6 embryos). (C, D) This is consistent with the increased cell death in this domain in *pac*-/-R embryos, as visualized by acridine orange staining. (E) The amount of cell death in the cerebellum of *pac*-/-R embryos significantly increases with continuing granule cell differentiation (WT, 4dpf: 2.0 ±2.0 vs. 5dpf: 7.85 ±3.89 and *pac*-/-R, 4dpf: 13 ±1.82 vs. 5dpf 34.5 ±6.19, ***p<000.1). Asterisks indicate significant differences at ***p<0.0001 and **p<0.01. Statistical values and error bars are represented as mean ± SD, standard deviations (Student t test).

To construct a Cadherin-2 deletion variant that does not exert phenotypes when ectopically expressed, several aspects needed to be considered. Classic Cadherins possess two important evolutionary highly conserved structural features in the first ectodomain, a tryptophane residue at amino acid position 2 and a motif containing the three conserved amino acid residues His-Ala-Val (HAV). Both features have been shown to be necessary for strand and trans dimer formation of classic type I Cadherins (Williams et al., 2000, Kim et al., 2005). Furthermore, alanine 80 lines a hydrophobic acceptor pocket for tryptophane 2 of a second Cadherin-2 monomer and has also been proposed to be involved in trans-

dimer formation. In addition to these structural functions of the ectodomains, the cytoplasmic domain has an important signaling role in the crosstalk with other intracellular pathways. Thus, two Cadherin-2 deletion variants were constructed that were expected to be non-functional when ectopically expressed, as both constructs are missing important structural features, necessary for dimer formation. In one construct, termed Cdh2Δ1-3ΔC, ectodomains 1-3 and the cytoplasmic domain, except for 6 amino acids following the transmembrane domain, were deleted (Suppl. Fig. 3C). In a second construct, termed Cdh2Δ2-4ΔC, the cytoplasmic domain and ectodomains 2-4 were deleted, leaving the first ectodomain intact, which was fused to the C-terminal end of ectodomain 4 (Suppl. Fig. 3D). The remaining cytoplasmic tail of both variants was fused at its C-terminus to the fluorescent reporter monomeric Cherry (mCherry). Both constructs were expected to exert weak cis and trans dimer formation, while lacking intracellular signaling properties.

To ectopically express both variants, ~70pg of mRNA was injected into 1-cell stage zebrafish embryos. The phenotypes were monitored by *atonal1a* staining at 24hpf. Expression of Cdh2Δ1-3ΔC-mCherry resulted in severe phenotypes such as split axes and neurulation defects (Fig. 3.18D), while the expression of Cdh2Δ2-4ΔC-mCherry revealed no malformations of the differentiating cerebellum, when the URL was examined by *atonal1a* staining (Fig. 3.18E) and when the morphology of injected embryos was analyzed at 24hpf (Compare embryos in A, B injected with Cdh2Δ1-3ΔC-mCherry to C, D injected with Cdh2Δ2-4ΔC-mCherry). While only 15% of Cdh2Δ1-3ΔC-mCherry injected embryos revealed a morphological appearance comparable to wild type, 30% were severely malformed and 55% died during the first 24 hours. In contrast, 80% of Cdh2Δ2-4ΔC-mCherry-injected embryos appeared normal and only 9 and 11% were either malformed or dead, respectively (Fig. 3.18F). Furthermore, the Cdh2Δ2-4ΔC-mCherry variant was unable to rescue *pac*-/-R embryos (0/36) when mRNA was injected into *pac*R2.10 mutants. This indicated that this variant lacked wild type functionality.

To reveal the subcellular localization of Cdh2Δ2-4ΔC-mCherry, which was expected to be present along cellular contacts, mRNA-injected embryos were counterstained with Bodipy Ceramide to fluorescently outline cytoplasmic membranes. Analysis by confocal microscopy revealed a punctate appearance of Cadherin-2 clusters along contact sites of cerebellar rhombic lip cells at 24hpf (Fig. 3.19E, arrow).

Figure 3.18 *Atonal1a* expression analysis in embryos injected with different Cadherin-2 variants

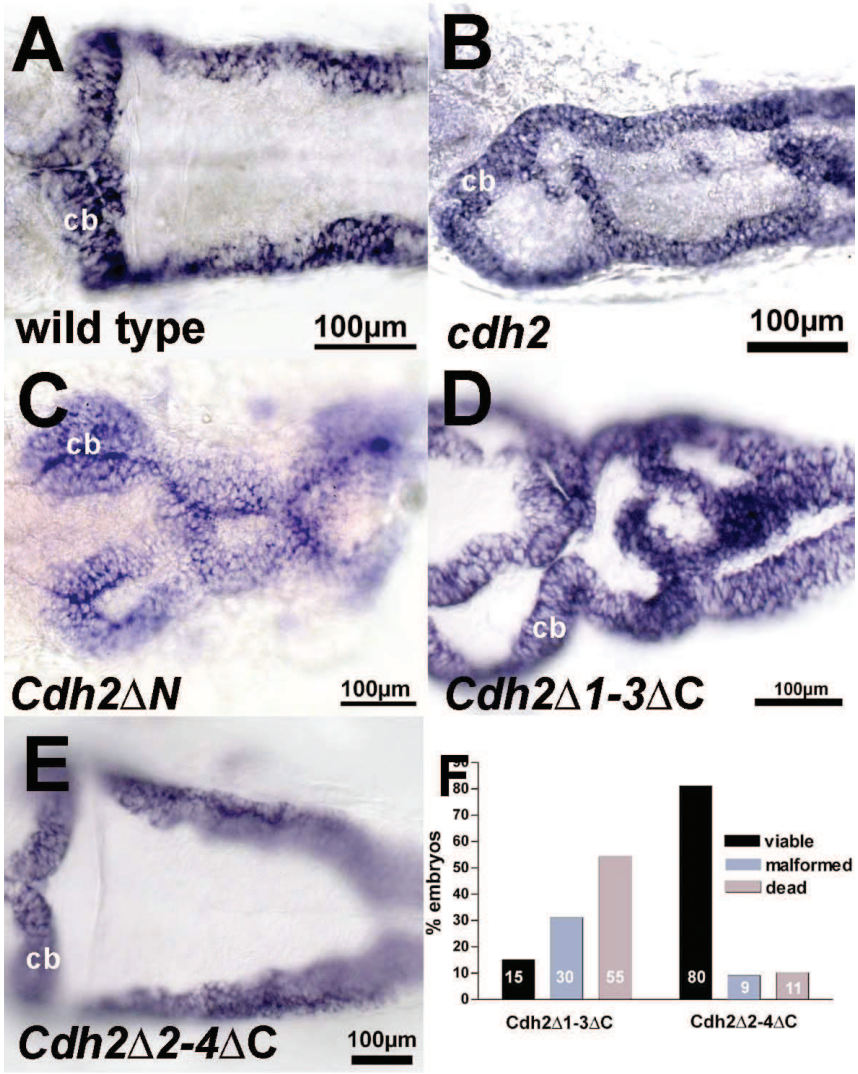

(Fig. 3.18) (A-E) Dorsal views of the zebrafish hindbrain at 24hpf. Embryos injected with different Cadherin2 variants showing *atonal1a* gene expression after *in situ* hybridization. (A) Wild type *atonal1a* staining marks the rhombic lip. (B-D) Ectopic expression of full-length Cadherin-2 (B), dominant-negative Cadherin-2 (C) and Cdh2Δ1-3ΔC-mCherry (D) results in severe hindbrain malformations. (E) In contrast, embryos ectopically expressing the non-functional Cadherin-2 variant Cdh2Δ2-4ΔC-mCherry show wild type appearance (E). (F) Column graph showing percentages of viable, malformed and dead embryos injected either with Cdh2Δ1-3ΔC or Cdh2Δ2-4ΔC-mCherry.

To further validate that this variant co-localizes with full-length Cadherin-2 fused to GFP, termed Cdh2:GFP, 100ng/μl plasmid DNA was co-electroporated with 100ng/μl Cdh2Δ2-4ΔC-mCherry into cells located within the URL. Both proteins co-localized within the cell (Fig. 3.19G-H), showing a clustered appearance rather than being uniformly distributed throughout the cytoplasm, thus suggesting that this deletion variant is recruited

to sites within the cell where wild type Cadherin-2 is localized. These findings show that Cdh2Δ2-4ΔC-mCherry is useful to monitor Cadherin-2-containing adherens junctions in migrating cerebellar GPCs.

Figure 3.19 Cdh2Δ2-4ΔC-mCherry can serve as *in vivo* reporter for adherens junctions

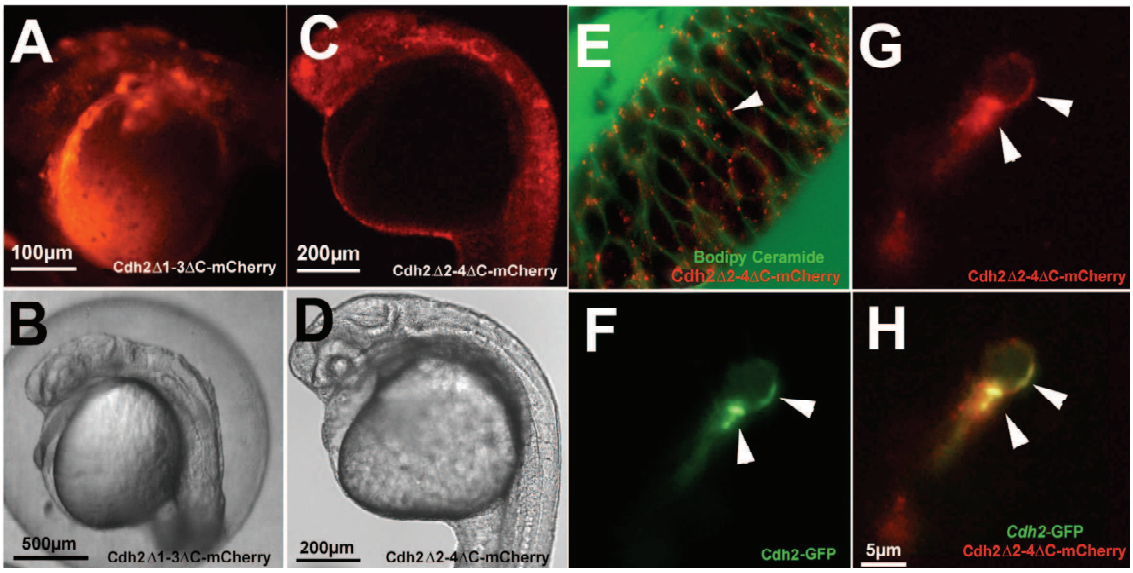

(Fig. 3.19) (A-D) Morphology of embryos expressing Cdh2Δ1-3ΔC-mCherry (A. B) and Cdh2Δ2-4ΔC-mCherry (C, D) at 24hpf after mRNA injection. All images show lateral views. Fluorescent images (A, C) and corresponding transmitted light images (B, D) reveal a strong phenotype evoked by ectopic expression of Cdh2Δ1-3ΔC-mCherry (A, B) and embryos with wild type appearance expressing Cdh2Δ2-4ΔC-mCherry (C, D). (E) Single optical section of the cerebellar primordium at 24hpf revealing a clustered localization of Cdh2Δ2-4ΔC-mCherry (red) along plasma membranes that have been counterstained with Bodipy Ceramide (green). (G-H) Single 1μm optical sections of a cerebellar cell co-electroporated with Cdh2Δ2-4ΔC-mCherry and Cdh2-GFP plasmid DNA. The red-fluorescent Cadherin-2 deletion variant (G) co-localizes with green-fluorescent full-length Cdh2-GFP protein (F) as shown in the overlay of both images (H). Both fusion proteins co-localize to clusters in the anterior cell compartment (lower arrowhead) and along one lateral wall (upper arrowhead).

3.1.12 GPCs dynamically relocate Cadherin-2 clusters during forward migration

To reveal the subcellular dynamics of Cadherin-2 in migrating GPCs, 70pg of the deletion variant Cdh2Δ2-4ΔC-mCherry was injected as heatshock-inducible plasmid into single cell stage embryos of the gata1:GFP transgenic line for transient expression after onset of GPC migration, thus serving as fluorescent adhesion reporter within migrating GPCs. Expression of this variant was activated by two repeated 1-hour heatshocks at 40°C at 48 and 51hpf, resulting in a high frequency of GPCs, co-expressing GFP and Cdh2Δ2-4ΔC-mCherry.

Double-fluorescent GPCs were subsequently followed by *in vivo* time-lapse confocal analysis at high magnification (Fig. 3.20A inset, migration of a red fluorescent GPC marked with white arrowhead is being followed in B-F, see Supplementary Movie 3.10, n=4). This showed that Cadherin-2 clusters are dynamically shifted within GPCs during migration. In the cell represented in Fig. 3.20, the majority of Cadherin-2 clusters are initially located at the leading edge (Fig. 3.20B, arrowheads) but re-locate to the rear end (Fig. 3.20C, arrowheads) and along one lateral wall as the cell moves (Fig. 3.20D, dashed box, arrowhead) as the cell contacts another co-migrating GPC (Supplementary Movie 3.10). Subsequently, these clusters slowly diminished at the rear (Fig. 3.20E yellow arrowhead) and are finally found in the anterior of the cell again (Fig. 3.20F, arrowheads). These findings suggest that Cadherin-2-mediated adherens junctions are dynamically reorganized in migrating GPCs.

3.1.13 Directed relocation of Cadherin-2 within the cell membrane

In order to understand how the dynamic re-positioning of Cadherin-2 clusters is regulated within migrating GPCs, mCherry of the Cadherin-2 deletion construct Cdh2Δ2-4ΔC was replaced by the UV-convertible fluorescent protein dEosFP. This photo-convertible fluorescent protein behaves as pseudo-monomer by homo-dimerization (Wiedenmann et al., 2004). To test the functionality of the fusion construct, PAC2 zebrafish fibroblast cells, also expressing endogenous Cadherin-2, were first transfected with 1μg Cdh2Δ2-4ΔC-dEosFP to analyze Cadherin-2 dynamics in cell culture. By using region-of-interest (ROI) excitation, a short UV-laser pulse was applied for 3 seconds to a small portion of Cdh2Δ2-4ΔC:dEosFP located at the plasma membrane. Cadherin-2 dynamics were subsequently followed within these cells (see Supplementary Movie 3.11, n=3). Immediately after conversion, the converted Cdh2Δ2-4ΔC:dEosFP diffused in the cytoplasm of lamellopods and disappeared within 1-2 minutes (Supplementary Movie 3.11, white arrowhead). When a second region was subsequently converted at a different site it appeared as if Cadherin-2 clusters were transported away from filopods in a microtubule dependent manner (Supplementary Movie 3.11, white arrow). These findings suggested that Cadherin-2 clusters are dynamically transport in living zebrafish cells.

To test whether cerebellar GPCs utilize a directed transport of Cadherin-2 in order to relocate adherens junctions during migration, 70pg of plasmid DNA of the heatshock-inducible and photo-convertible Cdh2Δ2-4ΔC:dEosFP was injected into 1-cell stage

zebrafish gata1:GFP embryos and activated at 51hpf. A short UV-laser pulse of 3sec was subsequently applied to a small region at the cell membrane using ROI, to convert Cdh2Δ2-4ΔC:dEosFP from green to red emission at the plasma membrane of migrating GPCs at 55hpf.

Figure 3.20 Cdh2Δ2-4ΔC-mCherry dynamics in migrating cerebellar GPCs

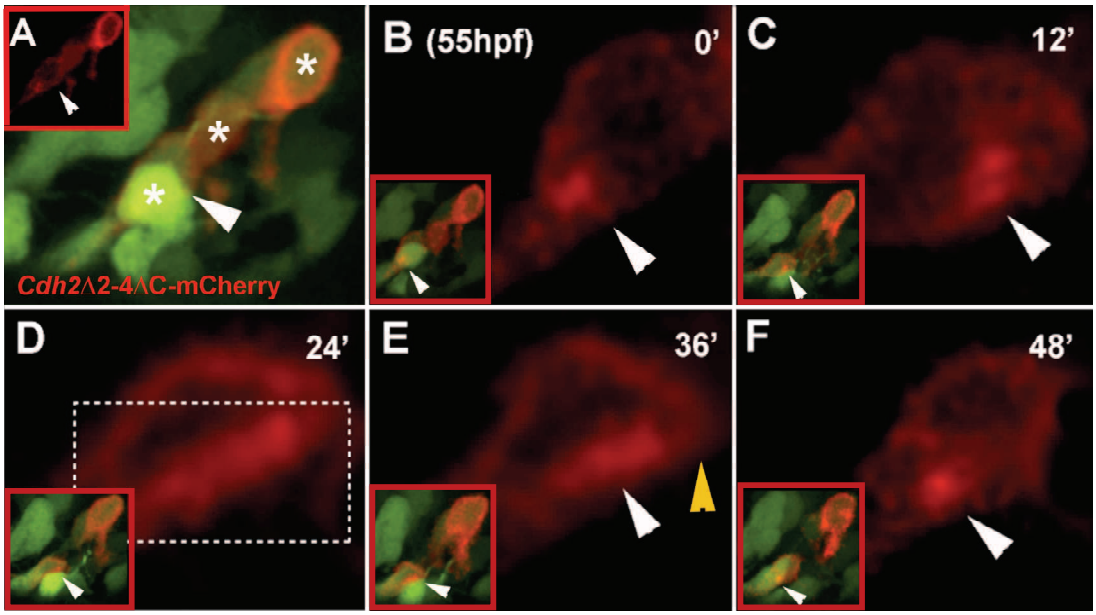

(Fig. 3.20) Cadherin-2 clusters are dynamically repositioned in migrating GPC. (A-F) Projections of 12μm stacks of a time-lapse movie showing heatshock-induced expression of the Cdh2Δ2-4ΔC-mCherry fusion protein in cerebellar GPCs of gata1:GFP embryos at 55hpf (white asterisks, see also insets and Supplementary Movie 3.10). (B-F) The cell marked by a white arrowhead in A is displayed at high magnification. (B) In preparation of a forward moving step most of Cdh2Δ2-4ΔC-mCherry is located at the leading edge of the cell (white arrowhead). (C) During cell movement Cdh2Δ2-4ΔC-mCherry clusters appear first in the rear (white arrowhead) and then along the lateral wall of the cell where it remains contact to a neighboring cell (D, E), while Cdh2Δ2-4ΔC-mCherry is released from the trailing edge (yellow arrowhead) as the contact is released. Cadherin-2 clusters are again found in the leading edge (F, white arrowhead).

The behavior of small clusters, containing photo-converted Cdh2Δ2-4ΔC:dEosFP (Fig. 3.21A-F, white arrowheads and Supplementary Movie 3.12, n=3) was subsequently analyzed by *in vivo* time-lapse imaging. During forward movement of the GPC, a photo-converted Cadherin-2 cluster remained strictly within the plasma membrane and was successively transported towards the leading edge during an interval of 25min (note the transport of Cadherin-2 clusters along the base of the neurite, Fig. 3.21D-F, arrows). These observations suggest that the dynamic establishment of cell-cell adhesion during zebrafish

cerebellar GPC migration is achieved by the translocation of Cadherin-2 within the cell membrane.

Figure 3.21 Directed relocation of Cadherin-2 clusters within the cell membrane

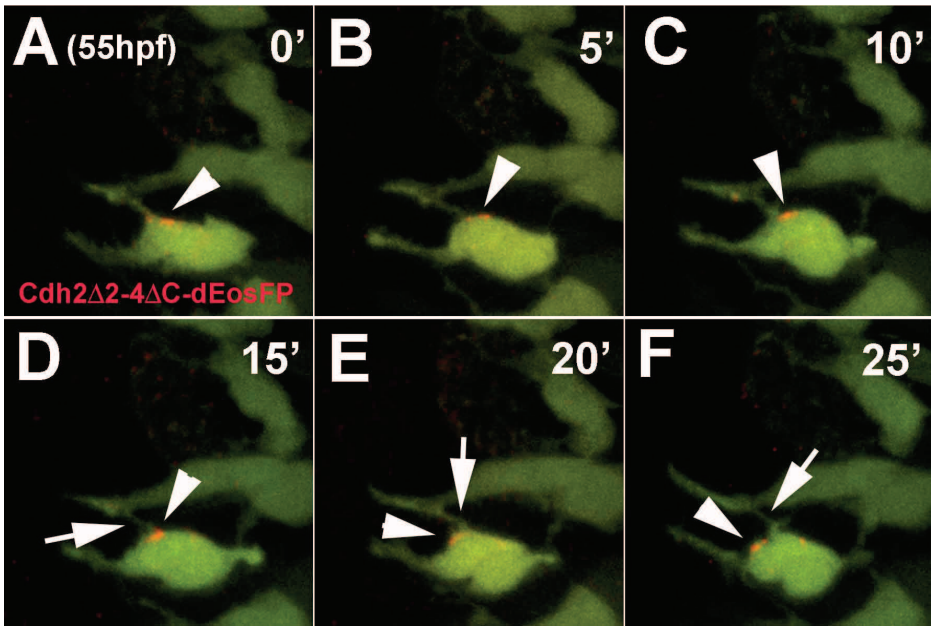

(Fig. 3.21) Cadherin-2 cluster relocates towards the leading edge of a cerebellar GPC. (A-F) *In vivo* time-lapse confocal microscopy showing projections of 10μm stacks recorded every 5 minutes. Clusters of Cdh2Δ2-4ΔC:dEosFP protein after UV-light conversion from green to red fluorescence emission (marked by white arrowheads) move in anterior direction. During forward movement of the GFP-expressing GPC, a Cadherin-2 cluster moves successively towards the leading edge and thereby passes along the base of a neurite (D-F, white arrows). See also Supplementary Movie 3.12.

Taken together, these findings show that Cadherin-2 is an important mediator of the coherent and directional migration of cerebellar GPCs along chains. Such a migratory behavior requires the constant reorganization of adherens junctions within cells, which could be shown to be achieved by the dynamic translocation of Cadherin-2 inside the plasma membrane.

3.2 PSA-NCAM

3.2.1 Cloning of the zebrafish polysialyltransferases STX and PST

Polysialylated NCAM (PSA-NCAM) has been implicated in the control of neuronal migration during mammalian nervous system development (Murakami et al., 2000, Marx et al., 2001, Ulfig and Chan, 2004). However, in zebrafish the role of PSA-NCAM in the regulation of neuronal progenitor migration remained unclear. Polysialylation of NCAM occurs through enzymatic addition of α2,8-linked sialic acid residues on NCAM by two known polysialyltransferases, St8sia2 (STX) and St8sia4 (PST). To analyze the expression of STX and PST in the differentiating zebrafish cerebellum, where neuronal migration is especially pronounced, and in the adult brain during ongoing neurogenesis, the full-length cDNAs of both polysialyltransferases were cloned. Specific primers were designed (see 2.1.9) from previously published sequences (Harduin-Lepers et al., 2005, Marx et al., 2007) and both full-length cDNAs were amplified via RT-PCR from 54hpf zebrafish embryos. The obtained cDNAs were further subcloned via TA cloning into pCRIITOPO and sequenced (see Supplementary Fig. 4 for sequences).

Both zebrafish polysialyltransferases are type II membrane proteins, containing three important structural features (Marx et al., 2007), that have been identified as large (L), small (S) and very small (VS) sialylmotifs (Harduin-Lepers et al., 2005). Sequence homology analysis revealed a high evolutionary conservation of all three motifs among zebrafish and other vertebrate species (Fig. 3.22). These motifs are moreover highly conserved between both polysialyltransferases (>70%), suggesting a similar enzymatic activity.

3.2.2 Polysialyltransferase expression in the developing zebrafish central nervous system

The two polysialyltransferases STX and PST are key enzymes in the synthesis of polysialic acid and its attachment to NCAM (Angata and Fukuda, 2003). To address possible functions of STX and PST during neuronal migration in the developing and mature zebrafish nervous system, first *in situ* hybridization for *stx* and *pst* was performed during stages when neuronal migration in the developing zebrafish central nervous system is prominent (Fig. 3.23). At 48hpf, highest *stx* expression was present in regions of pronounced neuronal migration, such as in the differentiating cerebellum and the dorsal

region of the caudal hindbrain (Fig. 3.23A). Low levels of *stx* were detected in the telencephalon, diencephalon, tectum and the anterior spinal cord. At 96hpf, *stx* expression declined and faint levels remained only in the cerebellum (Fig. 3.23B) and in ventral domains of the mid- and hindbrain.

Figure 3.22 Sequence alignment of zebrafish STX and PST compared to other vertebrates

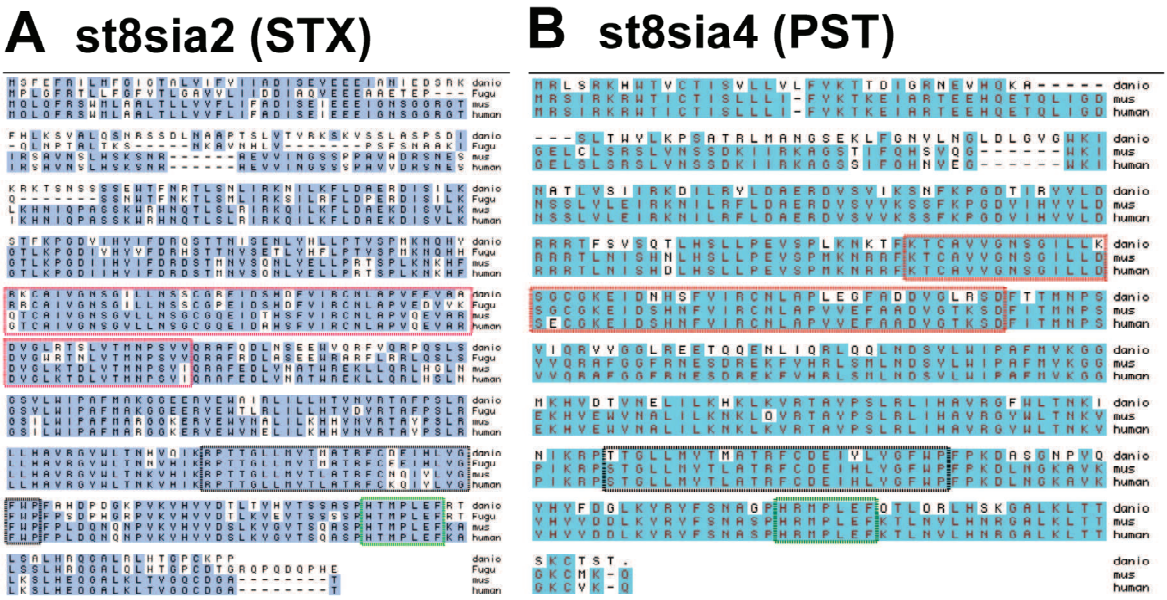

(Fig. 3.22) ClustalW alignments of amino acid sequences for zebrafish STX (A) and PST (B) compared to different vertebrate species. Shaded background depicts conserved amino acids while the predicted sialylmotifs are boxed in different colors. Red boxes represent L (large), black boxes S (small) and green boxes VS (very small) sialylmotifs. (A) The amino acid sequence of zebrafish polysialyltransferase St8sia2 (STX) is aligned to STX of Fugu, mouse and human. (B) Sequence alignment of zebrafish St8sia4 (PST), mouse and human PST. Homology analysis revealed no blast hit for PST in Fugu. The sialylmotifs of both zebrafish polysialyltransferases show more than 71% sequence homology to the sialylmotifs of the other vertebrates shown.

At 7dpf weak *stx* staining was retained in the medio-dorsal domain of the anterior hindbrain (Fig. 3.23C arrowhead), whereas all other brain regions did not show detectable *stx* expression levels anymore.

Expression of the second polysialyltransferase *pst* was generally weaker in the CNS throughout development when compared to *stx* (Fig. 3.23D-F). At 48hpf *pst* was detected in ventral regions of the fore-, mid- and hindbrain (Fig. 3.23D) and along the ventricles (Fig. 3.23G-I). *pst* expression in the hindbrain was most prominent in dorso-ventral stripes, delineating the central domains of individual rhombomeres (Fig. 3.23D inset, asterisks). Similar to the decline in *stx* expression, *pst* levels also diminished with progression of

organogenesis and low expression remained only in some patches of the posterior hindbrain at 96hpf (Fig. 3.23E).

Figure 3.23 Expression of *stx* and *pst* in the developing zebrafish brain

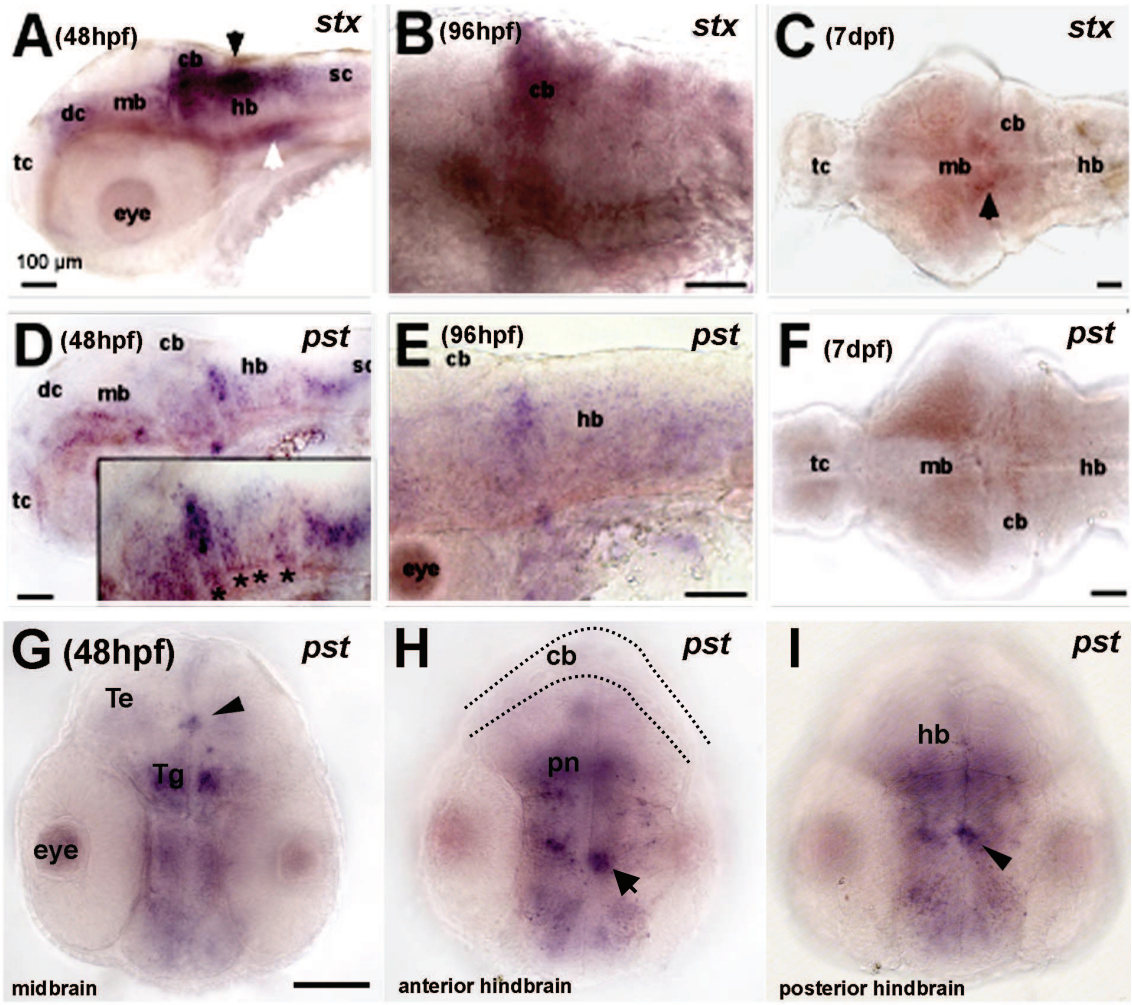

(Fig. 3.23) Panels (A, B, D, E) show lateral (C, F) dorsal and (G-I) transversal views, anterior is left. (A) At 48hpf *stx* expression is weakly present in the ventral telencephalon, in the diencephalon, midbrain and in the spinal cord. Strong expression is found in the in the floorplate (white arrowhead), differentiating cerebellum and along the fourth ventricle in the dorsal region of the caudal hindbrain (black arrowhead). (B) *stx* remains weakly expressed in the differentiating cerebellum and in ventral regions of the mid- and hindbrain at 96hpf. (C) At 7dpf only the dorso-medial domain of the cerebellum retains low levels of *stx* (arrow). (D) *pst* is expressed along the ventricles in the ventral for-, and midbrain. A striped pattern is present in the hindbrain confined to individual rhombomeres (inset, asterisks). (E) Only patchy expression of *pst* is retained in the hindbrain at 96hpf. (F) *pst* expression is not any longer detectable in the brain at 7dpf. (G-I) Transversal sections of zebrafish heads showing expression of *pst* at 48hpf. *pst* is in general not detectable in the dorsal brain, while its expression is found in the ventral brain along the ventricles (arrowheads) in the midbrain (G), anterior (H) and posterior hindbrain (I). The dashed lines in (H) delineate the cerebellum, where *pst* is not expressed. Abbr.: cb: cerebellum, dc: diencephalon, hb: hindbrain, mb: midbrain, pn: pons, sc: spinal cord, tc: telencephalon, Te: tectum, Tg: tegmentum. Scalebars: 100μm

At one-week post fertilization, *pst* expression could not be detected further in the nervous system (Fig. 3.23F). These findings show that the spatio-temporal expression pattern of *stx* in developing zebrafish is similar to that of mouse, where *stx* is the major polysialyltransferase during CNS development, but its expression declines at postnatal stages (Ong et al., 1998). In contrast, mouse *pst* expression is continuous and lasts at moderate levels from embryogenesis to adulthood, whereas in zebrafish *pst* expression is absent at larval stages.

3.2.3 *stx* and *pst* are both expressed in common and differential domains in the adult zebrafish brain

stx and *pst* polysialyltransferases show moderate expression levels in various regions of the adult brain in mammals (Angata et al., 1997, Kurosawa et al., 1997, Hildebrandt et al., 1998). To compare the expression patterns for both enzymes in the adult zebrafish brain, paraffin sections were analyzed by *in situ* hybridization. These results revealed that despite the decline in the expression levels of *stx* and *pst* at one-week post fertilization (Fig. 3.23C, F), expression of both enzymes reappeared in the mature brain (Fig. 3.24A, D). *In situ* hybridization analysis on adult brain sections revealed a clear tissue-specific expression for *stx* and *pst*.

By examining sagittal sections both enzyme-encoding genes could be detected in the outermost glomerular layer (GL), the adjacent external cellular layer (ECL) and the internal cellular layer (ICL) of the olfactory bulb (OB) (Reichert, 1996), in the pallium, and in stripes of the subpallium in the telencephalon (Fig. 3.24B, E), which has been considered to be an equivalent of the rostral migratory stream in mammals (Adolf et al., 2006). The expression domains of *stx* and *pst* in the subpallial stripe correlate well with the presence of PSA-NCAM in migrating proliferative neuroblasts in zebrafish (Adolf et al., 2006). Expression of both enzymes was also detected in the periventricular gray zone of the midbrain, the optic tectum (Fig. 3.24A, D), and along the lateral diencephalic ventricles of the hypothalamus (Fig. 3.24C, F). Furthermore, *stx* and *pst* expression was found in the molecular, Purkinje and granule cell layers of the corpus and valvula cerebelli (Fig. 3.24H-K), as well as in the crista cerebellaris (*pst* in Fig. 3.24D, not shown for *stx*). Interestingly, high *stx* but low *pst* levels were detected in the cerebellar Purkinje cell layer (PCL) (Fig. 3.24H, I). In contrast, cells in the cerebellar granule cell layer (GCL) revealed strong *pst* but weak *stx* expression (Fig. 3.24J, K).

Figure 3.24 Adult expression of *ncam* and the polysialyltransferases *stx* and *pst*

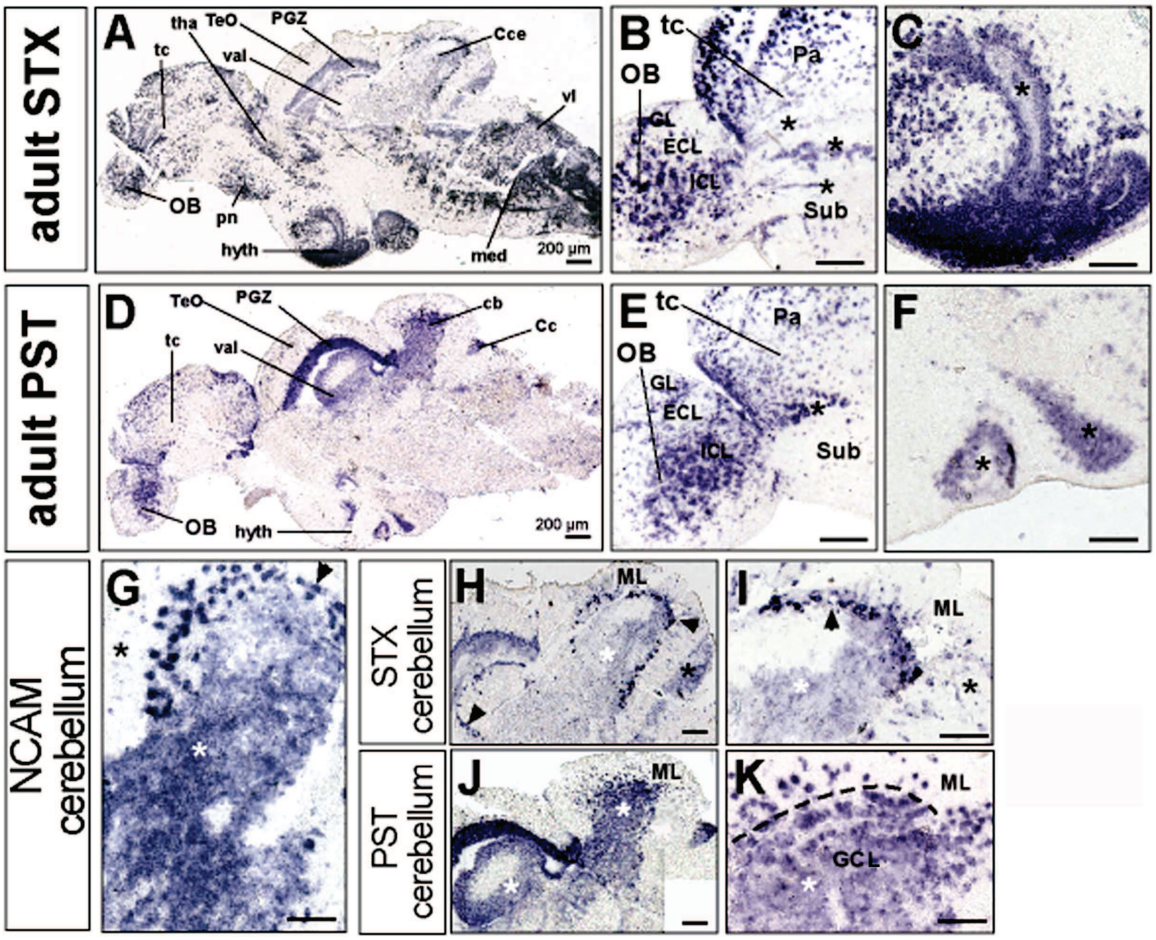

(Fig. 3.24) Comparison of *stx* and *pst* expression in the adult zebrafish brain. All panels show sagittal sections along the medial antero-posterior axis, anterior is to the left. (A–C, H, I) shows gene expression of *stx* and (D–F, J, K) of *pst*. (A) Overview of *stx* expression. (D) Overview of *pst* expression. (B, E) Cells in the pallial migratory domains of the telencephalon and olfactory bulb are marked by asterisks. (C, F) Ventricular staining in the hypothalamic region. (G) *ncam* expression in the molecular (black asterisk), Purkinje (arrow) and granule (white asterisk) cell layers of the cerebellum. (H) Higher magnification of the cerebellum, showing *stx* expression in some cells of the molecular layer, but especially pronounced in cells of the Purkinje cell layer (PCL), extending from the corpus into the valvula cerebelli (black arrowheads). Weak expression levels are present in the caudal lobe (black asterisk) and in the GCL (white asterisk). (I) Shows a higher magnification of (H). Black and white asterisks mark the ML and GC layer, respectively, black arrowhead marks the PCL. (J) Strong *pst* expression in the granule cell layer of the corpus and in the valvula cerebelli (white asterisks), being more pronounced than that of *stx* (H, white asterisk). (K) Shows a higher magnification of (J) where *pst* expression is detected in the ML and GCL, being separated by a dashed line. Cc, crista cerebellaris; Cce, corpus cerebelli; ECL, external cellular layer; GCL, granule cell layer; GL, glomerular layer; hyth, hypothalamus; IL, internal cellular layer; med, medulla; ML, molecular layer; OB, olfactory bulb; Pa, pallium; PGZ, periventricular gray zone of the optic tectum (TeO); pn, preoptic nucleus; Sub, subpallium; tha, thalamus; val, valvula; vl, vagal lobe

In addition, pronounced but unique expression of *stx* was found in the subpallial stripe of the telencephalon, the preoptic nucleus, the thalamic region (Fig. 3.24A), in the caudal

lobe of the cerebellum (Fig. 3.24H, black asterisk), in the vagal lobe of the hindbrain and in several regions of the medulla extending into the spinal cord (Fig. 3.24A).

The analysis of *stx* and *pst* expression in the adult brain showed that both polysialyltransferase genes are not ubiquitously expressed, but are confined to distinct brain regions. It is noteworthy that these tissues also express *ncam* (e.g. corpus cerebelli shown in Fig. 3.24G) and PSA (Adolf et al., 2006) (personal communication). These findings suggest that STX and PST function in the regulation of adult neurogenesis, neuronal migration and plasticity via modulation of NCAM polysialylation.

3.2.4 Co-expression of *ncam*, *stx* and PSA in domains of neuronal migration in the developing zebrafish cerebellum

Modulation of NCAM via PSA-addition has been shown to be important for neuronal migration (Cremer et al., 1994, Ono et al., 1994, Murakami et al., 2000), but in zebrafish such a function for PSA-NCAM remained elusive. Thus *stx* and *pst* expression was compared to that of *ncam* and PSA in the differentiating cerebellum at 30hpf and 48hpf, developmental stages during which intense neuronal migration occurs from the upper rhombic lip (URL) towards and along the MHB to ventral brain regions (Köster and Fraser, 2001). Consistent with playing a role in regulating migration, uniform but strong expression of *ncam* (Fig. 3.25A) and *stx* (Fig. 3.25B) was detected along this migratory path at 30hpf. In contrast, *pst* expression was absent from the differentiating cerebellum at all embryonic stages analyzed (Fig. 3.25C, G). This suggests that STX is the primary enzyme to mediate NCAM-polysialylation in migrating URL-derived neuronal progenitor cells. To test if polysialyltransferase expression in the differentiating cerebellum correlates with the polysialylation pattern of NCAM, PSA immunostaining was performed using the mAb735 antibody and compared to *ncam*, *stx* and *pst* gene expression. Strong PSA immunoreactivity was found in domains of pronounced *ncam* and *stx* expression at 30hpf (Fig. 3.25D compare to A and B).

Interestingly, at 48hpf expression of *ncam* (Fig. 3.25E) and PSA (Fig. 3.25H) became restricted to the rostral cerebellum along the MHB, whereas cells in the URL lost expression of both *ncam* and PSA (see Fig. 3.25E, H, dashed line between MHB and URL marks the rostral shift of expression). Consistent with this lack of *ncam* and PSA in the caudal cerebellum at 48hpf, *stx* expression was also less pronounced in the caudal region

(Fig. 3.25F). This decline correlated with the strong reduction of PSA levels around 60hpf in the cerebellar domain (Fig. 3.26B).

Figure 3.25 Expression of *ncam, stx*, *pst* and PSA expression at developmental stages of neuronal migration in the developing cerebellum

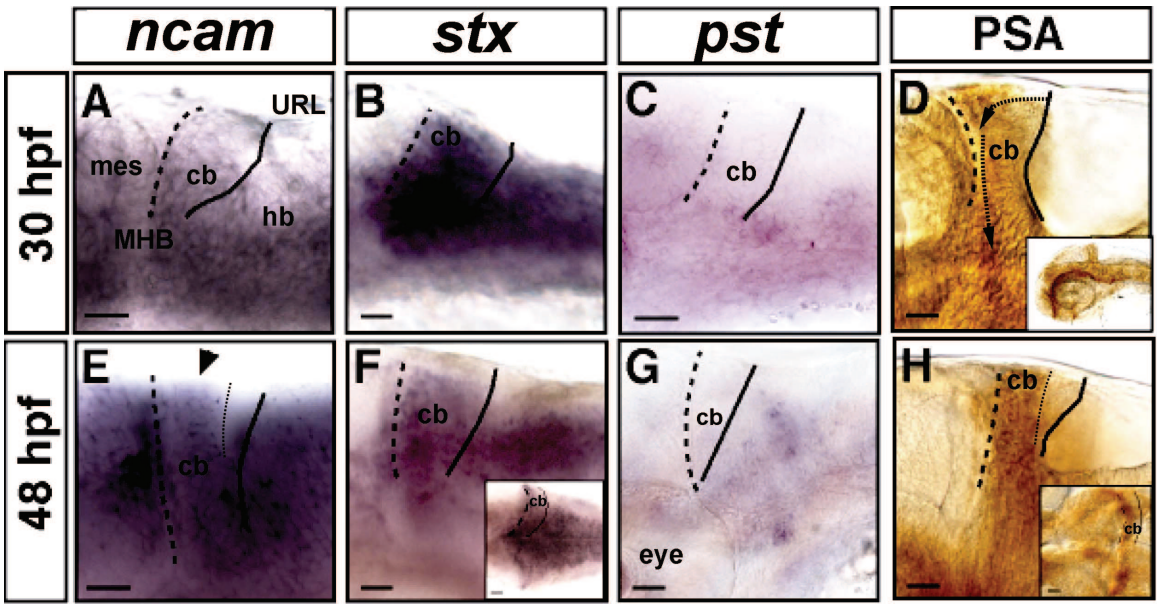

(Fig. 3.25) Comparison of *ncam*, *stx*, *pst* and PSA expression in the differentiating cerebellum at 30hpf (A–D) and 48hpf (E–H), during stages when neuronal migration occurs. Arrows in (D) mark routes of neuronal migration. High magnification lateral views of the cerebellar region are shown. The anterior cerebellar border at the MHB and the posterior edge of the cerebellum are marked with a dashed and solid line, respectively. ISH analysis was performed for *ncam* (A, E), *stx* (B, F) and *pst* (C, G), while PSA immunoreactivity was detected with mAb735 antibody staining (D, H). (A) Expression of *ncam* is strong in the cerebellum at 30hpf. (B, C) Both zebrafish polysialyltransferases *stx* (B) and *pst* (C) show expression in the ventral hindbrain, whereas only *stx* is also expressed in the differentiating cerebellum. (D) PSA signal correlates with cerebellar domains where *stx* and *ncam* are expressed. Inset shows an overview of total PSA expression in the CNS. (E) At 48hpf, the *ncam* expression domain has become restricted to the rostral cerebellum, as marked by the dashed line delineating the caudal edge of the shifted expression. The black arrowhead marks the *ncam* expression domain, whereas cells in the URL are devoid of *ncam*. (F) Expression of *stx* is found in the entire cerebellar anlage with strongest expression however in the rostral domain along the MHB, while declining in caudal cerebellar regions (inset) at 48hpf. (G) *pst* expression is still absent in the differentiating cerebellum at 48hpf. (H) Similar to *stx* expression, PSA expression has also shifted rostrally in the cerebellum at 48hpf. Inset shows a dorsal view of the mid- and anterior hindbrain region. Black line marks the caudal boundary of the cerebellum. Abbr.: cb: cerebellum, hb: hindbrain, mes: mesencephalon MHB: mid-hindbrain boundary, URL: upper rhombic lip. Scale bars: 50μm.

3.2.5 PSA removal impairs migration of neuronal progenitor cells from the URL

Given that PSA-NCAM is capable of regulating neuronal migration in mouse (Cremer et al., 1994, Ono et al., 1994) together with findings in this study that *ncam*, *stx* and PSA

are co-expressed along the major neuronal migratory pathway in the differentiating zebrafish cerebellum, it was investigated whether PSA-NCAM is capable of regulating URL-derived migration in the zebrafish cerebellum. The enzyme endoneuraminidase (EndoN), which selectively degrades polysialic acid on NCAM (Rutishauser et al., 1985, Marx et al., 2001, Franz et al., 2005) was therefore used to specifically remove PSA in the differentiating brain at 33hpf, shortly after onset of PSA-NCAM expression (Marx et al., 2001). For this, either 2-4nl of control PBS solution or 100ng/μl EndoN in PBS was injected at ~33hpf into the fourth ventricle of zebrafish embryos. The efficiency of PSA removal in the brain was first monitored 2 and 24 hours post injection by immunohistochemistry using the mAB735 antibody. While control embryos displayed no obvious reduction in the levels of PSA at both time points (Fig. 3.26A, B), PSA was completely absent in the CNS of EndoN-injected embryos already after 2 hours and lasted up to 24 hours (Fig. 3.26C, D). This demonstrated that EndoN sufficiently degrades PSA from neuronal progenitor cells in the differentiating cerebellum for at least 24 hours.

Figure 3.26 Immunohistochemical analysis of PSA-NCAM after PSA degradation in the zebrafish cerebellum

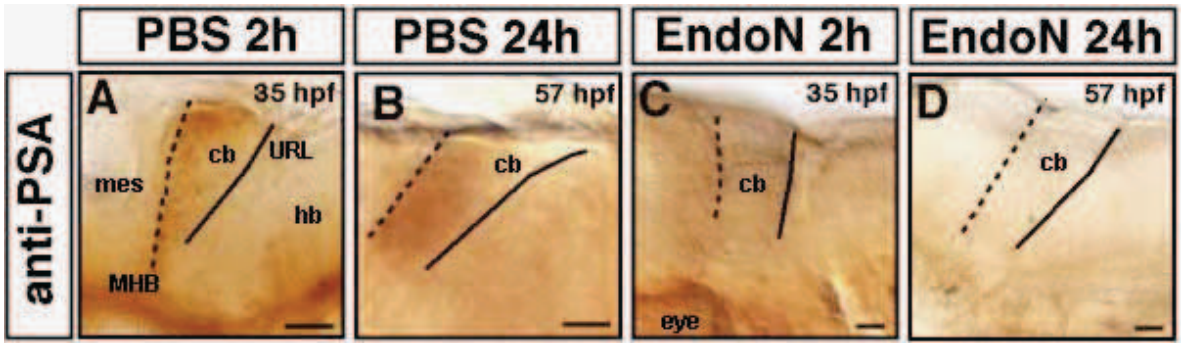

(Fig. 3.26) PSA removal after EndoN-injection is visualized by immunohistochemistry. All panels show a lateral view of the zebrafish cerebellum, anterior is to the left. Panels (A-D) show PSA staining in PBS-control (A, B) and EndoN-injected embryos (C, D). (A, B) PSA immunoreactivity is detected in the cerebellar domain of PBS-injected control embryos after 2 hours (A) and 24 hours (B). Note the weaker expression levels at 57hpf are due to endogenous down-regulation of PSA. (C, D) EndoN-injection at 33hpf completely abolished PSA immunoreactivity in the cerebellum already after 2 hours (C), lasting up to 24 hours (D). Abbr.: cb: cerebellum, hb: hindbrain, mes: mesencephalon, MHB: mid-hindbrain boundary, URL: upper rhombic lip.

Altered PSA levels in EndoN-injected embryos were not expected to result in any gross morphological changes. However, as PSA is found along paths of migrating cerebellar rhombic-lip derivatives, time-lapse confocal microscopy was employed to investigate

cerebellar migration on a single cell level when PSA is ablated by EndoN treatment of embryos. For this, neuronal progenitor cells were labeled mosaically by injection of atubGVP-UuncGFP (Köster and Fraser, 2001) into 1-cell stage zebrafish embryos. This allowed for cytoplasmic staining, with nuclei being devoid of GFP-expression.

Figure 3.27 Loss of PSA influences motility of cerebellar neuronal progenitor cells

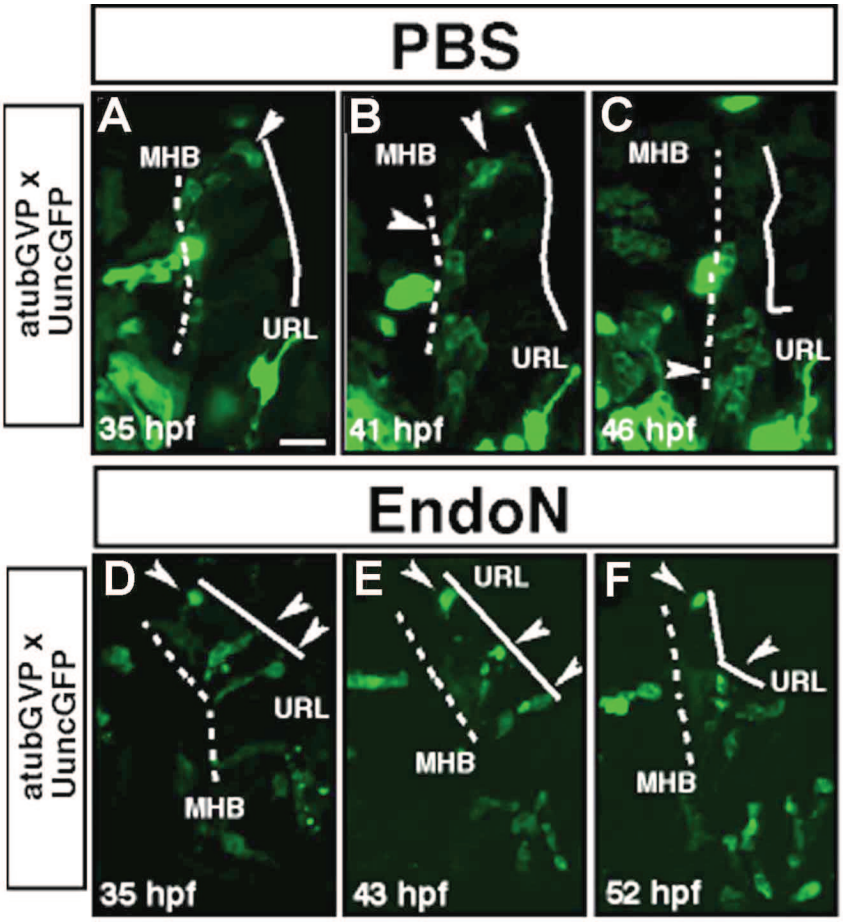

(Fig. 3.27) Loss of PSA impairs cell migration emanating from the cerebellar rhombic lip. Panels (A–F) show projections of migrating neuronal progenitor cells in the differentiating cerebellum after PBS (n=3) (A–C) and EndoN-treatment (n=3) (D–F), recorded by *in vivo* time-lapse confocal microscopy. (A) A group of neuronal progenitor cells at the URL in the control embryo at 2 hours post injection is marked by a white arrowhead. (B) These cells migrated about half way between URL and MHB after 6 hours, while others have reached the MHB. (C) A white arrowhead depicts the ventral region of the cerebellum where cells become stationary and form clusters. (D) Neuronal progenitor cells (arrowheads) are positioned at the URL or between the URL and MHB, two hours after EndoN-injection into the hindbrain ventricle of 33hpf embryos. (E) Ten hours later at 43hpf, these neuronal progenitors are stalled in the cerebellum and remain in this position for up to 17 hours of time-lapse recording (F). See Supplementary Movies 3.13 and 3.14. Abbr.: MHB: mid-hindbrain boundary, URL: upper rhombic lip.

At 33hpf, selected embryos expressing this construct in migrating URL-derived cerebellar cells were injected either with PBS or EndoN and migration of GFP-expressing neuronal progenitors was subsequently monitored by *in vivo* time-lapse confocal microscopy, starting 2 hours post injection (n=3) (see Supplementary Movies 3.13 and 3.14). In control embryos clusters of labeled neuronal progenitor cells initiated migration by becoming polarized and extending long leading processes in direction of the MHB (Fig. 3.27A, see Supplementary Movie 3.13, n=3). Migration of such cells then followed the previously characterized antero-ventral pathway towards and along the MHB (Fig. 3.27B) to ventral regions of the anterior hindbrain (Fig. 3.27C) (Köster and Fraser, 2001). In contrast, URL-derived neuronal progenitors in EndoN-injected embryos exhibited severe migration defects after PSA removal (see Supplementary Movie 3.14, n= 5). About two hours after EndoN-injection, URL-positioned cells failed to polarize and stabilize a leading process, despite filopodial activity (Fig. 3.27D). In addition, these progenitors never initiated migration. In addition, neuronal progenitors that had already left the URL before EndoN-injection first displayed a polarized cell morphology with their leading processes directed towards the MHB. These cells did however not pursue antero-ventral migration and remained stalled at their position close to the URL during the entire period of time-lapse recordings (Fig. 3.27E, F arrowheads). These findings suggest that PSA is essential for regulating cellular motility of migratory neurons emanating from the zebrafish cerebellar rhombic lip.

Taken together, the motility of neuronal progenitor cells in the differentiating zebrafish cerebellum is promoted by NCAM polysialylation, likely through polysialylation of NCAM by STX. In addition, based on their tissue-specific expression both STX and PST are good candidates to regulate adult neurogenesis, neuronal migration and plasticity in the zebrafish cerebellum through differential polysialylation of NCAM.

4 Discussion

Neuronal progenitors born in the upper rhombic lip of the differentiating zebrafish cerebellum migrate over long distances before reaching their terminal differentiation domains. Although their migration routes have been well described, their migration mode and the underlying cell biological events that control their migration behavior remained elusive. Two candidates, the cell-cell adhesion factor Cadherin-2 and polysialylated NCAM (PSA-NCAM), which has been previously already shown to participate in long-distance migration of neuronal progenitors in other brain regions, have been identified in this study to mediate essential processes of neuronal progenitor migration in the developing zebrafish cerebellum.

4.1 Cadherin-2 regulates migration of granule progenitor cells in the differentiating zebrafish cerebellum

4.1.1 Glia cell-independent migration of cerebellar GPCs

The coordinated migration of neuronal progenitors during embryonic differentiation of the brain is essential for their correct positioning and proper integration into functional neuronal networks of the mature brain. In the differentiating avian and mammalian cerebellum, migration of granule progenitor cells (GPCs) is characterized by a biphasic migration mode. Initially GPC migration occurs in a tangential homotypic manner. Cells emanate from the URL and migrate across the dorsal surface of the cerebellum to form the external granule cell layer (EGL). This homotypic migration is followed by a heterotypic radial inward migration of GPCs along Bergman glia cells into deeper layers of the cerebellum, where GPCs finally settle in the internal granule cell layer (IGL) (Rakic, 1971, Rakic, 1990). Intriguingly, this study revealed that in zebrafish a tangential homotypic mode is the predominant form of GPC migration as glia cells are not present during the peak of GPC migration. This may be interpreted as evidence that granule cell migration has not been well conserved during evolution. *In vitro* and *in vivo* evidence however suggests that GPCs in the early differentiating mammalian cerebellum also do not strictly migrate along glial fibers towards the IGL (Zagon et al., 1985, Liesi, 1992, Liesi and Wright, 1996, Kawaji et al., 2004, Wang et al., 2007). Rather a large number of GPCs seems to migrate in intimate contact with each other along fasciculated fibers of co-migrating GPCs. In fact, it has been

postulated that tangential and radial GPC migration can occur simultaneously and that glial involvement in GPC migration might play a minor role during early cerebellar differentiation (Hager et al., 1995, Liesi et al., 2003). During onset of GPC inward migration in mouse, many Bergman glia cells are still immature and have not yet reached the EGL (Bignami and Dahl, 1974, Das et al., 1974, Sotelo and Changeux, 1974, Zagon et al., 1985, Hager et al., 1995). In addition, GPCs are capable of inward migration even in the absence of Bergman glia cells or when they are distorted (Sotelo and Rio, 1980, Colucci-Guyon et al., 1999). Thus observations made in this study showing that GPC migration in the differentiating zebrafish cerebellum occurs independently of glia cells is in good agreement with cerebellar development in mammals and rather underscores an exceptional high degree of conservation among mammals and teleosts. Furthermore, during ongoing adult neurogenesis, zebrafish cerebellar migration has been proposed to occur radial along glia fiber processes (Zupanc and Clint, 2003). Thus similarly to mammals, GPCs in zebrafish use a homotypic chain-like migration during cerebellar development while this migration mode becomes most likely replaced by heterotypic glia-dependent migration during juvenile stages and during adult neurogenesis.

4.1.2 Cadherin-2 has several migration-regulating functions for zebrafish cerebellar GPCs

During migration, Cadherin-2 activity can serve several functions by enabling onset of migration (Nakagawa and Takeichi, 1998, Shoval et al., 2007), in the segregation of different migratory subpopulations (Takeichi, 1995, Luo et al., 2004), by influencing cellular motility (Kim et al., 2005, Taniguchi et al., 2006), regulating guidance of migration (Rhee et al., 2002, Wang et al., 2007) and controlling condensation of migratory cells (Kasemeier-Kulesa et al., 2006). Earlier in development, Cadherin-2 has been shown to possess polarizing activity for neural cells that converge and intercalate along the midline to drive zebrafish neurulation (Hong and Brewster, 2006). The analysis of Cadherin-2 deficient *pac*R2.10 mutant embryos in this study revealed additional functions for Cadherin-2 in the regulation of polarization of cerebellar GPCs and in mediating their chain-like coherent and directional migration behavior. These late functions became only evident when the neurulation defect of *pac*R2.10 mutants was overcome by temporally restoring the expression of wild type Cadherin-2. Thus, it could be shown that Cadherin-2 functions in the establishment and maintenance of cell polarity for cerebellar GPCs. An additional role for

Cadherin-2 was revealed in the regulation of coherence and directionality of migrating cerebellar GPCs by mediating the formation of stable homotypic contacts during chain-like migration, similarly to its migration regulating function during tangential migration of precerebellar neurons in the mouse hindbrain (Taniguchi et al., 2006). This shows that zebrafish Cadherin-2 exerts different functions within one cell type, the cerebellar granule cell population.

4.1.3 Cadherin-2 is the prominent classic Cadherin mediating homotypic contacts between migrating cerebellar GPCs

Observations by transmission electron microscopy (TEM) showed that GPCs in wild type embryos form adherens junctions en route to the MHB, while no such intercellular junctions could be detected in GPCs of *pac*-/-R mutants. This indicates that Cadherin-2 is likely to be the predominant classic Cadherin expressed by migrating differentiating cerebellar GPCs in zebrafish. Such a dominant role for Cadherin-2 differs from that in the rodent cerebellum, where postmitotic cerebellar GPCs co-express several classic Cadherins, such as M-, N- and R-Cadherin (Gliem et al., 2006). Several classic Cadherins, including N-cadherin are also co-expressed by migrating precerebellar progenitors derived from the lower rhombic lip (LRL) in the rat brain (Taniguchi et al., 2006). Ablation of N-cadherin in LRL cells results however primarily in the delay of neuronal migration, being different from the misrouting of Cadherin-2 deficient GPCs in the differentiating zebrafish cerebellum. This less severe phenotype might be explained by the functional redundancy of classic Cadherins in LRL progenitors. Alternatively, this divergence might be in fact not so different when considering that LRL-derived neurons remain on the ipsilateral site in the presence of dominant-negative Cadherin-2, whereas wild type EGFP expressing cells crossed the ventral midline and migrated to the contra-lateral side. It could thus be possible that similar to GPC migration in zebrafish this observed clustering resulted from a misrouting of neuronal progenitor cells.

4.1.4 Impaired differentiation and increased cell death of GPCs in dorsal domains of rescued *pac*-/-R cerebelli

The analysis of Cadherin-2 deficient *pac*-/-R gata1:GFP embryos revealed that migrating GPCs are misrouted and finally remain in ectopic positions of the dorsal cerebellum. Nevertheless, they initiate proper differentiation as observed by their *neuroD* expression.

This supports the findings that lack of Cadherin-2 does not affect initial differentiation of neuronal cells (Noles and Chenn, 2007). GPCs in dorsal regions of the differentiating *pac*-/-R cerebellum however fail to terminate their differentiation and undergo increasingly cell death at 5dpf. The increasing cell death in the cerebellum of *pac*-/-R embryos can not be attributed to apoptosis, as TUNEL staining and immunohistochemical analysis for activated caspase-3 (not shown) did not reveal any significant changes in the numbers of labeled cells. Currently, it cannot be excluded that a decline in health caused by other factors, unrelated to improper GPC migration, such as the insufficient delivery of oxygen or nutrients in dorsal regions of *pac*-/-R embryos contributes to the increase in non-apoptotic cell death. Interestingly, the increase in cell death begins already between 4 and 5dpf, while *pac*-/-R larvae die only later than 7dpf. The late death of Cadherin-2 deficient *pac*-/-R embryos might therefore be due to improper heart maturation as Cadherin-2 has been implicated in heart development (Radice et al., 1997, Bagatto et al., 2006, Luo et al., 2006). Furthermore, *pac*-/-R mutants show an enlargement of their heart sacs with progressing development (not shown). It thus seems more likely that the ectopic positioning of differentiating GPCs in dorsal regions of the *pac*-/-R cerebellum leads to a failure to respond to appropriate differentiation signals, therefore leading to their subsequent non-apoptotic cell death.

4.1.5 Cadherin-2 mediates GPC polarization in the URL

Cadherin-2 deficient GPCs in the URL of *pac*R2.10 embryos fail to polarize, while this polarization is restored in cerebellar GPCs of *pac*-/-R mutants, being rescued for their neurulation defects. Interestingly, late transient activation of dominant-negative Cadherin-2 (Cdh2ΔN-mCherry) via heatshock-induction did not re-induce loss of polarization in GPCs when Cdh2ΔN-mCherry was strongly expressed in these cells. These findings suggest that Cadherin-2 might function early in URL development in the irreversible establishment of cell polarity and the assignment of neuroepithelial character to GPCs. Recently, another classic Cadherin, type II Cadherin-6 was identified in zebrafish and has been shown to be expressed in URL-derived cells before onset of GPC migration (Liu et al., 2006b). Although Cadherin-6 is first broadly expressed in the developing zebrafish cerebellum before ~40hpf, its expression becomes restricted to the upper rhombic lip during onset of GPC migration. A role for Cadherin-6 in mediating GPC polarization within the URL might however play a minor role as the loss of Cadherin-2 in *pac*R2.10 embryos results in the failure of GPCs to polarize although Cadherin-6 remains expressed in mutant cerebelli (not shown), suggesting

that Cadherin-6 alone cannot mediate polarization. It is therefore possible that Cadherin-6 rather plays a structural role by maintaining the integrity of polarized GPCs in the URL during onset of GPC migration. This is supported by TEM analyses of *pac*-/-R embryos after onset of GPC migration, where adherens junctions were found to remain on cells that are located in the URL (not shown), being consistent with the restricted expression of Cadherin-6 in the URL at this stage. A cooperative role for Cadherin-2 and Cadherin-6 in the establishment of GPC polarization via *cis*-dimer formation also seems unlikely in mediating polarization, as the EC1 domains of type I and type II Cadherins can only interact poorly with each other due to structural constraints, making them incompatible (Patel et al., 2006). This is further supported by co-aggregation assays of type I and II Cadherins leading to the segregation of cells expressing either Cadherin type (Patel et al., 2006). Together, these findings suggest that Cadherin-2 is likely the solitary Cadherin to mediate polarization of GPCs within the URL before onset of GPC migration. In *pac*-/-R GPCs, early supplied Cadherin-2 could function in the recruitment of polarity proteins to the plasma membrane, thus conferring apical and basal identity to the cell. This might lead to an irreversible polarization of these cells, while the maintenance of this polarization becomes independent of Cadherin-2. Such a mechanism is supported by the observation that transient heatshock activation of Cdh2ΔN-mCherry in GPCs within the URL did not abolish their polarization.

4.1.6 Coherent migration of GPCs mediated by dynamic shifts of Cadherin-2 along cell-cell contacts

In the zebrafish cerebellum upper rhombic lip-derived GPCs migrate in a chain-like manner via the formation of adherens junctions to migrate across and through layers of ventricular zone-derived cells (A. Barbaryka & R. W. Köster, unpublished). Cadherin-2 has been shown to be present in GPCs and to be required for mediating their chain-like migration behavior. Cerebellar GPCs take turns in forward migration along a chain and rest between migratory phases. At the same time GPCs also provide a template for co-migrating cells, similarly to the migratory behavior of postmitotic granule cells during early mammalian cerebellar development, such as migrating neuroblasts in the rodent RMS (Doetsch et al., 1997, Liesi et al., 2003). Observations of GPCs expressing the adhesion reporter Cdh2Δ2-4ΔC-mCherry revealed that migrating GPCs dynamically reposition Cadherin-2-containing clusters along at the plasma membrane towards contacts sites with neighboring cells as they migrate along other GPCs. Such Cadherin-2 clusters are shifted

between the leading edge and the rear end, consistent with the movement of the cell. Such a highly dynamic redistribution of Cadherin-2 clusters in GPCs may explain the highly coherent migration behavior of GPCs.

4.1.7 Dynamics of Cadherin-2 in migrating GPCs

Type I Cadherins are down-regulated in epithelial cells during epithelial-to-mesenchymal transition (EMT), when cells with epithelial character acquire motility. For example, this has been shown to occur during gastrulation (Zohn et al., 2006), neural crest emigration (Taneyhill et al., 2007) and cancer invasion (Weidner et al., 1990, Behrens, 1993). In these processes, disruption of intercellular connections and disassembly of adherens junction has been proposed to be a prerequisite for onset of cell migration. Over the past years, evidence has emerged showing that type I Cadherins can however also be upregulated as cells undergo a transition from a steady into a motile state (Chen and Ma, 2007, Guo et al., 2007, Shintani et al., 2007, Theisen et al., 2007). These findings support the idea that adherens junctions undergo a dynamic remodeling in migrating cells.

Taking advantage of the clarity and external development of zebrafish embryos, it was demonstrated by *in vivo* time-lapse microscopy that Cadherin-2 clusters are continuously adjusted in migrating GPCs during migration, most likely to allow a coherent migratory behavior along chains. Recently, it has been shown that Cadherins are transported in vesicles along the microtubule network (Mary et al., 2002, Jontes et al., 2004), that they can flow in a directional manner at cell junctions associated with reorganization of actin filaments in migrating cells (Kametani and Takeichi, 2007) or they can be internalized via endocytosis and processed either for degradation or redeployed to novel sites adhesion sites (Fukuhra et al., 2006, Ogata et al., 2007). Such a transport of Cadherin-2 might facilitate the rapid re-assembly of adherens junctions in migrating cells. Time-lapse imaging of photo-convertible Cadherin Cdh2Δ2-4ΔC-EosFP revealed distinct dynamics for Cadherin-2 in cultured zebrafish PAC2-fibroblast (see Supplementary Movie 12) and migrating GPCs. While photo-converted Cadherin-2 in PAC2 cells diffused in the cytoplasm of lamellopods within 1-2 minutes after UV-light conversion, it also appeared as Cadherin-2 clusters were transported away from filopods in a directional, such as in a microtubule-dependent manner. In contrast, *in vivo* tracing of Cdh2Δ2-4ΔC-EosFP in migrating cerebellar GPCs indicated that photo-converted Cadherin-2 clusters are not quickly removed from the plasma membrane but rather appeared to be slowly but directionally moving within the membrane

towards the leading edge. This moving behavior of Cadherin-2 clusters is most reminiscent of the previously shown Cadherin flow (Kametani and Takeichi, 2007), suggesting that migrating cerebellar GPCs may use such a mechanism to rapidly relocate adherens junctions in response to environmental changes.

4.1.8 Possible guidance mechanisms for GPC migration towards the MHB

A key question will be what molecular factors guide migrating GPCs towards the MHB. Early during zebrafish cerebellar development at about 24hpf, when the cerebellar primordium is one cell diameter in width, neural progenitors span the entire cerebellum from the rhombic lip to the MHB. With ongoing cerebellar growth and differentiation this initial orientation of neuronal progenitors could be inherited to migratory chains by first forming chains consisting of two progenitors, which together span the cerebellum and subsequently adding more and more GPCs to these chains as cerebellar growth and differentiation progresses. Although this model could explain how GPCs obtain their proper initial directionality, this mechanism is error-prone as proper migration is dependent on the integrity of the migratory chains at all times.

An alternative explanation involving Cadherin-2 can be drawn from the observation that Cadherin-2 is not only involved in mediating adhesion, but also contributes to signal transduction. For example, Cadherin-2 interacts with FGF-receptors and can mediate cell motility through this receptor (Nieman et al., 1999, Peluso, 2000, Suyama et al., 2002). This may be an interesting model to explain the directionality of zebrafish GPCs with FGF-ligands emanating from the MHB and promoting GPC motility towards anterior directions. Nevertheless Cadherin-2-mediated FGF-signal transduction is unlikely to play a major role in the directed migration of cerebellar GPCs in zebrafish, as it was previously shown that inhibition of FGF-signaling in zebrafish does not significantly affect GPC migration in gata1:GFP transgenic embryos (Köster and Fraser, 2006). More attractive is a possible role for the Slit-receptor Roundabout (Robo) in guiding cerebellar GPCs towards the MHB. It was demonstrated that Robo, upon binding to its ligand Slit, interacts with Cadherin-2 and inhibits its adhesive properties by triggering the dissociation of β-catenin from the adhesion complex (Rhee et al., 2002). Interestingly, *slit2* (Miyasaka et al., 2005) and *robo3* (Challa et al., 2001) are expressed in a mediolateral domain close to the URL during stages of GPC migration. Thus, secreted Slit2 in the rhombic lip could act as repulsive cue on migrating

GPCs as they leave the URL, by weakening Cadherin-2-mediated adhesion in the trailing edge thus driving cells towards the MHB.

4.1.9 Model of coherent and directional GPC migration

GPCs migrate via nucleokinesis by sequentially translocating the centrosome and the nucleus towards the leading edge. Although a detailed study of the subcellular dynamics of zebrafish GPC migration has not been performed so far, many of the observations made by high-resolution time-lapse imaging, such as the saltatory nuclear movements into the leading edge and trailing of the cell soma (M. Distel & R. W. Köster, unpublished) are in good agreement with a nucleokinetic migration mode of zebrafish GPCs. Nucleokinesis is largely mediated through the microtubule skeleton, connecting adherens junctions with the centrosome and nucleus.

Time-lapse observations of migratory GPCs expressing the fluorescently tagged centrosomal marker Centrin2-tdTomato demonstrated that the centrosome is moving in front of the cell during forward movement. In contrast, Cadherin-2 deficient GPCs in *pac*-/-R gata1:GFP embryos showed a randomized centrosome distribution. This is in good agreement with an impairment of GPCs in directional and coherent migration. Based on findings in this study in conjunction with previous detailed descriptions of neuronal translocation during nucleokinesis (Schaar and McConnell, 2005, Tsai and Gleeson, 2005, Higginbotham and Gleeson, 2007), a model can be proposed illustrating the dynamic but coordinated shifts of the centrosome and Cadherin-2 clusters within the migrating GPC to enable the directional migration along chains (Fig. 4). In this model, in response to repulsive cues emanating from the URL, GPCs relocate Cadherin-2 clusters into the anterior cell compartment to stabilize their front towards the MHB, the direction of cell movement. A small pool of Cadherin-2 in the anterior cell may further serve to quickly transport Cadherin-2 into the leading process, similar to Cadherin-2 function in other neurons (Jontes et al., 2004). This may help facilitating pathfinding decisions of the GPC. As the GPC reorients its centrosome into the leading process due to forces from adherens junctions-coupled MT in the cortex, the cell further stabilizes its rear via transport of Cadherin-2 clusters into the posterior compartment. The GPC subsequently starts migration while maintaining Cadherin-2 mediated adherens junctions along cell-cell contacts, thus allowing for a coherent and directional migration along other GPCs. At the end of cell movement,

Cadherin-2-containing adherens junctions are disassembled and transported back into the front compartment during resting of the cell.

Figure 4 Model for Cadherin-2-dependent directional and coherent migration of GPCs during zebrafish cerebellar development

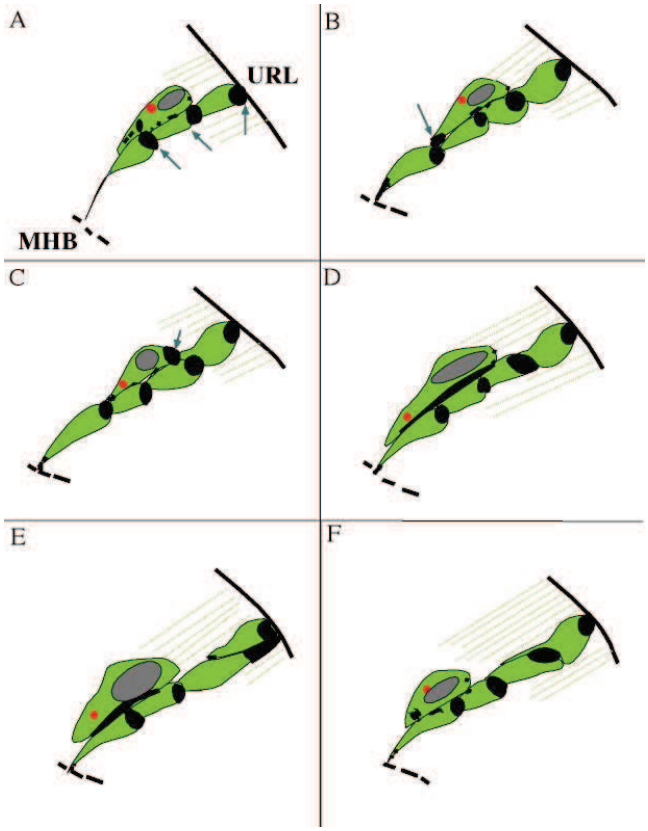

(Fig. 4) Model for directional migration of GPCs along chains mediated by Cadherin-2. (A) A repulsive cue emanating from the URL is sensed by a GPC as it prepares to move along a chain, that spans across the anteroposterior aspect of the cerebellum. GPCs are thereby attached to each other at the front and rear ends via Cadherin-2-mediated adherens junctions (arrows). (B) The repulsive cue triggers signaling cascades leading to a Cadherin-2-mediated stabilization of the leading process towards the MHB (black dots, arrow), while the GPC maintains contact with the chain. (C) The centrosome (red) is subsequently repositioned into the leading process, likely due to pulling from the MT plus ends, while the rear end of the GPC is further stabilized via Cadherin-2 (arrow). (D) During soma translocation, the nucleus (gray) elongates due to pulling forces from the centrosome while Cadherin-2-mediated adherens junctions become relocated along the lateral wall, as the GPC starts moving along the chain to maintain directionality and coherence. (E) The cell translocates its soma towards the MHB, while Cadherin-2 is disassembled in the rear for releasing the cell as it moves forward along the chain. (F) The majority of Cadherin-2-clusters are then transported again into the front of the cell, where they might serve as pool for transport into the leading process during path finding decisions.

4.1.10 Outlook

Time lapse analyses of GPCs in the cerebellum of *pac*R2.10 gata1:GFP embryos revealed that these cells fail to polarize. In contrast, *pac*-/-R mutants show that polarization is restored in GPCs of the URL after transient expression of wild type Cadherin-2 during neurulation. This suggests that Cadherin-2 plays a role in the establishment of GPC polarity prior to onset of migration. Cell polarization within the neuroepithelium is an important step during asymmetric cell division to allow transmission of neurogenic determinants into only one daughter cell, which is destined to become a neuron. Several proteins have been implicated in polarity establishment of neuroepithelial cells. For example, in the early mouse telencephalon, the polarity protein aPKC first regulates integrity of tight junctions in epithelial cells through interactions with mPar3 and mPar6 (Ohno, 2001) in a Par protein complex, located at these intercellular connections. This type of junctions is then replaced as cells acquire a neuroepithelial character, and adherens junctions remain associated with this complex (Aaku-Saraste et al., 1996). In this manner, polarity is conferred from epithelial to neuroepithelial cells. The role for Par complex proteins, such as Par-3/ASIP and aPKC has been conserved in zebrafish where these factors have been implicated in regulating cell division of neuroepithelial cells during zebrafish neurulation (Horne-Badovinac et al., 2001, von Trotha et al., 2006). It remains however elusive whether these Par complex proteins are involved in polarity establishment of GPCs in the URL and whether this is mediated by interactions with Cadherin-2-containing adherens junctions before onset of GPC migration.

To identify potential mechanisms, antibody co-expression studies have to clarify which of these polarity proteins are co-localized with Cadherin-2 in GPCs of the URL. Using this information, green-fluorescent fusion proteins can be generated and co-expressed together with the Cadherin-2 reporter Cdh2Δ2-4ΔC-mCherry in cells located in the URL, thus allowing one to study their association with adherens junctions by *in vivo* confocal microscopy. Time-lapse studies will furthermore reveal, whether adherens junctions and the associated polarity proteins are asymmetrically distributed into daughter cells during cell division and how these proteins contribute to the maintenance of cell polarity in migrating GPCs.

IQGAP1 is a key mediator in the regulation of adhesion and migration by anchoring MT plus-ends in the cell cortex of the leading edge to the actin cytoskeleton at adherens junctions (Noritake et al., 2005). To identify whether IQGAP1 also mediates MT anchoring

in migrating GPCs, antibody expression studies for IQGAP1 could be performed in conjunction with fluorescence-tagged phalloidin staining, to co-label the actin cytoskeleton and to determine the subcellular localization, which would be expected in actin-rich sites of the leading process. To test *in vivo* the possibility that IQGAP1 regulates MT anchoring in migrating GPCs, a red fluorescently tagged IQGAP1 fusion protein could be expressed in migrating GPCs together with the MT plus-end protein EB3, being fused to GFP. Both proteins would be expected to be co-localized in the leading edge. As IQGAP1 also interacts with adherens junctions it could be tested if the tethering of MTs is lacking or destabilized in *pac*-/-R GPCs, being deficient of Cadherin-2. In contrast, the ectopic expression of IQGAP1 in wild type GPCs would be expected to stabilize MT plus-ends or lead to their ectopic placement in the leading edge of migrating GPCs thus disturbing their coordinated migration. To show the involvement of adherens junctions in this process, low amounts of a yellow fluorescent IQGAP1 fusion protein could be co-expressed with the Cadherin reporter Cdh2Δ2-4ΔC-mCherry and low amounts of a cyanine-tagged EB3 fusion protein to mark MTs in blue, to prevent overexpression of these proteins and ectopic defects. All three proteins would be expected to co-localize at the cell cortex in the leading edge of polarized GPCs during preparation and active forward migration.

This study showed that Cadherin-2 clusters accumulate in migrating GPCs and become redistributed as the cell migrates. In addition it was shown that photo-converted Cadherin-2 clusters are directionally transported into leading edge. Distinctive mechanisms might control the redistribution of such Cadherin-2 clusters within migrating GPCs. For example, it has been shown that the transport of receptors located at the cell surface can be achieved through lateral diffusion. Such lateral diffusion has been however mostly studied on a single molecule level during clustering of membrane receptors, suggesting that this mechanism occurs rather randomly by trapping of molecules within certain sites of the membrane (Poo, 1982, Sako and Kusumi, 1994). This however contrasts the observations made herein, showing that Cadherin-2 clusters are transported in a directional manner, consistent with individual moving steps of migrating GPCs. Recently, the directed flow of VE-cadherin clusters has been reported to contribute to the dislocation of adherens junctions in the leading edge of migrating cells (Kametani and Takeichi, 2007). This directed transport has been suggested to depend on interactions of actin fibers with VE-cadherin and the indirect regulation of actin flow at sites of adherens junction via Myosin IIA. It is likely that the observed transport behavior for Cadherin-2 clusters in migrating GPCs occurs in a similar

manner as the directed flow of VE-cadherin clusters. Another possibility could be the internalization of Cadherin-2 clusters via Clathrin-coated vesicles. For example, internalization of VE-Cadherin is regulated via p120 catenin and involves Clathrin-coated vesicles as part of an early endosomal trafficking machinery (Xiao et al., 2005, Popoff et al., 2007). Interestingly, Clathrin has been found to rapidly and directionally move over micrometer distances within the plasma membrane (Keyel et al., 2004), which could be another mechanism to explain the directional transport of Cadherin-2 clusters within the cell membrane of GPCs. Interestingly, *in situ* analyses by Thisse et al. 2001 showed that zebrafish *clathrin (cltc)* is expressed in the CNS during stages of GPC migration. To test the possibility of Cadherin-2 internalization in a Clathrin-dependent manner during GPC migration, first immunohistochemistry for Cltc would have to clarify whether this molecule co-localizes with Cadherin-2 at the cell surface of GPCs, thus indicating its potential involvement in Cadherin-2 transport. Further analyses could be performed by *in vivo* time-lapse imaging via a fluorescently tagged Clathrin fusion protein, being co-expressed with CdhΔ2-4ΔC-mCherry in migrating GPCs to directly show potential involvement of Clathrin in the internalization and lateral movement of Cadherin-2 clusters. Loss of function studies for Clathrin could further clarify whether Cadherin-2 internalization is dependent on Clathrin. The loss of functional Clathrin would thereby be expected to lead to an accumulation of Cadherin-2 at the membrane, while internalization is disturbed.

Time-lapse analyses of GPCs in *pac* mutant embryos showed that GPCs are still motile in the absence of Cadherin-2, the only classic Cadherin present in these cells. This motility therefore most likely involves other adhesion systems. For example, GPCs have been shown to possess intrinsic motility and turning behavior when cultured on laminin-coated glass coverslips (Yacubova and Komuro, 2002). Receptors for laminins are some members of the β1-integrin family. It is therefore conceivable that GPC motility is conferred through integrin-mediated signaling. Interestingly, integrin beta 1b.2 (*itgb1b.2*), which is most similar to β1-subunits found in mammals is expressed in the developing zebrafish cerebellum (Thisse et al., 2004), therefore making it a good candidate to mediate GPCs motility. Furthermore, integrins have been implicated in mediating both radial and tangential migration of neuronal progenitors. For example, mutant mice being deficient for α3β1-integrin, a receptor for laminin, show disruption of neuronal migration in the developing cortex, caused by defects in the response to migration-modulating cues, disorganization of the actin cytoskeleton and reduced filopodial and lamellipodial activity (Schmid et al.,

2004). To test whether GPC migration in the cerebellum depends on laminin-mediated integrin signaling, the zebrafish laminin mutant *bashful* (Schier et al., 1996) could be analyzed for the migration behavior of cerebellar GPCs by crossing the gata1:GFP transgenic line into *bashful* mutants to allow investigations of migrating GPCs by *in vivo* time-lapse imaging, bearing a mutation in the *laminin alpha 1* gene. Interestingly, this gene is also expressed in the cerebellum at stages of GPC migration (Zinkevich et al., 2006). Similar to neuronal cells in mutant mice, laminin-deficient GPCs might show a perturbed migration behavior due to lacking or reduced actin filament organization or filopodial activity in the leading edge, which could be tested by co-staining of the actin cytoskeleton using fluorescently tagged phalloidin.

4.2 PSA-NCAM regulates neuronal progenitor migration in the zebrafish cerebellum

4.2.1 Divergence of PST and STX expression in the zebrafish embryo

STX is the predominant polysialyltransferase expressed during brain differentiation being consistent with previous findings (Marx et al., 2007). Interestingly, besides ventral diencephalic and tegmental brain regions STX expression was mostly confined to dorsal hindbrain structures including the rhombic lip from where neuronal progenitors have been shown to initiate long-distance migration (Köster and Fraser, 2001, Kawaji et al., 2004, Denaxa et al., 2005, Taniguchi et al., 2006). Also in the cerebellum, neuronal migration initiated from the upper rhombic lip occurs towards and along the midbrain-hindbrain boundary (Köster and Fraser, 2001) where STX-expression together with expression of NCAM and PSA was found to delineate this migratory pathway (Fig. 3.25).

PST expression was generally weaker than STX expression and in contrast not found in the differentiating cerebellum. Interestingly, PST expression was detected in rhombomeres of the caudal hindbrain, reaching from the dorsally positioned rhombic lip, which also expresses high levels of STX towards the floorplate where neuronal differentiation occurs (Cheng et al., 2004). At 4dpf, expression of both polysialyltransferases had declined to minute amounts. During this embryonic stage, neuronal migration in the hindbrain and particularly in the cerebellum ceases and terminal differentiation of neuronal populations is well under way (Volkmann et al., 2007). These findings show that besides axonal

pathfinding (Marx et al., 2001), polysialylation of NCAM could well play a role in regulating neuronal migration in zebrafish, similarly to higher vertebrates (Chazal et al., 2000, Murakami et al., 2000, Ulfig and Chan, 2004).

Imaging rhombic lip-derived migration in the differentiating cerebellum by time-lapse confocal microscopy revealed that the removal of PSA by EndoN-injection resulted in impaired cell migration. The observation that neuronal progenitors remained stalled in the rhombic lip or in close neighborhood after PSA removal suggests that polysialylated NCAM is required for mediating their cellular motility. These findings are in good agreement with results from migrating neuronal progenitors in the postnatal and adult rostral migratory stream of mammals. Tangential migration is severely decreased in mice lacking PSA-NCAM in the RMS, leading to a significant size reduction of the olfactory bulb (Cremer et al., 1994, Chazal et al., 2000).

4.2.2 STX polysialylates NCAM in the developing zebrafish cerebellum

Recently, the cerebellar rhombic lip in mice has been shown to produce different neuronal cell populations over time (Machold and Fishell, 2005, Wang et al., 2005). Similarly in the zebrafish cerebellum, the rhombic lip produces different cell types in a temporal manner (Köster and Fraser, 2001, Volkmann et al., 2007). Neuronal migration starts at about 28hpf, but granule cell precursors do not initiate migration prior to 50hpf, reaching its peak of migration between 60 and 80hpf (Volkmann et al., 2007). The successive decline of high expression levels of NCAM, STX and PSA in the zebrafish cerebellum after 48hpf indicates that PSA-NCAM regulates early neuronal progenitor migration. In contrast, the lack of PST in the cerebellum but its presence in rhombomeres of the caudal hindbrain suggests that PST might function in the polysialylation of rhombic lip-derived neuronal progenitors, most likely confined to the precerebellar system. Accordingly, findings in mice show that PSA-NCAM is expressed in ventrally migrating superficial cells, being destined to form the precerebellar LRN and ECN nuclei in the caudal hindbrain (Kyriakopoulou et al., 2002). Intriguingly, migration of the later granule cell progenitor population relies on a Cadherin-mediated adhesion system for proper migration. This suggests that different adhesion systems and their specific spatio-temporal regulation may discriminate between different neuronal populations within the cerebellum to regulate their migratory behavior.

4.2.3 Differential expression of STX and PST may establish functional differences for PSA-NCAM in the adult CNS

PST expression was found in several regions of the adult zebrafish brain. These results clearly contrast previous results in which zebrafish PST expression was reported to be absent in the adult CNS (Marx et al., 2007). Similarly to the expression during embryogenesis, many cooperative but also unique expression domains for PST and STX could be found in the mature brain. For example, both genes were detected in the RMS, olfactory bulb, along the hypothalamic lateral ventricles and in the cerebellum. In contrast, STX and PST also showed unique expression patterns in specific compartments of the cerebellum with STX being furthermore exclusively expressed in the caudal lobe. These findings suggest that PST and STX activity might act synergistically or in a redundant manner in the adult zebrafish CNS. In general, the expression of both polysialyltransferases is confined to many regions with ongoing adult neurogenesis and neuronal migration, which occurs more widespread in zebrafish than in higher vertebrates (Zupanc et al., 2005, Adolf et al., 2006, Grandel et al., 2006). PST and STX expression is found in the subpallial stripe, the zebrafish equivalent of the mammalian RMS and in other ventricular regions such as in the periventricular gray zone of the optic tectum or in the hypothalamic region.

Notably, in the cerebellum, complementary patterns of STX and PST expression are found in adjacent neuronal layers of synaptic partners. For example, Purkinje cells express high levels of STX and low levels of PST, whereas granule cells show the opposite expression pattern with low STX and high PST expression levels. Interestingly, PSA is restricted to axons (parallel fibers) and dendrites of the granule cells, but excluded from the soma (not shown). Therefore, based on the differential polysialyltransferase expression pattern in the mature cerebellum, variances in polysialylation could play a role in mediating synaptic plasticity as it has been shown in mice, where PSA and polysialyltransferases can influence synaptic plasticity and long-term potentiation (Becker et al., 1996, Muller et al., 1996, Eckhardt et al., 2000). Thus, like in higher vertebrates and mammals the spatio-temporal regulation of NCAM-polysialylation is highly regulated during development and adulthood.

4.2.4 Outlook

In this study, STX was shown to be the primary polysialyltransferase in the cerebellum during embryonic differentiation, consistent with PSA-NCAM expression during early

stages of cerebellar development. PST expression was generally weaker and mostly found in the ventral brain, while being stronger expressed in rhombomeres of the caudal hindbrain, where its expression partly overlapped in dorsal domains with strong STX expression. Based on these similar expression domains and the high conservation of their catalytic domains, both enzymes could well have a synergistic or redundant function during modulation of NCAM-mediated adhesion in the caudal hindbrain. This idea could be tested by morpholino knockdown of STX and PST to differentiate between the specific contributions of these enzymes to NCAM polysialylation in the caudal hindbrain. To efficiently knockdown polysialyltransferase expression, morpholinos could be delivered by microinjection into 1-cell stage embryos. However, this injection might cause developmental defects early on and thus obscure late functions. In addition, dilution of morpholinos with ongoing developmental progression and proliferation makes it difficult to analyze specific effects during late developmental stages. Thus alternatively, electroporation of STX and PST morpholinos into the caudal hindbrain during stages of neuronal migration could be performed to directly interfere with the function of either polysialyltransferase in this domain. To monitor their distribution, fluorescently tagged morpholinos could be used. The polysialylation patterns after knockdown of STX or PST could be detected by immunohistochemistry using anti-PSA antibody staining. The presence or absence of PSA in specific hindbrain domains will then allow to discriminate between contributions of both polysialyltransferases to NCAM polysialylation. In addition, *in vivo* time-lapse imaging after knockdown of STX and PST could be performed to analyze neuronal migration of hindbrain progenitors in the absence of polysialyltransferase expression.

STX and PST were shown to be expressed in the adult zebrafish cerebellum. Interestingly, different levels of both genes were found in distinct cerebellar layers. However only STX expression was solely detectable in the cerebellar caudal lobe while PST expression was absent in this domain. This suggests that both enzymes might function in a differential or redundant manner by regulating distinct processes in the adult cerebellum via polysialylation of NCAM, including adult neurogenesis, neuronal migration and activity-induced synaptic plasticity. To distinguish between the contributions of both polysialyltransferases to these processes, antibody staining for PSA-NCAM could be performed after morpholino knockdown of STX and PST via electroporation into the adult cerebellum.

To identify further mechanisms regulated by PSA-NCAM in the adult zebrafish cerebellum, the subcellular localization of PSA-NCAM could be examined by immunohistochemistry. For example, localization on dendrites and axons could be interpreted to be important in the regulation of synaptic plasticity. In contrast, a function for PSA-NCAM in adult neuronal progenitor migration could be inferred when PSA-NCAM locates at the surface of neuronal cell bodies or in leading processes of migrating neuronal cells, thereby facilitating navigation and movement of the soma. Interestingly, PSA-NCAM has been recently implicated in the regulation of cognitive learning processes (Gascon et al., 2007b). Furthermore, the mammalian and teleost cerebellum has also been shown to be involved in cognitive learning (Timmann et al., 2002, Rodriguez et al., 2005). To identify a potential role for PSA-NCAM in mediating cognitive learning processes in the adult zebrafish cerebellum, loss of function experiments could be performed. Modulation of PSA-NCAM activity could be achieved by gradual injection of EndoN into the hindbrain ventricle over several days, as learning processes are fairly slow. Differences in the ability of cognitive learning in fish lacking polysialic acid could be assessed through behavioral tests.

PSA-NCAM has been shown to be involved in the regulation of neuronal migration during adult neurogenesis of the olfactory system in rodents (Doetsch et al., 1997). In addition, evidence suggests that the adult CNS in zebrafish undergoes constant neurogenesis in many brain regions including the cerebellum (Zupanc and Clint, 2003, Adolf et al., 2006, Grandel et al., 2006). PSA-NCAM is therefore a likely candidate to regulate neuronal migration in the adult zebrafish cerebellum. Interestingly, adult cerebellar migration in teleosts has been proposed to depend on guidance along vimentin and GFAP positive radial glia fibers (Zupanc and Clint, 2003), similar to cerebellar development during postnatal stages in mammals. The true existence of glial-guided migration in the adult zebrafish cerebellum remains however elusive. To assess whether PSA-NCAM is involved in neuronal migration during adult cerebellar neurogenesis, and whether migration occurs along radial glia fibers into prospective target layers, newborn neurons could be labeled by incorporation of BrdU during recent cell divisions. BrdU-positive neurons could then be visualized together with PSA-NCAM indicating that PSA-NCAM might function in the regulation of neuronal migration. Furthermore, the association of glia cells with migrating neurons could be visualized by triple staining in the cerebellum using antibodies for PSA-

NCAM, BrdU and Vimentin or GFAP to support the migration-regulating function of PSA-NCAM in the adult zebrafish cerebellum.

PSA-NCAM has been implicated in promoting the regeneration of lesions in the adult rodent brain, including spinal cord injuries in mice (Papastefanaki et al., 2007), unilateral lesions in the nigrostriatal pathway in rats (Liu et al., 2006a) and restoration of motor functions in rats with neurotoxin-induced damage of the olivo-cerebellar circuitry (Fernandez et al., 1999). Given that the adult zebrafish CNS has a high regenerative capacity and that PSA-NCAM functions in the regeneration of olivo-cerebellar afferents in rats, PSA-NCAM might also regulate regeneration of the adult zebrafish cerebellum. To assess this possibility, loss of PSA or ectopic expression of PSA could be induced in lesions of the adult cerebellum. For ectopic PSA synthesis, plasmids encoding for both polysialyltransferases could be targeted to the proliferation zones through electroporation. The number of cerebellar neurons at the lesion site would be expected to increase when PSA-NCAM positively regulates this process. This could be visualized by BrdU labeling and antibody staining using neuronal differentiation markers. Loss of PSA-NCAM via electroporation of STX and PST morpholinos into ependymal cells or via EndoN-injection into the IV. ventricle could be further performed, which would be expected to reduce the regeneration capacity of the lesion site. Such a regeneration promoting function for PSA-NCAM might be conserved in mammals and may help in the identification of new treatment strategies for cerebellar neurodegenerative diseases, such as for spinocerebellar ataxia.

5 References

Aaku-Saraste, E., Hellwig, A. and Huttner, W. B., 1996. Loss of occludin and functional tight junctions, but not ZO-1, during neural tube closure--remodeling of the neuroepithelium prior to neurogenesis. Dev Biol. 180, 664-679.

Adams, J. C. and Tucker, R. P., 2000. The thrombospondin type 1 repeat (TSR) superfamily: diverse proteins with related roles in neuronal development. Dev Dyn. 218, 280-299.

Adolf, B., Chapouton, P., Lam, C. S., Topp, S., Tannhauser, B., Strahle, U., Gotz, M. and Bally-Cuif, L., 2006. Conserved and acquired features of adult neurogenesis in the zebrafish telencephalon. Dev Biol. 295, 278-293.

Ahrens, T., Pertz, O., Haussinger, D., Fauser, C., Schulthess, T. and Engel, J., 2002. Analysis of heterophilic and homophilic interactions of cadherins using the c-Jun/c-Fos dimerization domains. J Biol Chem. 277, 19455-19460.

Alder, J., Cho, N. K. and Hatten, M. E., 1996. Embryonic precursor cells from the rhombic lip are specified to a cerebellar granule neuron identity. Neuron. 17, 389-399.

Alder, J., Lee, K. J., Jessell, T. M. and Hatten, M. E., 1999. Generation of cerebellar granule neurons in vivo by transplantation of BMP-treated neural progenitor cells. Nature Neuroscience. 2, 535-540.

Altman, J. B., S. A., 1997. Development of the Cerebellar System in Relation to its Evolution, Structure, and Functions, P. Petralia ed. (Boca Raton, Fl: CRC Press, Inc.).

Angata, K., Chan, D., Thibault, J. and Fukuda, M., 2004. Molecular dissection of the ST8Sia IV polysialyltransferase. Distinct domains are required for neural cell adhesion molecule recognition and polysialylation. J Biol Chem. 279, 25883-25890.

Angata, K. and Fukuda, M., 2003. Polysialyltransferases: major players in polysialic acid synthesis on the neural cell adhesion molecule. Biochimie. 85, 195-206.

Angata, K., Nakayama, J., Fredette, B., Chong, K., Ranscht, B. and Fukuda, M., 1997. Human STX polysialyltransferase forms the embryonic form of the neural cell adhesion molecule. Tissue-specific expression, neurite outgrowth, and chromosomal localization in comparison with another polysialyltransferase, PST. J Biol Chem. 272, 7182-7190.

Angata, K., Suzuki, M. and Fukuda, M., 1998. Differential and cooperative polysialylation of the neural cell adhesion molecule by two polysialyltransferases, PST and STX. J Biol Chem. 273, 28524-28532.

Aruga, J., Yokota, N., Hashimoto, M., Furuichi, T., Fukuda, M. and Mikoshiba, K., 1994. A novel zinc finger protein, zic, is involved in neurogenesis, especially in the cell lineage of cerebellar granule cells. J Neurochem. 63, 1880-1890.

Bagatto, B., Francl, J., Liu, B. and Liu, Q., 2006. Cadherin2 (N-cadherin) plays an essential role in zebrafish cardiovascular development. BMC Dev Biol. 6, 23.

Bahn, S., Harvey, R. J., Darlison, M. G. and Wisden, W., 1996. Conservation of gamma-aminobutyric acid type A receptor alpha 6 subunit gene expression in cerebellar granule cells. Journal of Neurochemistry. 66, 1810-1818.

Bajoghli, B., Aghaallaei, N., Heimbucher, T. and Czerny, T., 2004. An artificial promoter construct for heat-inducible misexpression during fish embryogenesis. Dev Biol. 271, 416-430.

Barth, A. I., Siemers, K. A. and Nelson, W. J., 2002. Dissecting interactions between EB1, microtubules and APC in cortical clusters at the plasma membrane. J Cell Sci. 115, 1583-1590.

References

Becker, C. G., Artola, A., Gerardy-Schahn, R., Becker, T., Welzl, H. and Schachner, M., 1996. The polysialic acid modification of the neural cell adhesion molecule is involved in spatial learning and hippocampal long-term potentiation. J Neurosci Res. 45, 143-152.

Becker, C. G., Schweitzer, J., Feldner, J., Schachner, M. and Becker, T., 2004. Tenascin-R as a repellent guidance molecule for newly growing and regenerating optic axons in adult zebrafish. Mol Cell Neurosci. 26, 376-389.

Behrens, J., 1993. The role of cell adhesion molecules in cancer invasion and metastasis. Breast Cancer Res Treat. 24, 175-184.

Behrens, J., Vakaet, L., Friis, R., Winterhager, E., Van Roy, F., Mareel, M. M. and Birchmeier, W., 1993. Loss of epithelial differentiation and gain of invasiveness correlates with tyrosine phosphorylation of the E-cadherin/beta-catenin complex in cells transformed with a temperature-sensitive v-SRC gene. J Cell Biol. 120, 757-766.

BenArie, N., Bellen, H. J., Armstrong, D. L., McCall, A. E., Gordadze, P. R., Guo, Q. X., Matzuk, M. M. and Zoghbi, H. Y., 1997. Math1 is essential for genesis of cerebellar granule neurons. Nature. 390, 169-172.

Bignami, A. and Dahl, D., 1974. The development of Bergmann glia in mutant mice with cerebellar malformations: reeler, staggerer and weaver. Immunofluorescence study with antibodies to the glial fibrillary acidic protein. J Comp Neurol. 155, 219-229.

Bitzur, S., Kam, Z. and Geiger, B., 1994. Structure and distribution of N-Cadherin in developing zebrafish embryos: morphogenetic effects of ectopic over-expression. Developmental Dynamics. 201, 121-136.

Blaschuk, O. W., Sullivan, R., David, S. and Pouliot, Y., 1990. Identification of a cadherin cell adhesion recognition sequence. Dev Biol. 139, 227-229.

Bonifacino, J. S. and Weissman, A. M., 1998. Ubiquitin and the control of protein fate in the secretory and endocytic pathways. Annu Rev Cell Dev Biol. 14, 19-57.

Bradley, R. S., Cowin, P. and Brown, A. M., 1993. Expression of Wnt-1 in PC12 cells results in modulation of plakoglobin and E-cadherin and increased cellular adhesion. J Cell Biol. 123, 1857-1865.

Brieher, W. M., Yap, A. S. and Gumbiner, B. M., 1996. Lateral dimerization is required for the homophilic binding activity of C-cadherin. J Cell Biol. 135, 487-496.

Bronner-Fraser, M., Wolf, J. J. and Murray, B. A., 1992. Effects of antibodies against N-cadherin and N-CAM on the cranial neural crest and neural tube. Dev Biol. 153, 291-301.

Bruchez, M. J., Moronne, M., Gin, P., Weiss, S. and Alivisatos, A. P., 1998. Semiconductor nanocrystals as fluorescent biological labels. Science. 281, 2013-2016.

Challa, A. K., Beattie, C. E. and Seeger, M. A., 2001. Identification and characterization of roundabout orthologs in zebrafish. Mechanisms of Development. 101, 249-253.

Chappuis-Flament, S., Wong, E., Hicks, L. D., Kay, C. M. and Gumbiner, B. M., 2001. Multiple cadherin extracellular repeats mediate homophilic binding and adhesion. J Cell Biol. 154, 231-243.

Chazal, G., Durbec, P., Jankovski, A., Rougon, G. and Cremer, H., 2000. Consequences of neural cell adhesion molecule deficiency on cell migration in the rostral migratory stream of the mouse. J Neurosci. 20, 1446-1457.

Chen, H. J. and Ma, Z. Z., 2007. N-cadherin expression in a rat model of retinal detachment and reattachment. Invest Ophthalmol Vis Sci. 48, 1832-1838.

Chen, W., Burgess, S., Golling, G., Amsterdam, A. and Hopkins, N., 2002. High-throughput selection of retrovirus producer cell lines leads to markedly improved efficiency of germ line-transmissible insertions in zebra fish. J Virol. 76, 2192-2198.

Cheng, Y. C., Amoyel, M., Qiu, X., Jiang, Y. J., Xu, Q. and Wilkinson, D. G., 2004. Notch activation regulates the segregation and differentiation of rhombomere boundary cells in the zebrafish hindbrain. Dev Cell. 6, 539-550.

Cheung, I. Y., Vickers, A. and Cheung, N. K., 2006. Sialyltransferase STX (ST8SiaII): a novel molecular marker of metastatic neuroblastoma. Int J Cancer. 119, 152-156.

Chizhikov, V., Steshina, E., Roberts, R., Ilkin, Y., Washburn, L. and Millen, K. J., 2006. Molecular definition of an allelic series of mutations disrupting the mouse Lmx1a (dreher) gene. Mamm Genome. 17, 1025-1032.

Colucci-Guyon, E., Gimenez, Y. R. M., Maurice, T., Babinet, C. and Privat, A., 1999. Cerebellar defect and impaired motor coordination in mice lacking vimentin. Glia. 25, 33-43.

Cremer, H., Chazal, G., Goridis, C. and Represa, A., 1997. NCAM is essential for axonal growth and fasciculation in the hippocampus. Mol Cell Neurosci. 8, 323-335.

Cremer, H., Lange, R., Christoph, A., Plomann, M., Vopper, G., Roes, J., Brown, R., Baldwin, S., Kraemer, P., Scheff, S. and et al., 1994. Inactivation of the N-CAM gene in mice results in size reduction of the olfactory bulb and deficits in spatial learning. Nature. 367, 455-459.

D'Souza-Schorey, C., 2005. Disassembling adherens junctions: breaking up is hard to do. Trends Cell Biol. 15, 19-26.

Daniel, J. M. and Reynolds, A. B., 1997. Tyrosine phosphorylation and cadherin/catenin function. Bioessays. 19, 883-891.

Das, G. D., Lammert, G. L. and McAllister, J. P., 1974. Contact guidance and migratory cells in the developing cerebellum. Brain Res. 69, 13-29.

Daston, M. M., Bastmeyer, M., Rutishauser, U. and O'Leary, D. D., 1996. Spatially restricted increase in polysialic acid enhances corticospinal axon branching related to target recognition and innervation. J Neurosci. 16, 5488-5497.

Denaxa, M., Kyriakopoulou, K., Theodorakis, K., Trichas, G., Vidaki, M., Takeda, Y., Watanabe, K. and Karagogeos, D., 2005. The adhesion molecule TAG-1 is required for proper migration of the superficial migratory stream in the medulla but not of cortical interneurons. Dev Biol. 288, 87-99.

Desclin, J., 1974. [Demonstration by light microscopy of the terminal degeneration of afferents of inferior olivary origin in the lateral vestibular (Deiter's) nucleus of the rat]. C R Acad Sci Hebd Seances Acad Sci D. 278, 2931-2934.

Dino, M. R., Willard, F. H. and Mugnaini, E., 1999. Distribution of unipolar brush cells and other calretinin immunoreactive components in the mammalian cerebellar cortex. J Neurocytol. 28, 99-123.

Distel, M., Babaryka, A. and Koster, R. W., 2006. Multicolor in vivo time-lapse imaging at cellular resolution by stereomicroscopy. Dev Dyn. 235, 1100-1106.

Doetsch, F., Garcia-Verdugo, J. M. and Alvarez-Buylla, A., 1997. Cellular composition and three-dimensional organization of the subventricular germinal zone in the adult mammalian brain. J Neurosci. 17, 5046-5061.

Doherty, P., Rowett, L. H., Moore, S. E., Mann, D. A. and Walsh, F. S., 1991. Neurite outgrowth in response to transfected N-CAM and N-cadherin reveals fundamental differences in neuronal responsiveness to CAMs. Neuron. 6, 247-258.

Dubertret, B., Skourides, P., Norris, D. J., Noireaux, V., Brivanlou, A. H. and Libchaber, A., 2002. In Vivo Imaging of Quantum Dots Encapsulated in Phospholipid micelles. Science. 298, 1759-1762.

Duncan, M. K., Bordas, L., Dicicco-Bloom, E. and Chada, K. K., 1997. Expression of the helix-loop-helix genes Id-1 and NSCL-1 during cerebellar development. Dev Dyn. 208, 107-114.

Dynes, J. L. and Ngai, J., 1998. Pathfinding of olfactory neuron axons to stereotyped glomerular targets revealed by dynamic imaging in living zebrafish embryos. Neuron. 20, 1081-1091.

Eckhardt, M., Bukalo, O., Chazal, G., Wang, L., Goridis, C., Schachner, M., Gerardy-Schahn, R., Cremer, H. and Dityatev, A., 2000. Mice deficient in the polysialyltransferase ST8SiaIV/PST-1 allow discrimination of the roles of neural cell adhesion molecule protein and polysialic acid in neural development and synaptic plasticity. J Neurosci. 20, 5234-5244.

Edmondson, J. C. and Hatten, M. E., 1987. Glial-guided granule neuron migration in vitro: a high-resolution time-lapse video microscopic study. J Neurosci. 7, 1928-1934.

Engelkamp, D., Rashbass, P., Seawright, A. and van Heyningen, V., 1999. Role of Pax6 in development of the cerebellar system. Development. 126, 3585-3596.

Englund, C., Kowalczyk, T., Daza, R. A., Dagan, A., Lau, C., Rose, M. F. and Hevner, R. F., 2006. Unipolar brush cells of the cerebellum are produced in the rhombic lip and migrate through developing white matter. J Neurosci. 26, 9184-9195.

Etienne-Manneville, S. and Hall, A., 2001. Integrin-mediated activation of Cdc42 controls cell polarity in migrating astrocytes through PKCzeta. Cell. 106, 489-498.

Etienne-Manneville, S. and Hall, A., 2003. Cdc42 regulates GSK-3beta and adenomatous polyposis coli to control cell polarity. Nature. 421, 753-756.

Fernandez, A. M., Gonzalez de la Vega, A. G., Planas, B. and Torres-Aleman, I., 1999. Neuroprotective actions of peripherally administered insulin-like growth factor I in the injured olivo-cerebellar pathway. Eur J Neurosci. 11, 2019-2030.

Franz, C. K., Rutishauser, U. and Rafuse, V. F., 2005. Polysialylated neural cell adhesion molecule is necessary for selective targeting of regenerating motor neurons. J Neurosci. 25, 2081-2091.

Fricke, C., Lee, J. S., Geiger-Rudolph, S., Bonhoeffer, F. and Chien, C. B., 2001. astray, a zebrafish roundabout homolog required for retinal axon guidance. Science. 292, 507-510.

Fujita, Y., Krause, G., Scheffner, M., Zechner, D., Leddy, H. E., Behrens, J., Sommer, T. and Birchmeier, W., 2002. Hakai, a c-Cbl-like protein, ubiquitinates and induces endocytosis of the E-cadherin complex. Nat Cell Biol. 4, 222-231.

Fukata, M., Watanabe, T., Noritake, J., Nakagawa, M., Yamaga, M., Kuroda, S., Matsuura, Y., Iwamatsu, A., Perez, F. and Kaibuchi, K., 2002. Rac1 and Cdc42 capture microtubules through IQGAP1 and CLIP-170. Cell. 109, 873-885.

Fukuhra, S., Sakurai, A., Yamagishi, A., Sako, K. and Mochizuki, N., 2006. Vascular endothelial cadherin-mediated cell-cell adhesion regulated by a small GTPase, Rap1. J Biochem Mol Biol. 39, 132-139.

Ganzler-Odenthal, S. I. and Redies, C., 1998. Blocking N-cadherin function disrupts the epithelial structure of differentiating neural tissue in the embryonic chicken brain. J Neurosci. 18, 5415-5425.

Gascon, E., Vutskits, L., Jenny, B., Durbec, P. and Kiss, J. Z., 2007a. PSA-NCAM in postnatally generated immature neurons of the olfactory bulb: a crucial role in regulating p75 expression and cell survival. Development. 134, 1181-1190.

Gascon, E., Vutskits, L. and Kiss, J. Z., 2007b. Polysialic acid-neural cell adhesion molecule in brain plasticity: From synapses to integration of new neurons. Brain Res Rev.

Gilthorpe, J. D., Papantoniou, E. K., Chedotal, A., Lumsden, A. and Wingate, R. J. T., 2002. The migration of cerebellar rhombic lip derivatives. Development. 129, 4719-4728.

Gliem, M., Weisheit, G., Mertz, K. D., Endl, E., Oberdick, J. and Schilling, K., 2006. Expression of classical cadherins in the cerebellar anlage: quantitative and functional aspects. Mol Cell Neurosci. 33, 447-458.

Goldowitz, D. and Hamre, K., 1998. The cells and molecules that make a cerebellum. Trends in Neurosciences. 21, 375-382.

Grandel, H., Kaslin, J., Ganz, J., Wenzel, I. and Brand, M., 2006. Neural stem cells and neurogenesis in the adult zebrafish brain: origin, proliferation dynamics, migration and cell fate. Dev Biol. 295, 263-277.

Gregory, W. A., Edmondson, J. C., Hatten, M. E. and Mason, C. A., 1988. Cytology and neuron-glial apposition of migrating cerebellar granule cells in vitro. J Neurosci. 8, 1728-1738.

Gumbiner, B. M., 2000. Regulation of cadherin adhesive activity. J Cell Biol. 148, 399-404.

Gundersen, G. G., 2002. Microtubule capture: IQGAP and CLIP-170 expand the repertoire. Curr Biol. 12, R645-647.

Guo, R., Sakamoto, H., Sugiura, S. and Ogawa, M., 2007. Endothelial cell motility is compatible with junctional integrity. J Cell Physiol. 211, 327-335.

Hager, G., Dodt, H. U., Zieglgansberger, W. and Liesi, P., 1995. Novel forms of neuronal migration in the rat cerebellum. J Neurosci Res. 40, 207-219.

Hamre, K. M. and Goldowitz, D., 1997. meander tail acts intrinsic to granule cell precursors to disrupt cerebellar development: analysis of meander tail chimeric mice. Development. 124, 4201-4212.

Harduin-Lepers, A., Mollicone, R., Delannoy, P. and Oriol, R., 2005. The animal sialyltransferases and sialyltransferase-related genes: a phylogenetic approach. Glycobiology. 15, 805-817.

Hatten, M. E., 1999. Central nervous system neuronal migration. Annual Review of Neuroscience. 22, 511-539.

Hatten, M. E. and Heintz, N., 1995. Mechanisms of Neural Patterning and Specification in the Developing Cerebellum. Annual Review of Neuroscience. 18, 385-408.

Higashijima, S., Mandel, G. and Fetcho, J. R., 2004. Distribution of prospective glutamatergic, glycinergic, and GABAergic neurons in embryonic and larval zebrafish. J Comp Neurol. 480, 1-18.

Higginbotham, H. R. and Gleeson, J. G., 2007. The centrosome in neuronal development. Trends Neurosci. 30, 276-283.

Hildebrandt, H., Becker, C., Murau, M., Gerardy-Schahn, R. and Rahmann, H., 1998. Heterogeneous expression of the polysialyltransferases ST8Sia II and ST8Sia IV during postnatal rat brain development. J Neurochem. 71, 2339-2348.

Hinck, L., Nathke, I. S., Papkoff, J. and Nelson, W. J., 1994. Dynamics of cadherin/catenin complex formation: novel protein interactions and pathways of complex assembly. J Cell Biol. 125, 1327-1340.

Hirotsune, S., Fleck, M. W., Gambello, M. J., Bix, G. J., Chen, A., Clark, G. D., Ledbetter, D. H., McBain, C. J. and Wynshaw-Boris, A., 1998. Graded reduction of Pafah1b1 (Lis1) activity results in neuronal migration defects and early embryonic lethality. Nat Genet. 19, 333-339.

Hong, E. and Brewster, R., 2006. N-cadherin is required for the polarized cell behaviors that drive neurulation in the zebrafish. Development. 133, 3895-3905.

Horne-Badovinac, S., Lin, D., Waldron, S., Schwarz, M., Mbamalu, G., Pawson, T., Jan, Y., Stainier, D. Y. and Abdelilah-Seyfried, S., 2001. Positional cloning of heart and soul reveals multiple roles for PKC lambda in zebrafish organogenesis. Curr Biol. 11, 1492-1502.

Hoshino, M., Nakamura, S., Mori, K., Kawauchi, T., Terao, M., Nishimura, Y. V., Fukuda, A., Fuse, T., Matsuo, N., Sone, M., Watanabe, M., Bito, H., Terashima, T., Wright, C. V. E., Kawaguchi, Y., Nakao, K. and Nabeshima, Y., 2005. Ptf1a, a bHLH transcriptional gene, defines the GABAergic neuronal fates in cerebellum. Neuron. 47, 201-213.

Hove, J. R., Koster, R. W., Forouhar, A. S., Acevedo-Bolton, G., Fraser, S. E. and Gharib, M., 2003. Intracardiac fluid forces are an essential epigenetic factor for embryonic cardiogenesis. Nature. 421, 172-177.

Hu, H., Tomasiewicz, H., Magnuson, T. and Rutishauser, U., 1996. The role of polysialic acid in migration of olfactory bulb interneuron precursors in the subventricular zone. Neuron. 16, 735-743.

Huard, J. M., Forster, C. C., Carter, M. L., Sicinski, P. and Ross, M. E., 1999. Cerebellar histogenesis is disturbed in mice lacking cyclin D2. Development. 126, 1927-1935.

Husmann, K., Faissner, A. and Schachner, M., 1992. Tenascin promotes cerebellar granule cell migration and neurite outgrowth by different domains in the fibronectin type III repeats. J Cell Biol. 116, 1475-1486.

Inoue, T., Tanaka, T., Takeichi, M., Chisaka, O., Nakamura, S. and Osumi, N., 2001. Role of cadherins in maintaining the compartment boundary between the cortex and striatum during development. Development. 128, 561-569.

Jones, M. C., Caswell, P. T. and Norman, J. C., 2006. Endocytic recycling pathways: emerging regulators of cell migration. Curr Opin Cell Biol. 18, 549-557.

Jontes, J. D., Emond, M. R. and Smith, S. J., 2004. In vivo trafficking and targeting of N-cadherin to nascent presynaptic terminals. J Neurosci. 24, 9027-9034.

Junghans, D., Haas, I. G. and Kemler, R., 2005. Mammalian cadherins and protocadherins: about cell death, synapses and processing. Curr Opin Cell Biol. 17, 446-452.

Kadowaki, M., Nakamura, S., Machon, O., Krauss, S., Radice, G. L. and Takeichi, M., 2007. N-cadherin mediates cortical organization in the mouse brain. Dev Biol. 304, 22-33.

Kalinichenko, S. G. and Okhotin, V. E., 2005. Unipolar brush cells--a new type of excitatory interneuron in the cerebellar cortex and cochlear nuclei of the brainstem. Neurosci Behav Physiol. 35, 21-36.

Kametani, Y. and Takeichi, M., 2007. Basal-to-apical cadherin flow at cell junctions. Nat Cell Biol. 9, 92-98.

Karam, S. D., Kim, Y. S. and Bothwell, M., 2001. Granule cells migrate within raphes in the developing cerebellum: an evolutionarily conserved morphogenic event. J Comp Neurol. 440, 127-135.

Kasemeier-Kulesa, J. C., Bradley, R., Pasquale, E. B., Lefcort, F. and Kulesa, P. M., 2006. Eph/ephrins and N-cadherin coordinate to control the pattern of sympathetic ganglia. Development. 133, 4839-4847.

Kawaji, K., Umeshima, H., Eiraku, M., Hirano, T. and Kengaku, M., 2004. Dual phases of migration of cerebellar granule cells guided by axonal and dendritic leading processes. Mol Cell Neurosci. 25, 228-240.

Kemphues, K. J., Priess, J. R., Morton, D. G. and Cheng, N. S., 1988. Identification of genes required for cytoplasmic localization in early C. elegans embryos. Cell. 52, 311-320.

Keyel, P. A., Watkins, S. C. and Traub, L. M., 2004. Endocytic adaptor molecules reveal an endosomal population of clathrin by total internal reflection fluorescence microscopy. J Biol Chem. 279, 13190-13204.

Kholmanskikh, S. S., Koeller, H. B., Wynshaw-Boris, A., Gomez, T., Letourneau, P. C. and Ross, M. E., 2006. Calcium-dependent interaction of Lis1 with IQGAP1 and Cdc42 promotes neuronal motility. Nat Neurosci. 9, 50-57.

Kim, C. H., Bae, Y. K., Yamanaka, Y., Yamashita, S., Shimizu, T., Fujii, R., Park, H. C., Yeo, S. Y., Huh, T. L., Hibi, M. and Hirano, T., 1997. Overexpression of neurogenin induces ectopic expression of HuC in zebrafish. Neuroscience Letters. 239, 113-116.

Kim, Y. J., Johnson, K. R. and Wheelock, M. J., 2005. N-cadherin-mediated cell motility requires cis dimers. Cell Commun Adhes. 12, 23-39.

Kimmel, C. B., Ballard, W. W., Kimmel, S. R., Ullmann, B. and Schilling, T. F., 1995. Stages of embryonic development of the zebrafish. Developmental Dynamics. 203, 235-310.

Köster, R. W. and Fraser, S. E., 2001. Direct imaging of in vivo neuronal migration in the developing cerebellum. Current Biology. 11, 1858-1863.

Köster, R. W. and Fraser, S. E., 2004. Time-lapse microscopy of brain development. In: H. William Detrich, M. W., Leonard I. Zon (Ed.), The Zebrafish: Cellular and Developmental Biology, vol.76. Academic Press, San Diego, pp. 205-233.

Köster, R. W. and Fraser, S. E., 2006. FGF signaling mediates regeneration of the differentiating cerebellum through repatterning of the anterior hindbrain and reinitiation of neuronal migration. Journal of Neuroscience. 26, 7293-7304.

Kostetskii, I., Moore, R., Kemler, R. and Radice, G. L., 2001. Differential adhesion leads to segregation and exclusion of N-cadherin-deficient cells in chimeric embryos. Dev Biol. 234, 72-79.

Kuroda, S., Fukata, M., Nakagawa, M., Fujii, K., Nakamura, T., Ookubo, T., Izawa, I., Nagase, T., Nomura, N., Tani, H., Shoji, I., Matsuura, Y., Yonehara, S. and Kaibuchi, K., 1998. Role of IQGAP1, a target of the small GTPases Cdc42 and Rac1, in regulation of E-cadherin- mediated cell-cell adhesion. Science. 281, 832-835.

Kurosawa, N., Yoshida, Y., Kojima, N. and Tsuji, S., 1997. Polysialic acid synthase (ST8Sia II/STX) mRNA expression in the developing mouse central nervous system. J Neurochem. 69, 494-503.

Kyriakopoulou, K., de Diego, I., Wassef, M. and Karagogeos, D., 2002. A combination of chain and neurophilic migration involving the adhesion molecule TAG-1 in the caudal medulla. Development. 129, 287-296.

Landsberg, R. L., Awatramani, R. B., Hunter, N. L., Farago, A. F., DiPietrantonio, H. J., Rodriguez, C. I. and Dymecki, S. M., 2005. Hindbrain rhombic lip is comprised of discrete progenitor cell populations allocated by Pax6. Neuron. 48, 933-947.

Lavdas, A. A., Franceschini, I., Dubois-Dalcq, M. and Matsas, R., 2006. Schwann cells genetically engineered to express PSA show enhanced migratory potential without impairment of their myelinating ability in vitro. Glia. 53, 868-878.

Le, T. L., Yap, A. S. and Stow, J. L., 1999. Recycling of E-cadherin: a potential mechanism for regulating cadherin dynamics. J Cell Biol. 146, 219-232.

Lele, Z., Folchert, A., Concha, M., Rauch, G.-J., Geisler, R., Rosa, F. M., Wilson, S. W., Hammerschmidt, M. and Bally-Cuif, L., 2002. parachute/n-cadherin is required for morphogenesis and maintained integrity of the zebrafish neural tube. Development. 129, 3281-3294.

Liesi, P., 1992. Neuronal migration on laminin involves neuronal contact formation followed by nuclear movement inside a preformed process. Exp Neurol. 117, 103-113.

Liesi, P., Akinshola, E., Matsuba, K., Lange, K. and Morest, K., 2003. Cellular migration in the postnatal rat cerebellar cortex: confocal-infrared microscopy and the rapid Golgi method. J Neurosci Res. 72, 290-302.

Liesi, P. and Wright, J. M., 1996. Weaver granule neurons are rescued by calcium channel antagonists and antibodies against a neurite outgrowth domain of the B2 chain of laminin. J Cell Biol. 134, 477-486.

Liu, B. F., Gao, E. J., Zeng, X. Z., Ji, M., Cai, Q., Lu, Q., Yang, H. and Xu, Q. Y., 2006a. Proliferation of neural precursors in the subventricular zone after chemical lesions of the nigrostriatal pathway in rat brain. Brain Res. 1106, 30-39.

Liu, Q., Azodi, E., Kerstetter, A. E. and Wilson, A. L., 2004. Cadherin-2 and cadherin-4 in developing, adult and regenerating zebrafish cerebellum. Developmental Brain Research. 150, 63-71.

Liu, Q., Liu, B., Wilson, A. L. and Rostedt, J., 2006b. cadherin-6 message expression in the nervous system of developing zebrafish. Dev Dyn. 235, 272-278.

Lock, J. G. and Stow, J. L., 2005. Rab11 in recycling endosomes regulates the sorting and basolateral transport of E-cadherin. Mol Biol Cell. 16, 1744-1755.

Long, Q., Meng, A., Wang, H., Jessen, J. R., Farrell, M. J. and Lin, S., 1997. GATA-1 expression pattern can be recapitulated in living transgenic zebrafish using GFP reporter gene. Development. 124, 4105-4111.

Lu, X., Le Noble, F., Yuan, L., Jiang, Q., De Lafarge, B., Sugiyama, D., Breant, C., Claes, F., De Smet, F., Thomas, J. L., Autiero, M., Carmeliet, P., Tessier-Lavigne, M. and Eichmann, A., 2004. The netrin receptor UNC5B mediates guidance events controlling morphogenesis of the vascular system. Nature. 432, 179-186.

Luckner, R., Obst-Pernberg, K., Hirano, S., Suzuki, S. T. and Redies, C., 2001. Granule cell raphes in the developing mouse cerebellum. Cell Tissue Res. 303, 159-172.

Luo, J., Treubert-Zimmermann, U. and Redies, C., 2004. Cadherins guide migrating Purkinje cells to specific parasagittal domains during cerebellar development. Mol Cell Neurosci. 25, 138-152.

Luo, Y., Ferreira-Cornwell, M., Baldwin, H., Kostetskii, I., Lenox, J., Lieberman, M. and Radice, G., 2001. Rescuing the N-cadherin knockout by cardiac-specific expression of N- or E-cadherin. Development. 128, 459-469.

Luo, Y., High, F. A., Epstein, J. A. and Radice, G. L., 2006. N-cadherin is required for neural crest remodeling of the cardiac outflow tract. Dev Biol. 299, 517-528.

Machold, R. and Fishell, G., 2005. Math1 is expressed in temporally discrete pools of cerebellar rhombic-lip neural progenitors. Neuron. 48, 17-24.

Malicki, J., Jo, H. and Pujic, Z., 2003. Zebrafish N-cadherin, encoded by the glass onion locus, plays an essential role in retinal patterning. Dev Biol. 259, 95-108.

Marx, M., Rivera-Milla, E., Stummeyer, K., Gerardy-Schahn, R. and Bastmeyer, M., 2007. Divergent evolution of the vertebrate polysialyltransferase Stx and Pst genes revealed by fish-to-mammal comparison. Dev Biol. 306, 560-571.

Marx, M., Rutishauser, U. and Bastmeyer, M., 2001. Dual function of polysialic acid during zebrafish central nervous system development. Development. 128, 4949-4958.

Mary, S., Charrasse, S., Meriane, M., Comunale, F., Travo, P., Blangy, A. and Gauthier-Rouviere, C., 2002. Biogenesis of N-cadherin-dependent cell-cell contacts in living fibroblasts is a microtubule-dependent kinesin-driven mechanism. Mol Biol Cell. 13, 285-301.

Mathis, L., Bonnerot, C., Puelles, L. and Nicolas, J. F., 1997. Retrospective clonal analysis of the cerebellum using genetic laacZ/lacZ mouse mosaics. Development. 124, 4089-4104.

Matsunaga, M., Hatta, K., Nagafuchi, A. and Takeichi, M., 1988. Guidance of optic nerve fibres by N-cadherin adhesion molecules. Nature. 334, 62-64.

Matsuyoshi, N., Hamaguchi, M., Taniguchi, S., Nagafuchi, A., Tsukita, S. and Takeichi, M., 1992. Cadherin-mediated cell-cell adhesion is perturbed by v-src tyrosine phosphorylation in metastatic fibroblasts. J Cell Biol. 118, 703-714.

McManus, M. F., Nasrallah, I. M., Pancoast, M. M., Wynshaw-Boris, A. and Golden, J. A., 2004. Lis1 is necessary for normal non-radial migration of inhibitory interneurons. Am J Pathol. 165, 775-784.

Mege, R. M., Goudou, D., Diaz, C., Nicolet, M., Garcia, L., Geraud, G. and Rieger, F., 1992. N-cadherin and N-CAM in myoblast fusion: compared localisation and effect of blockade by peptides and antibodies. J Cell Sci. 103 (Pt 4), 897-906.

Mimori-Kiyosue, Y., Shiina, N. and Tsukita, S., 2000. Adenomatous polyposis coli (APC) protein moves along microtubules and concentrates at their growing ends in epithelial cells. J Cell Biol. 148, 505-518.

Miyasaka, N., Sato, Y., Yeo, S. Y., Hutson, L. D., Chien, C. B., Okamoto, H. and Yoshihara, Y., 2005. Robo2 is required for establishment of a precise glomerular map in the zebrafish olfactory system. Development. 132, 1283-1293.

Miyata, T., Maeda, T. and Lee, J. E., 1999. NeuroD ir required for differentiation of the granule cells in the cerebellum and hippocampus. Genes & Development. 13, 1647-1652.

Miyazaki, T., Fukaya, M., Shimizu, H. and Watanabe, M., 2003. Subtype switching of vesicular glutamate transporters at parallel fibre-Purkinje cell synapses in developing mouse cerebellum. Eur J Neurosci. 17, 2563-2572.

Muller, D., Djebbara-Hannas, Z., Jourdain, P., Vutskits, L., Durbec, P., Rougon, G. and Kiss, J. Z., 2000. Brain-derived neurotrophic factor restores long-term potentiation in polysialic acid-neural cell adhesion molecule-deficient hippocampus. Proc Natl Acad Sci U S A. 97, 4315-4320.

Muller, D., Wang, C., Skibo, G., Toni, N., Cremer, H., Calaora, V., Rougon, G. and Kiss, J. Z., 1996. PSA-NCAM is required for activity-induced synaptic plasticity. Neuron. 17, 413-422.

Mumm, J. S., Williams, P. R., Godinho, L., Koerber, A., Pittman, A. J., Roeser, T., Chien, C. B., Baier, H. and Wong, R. O., 2006. In vivo imaging reveals dendritic targeting of laminated afferents by zebrafish retinal ganglion cells. Neuron. 52, 609-621.

Murakami, S., Seki, T., Rutishauser, U. and Arai, Y., 2000. Enzymatic removal of polysialic acid from neural cell adhesion molecule perturbs the migration route of luteinizing hormone-releasing hormone neurons in the developing chick forebrain. J Comp Neurol. 420, 171-181.

Nakagawa, S. and Takeichi, M., 1998. Neural crest emigration from the neural tube depends on regulated cadherin expression. Development. 125, 2963-2971.

Nakayama, J., Angata, K., Ong, E., Katsuyama, T. and Fukuda, M., 1998. Polysialic acid, a unique glycan that is developmentally regulated by two polysialyltransferases, PST and STX, in the central nervous system: from biosynthesis to function. Pathol Int. 48, 665-677.

Niell, C. M., Meyer, M. P. and Smith, S. J., 2004. In vivo imaging of synapse formation on a growing dendritic arbor. Nature Neuroscience. 7, 254-260.

Nieman, M. T., Prudoff, R. S., Johnson, K. R. and Wheelock, M. J., 1999. N-cadherin promotes motility in human breast cancer cells regardless of their E-cadherin expression. J Cell Biol. 147, 631-644.

Noles, S. R. and Chenn, A., 2007. Cadherin inhibition of beta-catenin signaling regulates the proliferation and differentiation of neural precursor cells. Mol Cell Neurosci. 35, 549-558.

Noritake, J., Fukata, M., Sato, K., Nakagawa, M., Watanabe, T., Izumi, N., Wang, S., Fukata, Y. and Kaibuchi, K., 2004. Positive role of IQGAP1, an effector of Rac1, in actin-meshwork formation at sites of cell-cell contact. Mol Biol Cell. 15, 1065-1076.

Noritake, J., Watanabe, T., Sato, K., Wang, S. and Kaibuchi, K., 2005. IQGAP1: a key regulator of adhesion and migration. J Cell Sci. 118, 2085-2092.

Nunzi, M. G., Birnstiel, S., Bhattacharyya, B. J., Slater, N. T. and Mugnaini, E., 2001. Unipolar brush cells form a glutamatergic projection system within the mouse cerebellar cortex. J Comp Neurol. 434, 329-341.

Nunzi, M. G., Shigemoto, R. and Mugnaini, E., 2002. Differential expression of calretinin and metabotropic glutamate receptor mGluR1alpha defines subsets of unipolar brush cells in mouse cerebellum. J Comp Neurol. 451, 189-199.

Ogata, S., Morokuma, J., Hayata, T., Kolle, G., Niehrs, C., Ueno, N. and Cho, K. W., 2007. TGF-beta signaling-mediated morphogenesis: modulation of cell adhesion via cadherin endocytosis. Genes Dev. 21, 1817-1831.

Ohno, S., 2001. Intercellular junctions and cellular polarity: the PAR-aPKC complex, a conserved core cassette playing fundamental roles in cell polarity. Curr Opin Cell Biol. 13, 641-648.

Ong, E., Nakayama, J., Angata, K., Reyes, L., Katsuyama, T., Arai, Y. and Fukuda, M., 1998. Developmental regulation of polysialic acid synthesis in mouse directed by two polysialyltransferases, PST and STX. Glycobiology. 8, 415-424.

Ono, K., Tomasiewicz, H., Magnuson, T. and Rutishauser, U., 1994. N-CAM mutation inhibits tangential neuronal migration and is phenocopied by enzymatic removal of polysialic acid. Neuron. 13, 595-609.

Ozawa, M., 2002. Lateral dimerization of the E-cadherin extracellular domain is necessary but not sufficient for adhesive activity. J Biol Chem. 277, 19600-19608.

Papastefanaki, F., Chen, J., Lavdas, A. A., Thomaidou, D., Schachner, M. and Matsas, R., 2007. Grafts of Schwann cells engineered to express PSA-NCAM promote functional recovery after spinal cord injury. Brain. 130, 2159-2174.

Park, K. W., Crouse, D., Lee, M., Karnik, S. K., Sorensen, L. K., Murphy, K. J., Kuo, C. J. and Li, D. Y., 2004. The axonal attractant Netrin-1 is an angiogenic factor. Proc Natl Acad Sci U S A. 101, 16210-16215.

Pascual, M., Abasolo, I., Mingorance-Le Meur, A., Martinez, A., Del Rio, J. A., Wright, C. V., Real, F. X. and Soriano, E., 2007. Cerebellar GABAergic progenitors adopt an external granule cell-like phenotype in the absence of Ptf1a transcription factor expression. Proc Natl Acad Sci U S A. 104, 5193-5198.

Patel, S. D., Ciatto, C., Chen, C. P., Bahna, F., Rajebhosale, M., Arkus, N., Schieren, I., Jessell, T. M., Honig, B., Price, S. R. and Shapiro, L., 2006. Type II cadherin ectodomain structures: implications for classical cadherin specificity. Cell. 124, 1255-1268.

Paulin, M. G., 2005. Evolution of the cerebellum as a neuronal machine for Bayesian state estimation. J Neural Eng. 2, S219-234.

Pece, S. and Gutkind, J. S., 2002. E-cadherin and Hakai: signalling, remodeling or destruction? Nat Cell Biol. 4, E72-74.

Peluso, J. J., 2000. N-cadherin-mediated cell contact regulates ovarian surface epithelial cell survival. Biol Signals Recept. 9, 115-121.

Pogoriler, J., Millen, K., Utset, M. and Du, W., 2006. Loss of cyclin D1 impairs cerebellar development and suppresses medulloblastoma formation. Development. 133, 3929-3937.

Pokutta, S., Herrenknecht, K., Kemler, R. and Engel, J., 1994. Conformational changes of the recombinant extracellular domain of E-cadherin upon calcium binding. Eur J Biochem. 223, 1019-1026.

Ponti, G., Peretto, P. and Bonfanti, L., 2006. A subpial, transitory germinal zone forms chains of neuronal precursors in the rabbit cerebellum. Dev Biol. 294, 168-180.

Poo, M., 1982. Rapid lateral diffusion of functional A Ch receptors in embryonic muscle cell membrane. Nature. 295, 332-334.

Popoff, V., Mardones, G. A., Tenza, D., Rojas, R., Lamaze, C., Bonifacino, J. S., Raposo, G. and Johannes, L., 2007. The retromer complex and clathrin define an early endosomal retrograde exit site. J Cell Sci. 120, 2022-2031.

Puzdrowski, R. L., 1989. Peripheral distribution and central projections of the lateral-line nerves in goldfish. Brain Behavior and Evolution. 34, 110-131.

Radice, G. L., Rayburn, H., Matsunami, H., Knudsen, K. A., Takeichi, M. and Hynes, R. O., 1997. Developmental defects in mouse embryos lacking N-cadherin. Dev Biol. 181, 64-78.

Raetzman, L. T. and Siegel, R. E., 1999. Immature granule neurons from cerebella of different ages exhibit distinct developmental potentials. J Neurobiol. 38, 559-570.

Rakic, P., 1971. Neuron-glia relationship during granule cell migration in developing cerebellar cortex. A Golgi and electronmicroscopic study in Macacus Rhesus. J Comp Neurol. 141, 283-312.

Rakic, P., 1990. Principles of neural cell migration. Experientia. 46, 882-891.

Redies, C., 2000. Cadherins in the central nervous system. Prog Neurobiol. 61, 611-648.

Reichert, M. F. W. B. R. H., 1996. Neuroanatomy of the zebrafish brain. Birkhaeuser Verlag, CH-4010 Basel, Switzerland.

Reiss, K., Maretzky, T., Ludwig, A., Tousseyn, T., de Strooper, B., Hartmann, D. and Saftig, P., 2005. ADAM10 cleavage of N-cadherin and regulation of cell-cell adhesion and beta-catenin nuclear signalling. Embo J. 24, 742-752.

Rhee, J., Mahfooz, N. S., Arregui, C., Lilien, J., Balsamo, J. and VanBerkum, M. F., 2002. Activation of the repulsive receptor Roundabout inhibits N-cadherin-mediated cell adhesion. Nat Cell Biol. 4, 798-805.

Ridley, A. J., Schwartz, M. A., Burridge, K., Firtel, R. A., Ginsberg, M. H., Borisy, G., Parsons, J. T. and Horwitz, A. R., 2003. Cell migration: integrating signals from front to back. Science. 302, 1704-1709.

Rieger, S., Kulkarni, R. P., Darcy, D., Fraser, S. E. and Koster, R. W., 2005. Quantum dots are powerful multipurpose vital labeling agents in zebrafish embryos. Dev Dyn. 234, 670-681.

Rieger, S. K., RW, 2007. Preparation of Zebrafish Embryos for Transmission Electron Microscopy. Cold Spring Harbor Protocols. 2.

Riehl, R., Johnson, K., Bradley, R., Grunwald, G. B., Cornel, E., Lilienbaum, A. and Holt, C. E., 1996. Cadherin function is required for axon outgrowth in retinal ganglion cells in vivo. Neuron. 17, 837-848.

Rio, C., Rieff, H. I., Qi, P., Khurana, T. S. and Corfas, G., 1997. Neuregulin and erbB receptors play a critical role in neuronal migration. Neuron. 19, 39-50.

Rivas, R. J. and Hatten, M. E., 1995. Motility and cytoskeletal organization of migrating cerebellar granule neurons. J Neurosci. 15, 981-989.

Rodriguez, C. I. and Dymecki, S. M., 2000. Origin of the precerebellar system. Neuron. 27, 475-486.

Rodriguez, F., Duran, E., Gomez, A., Ocana, F. M., Alvarez, E., Jimenez-Moya, F., Broglio, C. and Salas, C., 2005. Cognitive and emontional functions of the teleost fish cerebellum. Brain Research Bulletin. 66, 365-370.

Ross, M. E., Fletcher, C., Mason, C. A., Hatten, M. E. and Heintz, N., 1990. Meander tail reveals a discrete developmental unit in the mouse cerebellum. Proc Natl Acad Sci U S A. 87, 4189-4192.

Rupp, R. A., Snider, L. and Weintraub, H., 1994. Xenopus embryos regulate the nuclear localization of XMyoD. Genes Dev. 8, 1311-1323.

Rutishauser, U., 1998. Polysialic acid at the cell surface: biophysics in service of cell interactions and tissue plasticity. J Cell Biochem. 70, 304-312.

Rutishauser, U. and Landmesser, L., 1996. Polysialic acid in the vertebrate nervous system: a promoter of plasticity in cell-cell interactions. Trends Neurosci. 19, 422-427.

Rutishauser, U., Watanabe, M., Silver, J., Troy, F. A. and Vimr, E. R., 1985. Specific alteration of NCAM-mediated cell adhesion by an endoneuraminidase. J Cell Biol. 101, 1842-1849.

Sako, Y. and Kusumi, A., 1994. Compartmentalized structure of the plasma membrane for receptor movements as revealed by a nanometer-level motion analysis. J Cell Biol. 125, 1251-1264.

Salinas, P. C., Fletcher, C., Copeland, N. G., Jenkins, N. A. and Nusse, R., 1994. Maintenance of Wnt-3 expression in Purkinje cells of the mouse cerebellum depends on interactions with granule cells. Development. 120, 1277-1286.

Schaar, B. T. and McConnell, S. K., 2005. Cytoskeletal coordination during neuronal migration. Proc Natl Acad Sci U S A. 102, 13652-13657.

Schier, A. F., Neuhauss, S. C., Harvey, M., Malicki, J., Solnica-Krezel, L., Stainier, D. Y., Zwartkruis, F., Abdelilah, S., Stemple, D. L., Rangini, Z., Yang, H. and Driever, W., 1996. Mutations affecting the development of the embryonic zebrafish brain. Development. 123, 165-178.

Schmahmann, J. D., 2004. Disorders of the cerebellum: ataxia, dysmetria of thought, and the cerebellar cognitive affective syndrome. J Neuropsychiatry Clin Neurosci. 16, 367-378.

Schmahmann, J. D. and Caplan, D., 2006. Cognition, emotion and the cerebellum. Brain. 129, 290-292.

Schmid, R. S., Shelton, S., Stanco, A., Yokota, Y., Kreidberg, J. A. and Anton, E. S., 2004. alpha3beta1 integrin modulates neuronal migration and placement during early stages of cerebral cortical development. Development. 131, 6023-6031.

Sehnert, A. J. and Stainier, D. Y., 2002. A window to the heart: can zebrafish mutants help us understand heart disease in humans? Trends Genet. 18, 491-494.

Seidenfaden, R., Krauter, A., Schertzinger, F., Gerardy-Schahn, R. and Hildebrandt, H., 2003. Polysialic acid directs tumor cell growth by controlling heterophilic neural cell adhesion molecule interactions. Mol Cell Biol. 23, 5908-5918.

Sekerkova, G., Ilijic, E. and Mugnaini, E., 2004. Time of origin of unipolar brush cells in the rat cerebellum as observed by prenatal bromodeoxyuridine labeling. Neuroscience. 127, 845-858.

Seki, T. and Rutishauser, U., 1998. Removal of polysialic acid-neural cell adhesion molecule induces aberrant mossy fiber innervation and ectopic synaptogenesis in the hippocampus. J Neurosci. 18, 3757-3766.

Sgaier, S. K., Millet, S., Villanueva, M. P., Berenshteyn, F., Song, C. and Joyner, A. L., 2005. Morphogenetic and cellular movements that shape the mouse cerebellum: insights from genetic fate mapping. Neuron. 45, 27-40.

Shaner, N. C., Campbell, R. E., Steinbach, P. A., Giepmans, B. N., Palmer, A. E. and Tsien, R. Y., 2004. Improved monomeric red, orange and yellow fluorescent proteins derived from Discosoma sp. red fluorescent protein. Nat Biotechnol. 22, 1567-1572.

Shapiro, L., Fannon, A. M., Kwong, P. D., Thompson, A., Lehmann, M. S., Grubel, G., Legrand, J. F., Als-Nielsen, J., Colman, D. R. and Hendrickson, W. A., 1995. Structural basis of cell-cell adhesion by cadherins. Nature. 374, 327-337.

Sharma, M. and Henderson, B. R., 2007. IQ-domain GTPase-activating protein 1 regulates beta-catenin at membrane ruffles and its role in macropinocytosis of N-cadherin and adenomatous polyposis coli. J Biol Chem. 282, 8545-8556.

Sharma, M., Leung, L., Brocardo, M., Henderson, J., Flegg, C. and Henderson, B. R., 2006. Membrane localization of adenomatous polyposis coli protein at cellular protrusions: targeting sequences and regulation by beta-catenin. J Biol Chem. 281, 17140-17149.

Shi, S. H., Jan, L. Y. and Jan, Y. N., 2003. Hippocampal neuronal polarity specified by spatially localized mPar3/mPar6 and PI 3-kinase activity. Cell. 112, 63-75.

Shibamoto, S., Hayakawa, M., Takeuchi, K., Hori, T., Oku, N., Miyazawa, K., Kitamura, N., Takeichi, M. and Ito, F., 1994. Tyrosine phosphorylation of beta-catenin and

plakoglobin enhanced by hepatocyte growth factor and epidermal growth factor in human carcinoma cells. Cell Adhes Commun. 1, 295-305.
Shih, J. and Keller, R., 1992. Patterns of cell motility in the organizer and dorsal mesoderm of Xenopus laevis. Development. 116, 915-930.
Shintani, Y., Fukumoto, Y., Chaika, N., Grandgenett, P. M., Hollingsworth, M. A., Wheelock, M. J. and Johnson, K. R., 2007. ADH-1 suppresses N-cadherin-dependent pancreatic cancer progression. Int J Cancer.
Shoval, I., Ludwig, A. and Kalcheim, C., 2007. Antagonistic roles of full-length N-cadherin and its soluble BMP cleavage product in neural crest delamination. Development. 134, 491-501.
Shu, T., Ayala, R., Nguyen, M. D., Xie, Z., Gleeson, J. G. and Tsai, L. H., 2004. Ndel1 operates in a common pathway with LIS1 and cytoplasmic dynein to regulate cortical neuronal positioning. Neuron. 44, 263-277.
Solecki, D. J., Govek, E. E., Tomoda, T. and Hatten, M. E., 2006. Neuronal polarity in CNS development. Genes Dev. 20, 2639-2647.
Solecki, D. J., Model, L., Gaetz, J., Kapoor, T. M. and Hatten, M. E., 2004. Par6alpha signaling controls glial-guided neuronal migration. Nat Neurosci. 7, 1195-1203.
Sotelo, C., 2004. Cellular and genetic regulation of the development of the cerebellar system. Progress in Neurobiology. 72, 295-449.
Sotelo, C. and Changeux, J. P., 1974. Bergmann fibers and granular cell migration in the cerebellum of homozygous weaver mutant mouse. Brain Res. 77, 484-491.
Sotelo, C., Hillman, D. E., Zamora, A. J. and Llinas, R., 1975. Climbing fiber deafferentation: its action on Purkinje cell dendritic spines. Brain Res. 98, 574-581.
Sotelo, C. and Rio, J. P., 1980. Cerebellar malformation obtained in rats by early postnatal treatment with 6-aminonicotinamide. Role of neuron-glia interactions in cerebellar development. Neuroscience. 5, 1737-1759.
Steinberg, M. S. and McNutt, P. M., 1999. Cadherins and their connections: adhesion junctions have broader functions. Curr Opin Cell Biol. 11, 554-560.
Su, H. L., Muguruma, K., Matsuo-Takasaki, M., Kengaku, M., Watanabe, K. and Sasai, Y., 2006. Generation of cerebellar neuron precursors from embryonic stem cells. Dev Biol. 290, 287-296.
Suyama, K., Shapiro, I., Guttman, M. and Hazan, R. B., 2002. A signaling pathway leading to metastasis is controlled by N-cadherin and the FGF receptor. Cancer Cell. 2, 301-314.
Takeichi, M., 1995. Morphogenetic roles of classic cadherins. Curr Opin Cell Biol. 7, 619-627.
Tamura, K., Shan, W. S., Hendrickson, W. A., Colman, D. R. and Shapiro, L., 1998. Structure-function analysis of cell adhesion by neural (N-) cadherin. Neuron. 20, 1153-1163.
Tanaka, T., Serneo, F. F., Higgins, C., Gambello, M. J., Wynshaw-Boris, A. and Gleeson, J. G., 2004. Lis1 and doublecortin function with dynein to mediate coupling of the nucleus to the centrosome in neuronal migration. J Cell Biol. 165, 709-721.
Taneyhill, L. A., Coles, E. G. and Bronner-Fraser, M., 2007. Snail2 directly represses cadherin6B during epithelial-to-mesenchymal transitions of the neural crest. Development. 134, 1481-1490.
Tang, J., Landmesser, L. and Rutishauser, U., 1992. Polysialic acid influences specific pathfinding by avian motoneurons. Neuron. 8, 1031-1044.
Taniguchi, H., Kawauchi, D., Nishida, K. and Murakami, F., 2006. Classic cadherins regulate tangential migration of precerebellar neurons in the caudal hindbrain. Development. 133, 1923-1931.

Teruel, M. N., Blanpied, T. A., Shen, K., Augustine, G. J. and Meyer, T., 1999. A versatile microporation technique for the transfection of cultured CNS neurons. Journal of Neuroscience Methods. 93, 37-48.

Theisen, C. S., Wahl, J. K., 3rd, Johnson, K. R. and Wheelock, M. J., 2007. NHERF links the N-cadherin/catenin complex to the platelet-derived growth factor receptor to modulate the actin cytoskeleton and regulate cell motility. Mol Biol Cell. 18, 1220-1232.

Thisse, B., Heyer, V., Lux, A., Alunni, V., Degrave, A., Seiliez, I., Kirchner, J., Parkhill, J. P. and Thisse, C., 2004. Spatial and temporal expression of the zebrafish genome by large-scale in situ hybridization screening. Methods Cell Biol. 77, 505-519.

Timmann, D., Drepper, J., Maschke, M., Kolb, F. P., Boring, D., Thilmann, A. F. and Diener, H. C., 2002. Motor deficits cannot explain impaired cognitive associative learning in cerebellar patients. Neuropsychologia. 40, 788-800.

Togashi, H., Abe, K., Mizoguchi, A., Takaoka, K., Chisaka, O. and Takeichi, M., 2002. Cadherin regulates dendritic spine morphogenesis. Neuron. 35, 77-89.

Tsai, J. W., Chen, Y., Kriegstein, A. R. and Vallee, R. B., 2005. LIS1 RNA interference blocks neural stem cell division, morphogenesis, and motility at multiple stages. J Cell Biol. 170, 935-945.

Tsai, L. H. and Gleeson, J. G., 2005. Nucleokinesis in neuronal migration. Neuron. 46, 383-388.

Ulfig, N. and Chan, W. Y., 2004. Expression patterns of PSA-NCAM in the human ganglionic eminence and its vicinity: role of PSA-NCAM in neuronal migration and axonal growth? Cells Tissues Organs. 177, 229-236.

Volkmann, K., Rieger, S., Babaryka, A. and Köster, R. W., 2007. The zebrafish cerebellar rhombic lip is spatially patterned in producing granule cell populations of different functional compartments. Developmental Biology.

von Trotha, J. W., Campos-Ortega, J. A. and Reugels, A. M., 2006. Apical localization of ASIP/PAR-3:EGFP in zebrafish neuroepithelial cells involves the oligomerization domain CR1, the PDZ domains, and the C-terminal portion of the protein. Dev Dyn. 235, 967-977.

Vutskits, L., Gascon, E., Zgraggen, E. and Kiss, J. Z., 2006. The polysialylated neural cell adhesion molecule promotes neurogenesis in vitro. Neurochem Res. 31, 215-225.

Walkenhorst, J., Dutting, D., Handwerker, C., Huai, J. S., Tanaka, H. and Drescher, U., 2000. The EphA4 receptor tyrosine kinase is necessary for the guidance of nasal retinal ganglion cell axons in vitro. Molecular and Cellular Neuroscience. 16, 365-375.

Wallingford, J. B., Rowning, B. A., Vogeli, K. M., Rothbacher, U., Fraser, S. E. and Harland, R. M., 2000. Dishevelled controls cell polarity during Xenopus gastrulation. Nature. 405, 81-85.

Wang, C., Rougon, G. and Kiss, J. Z., 1994. Requirement of polysialic acid for the migration of the O-2A glial progenitor cell from neurohypophyseal explants. J Neurosci. 14, 4446-4457.

Wang, V. Y., Rose, M. F. and Zoghbi, H. Y., 2005. Math1 expression redefines the rhombic lip derivatives and reveals novel lineages within the brainstem and cerebellum. Neuron. 48, 31-48.

Wang, V. Y. and Zoghbi, H. Y., 2001. Genetic regulation of cerebellar development. Nature Reviews Neuroscience. 2, 484-491.

Wang, W., Mullikin-Kilpatrick, D., Crandall, J. E., Gronostajski, R. M., Litwack, E. D. and Kilpatrick, D. L., 2007. Nuclear factor I coordinates multiple phases of cerebellar granule cell development via regulation of cell adhesion molecules. J Neurosci. 27, 6115-6127.

Watanabe, T., Wang, S., Noritake, J., Sato, K., Fukata, M., Takefuji, M., Nakagawa, M., Izumi, N., Akiyama, T. and Kaibuchi, K., 2004. Interaction with IQGAP1 links APC to Rac1, Cdc42, and actin filaments during cell polarization and migration. Dev Cell. 7, 871-883.

Weidner, K. M., Behrens, J., Vandekerckhove, J. and Birchmeier, W., 1990. Scatter factor: molecular characteristics and effect on the invasiveness of epithelial cells. J Cell Biol. 111, 2097-2108.

Weinhold, B., Seidenfaden, R., Rockle, I., Muhlenhoff, M., Schertzinger, F., Conzelmann, S., Marth, J. D., Gerardy-Schahn, R. and Hildebrandt, H., 2005. Genetic ablation of polysialic acid causes severe neurodevelopmental defects rescued by deletion of the neural cell adhesion molecule. J Biol Chem. 280, 42971-42977.

Westerfield, M., 1995. The Zebrafish Book. A Guide for the Laboratory Use of Zebrafish (Danio rerio), 3rd Edition. Eugene, OR, University of Oregon Press,385 (Book).

Wichterle, H., Garcia-Verdugo, J. M., Herrera, D. G. and Alvarez-Buylla, A., 1999. Young neurons from medial ganglionic eminence disperse in adult and embryonic brain. Nat Neurosci. 2, 461-466.

Wichterle, H., GarciaVerdugo, J. M. and AlvarezBuylla, A., 1997. Direct evidence for homotypic, glia-independent neuronal migration. Neuron. 18, 779-791.

Wiedenmann, J., Ivanchenko, S., Oswald, F., Schmitt, F., Rocker, C., Salih, A., Spindler, K. D. and Nienhaus, G. U., 2004. EosFP, a fluorescent marker protein with UV-inducible green-to-red fluorescence conversion. Proc Natl Acad Sci U S A. 101, 15905-15910.

Williams, J. A., Barrios, A., Gatchalian, C., Rubin, L., Wilson, S. W. and Holder, N., 2000. Programmed cell death in zebrafish Rohon Beard neurons is influenced by TrkC1/NT-3 signaling. Developmental Biology. 226, 220-230.

Wilson, L. J. and Wingate, R. J. T., 2006. Temporal identity transition in the avian cerebellar rhombic lip. Developmental Biology. 297, 508-521.

Wingate, R. J. T., 2001. The rhombic lip and early cerebellar development. Current Opinion in Neurobiology. 11, 82-88.

Wingate, R. J. T., 2005. Math-Map(ic)s. Neuron. 48, 1-7.

Wingate, R. J. T. and Hatten, M. E., 1999. The role of the rhombic lip in avian cerebellum development. Development. 126, 4395-4404.

Wullimann, M. F., 1998. The Central Nervous System. In: Evans, D. H. (Ed.), The Physiology of Fishes. CRC Press, Boca Raton, New York, pp. 245-282.

Wullimann, M. F. and Northcutt, R. G., 1988. Connections of the Corpus Cerebelli in the Green Sunfish and the Common Goldfish - a Comparison of Perciform and Cypriniform Teleosts. Brain Behavior and Evolution. 32, 293-316.

Wullimann, M. F. and Northcutt, R. G., 1989. Afferent connections of the valvula cerebelli in two teleosts, the common goldfish and the green sunfish. Journal of Comparative Neurology. 289, 554-567.

Wurst, W. and Bally-Cuif, L., 2001. Neural plate patterning: upstream and downstream of the isthmic organizer. Nature Reviews Neuroscience. 2, 99-108.

Xiao, K., Garner, J., Buckley, K. M., Vincent, P. A., Chiasson, C. M., Dejana, E., Faundez, V. and Kowalczyk, A. P., 2005. p120-Catenin regulates clathrin-dependent endocytosis of VE-cadherin. Mol Biol Cell. 16, 5141-5151.

Xie, Z., Sanada, K., Samuels, B. A., Shih, H. and Tsai, L. H., 2003. Serine 732 phosphorylation of FAK by Cdk5 is important for microtubule organization, nuclear movement, and neuronal migration. Cell. 114, 469-482.

Yacubova, E. and Komuro, H., 2002. Intrinsic program for migration of cerebellar granule cells in vitro. J Neurosci. 22, 5966-5981.

Yap, A. S., Brieher, W. M., Pruschy, M. and Gumbiner, B. M., 1997. Lateral clustering of the adhesive ectodomain: a fundamental determinant of cadherin function. Curr Biol. 7, 308-315.

Zagon, I. S., McLaughlin, P. J. and Rogers, W. E., 1985. Neuronal migration independent of glial guidance: light and electron microscopic studies in the cerebellar cortex of neonatal rats. Acta Anat (Basel). 122, 77-86.

Zhang, Y., Zhang, X., Yeh, J., Richardson, P. and Bo, X., 2007. Engineered expression of polysialic acid enhances Purkinje cell axonal regeneration in L1/GAP-43 double transgenic mice. Eur J Neurosci. 25, 351-361.

Zinkevich, N. S., Bosenko, D. V., Link, B. A. and Semina, E. V., 2006. laminin alpha 1 gene is essential for normal lens development in zebrafish. BMC Dev Biol. 6, 13.

Zohn, I. E., Li, Y., Skolnik, E. Y., Anderson, K. V., Han, J. and Niswander, L., 2006. p38 and a p38-interacting protein are critical for downregulation of E-cadherin during mouse gastrulation. Cell. 125, 957-969.

Zupanc, G. K. and Clint, S. C., 2003. Potential role of radial glia in adult neurogenesis of teleost fish. Glia. 43, 77-86.

Zupanc, G. K., Hinsch, K. and Gage, F. H., 2005. Proliferation, migration, neuronal differentiation, and long-term survival of new cells in the adult zebrafish brain. J Comp Neurol. 488, 290-319.

Zupanc, G. K. and Zupanc, M. M., 2006. New neurons for the injured brain: mechanisms of neuronal regeneration in adult teleost fish. Regen Med. 1, 207-216.

6 Appendix

6.1 Supplementary Figures

Supplementary Figure 1 Semi-thin section of wild type embryo showing region of ultrastructural analysis

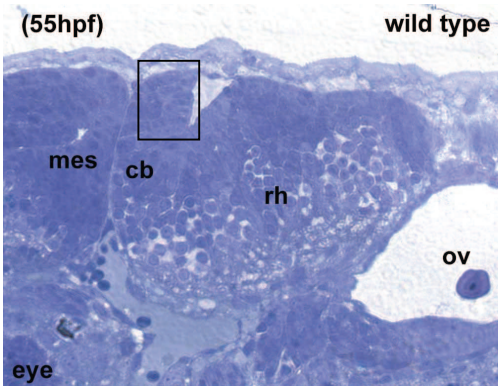

(Suppl. Fig. 1) Sagittal section (20μm) of a wild type embryo at 55hpf stained with toluidine blue before preparation of ultra-thin sections (60nm) from the region marked by a black box for TEM analysis (see Fig. 3.3). Abbr.: mes, mesencephalon; cb, cerebellum; rh, rhombencephalon; ov, otic vesicle

Supplementary Figure 2 Semi-thin section of rescued *pac*-/-R embryo showing region of ultrastructural analysis

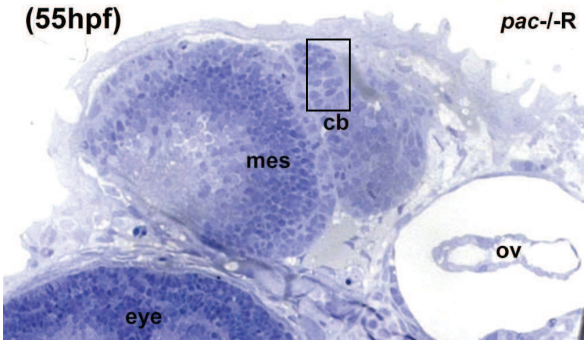

(Suppl. Fig. 2) Sagittal section (20μm) of a *pac*-/-R embryo at 55hpf stained with toluidine blue before preparation of ultra-thin sections (60nm) from the region marked by a black box for TEM analysis (see Fig. 3.9F, G).

Supplementary Figure 3 Schematic representation of Cadherin-2 deletion variants

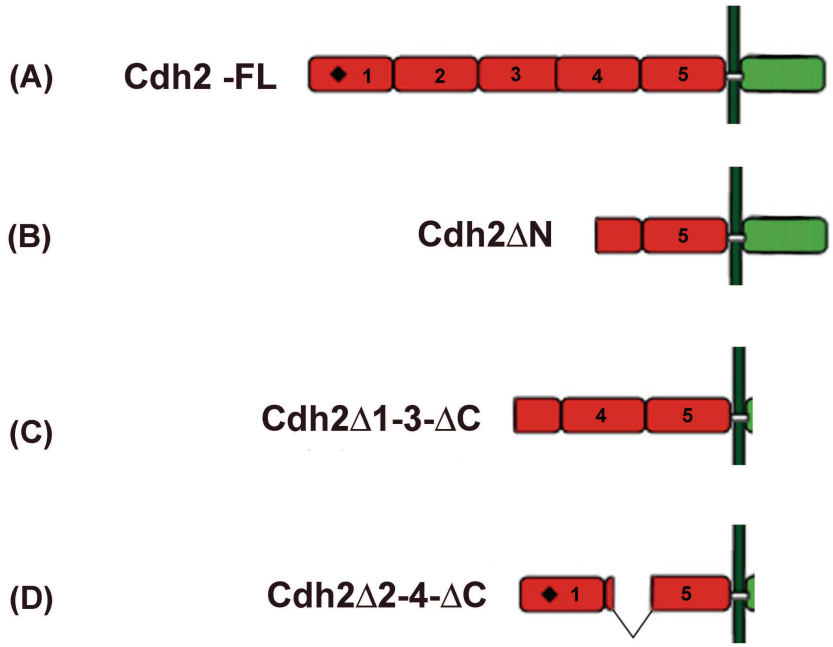

(Suppl. Fig. 3) Structural features of Cadherin-2 variants. (A) Full-length Cadherin-2 possesses 5 ectodomains (red), a single-pass transmembrane domain (white) and a cytoplasmic domain (green). Ectodomains are numbered from 1 to 5. The black square shown in ectodomain 1 designates two important structural features for cis-dimer formation, the conserved tryptophane residue at amino acid position 2 (Trp2) and an HAV motif. (B) The dominant-negative Cadherin-2-variant (Cdh2ΔN) has the first four ectodomains deleted, while ectodomains 1, 2, 3 and the cytoplasmic were deleted in the Cdh2Δ1-3ΔC variant (C), including the Trp2 and HAV motif. (D) In contrast, deletion of ectodomains 2, 3, 4 and the cytoplasmic tail of Cdh2Δ2-4ΔC retained the Trp2 and HAV motif in ectodomain 1. Note that the missing cytoplasmic domains of Cdh2Δ1-3ΔC and Cdh2Δ2-4ΔC were replaced by fusion to monomeric cherry.

Supplementary Figure 4 Nucleotide sequences of cloned *stx* and *pst*

st8sia2 (stx) 1,146bp

ATGTCTTTTGAATTCCGAATACTGATGTTTGGAATCGGGACAGCGCTGGTTATATTTGTGATTATA
GCTGATATATCGGAAGTGGAGGAAGAAATCGCGAACATTGAGGATTCACGGAAATTCCACTTAA
AAAGTGTCGCCCTTCAGTCCAACAGAAGTTCAGATCTGAATGCTGCCCCTACTTCTCTAGTCACAT
ATAGAAAGAGCAAAGTCTCCTCTCTAGCTTCACCGTCTGACATAAAGCGCAAAACCAGCAATTCA
TCCTCATCTGAATGGACTTTCAACAGAACCTTGTCTAACCTCATCAGGAAAAACATTTTGAAATTC
CTGGATGCTGAGAGGGACATCTCAATTCTGAAGAGCACCTTTAAACCTGGTGATGTAATTCATTA
TATATTTGACCGTCAGAGCACCACAAACATCTCAGAGAATCTGTACCACCTTTTACCAACTGTGTC
GCCCATGAAGAATCAGCATTACAGAAAGTGTGCCATCGTAGGGAACTCTGGCATACTACTGAAC
AGCAGCTGCGGCAGAGAGATTGACTCGCACGACTTTGTTATTAGGTGTAACTTGGCTCCGGTGGA
GGAGTATGCTGCTGACGTGGGCCTGCGCACCAGCCTGGTGACTATGAACCCCTCAGTGGTGCAGC
GTGCCTTTCAGGACCTGAACAGCGAAGAGTGGGTGCAGCGTTTCGTCCAGCGGCCGCAAAGCCTT

AGTGGGAGTGTGTTGTGGATTCCTGCCTTTATGGCTAAAGGAGGAGAGGAGCGAGTGGAGTGGG
CCATTCGTCTCATTCTCCTGCATACGGTGAACGTCCGCACCGCCTTCCCCTCTCTGCGTCTGCTCC
ATGCTGTCAGAGGTTACTGGCTGACCAACCATGTCCAGATCAAACGTCCCACCACTGGACTGCTA
ATGTACACCATGGCTACTCGCTTTTGTGATGAGATCCACCTGTATGGCTTCTGGCCCTTCGCTCAC
GACCCTGACGGCAAACCAGTCAAGTATCACTACTATGATACACTAACTTACCACTACACATCTAG
TGCCAGTCCACACACAATGCCTCTGGAGTTTAGGACCTTAAGTGCTCTTCACAGACAGGGGGCGC
TGCGGCTGCACACGGGACCATGCAAACCTCCTACATGA

st8sia4 (pst) 1,077bp

ATGCGGCTTTCACGCAAACACTGGACGGTCTGTACCATTAGCGTTCTGCTTGTATTGTTTTACAAG
ACGACAGACATTGGCAGAAACGAAGTGCACCAGAAAGCTAGTCTGACATGGTACTTGGAGCCAA
GTGCTACTAGACTGATGGCCAATGGCTCTGAGAAACTTTTCGGCAATGTCTTGAATGGTCTTGACT
TGGGAGTTGGATGGAAGATTAATGCCACCCTTGTGTCCATAATAAGGAAAGACATACTCCGCTAC
TTGGACGCAGAGAGAGACGTGTCGGTTATCAAGAGCAATTTTAAGCCGGGCGACACCATCCGCT
ACGTTCTGGACAGACGCAGGACATTCAGCGTATCTCAAACTCTCCATAGTTTACTTCCTGAAGTCT
CTCCTCTGAAGAACAAGACGTTCAAGACATGTGCAGTGGTGGGAAACTCAGGCATTCTCCTGAAG
AGCGGATGTGGAAAGGAGATAGACAACCATAGTTTTGTTATACGATGTAACCTGGCTCCTCTGGA
GGGTTTCGCAGATGATGTAGGATTGCGGTCAGACTTCACCACGATGAACCCATCTGTGATCCAGC
GGGTGTACGGGGGTCTGCGGGAGGAAACCCAGCAGGAGAATCTCATCCAGCGCTTGCGGCAGCT
GAATGACAGCGTGCTCTGGATTCCTGCCTTCATGGTGAAGGGTGGCATGAAGCATGTGGACACGG
TCAATGAGCTCATCCTTAAACACAAGCTGAAAGTGCGCACAGCTTACCCTTCACTCCGCCTAATC
CACGCTGTACGAGGGTTTTGGCTTACAAATAAAATCAATATCAAACGACCCACTACTGGATTACT
GATGTACACGATGGCTACACGCTTCTGTGACGAGATCTACCTGTATGGATTCTGGCCTTTTCCCAA
AGACGCCAGCGGAAATCCTGTTCAATATCATTACTTTGATGGACTGAAATATCGATATTTTTCCAA
TGCGGGTCCTCACCGCATGCCACTGGAGTTTCAAACGCTGCAAAGACTGCACAGCAAGGGGGCG
CTGAAACTCACGACATCTAAATGCACATCAACTTAA

6.2 Movie legends

Supplementary Movie 1

This movie shows the rotation of the cerebellar anlage from an initial anteroposterior into a mediolateral orientation. The fourth ventricle of the hindbrain begins to open at ~13hpf (see black lines, arrow) and as the ventricle widens the cerebellar lobes are repositioned, such that the anterior cerebellum is bounded at the MHB (dashed black line) and its caudal aspect lines to the fourth ventricle (solid black line). The movie shows a dorsal view of 50μm projections of a time-lapse movie from 13hpf –26hpf. Individual stacks of 3μm sections were recorded in 12-minute intervals using the Zeiss C-Apochromat 40x water-immersion objective.

Supplementary Movie 3.1 GPC migration in the differentiating zebrafish cerebellum

This movie shows the homotypic neurophilic migration mode of zebrafish cerebellar GPCs, occurring in a highly directional manner. Movie sequence 1: Colored dots depict GPCs migrating in separate chains with arrows pointing to single GPCs within each chain adhering to other neuronal progenitors as they move along them towards the MHB. Movie sequence 2 shows pseudo-colored GPCs of several chains to illustrate their highly cohesive migratory behavior. 12μm stacks were recorded in 1μm sections every 12 minutes using a 63x water immersion objective. Each stack was projected into a single image for each time point and displayed as movie sequence using QuickTime Pro 7.2.

Supplementary Movie 3.2 GPC migration behavior in wild type gata1:GFP embryos

This movie shows a dorsal view of the antero-lateral migration mode of zebrafish cerebellar GPCs in the gata1:GFP transgenic line heading from the URL towards and along the MHB. Granule cell clusters along the MHB in dorso-medial domains constitute the future corpus cerebelli, while ventrolateral clusters form the future eminentia granularis. 50μm stacks were recorded in 3μm sections every 12 minutes using a 40x water immersion objective. Each stack was projected into a single image for each time point and displayed as movie sequence using QuickTime Pro 7.2.

Supplementary Movie 3.3 GPC migration behavior in *pac*R2.10 gata1:GFP embryos

This movie shows a dorsal view of migrating GPCs in *parachute* R2.10 gata1:GFP mutants, lacking functional Cadherin-2. Loss of Cadherin-2 results in impaired migration of cerebellar GPCs with the majority of cells, although motile remaining in positions close to the point where they emerge along the medio-lateral axis of the differentiating cerebellum. 50μm stacks were recorded in 3μm sections every 12 minutes using a 40x water immersion objective. Each stack was projected into a single image for each time point and displayed as movie sequence using QuickTime Pro 7.2.

Supplementary Movie 3.4 Coherent migration behavior of GPC in wild type gata1:GFP embryos

This movie shows a dorsal view of the migration of wild type GPCs of gata1:GFP embryos in higher magnification. Only one cerebellar lobe is presented for simplicity to emphasize the highly directional and coherent migration behavior of zebrafish cerebellar GPCs. Individual traces of GPCs are subsequently followed using ImageJ software and the manual tracking tool plug-in. The final arrows depict the overall migration direction of traced GPCs. 50μm stacks were recorded in 3μm sections every 12 minutes using a 40x water immersion objective. Each stack was projected into a single image for each time point and displayed as movie sequence using QuickTime Pro 7.2.

Supplementary Movie 3.5 Loss of directionality and coherence for GPCs of *pac*-/-R embryos

This movie shows a dorsal view of migrating zebrafish cerebellar GPCs after the temporal rescue of *pac*-/-R gata1:GFP embryos. Loss of Cadherin-2 around the onset of GPC migration results in loss of migratory directionality and coherence, also depicted by the following tracks showing randomized migratory behavior. Only one cerebellar half is presented. 50μm stacks were recorded in 3μm sections every 12 minutes using a 40x water immersion objective. Each stack was projected into a single image for each time point and displayed as movie sequence using QuickTime Pro 7.2.

Supplementary Movie 3.6 GPC migration after transplantation of wild type gata1:GFP host cells into wild type donor embryos

This movie shows a dorsal view of one cerebellar lobe after transplantation of gata1:GFP donor cells at sphere stage into wild type brass embryos, thus visualizing donor cells in the cerebellum by their GFP expression. Migration of these GPCs was followed by *in vivo* time-lapse imaging starting at 48hpf. This shows that wild type donor GPCs migrate in anterolateral directions from the URL towards the MHB in a wild type environment. Individual GPCs were further manually traced by using the ImageJ tracking tool. 30μm stacks were recorded in 3μm sections every 12 minutes using a 40x water immersion objective. Each stack was projected into a single image for each time point and displayed as movie sequence using QuickTime Pro 7.2.

Supplementary Movie 3.7 GPC migration after transplantation of *pac*-/-R gata1:GFP host cells into wild type donor embryos

This movie shows a dorsal view of migrating *pac*-/-R gata1:GFP-derived cerebellar GPCs in a wild type host cerebellum after transplantation. In contrast to transplanted control cells, GPCs of *pac*-/-R gata1:GFP fail to migrate in a directional manner. Subsequent cell tracing of individual cells reveals their high migratory motility but a lack in directionality, as depicted by their tracks. Only one cerebellar half is presented. 50μm stacks were recorded in 3μm sections every 12 minutes using a 40x water immersion objective. Each stack was projected into a single image for each time point and displayed as movie sequence using QuickTime Pro 7.2.

Supplementary Movie 3.8 Expression of dominant-negative Cadherin-2-mCherry in GPCs of the cerebellum

This movie shows strong transient expression of a heatshock-induced dominant-negative Cadherin-2 variant (8xHSE:*Cdh2*ΔN-mCherry) by cerebellar GPCs in the URL of the gata1:GFP transgenic line. GPCs expressing this construct fail to initiate migration and emigrate from the URL, while GFP-expressing GPCs in their vicinity exhibit a chain-like migration behavior towards the MHB. Only one cerebellar half is presented. 20μm stacks were recorded in 1μm sections every 12 minutes using a 63x water immersion objective.

Each stack was projected into a single image for each time point and displayed as movie sequence using QuickTime Pro 7.2.

Supplementary Movie 3.9 Expression of a non-functional Cadherin-2-mCherry deletion variant in migrating GPCs of the cerebellum

This movie shows control cerebellar GPCs in gata1:GFP embryos strongly expressing a non-functional Cadherin-2 variant (8xHSE:*Cdh2*Δ2-4ΔC-mCherry) after heatshock induction. GFP-expressing GPCs co-expressing this variant exhibit wild type-like directional migration behavior along other co-migrating GPCs towards the MHB. Only one cerebellar half is presented. 25μm stacks were recorded in 1μm sections every 12 minutes using a 63x water immersion objective. Each stack was projected into a single image for each time point and displayed as movie sequence using QuickTime Pro 7.2.

Supplementary Movie 3.10 Cadherin-2 dynamics in a migrating cerebellar GPC

This movie shows a higher magnification of one migrating GPC, shown in Movie 3.9, to reveal dynamics of Cadherin-2 clusters. The GPC expressing the non-functional Cdh2Δ2-4ΔC-mCherry deletion variant initially accumulates Cadherin-2 containing clusters in the leading edge (white arrow) at the onset of forward movement. During the following movement, Cadherin-2 clusters are dynamically shifted first into the rear and then become equally distributed along one lateral wall where the GPC remains in contact with another co-migrating cell (arrow, see also the slow motion and GFP overlay channel, following the initial red channel movie sequence). As soon as the contact is released Cadherin-2 clusters are disassembled in the trailing edge (yellow arrow). Cadherin-2 clusters are subsequently re-located into the anterior of the cell. 10μm stacks were recorded in 1μm sections every 12 minutes using a 63x water immersion objective. Each stack was projected into a single image for each time point and displayed as movie sequence using QuickTime Pro 7.2.

Supplementary Movie 3.11 Cadherin-2 dynamics in a zebrafish PAC2 fibroblast cell

This movie shows a zebrafish PAC2 fibroblast cell transfected with Cdh2Δ2-4ΔC-EosFP before and after photo-conversion. Besides the rapid diffusion of Cadherin-2 within the cell (right arrow) upon UV-laser conversion from green to red emission by ROI, Cadherin-2

clusters appear as if they are transported in a microtubule-like manner from the cell cortex into the cytoplasm, when a second patch in the membrane was converted (upper arrow). A single section was recorded every minute using a 63x water immersion objective. The images were assembled into a movie sequence using QuickTime Pro 7.2.

Supplementary Movie 3.12 Directed movement of Cadherin-2 within the plasma membrane of a migrating GPC

This movie shows the directed transport of UV-converted Cdh2Δ2-4ΔC-EosFP within the plasma membrane of a GPC. Cadherin-2 containing clusters move towards the leading edge, thereby passing along the base of an extended neurite. 10μm stacks were recorded in 1μm sections every 5 minutes using a 63x water immersion objective. Each stack was projected into a single image for each time point and displayed as movie sequence using QuickTime Pro 7.2.

Supplementary Movie 3.13 Neuronal migration of cerebellar progenitor cells after injection of PBS

Lateral view of migrating cerebellar neuronal progenitor cells in PBS-injected control embryo beginning at 35hpf. Neuronal migration of control cerebellar neuronal progenitors was analyzed by *in vivo* time-lapse confocal microscopy. Migrating cells are marked by expression of uncGFP, thus labeling the soma but not the nucleus. Recording of migratory neurons started at 35hpf, two hours after PBS injection into the hindbrain ventricle. All cells that are first positioned at the URL (solid line in first frame and then arrowhead) migrate rostrally toward the MHB. They further continue ventral migration along the MHB towards the brain stem. Approx. 11 hours later, neuronal cells assemble in a ventral target cluster and cease migration. 50μm stacks were recorded in 3μm sections every 12 minutes using a 40x water immersion objective. Each stack was projected into a single image for each time point and displayed as movie sequence using QuickTime Pro 7.2.

Supplementary Movie 3.14 Neuronal migration of cerebellar progenitor cells after injection of EndoN

Lateral view of migrating cerebellar neuronal progenitor cells in embryos lacking polysialic acid after EndoN-treatment. Migration of cerebellar neuronal progenitors after

loss of PSA was analyzed by *in vivo* time-lapse confocal microscopy, beginning at 35hpf. Neuronal cells are marked by expression of uncGFP, thus labeling the soma but not the nucleus. Recording started two hours after EndoN-injection into the hindbrain ventricle. Initially several neuronal cells are positioned at the URL (top) and extend processes. The top cell extends several filopodia into the periphery but never initiates migration during the length of the time-lapse movie. The cell located just below even retracts its process and becomes stationary at the URL. Over a period of 17 hours these neuronal progenitors remain stalled close to the URL and fail to migrate towards anteroventral brain regions. 50μm stacks were recorded in 3μm sections every 12 minutes using a 40x water immersion objective. Each stack was projected into a single image for each time point and displayed as movie sequence using QuickTime Pro 7.2.

6.3 List of Figures

Figure 1.1 Anatomical view of the zebrafish cerebellum

Figure 1.2 Rotation of the cerebellar anlage

Figure 1.3 Cerebellar proliferation zones and migration routes of URL-derived progenitors in zebrafish

Figure 1.4 Neuronal progenitor cells span the entire width of the early cerebellar anlage in zebrafish

Figure 1.5 Microtubule-based nuclear translocation in migrating neuronal cells

Figure 1.6 Model for cell polarization and centrosomal repositioning in response to cell-cell adhesion

Figure 1.7 The adherens junction complex

Figure 3.1 Absence of glial-like cell morphologies in the early differentiating cerebellum

Figure 3.2 Expression of glial markers in the caudal hindbrain but not in the differentiating cerebellum

Figure 3.3 Ultrastructural analyses of the differentiating cerebellum and caudal hindbrain

Figure 3.4 Chain-like migration behavior of cerebellar GPCs

Figure 3.5 Zebrafish Cadherin-2 is a candidate to mediate adhesive contacts between migrating GPCs

Figure 3.6 Atypical migration behavior of GPCs in *pac*R2.10 mutant embryos

Figure 3.7 Neurulation defects are rescued in *parachute* mutants by *cadherin-2* mRNA injection

Figure 3.8 GPCs in *pac*-/-R mutant embryos lack coherent and directional migration behavior

Figure 3.9 Reduction of contact stabilities among GPCs in *pac*-/-R embryos due to the absence of Cadherin-2

Figure 3.10 Length-width ratios and orientation angles of cerebellar GPCs

Figure 3.11 Randomized centrosomal positioning in GPCs of *pac*-/-R embryos

Figure 3.12 Migrating GPCs in *pac*-/-R embryos lack directionality but not motility

Figure 3.13 Genetic mosaic analysis and expression of Cadherin-2 deletion variants

Figure 3.14 Expression patterns of granule cell differentiation markers in the wild type and *pac*-/-R cerebellum

Figure 3.15 Absent expression of *vglut1* in the dorsal cerebellum of *pac*-/-R embryos at 6dpf

Figure 3.16 Expression of $gaba_A R\alpha 6$ is absent in the dorsal cerebellum of *pac*-/-R embryos at 6dpf

Figure 3.17 Increased neuronal cell death in the dorsal cerebellum of *pac*-/-R embryos

Figure 3.18 *Atonal1a* expression analysis in embryos injected with different Cadherin-2 variants

Figure 3.19 Cdh2Δ2-4ΔC-mCherry can serve as *in vivo* reporter for adherens junctions

Figure 3.20 Cdh2Δ2-4ΔC-mCherry dynamics in migrating cerebellar GPCs

Figure 3.21 Directed transport of Cadherin-2 within the cytoplasmic membrane

Figure 3.22 Sequence alignment of zebrafish STX and PST compared to other vertebrates

Figure 3.23 Expression of *stx* and *pst* in the developing zebrafish brain

Figure 3.24 Adult expression of *ncam* and the polysialyltransferases *stx* and *pst*

Figure 3.25 Expression of *ncam, stx*, *pst* and PSA expression at stages of neuronal migration in the developing cerebellum

Figure 3.26 Immunohistochemical analysis of PSA-NCAM after PSA degradation in the zebrafish cerebellum

Figure 3.27 Loss of PSA influences motility of cerebellar neuronal progenitor cells

Figure 4 Model for Cadherin-2 dependent directional and coherent migration of GPCs during zebrafish cerebellar development

Supplementary Figure 1 Semi-thin section of wild type embryo showing region of ultrastructural analysis

Supplementary Figure 2 Semi-thin section of rescued *pac*-/-R embryo showing region of ultrastructural analysis

Supplementary Figure 3 Schematic representation of Cadherin-2 deletion variants

Supplementary Figure 4 Nucleotide sequences of cloned *stx* and *pst*

6.4 List of Tables

Table 1: RNA probes used for in-situ hybridization sorted according to their function in the zebrafish central nervous system.

Table 2: Fluorescent proteins used for intravital labeling

Table 3: Plasmids used for RNA and DNA injections into zebrafish embryos

Table 4: Oligonucleotides for zebrafish cDNA amplification.

Table 5: PCR conditions for genotyping of wild type and *pac*R2.10 alleles

Table 6: Conditions used for time-lapse recordings of living specimens

6.5 Preparation of zebrafish embryos for transmission electron microscopy – online publication

Please cite as: CSH Protocols; 2007; doi:10.1101/pdb.prot4772

Protocol

Preparation of Zebrafish Embryos for Transmission Electron Microscopy

Sandra Rieger[1] and Reinhard W. Köster

GSF-National Research Center for Environment and Health, Institute of Developmental Genetics, 85764 München-Neuherberg, Germany

[1]Corresponding author (sandra.rieger{at}gsf.de)

INTRODUCTION

This protocol describes a procedure for the fixation and embedding of zebrafish embryos at organogenesis stages (48-72 hours post-fertilization [hpf]) for transmission electron microscopy (TEM). The lengths of individual steps may be adjusted according to the developmental stage of the specimen.

RELATED INFORMATION

TEM using the described method was performed to identify the ultrastructure of the neuronal precursors inside the embryonic zebrafish cerebellar rhombic lip (see Fig. 1 and Fig. 2).

6.6 Quantum Dots Are Powerful Multipurpose Vital Labeling Agents in Zebrafish Embryos

Summary

Existing imaging techniques in biology have been largely dependent on the use of organic fluorophores or fluorescent proteins. Most fluorescent molecules have however some limitations such as reduced photostability or short lifetimes. To establish fluorophores with improved properties for *in vivo* imaging applications, we characterized the use of quantum dots labeling in living zebrafish. Quantum dots are small inorganic semiconductor nanocrystals, which have high emission quantum yields and narrow emission spectra, they have a long shelf life and are extremely photostable. Depending on the nanocrystal size, their emission/emitted fluorescence fills the entire emission spectrum from blue to far-red. In general, smaller quantum dots tend to emit in the blue range whereas larger dots emit closer to the red spectrum. Although quantum dots are made of reactive nanocrystal cores, which are highly toxic such as cadmium-selenide, advances have been made to generate quantum dots with an additional non-reactive stabilizing shell, being made of zinc sulfide or silica to improve their optical properties. A further polymercoating on the outside makes them hydrophilic and renders them useful for conjugation to biological molecules to be used in intravital applications.

Using streptavidin-conjugated quantum dots 605 (QD605), made from a cadmium selenide core, a zinc sulfide shell, and a secondary outer coat conjugated to streptavidin, these nanocrystals could be proved useful for zebrafish imaging applications. To test whether living zebrafish embryos tolerate QD605, small quantities were injected into 1 to 4-cell stage embryos and analyzed by confocal microscopy at several developmental stages. In addition, QD605 were sonicated to reduce aggregation of these nanocrystals and tested for their *in vivo* tolerance, as sonication may destroy the non-reactive shell thereby releasing toxic core components. Such injected embryos displayed a bright red fluorescence and did not reveal any morphological alterations. These findings showed that QD605 are tolerated by zebrafish during embryonic development, thus making them useful for *in vivo* applications.

Quantum dots can be localized in different cell compartments, depending on their outer coat (Bruchez et al., 1998, Dubertret et al., 2002). To reveal the subcellular distribution of QD605 in zebrafish, the eyes of injected embryos were analyzed by comparing QD605 to

different fluorescent dyes thereby delineating distinct cellular compartments. While the location of the green fluorescent membrane-bound dye Bodipy Ceramide and a nuclear histone 2B fusion protein to monomeric red fluorescent protein (mRFP) did not reveal similarities to the subcellular distribution of QD605, the cytoplasmic staining of unc76:GFP, which is excluded from the nucleus, was most reminiscent of the QD605 distribution within the cell, showing that QD605 locate to the cytoplasm and are excluded from the nucleus.

The next challenge was to investigate whether QD605 are suitable for lineage tracing. QD605 were therefore co-injected with GFP messenger RNA into single blastomeres at the 32-cell and 64-cell stage. Like GFP, QD605 remained restricted to descendants of the injected blastomeres during proliferation and did not spread through cytoplasmic bridges into neighboring cells. This demonstrated that QD605 behave in a similar manner as GFP and therefore QD605 can be used for lineage tracing experiments in zebrafish embryos.

To test the photostability of QD605, microangiography was performed to outline individual blood vessels. Small amounts of QD605 were therefore injected into the heart ventricle of living zebrafish larvae at 5dpf. Following injection, QD605 were evenly distributed throughout the entire vascular system within a short period. Such larvae were further soaked in the green fluorescent dye Bodipy Ceramide to label cellular membranes. Subsequently, a frequency of high-power laser scans was applied to the trunk. While Bodipy Ceramide completely bleached within this region, QD605 labeling appeared almost as bright as before, thus confirming that QD605 are highly photostable fluorophores.

Many vital fluorescent proteins do not survive tissue fixations and therefore can only serve for *in vivo* imaging applications, thus making it difficult to analyze them in the context of expression analysis by immunohistochemistry. Microangiographed embryos were fixed and methanol dehydrated, followed by rehydration and immunostaining for anti-acetylated Tubulin to co-label dendritic and axonal processes within the embryonic brain. Neither the fixation nor the staining procedure resulted in a loss of fluorescence. This showed that QD605 can be used for multicolor labeling approaches in fixed specimens, to visualize axonal tracts in context with the vasculature of the brain.

Similar to GFP, QD605 are excited at a wavelength of 488nm. Thus, when present in one cell both could be co-excited. In contrast to GFP however QD605 have a large Stoke's shift, therefore the emission of QD605 will be easily separable from GFP. To demonstrate this, microangiography was performed in embryos of the stable gata1:GFP transgenic line (Long et al., 1997). Such embryos express GFP in erythrocytes and in migrating cerebellar granule

progenitor cells (Köster and Fraser, 2006, Volkmann et al., 2007). Imaging analyses of QD605-injected gata1:GFP embryos by confocal microscopy revealed that the emission spectrum of QD605 and GFP could be well separated in the same cell, although only a single excitation wavelength was used.

A known feature during CNS development is that blood vessels and axons share common trajectories during pathfinding, thereby using the same guidance molecules, as for example Netrin1 and its Receptor Unc5B (Lu et al., 2004, Park et al., 2004). The islet1:GFP stable transgenic line displays GFP expression in cranial motor neurons and their axon tracts. To test whether these axons use similar routes as blood vessels in the developing zebrafish nervous system, microangiography was performed on islet1:GFP transgenic embryos to co-label axons and blood vessels. It was found that in some brain regions, axon tracts and blood vessels did not share the same trajectories, while axons and blood vessels were found along the same routes in domains of the vagus sensory ganglion and the primordial hindbrain channel (PHBC), posterior to the otic vesicle. This demonstrates that pathfinding of blood vessels and axons is not strictly dependent on one another in the differentiating zebrafish brain.

DEVELOPMENTAL DYNAMICS 234:670–681, 2005

TECHNIQUES

Quantum Dots Are Powerful Multipurpose Vital Labeling Agents in Zebrafish Embryos

Sandra Rieger,[1] Rajan P. Kulkarni,[2] Dan Darcy,[2*] Scott E. Fraser,[2] and Reinhard W. Köster[1*]

Recently, inorganic fluorescent contrast agents composed of semiconductor materials have been introduced to biological imaging approaches. These so-called quantum dots provide unique and promising properties unreached by organic fluorophores, but their use as contrast agents within live organisms has been limited, probably due in part to concerns about their in vivo tolerance. Using transparent zebrafish embryos, we challenged quantum dots with a series of intravital imaging problems. We show that quantum dots provide a high fluorescent yield within targeted tissues, possess immense photostability, can be targeted to specific subcellular compartments, remain within targeted cells as lineage tracers, are easily separable from conventional organic fluorescent dyes, and are fixable, allowing them to be used in combination with immunohistochemistry after live recordings. Thus, quantum dots combine the specific advantages of different organic fluorescent contrast agents and promise to become the first fluorophore feasible for long-lasting intravital time-lapse studies. Finally, we show by colabeling blood vessels of the vasculature and major axon tracts of the nervous system that, for establishing these networks, the same guidance cues might be used in some body parts, whereas in others, both networks appear to develop independently from one another. Thus, the bright fluorescence of quantum dots will help to unravel many open questions in the fields of embryology, cell biology, as well as phenotyping and disease diagnosis. *Developmental Dynamics 234:670–681, 2005.* © 2005 Wiley-Liss, Inc.

Key words: zebrafish; bio-imaging; quantum dots; microangiography; contrast agent; lineage tracer

Received 9 February 2005; Revised 22 April 2005; Accepted 16 June 2005

INTRODUCTION

The ever-continuing demand for intravital contrast agents of different and brighter colors, reduced size, more stability, less toxicity, and greater versatility has led recently to the establishment of so-called quantum dots as biological labeling agents. Of these semiconductor nanocrystals, cadmium selenide quantum dots have been most commonly used for biological applications. Because crystal size alone determines the excitation and emission characteristics, a crayon box of fluorophores can be generated with a single synthesis strategy (Bruchez et al., 1998; Jaiswal et al., 2003). Also, appropriate masking and coupling chemistry has only to be developed once. Different coats using zinc sulfide (Mattoussi et al., 2001), silica (Bruchez et al., 1998; Chan and Nie, 1998), or micelles (Dubertret et al., 2002; Wu et al., 2003) have been developed to increase the fluorescence of the quantum dots and to render them soluble in aqueous medium. Such quantum dots have been found to be nontoxic in cultured cells (Jaiswal et al., 2003), within the mouse vasculature (Larson et al., 2003), in *Xenopus* embryos (Dubertret et al., 2002), and in tumor cells injected into mice embryos (Voura et al., 2004). Adapter molecules at-

The Supplementary Material referred to in this article can be accessed at www.interscience.wiley.com/jpages/1058-8388/suppmat
[1]GSF - National Research Center for Environment and Health, Institute of Developmental Genetics, Neuherberg-Munich, Germany
[2]Biological Imaging Center, Beckman Institute (139-74), California Institute of Technology, Pasadena, California
Grant sponsor: Caltech Biological Imaging Center; Grant sponsor: the German Bundesministerium für Bildung und Forschung; Grant number: Biofuture-Award 0311888.
*Dr. Darcy's present address is University of California San Diego, Division of Biology, San Diego, CA.
*Correspondence to: Reinhard W. Köster, GSF-National Research Center for Environment and Health, Institute of Developmental Genetics, 85764 Neuherberg, Munich, Germany. E-mail: reinhard.koester@gsf.de

DOI 10.1002/dvdy.20524
Published online 18 August 2005 in Wiley InterScience (www.interscience.wiley.com).

© 2005 Wiley-Liss, Inc.

6.7 List of publications

6.7.1 Publications

S. Rieger & R.W. Köster: **Preparation of zebrafish embryos for transmission electron microscopy.**

CSH Protocols Online; 2007; doi:10.1101/pdb.prot4772

Cover Image

Developmental Dynamics Special Edition: Developmental Neurobiology, November 2005

S. Rieger, R.P. Kulkarni, D. Darcy, S.E. Fraser & R.W. Köster: **Quantum dots are powerful multipurpose vital labeling agents in zebrafish embryos**.

Developmental Dynamics 234: 670–681, Nov 2005.

J. Beckers, F. Herrmann, S. Rieger, A.L. Drobyshev, M. Horsch, M. Hrabe de Angelis & B. Seliger: **Identification and validation of novel ERBB2 (HER2, NEU) targets including genes involved in angiogenesis**.

International Journal of Cancer 114(4): 590-597, Apr 2005.

B. Horr, H. Borck, M. Jones, A. Lebert, S. Rieger & F. Diel.: **Pyrethroids do not show relevant ex vivo histamine releasing potency in human basophils**.

Inflammation Research Center 52 Suppl 1: S11-2, Apr 2003

6.7.2 Submitted Publications & publications under review

S. Rieger, K. Volkmann & R.W. Köster: **Polysialyltransferase expression is linked to neuronal migration in the developing and adult zebrafish.**

Developmental Dynamics, under review

K. Volkmann, S. Rieger, A. Babaryka & R.W. Köster: **The zebrafish cerebellar rhombic lip is spatially patterned in producing granule cell populations of different functional compartments.**
Developmental Biology, submitted under review.

6.7.3 Publications in preparation

S. Rieger & R.W. Köster: Cadherin-2 regulates coherence and directionality of migrating cerebellar granule progenitor cells in zebrafish

6.8 Lebenslauf

Geboren am 10. Dezember 1972 in Bautzen, Sachsen.

Schulbildung & Studium

1979 – 1989	August-Fröhlich Gesamtschule Erfurt
9/1995 –7/1996	Fachabitur am Berufskolleg Backnang
9/1997 – 12/2002	Studium der Ernährungswissenschaft, Fachhochschule Fulda Dipl. Oec. Troph. (FH)
2/2000 – 8/2001	Biochemisches Praktikum in der Protein Engineering Group, Zyomyx Inc., Hayward CA, USA
2/2002 – 11/2002	Diplomarbeit zum Thema "Selection of protein-binding agents from libraries of partially randomized proteins", Protein Engineering Group, Zyomyx Inc., Hayward CA, USA
4/2004 – 9/2007	Doktorarbeit am Institut für Entwicklungsgenetik im GSF-Forschungszentrum für Umwelt und Gesundheit in der Helmholtz-Gemeinschaft München-Neuherberg zum Thema „ The regulation of neuronal progenitor cell migration by cell-cell adhesion factors during zebrafish cerebellar development" unter Betreuung Dr. Reinhard W. Köster und Professor Dr. Wolfgang Wurst, in Zusammenarbeit mit der Technischen Universität München

Stipendien & Auszeichnungen

1/2004	Auszeichnung vom Europäischem Allergie Verein - AVE für eine exzellente Diplomarbeit im Bereich der Biowissenschaften, dotiert mit 500 Euro
08/2004	Reisestipendium der Boehringer-Ingelheim Fonds und des Marine

	Biology Labs (MBL) für die Teilnahme am Kurs "Neural Development and Genetics of Zebrafish", Woods Hole MA, USA
06/2006	Doktorandenreisestipendium der GSF zur Teilnahme an der 7. Internationalen Konferenz „Zebrafish Development and Genetics" in Madison, Wisconsin, USA

Beruf & Berufsausbildung

9/1990 – 1/1993	Berufsausbildung Kauffrau im Einzelhandel bei Breuninger GmbH, Stuttgart
2/1993 – 2/1995	Verwaltungsanstellung bei Mercedes-Benz, Stuttgart-Möhringen
3/1995 – 8/1995	Au Pair in Maryland, USA
12/2002 – 2/2004	Wissenschaftliche Assistenzstelle am Institut für Experimentelle Genetik im GSF-Forschungszentrum für Umwelt und Gesundheit in der Helmholtz-Gemeinschaft München-Neuherberg, Untersuchung der Dll3 Mutante und Analyse von DNA Microarrays im Rahmen des „NGFN Express" Forschungsnetzwerkes